

Model-based Analysis of Chromatographic Processes with Implicit Sorption Isotherms

Dissertation

zur Erlangung des akademischen Grades

Doktoringenieur

(Dr.-Ing.)

von M.Sc. Marcus Fechtner
geboren am 19.12.1985 in Osterburg (Altmark)

genehmigt durch die Fakultät für Elektrotechnik und Informationstechnik
der Otto-von-Guericke-Universität

Gutachter:

Prof. Dr.-Ing. Achim Kienle
Prof. Dr.-Ing. Malte Kaspereit

Promotionskolloquium am 26.11.2020

This page intentionally left blank.

Foreword

This thesis is the result of research conducted at the chair for Automation/Modeling at the Otto von Guericke University and the Process Synthesis and Process Dynamics group of the Max Planck Institute for Dynamics of Complex Technical Systems in Magdeburg from 2015 to 2020. This research was funded by the state of Saxony-Anhalt within the International Max Planck Research School Magdeburg for Advanced Methods in Process and Systems Engineering and by the European Regional Development Fund within the Center of Dynamic systems. Both funding sources are hereby gratefully acknowledged.

I am grateful to all people who supported me on this journey.

This page intentionally left blank.

Abstract

Chromatography is a powerful separation method that is used in many different industries like chemical, pharmaceutical, and food industry. In the last two decades, chromatography received an immensely increased attention in biotechnology involving the separation of amino acids or even more importantly the separation of proteins. In general, chromatographic processes contribute crucially to a high cost of the corresponding overall process chains. Consequently, there is a high demand on their optimization through efficient process design and control. Both, design and control require a deep understanding of the process, which can be model-based or data-driven. In this thesis, model-based analysis is applied in order to predict qualitative process properties as well as quantitatively the process behavior through an analytical and a numerical approach, respectively.

The analytical approach used in this work results from the application of the equilibrium theory, which is based on an idealized model of spatially distributed packed bed sorption units assuming thermodynamic equilibrium between the fluid and the solid phase. The model represents a system of first-order quasi-linear partial differential equations and admits the analytical approach using the method of characteristics if the system is also hyperbolic. Thermodynamic equilibrium is described by the sorption isotherm, which represents the essential non-linearity of the system and determines crucial properties like hyperbolicity. Previous approaches have been limited to explicit sorption isotherms including Langmuir, Bi-Langmuir, and generalized Langmuir isotherms. In this work, processes with implicit sorption isotherms are considered. This generalized class of sorption isotherm is often required for an accurate process description. Consequently, the numerical approach presented in this thesis aims at an efficient numerical simulation of idealized chromatographic processes with implicit sorption isotherms. For demonstration purposes, two important classes of implicit sorption isotherms are considered for both approaches. One is derived from the ideal adsorbed solution theory, while the other results from the law of mass action.

First, focus is on the applicability of the numerical approach to an idealized chromatographic model with adsorption described by the ideal adsorbed solution theory. In particular, a reformulation strategy is introduced, which is combined with a method of lines approach. As a result, the simultaneous solution of the resulting differential algebraic equations (DAEs) is possible, thus avoiding explicit differentiation of the sorption isotherm. Efficiency of this approach and applicability of standard DAE software requires a differential index of one. For this purpose, the relation between the differential index of the DAE system and the spectral properties of the underlying adsorption equilibrium is established. In particular, it is shown that real and positive eigenvalues of the Jacobian derived from the adsorption isotherm represent a sufficient condition. This condition is also shown to be satisfied necessarily for binary mixtures with any type of single component adsorption isotherm or for multicomponent mixtures with certain restricted types

of single component isotherms. The new method is illustrated for different explicit and even implicit single component adsorption isotherms belonging to this class. Numerical efficiency is quantitatively demonstrated through comparison with various solution approaches using the state-of-the-art modified FastIAS method. An additional validation of numerical solutions is realized through comparison with semi-analytically obtained solutions from equilibrium theory.

Second, versatility of the numerical approach through application to an idealized chromatographic model with a significantly different sorption isotherm, the stoichiometric mass action law with constant solution normality for classical ion exchange processes, is demonstrated. It is proven that hyperbolicity of the model equations and non-negativity of the related eigenvalues implies a differential index of one, which greatly alleviates the numerical solution since it is often satisfied for thermodynamically consistent sorption isotherms. Classical theoretical results from equilibrium theory are summarized and further extended to full chromatographic cycles and pulse patterns, which are of major interest in chromatography. For validation purposes, semi-analytical solutions are compared to the numerical calculations for different scenarios. Focus is on selectivity reversals and their influence on process operation in general. Further, specific phenomena are discussed including the singular character of the origin with respect to a selectivity reversal as well as additional effects of multiple reversals.

Third, the analytical approach is extended by applying the equilibrium theory rigorously to advanced ion exchange processes that account for steric effects and a variable solution normality. This extension allows the equilibrium theory-based results to become available for applications in the field of bioseparations including the important separation of proteins. Analytical solutions are obtained for full chromatographic cycles consisting of the loading of an empty bed equilibrated at different counter-ion concentrations followed by the complete regeneration of the target components. Theoretical results regarding selectivity reversals are extended as well. A variable solution normality is shown to potentially introduce selectivity reversals and / or increase the number of selectivity reversals that affect the chromatographic cycle. For an improved understanding, the effect of steric hindrance and variable solution normality are investigated both separately as well as jointly in three suitable case studies. Theoretical findings for all cases were validated by comparison with results obtained from the numerical approach, which is extended accordingly. New phenomena such as the unique solution to non-strict hyperbolic cases or the global properties of the ion exchange sorption are analyzed in detail.

Finally, an extension of the triangle theory, which is based on results of the equilibrium theory for true moving bed processes involving two components, to classical ion exchange sorption is presented. Thus, rational design of the related simulated moving bed processes in conjunction with ion exchange sorption becomes available. Results are verified by simulations of the true moving bed process. For this purpose, the numerical approach is also extended to this advanced separation method.

Zusammenfassung

Eines der wichtigsten Trennverfahren für Mehrkomponentengemische im flüssigen oder gasförmigen Zustand ist die Chromatographie. Sie ist etabliert in einer Vielzahl von Industrien, wie z.B. der chemischen und der pharmazeutischen Industrie oder auch der Nahrungsmittelindustrie. In den letzten zwei Jahrzehnten hat sich das Hauptanwendungsgebiet mehr und mehr in den Bereich der Biotechnologie verschoben, da sich die Chromatographie hier als effektives Trennverfahren für Grundbausteine biotechnologischer Anwendungen, den Aminosäuren und den Proteinen, erwiesen hat. Sind chromatographische Prozesse Teil einer industriellen Prozesskette, tragen diese meist zu einem erheblichen Teil an den gesamten Prozesskosten bei. Aus diesem Grund ist die Optimierung chromatographischer Prozesse von zentraler Bedeutung. Umsetzung der Optimierung erfolgt durch entsprechend effizientes Prozessdesign und / oder Regelungsstrategien. Grundvoraussetzung für beide Optimierungskonzepte ist ein tiefgründiges Prozessverständnis. Dieses Verständnis kann entweder auf der Grundlage von physikalischen Gesetzen oder allein auf Grundlage von messbaren Daten gewonnen werden. Ersteres erlaubt eine prädiktive mathematische Darstellung des Prozesses durch klassische Modelle, während letzteres auf eine mathematische Darstellung durch Ersatzmodelle beschränkt ist die eine Reproduzierbarkeit der Messdaten erlaubt aber keine Prädiktion darüber hinaus. In dieser Dissertation werden analytische und numerische Ansätze für die Analyse klassischer Modelle entwickelt, welche dementsprechend die Vorhersage von qualitativen Prozesseigenschaften und auch des quantitativen Prozessverhaltens ermöglichen.

Der in dieser Arbeit verwendete analytische Ansatz basiert auf der Anwendung der sogenannten Gleichgewichtstheorie. Diese Theorie resultiert aus der Annahme eines bestimmten Gleichgewichtsmodells, dem idealen Modell örtlich verteilter Festbettprozess in der Chromatographie. Gleichgewicht bezieht sich in diesem Fall auf das thermodynamische Gleichgewicht zwischen fluider und fester Phase. Die Modellierung führt auf ein System quasi-linearer partieller Differentialgleichungen erster Ordnung, welches die Möglichkeit analytischer Lösungen basierend auf der Methode der Charakteristiken eröffnet. Die Anwendbarkeit der Methode setzt jedoch Hyperbolizität des Gleichungssystems voraus. Die Nicht-linearität in diesem Gleichungssystem wird allein durch die Sorptionsisotherme definiert, und sie bestimmt damit wichtige Eigenschaften des Gleichungssystems wie z.B. Hyperbolizität. Die Isotherme resultiert aus der Modellierung des thermodynamischen Gleichgewichts. In der Vergangenheit wurde die Anwendung der Gleichgewichtstheorie stets auf explizite Sorptionsisothermen beschränkt. Die wichtigsten Vertreter sind die Langmuir-, die Bi-Langmuir- und die verallgemeinerte Langmuir-Isotherme. Mit Hinblick auf eine erweiterte Anwendbarkeit wird in dieser Arbeit die verallgemeinerte Klasse der impliziten Sorptionsisothermen betrachtet. Dies gilt auch für die Entwicklung effizienter numerischer Lösungsverfahren. Zu Demonstrationszwecken werden zwei der wichtig-

sten impliziten Sorptionsisothermen basierend auf der Theorie der ideal adsorbierten Lösung beziehungsweise auf dem Massenwirkungsgesetz für den analytischen wie auch den numerischen Ansatz betrachtet.

Zuerst wird die Anwendbarkeit des entwickelten numerischen Lösungsansatzes an Hand des idealen Modells mit Adsorptionsisothermen basierend auf der Theorie der ideal adsorbierten Lösung demonstriert. Hierbei wird die Kernidee der Umformulierung des Systems partieller Differentialgleichungen präsentiert. Dieses neu formulierte Gleichungssystem wird anschließend mittels der Linienmethode in ein System bestehend aus Differential-algebraischen Gleichungen überführt, welche simultan ohne explizites Differenzieren der Adsorptionsisothermen gelöst werden können. Das effiziente numerische Lösen von Differential-algebraischen Gleichungssystemen, insbesondere bei der Nutzung von geeigneter Standardsoftware, erfordert einen Differentiationsindex gleich eins. Zu diesem Zweck wurde ein Zusammenhang zwischen dem Differentiationsindex und der Spektraleigenschaften des zu Grunde liegenden Adsorptionsgleichgewichts hergestellt. Sind die Eigenwerte der Jacobi-Matrix abgeleitet aus der Isothermen reell und positiv, so ist dies hinreichend für einen Differentiationsindex gleich eins. Es wird zudem gezeigt, dass diese hinreichende Bedingung im Falle von binären Gemischen für beliebige Reinstoffisothermen erfüllt ist jedoch nicht für Mehrstoffgemischen mit mehr als zwei Komponenten. Letzter Fall bedarf weiterer Einschränkungen bezüglich der Reinstoffisothermen. Das entwickelte numerische Lösungsverfahren wird durch Beispiele mit kompatiblen expliziten und sogar kompatiblen impliziten Reinstoffisothermen veranschaulicht. Für explizite Reinstoffisothermen gibt es die numerisch sehr effiziente 'modified FastIAS' Lösungsmethode, welche durch Vergleich mit dem entwickelten numerischen Lösungsansatz dessen Effizienz quantitativ bestätigt. Zudem werden die numerisch bestimmten Lösungen mit Hilfe der Gleichgewichtstheorie durch entsprechende semi-analytische Lösungen validiert.

Als zweites wird der numerische Lösungsansatz auf das ideale Modell mit einer sich zur obigen grundlegend unterscheidenden impliziten Isothermen basierend auf dem Massenwirkungsgesetz mit konstanter Lösungsnormalität für den klassischen Ionenaustausch angewendet, wodurch die Flexibilität der Anwendbarkeit des numerischen Ansatzes veranschaulicht wird. In diesem Fall ist ein Differentiationsindex von eins garantiert, wenn die Modellgleichungen hyperbolisch sind und die damit in Verbindung stehenden Eigenwerte nichtnegativ sind. Diese Bedingung ist für thermodynamisch konsistente Isothermen häufig erfüllt. Zudem werden klassische Ergebnisse der Gleichgewichtstheorie zusammengefasst und durch die Einbeziehung von chromatographischen Zyklen sowie von Pulsmustern erweitert. Die Validierung numerischer Ergebnisse erfolgt durch Vergleich mit semi-analytischen Ergebnissen der Gleichgewichtstheorie für verschiedene Prozessszenarien. Hauptaugenmerk liegt bei Simulationen und theoretischer Analyse auf dem Phänomen der Selektivitätsumkehr und den damit verbundenen allgemeinen Auswirkungen auf den Trennprozess. Des Weiteren wird zum einen die Rolle des Koordinatenursprungs im Zusammenhang mit der Selektivitätsumkehr diskutiert und zum an-

deren werden die Auswirkungen mehrerer Selektivitätsumkehrungen untersucht.

Als drittes wird der analytische Ansatz durch rigorose Anwendung der Gleichgewichtstheorie auf Ionenaustauschprozesse mit variabler Lösungsnormalität und sterischen Effekten erweitert. Folglich stehen die mit der Gleichgewichtstheorie verbundenen Ergebnisse auch im Bereich der Bioseparation zur Verfügung. Dies gilt insbesondere auch für die bedeutende Trennung von Proteinen. Analytische Lösungen werden für vollständige chromatische Zyklen bestimmt. Dabei besteht ein Zyklus aus der zusätzlichen Beladung einer ausschließlich mit Gegenionen beladenen und auch im Gleichgewicht stehenden Ionenaustauschsäule mit zu trennenden Zielkomponenten und weiteren Gegenionen gefolgt von der vollständigen Regeneration der Zielkomponenten. Eine weitere wichtige Erweiterung theoretischer Ergebnisse erfolgt in Bezug auf die Selektivitätsumkehr. Die nun variable Lösungsnormalität kann die unmittelbare Ursache einer Selektivitätsumkehr während eines chromatographischen Zyklus sein und / oder allgemein die Anzahl an Selektivitätsumkehrungen in einem Zyklus erhöhen. Um die verschiedenen Effekte der variablen Lösungsnormalität und der sterischen Hinderung zu verdeutlichen werden beide Eigenschaften in zwei Fallstudien getrennt voneinander betrachtet. Eine dritte Fallstudie untersucht die Effekte unter der Annahme dass beide Eigenschaften gleichzeitig präsent sind. Die semi-analytischen Ergebnisse aller drei Fallstudien werden zur Validierung mit Simulationen basierend auf dem entwickelten numerischen Lösungsansatz abgeglichen. Zu diesem Zweck wurde der numerische Lösungsansatz entsprechend auf diese Ionenaustauschprozesse erweitert. Zudem werden weitere Phänomene wie die Eindeutigkeit der Lösung eines nicht strikt hyperbolischen Spezialfalles wie auch globale Eigenschaften des Ionenaustausches im Detail untersucht.

Zuletzt wird eine Erweiterung der Dreieckstheorie auf klassische Ionenaustauschprozesse präsentiert. Diese Theorie basiert auf den Ergebnissen der Gleichgewichtstheorie angewendet auf 'True Moving Bed'-Prozesse für Zweikomponentengemische. Dementsprechend ist die darauf basierende Designprozedur für 'Simulated Moving Bed'-Prozesse auch bei Verwendung von Ionenaustauschsäulen verfügbar. Die theoretischen Ergebnisse werden durch Simulationen des 'True Moving Bed'-Prozesses validiert, wofür der numerische Ansatz entsprechend auf diese weiterentwickelten Trenntechnologie erweitert wurde.

This page intentionally left blank.

Contents

1	Introduction	1
1.1	Motivation and Scope	1
1.1.1	Chromatographic Processes	1
1.1.2	Model-based Design and Analysis	3
1.1.3	Implicit Sorption Isotherms	4
1.2	State of the Art	5
1.2.1	Numerical Approaches	5
1.2.2	Analytical Approaches	6
1.3	Objectives	7
1.4	Outline	9
2	Theoretical Background	11
2.1	Model Equations	11
2.2	Equilibrium Theory	20
2.3	Numerical Solution Methods	25
3	Ideal Adsorbed Solution Theory	29
3.1	Introduction	29
3.2	Reformulation and Solution Strategy	30
3.3	Applications	34
3.3.1	Example with Explicit SCIs	35
3.3.2	Example with Implicit SCIs	40
3.4	Summary	44
4	Classical Ion Exchange (CIE)	45
4.1	Introduction	45
4.2	Reformulation and Solution Strategy	46
4.3	Equilibrium Theory	47
4.4	Results	50
4.5	Summary	63
5	Advanced Ion Exchange (AIE)	65
5.1	Introduction	65
5.2	Extension of the Solution Strategy	66
5.3	Equilibrium Theory	68

5.4	Selectivity Reversals	73
5.5	Application Examples	75
5.5.1	Effect of the Variable Solution Normality	76
5.5.2	Effect of the Steric Factors	82
5.5.3	Joint Effects	84
5.6	Summary	90
6	Continuous Separation Processes	91
6.1	Introduction	91
6.2	Triangle Theory	91
6.3	Results	95
6.4	Summary	102
7	Concluding Remarks	103
7.1	Analytical Approach	103
7.2	Numerical Approach	105
7.3	Future Research	106
	Appendix	109
Appendix A	IAST: Spectral properties	109
Appendix B	CIE: Differential Index	114
Appendix C	AIE: Genuine Non-linearity	115
Appendix D	AIE: Reversal Intersections	119
Appendix E	AIE: Reversal Zones	120
Appendix F	AIE: Steric Factors	122
Appendix G	AIE: Experimental Test System	124
Appendix H	AIE: Non-strict Hyperbolicity	127
Appendix H.1	The $j, j + 1$ selectivity reversal	127
Appendix H.2	Two Coinciding Reversal Hyperplanes	128
Appendix H.3	Multiple Coinciding Reversal Hyperplanes	135
Appendix I	AIE: Global Properties on \mathcal{CH} hyperplanes	137
Appendix I.1	Existence of a Bijective Function	137
Appendix I.2	Application of the Global Inverse Theorem	141
Appendix I.3	Remarks	146
	Bibliography	159

List of Figures

1.1	Single column process	1
1.2	SMB process	2
2.1	Simplified single column process	12
3.1	SCIs of the first example.	36
3.2	Breakthrough curves for the first example.	37
3.3	Hodograph validation of the first example.	39
3.4	SCIs of the second example.	41
3.5	Eluted peaks for the second example.	42
3.6	Hodograph validation of the second example.	43
4.1	Concentration phase space with one selectivity reversal.	50
4.2	Loading with feed in I	52
4.3	Loading with feed in II	53
4.4	Concentration phase space: Loading with feed on reversal.	54
4.5	Profiles: Loading with feed on reversal.	55
4.6	Chromatographic cycle with feed in I	56
4.7	Spatial profiles with feed in I	57
4.8	Chromatographic cycle with feed in II	58
4.9	Spatial profiles with feed in II	59
4.10	Chromatographic cycles with feed on reversal	60
4.11	Concentration phase space with two selectivity reversals	61
5.1	Linear gradient elution	68
5.2	Stoichiometric ion exchange with constant solution normality	77
5.3	Stoichiometric ion exchange with variable solution normality	79
5.4	Loading on $c_{\text{tot}} = 2 \frac{\text{mol}}{\text{m}^3}$ plane	80
5.5	Regeneration on $c_{\text{tot}} = 0.5 \frac{\text{mol}}{\text{m}^3}$ plane	81
5.6	Comparison of c_{tot} planes differing in steric factors	83
5.7	Chromatographic cycle without steric hindrance	85
5.8	Chromatographic cycle with steric hindrance	86
5.9	Chromatographic cycle without steric hindrance and const. feed	88
5.10	Chromatographic cycle with steric hindrance and const. feed	89
6.1	TMB process	92

6.2	Fluxes in a TMB	93
6.3	TMB profile	94
6.4	TMB triangle of the CIE	97
6.5	Dynamic TMB simulation	99
6.6	Triangle comparison	100
6.7	Triangle dependency on c_{tot}	101
Appendix A.1 Counter-example.		112
Appendix G.1 Proof of principle		125
Appendix H.1 Non-strictly hyperbolic example		133
Appendix I.1 Watershed curves		147

List of Tables

3.1	Parameters of the first IAST example.	35
3.2	Execution times of the first IAST example.	37
3.3	Parameters of the second IAST example.	40
4.1	Parameters of the example with one selectivity reversal.	51
4.2	Parameters of the example with two selectivity reversals.	62
5.1	Basic Parameters.	76
5.2	CIE-based model parameters.	76
5.3	SMA-based model parameters.	82
6.1	TMB process and simulation parameters.	98
Appendix A.1	Parameters of the Tóth isotherm.	113
Appendix G.1	Experimental parameters.	124
Appendix H.1	Non-strictly hyperbolic example.	134

This page intentionally left blank.

Notation

Abbreviations

C_1	2-phenylethanol
C10	phenyl-n-decane
C11	phenyl-n-undecane
C_2	3-phenylpropanol
CIE	classical ion exchange
const	constant
CS	Column section
DAE	differential algebraic equation
Eq.	Equation
Eqs.	Equations
FD	finite differences
FDM	full discretization method
FE	finite elements
Fig.	Figure
Figs.	Figures
FV	finite volumes
IAST	ideal adsorbed solution theory
MOC	method of characteristics
MOL	method of lines
MOR	method of Rothe
ODE	ordinary differential equation
PDAE	partial differential and algebraic equation
PDE	partial differential equation
SCI	single component isotherm
SMA	steric mass action law
SMB	simulated moving bed
Tab.	Table
Tab.	Tables
TMB	true moving bed

List of Symbols

Latin letters

$\mathbf{0}$	zero vector	---
$\mathbf{0}_N$	matrix of dimension $N \times N$ with all entries equal to zero	---
$\mathbf{0}$	vector with all entries equal to one	---
$\mathbf{1}_N$	matrix of dimension $N \times N$ with all entries equal to one	---
a	supplementary variable	[.]
a_i^0	hypothetical covered surface area of component i	$[m^2]$
a_{tot}	totally covered surface area	$[m^2]$
\mathcal{A}	specific surface area of the solid phase	$[\frac{m^2}{m^3_{\text{solid}}}]$
A_c	cross-sectional area of the column	$[m^2]$
b	supplementary variable	[.]
b_i	SCI parameter	[.]
\mathbf{B}	flux matrix	$[\frac{m}{s}]$
c	supplementary variable	[.]
\mathbf{c}	fluid phase concentration vector	---
c_i	fluid phase concentration of component i	$[\frac{mol}{m^3}]$
c_{tot}	modified (generalized) solution normality	$[\frac{mol}{m^3}]$
\tilde{c}_{tot}	constant solution normality	$[\frac{mol}{m^3}]$
\mathbf{c}_j	fluid phase concentration vector in column section j	---
$\mathbf{c}_{\text{extract}}$	fluid phase concentration vector in outlet extract stream j	---
\mathbf{c}_{feed}	fluid phase concentration vector in inlet feed stream j	---
$\mathbf{c}_{\text{raffinat}}$	fluid phase concentration vector in outlet raffinat stream j	---
\tilde{c}_k	k th transition curve in concentration phase space	---
$c_{i,j}$	fluid phase concentration of component i in column section j	$[\frac{mol}{m^3}]$
$\tilde{c}_{i,k}$	k th transition curve of component i	$[\frac{mol}{m^3}]$
\mathbf{c}^0	hypothetical fluid phase concentration vector	---
c_i^0	hypothetical fluid phase concentration of component i	$[\frac{mol}{m^3}]$
\mathcal{C}	subset of fluid concentration phase space	---
\mathcal{C}^1	class of continuously differentiable functions	---
\mathcal{C}^i	i th state (plateau) in the fluid concentration phase space	---
\mathcal{CD}_i	i th contact discontinuity	---
\mathcal{CH}	hyperplane of constant c_{tot}	---
\mathbf{D}_a	constant matrix of apparent dispersion	---
$D_{a,i}$	constant apparent dispersion coefficient of component i	$[\frac{m^2}{s}]$
\mathbf{E}	matrix with zero main diagonal and all entries equal to one	---
f	function symbol	---
\mathbf{f}	function symbol	---
F	phase ratio	$[-]$
\mathcal{F}	flux vector function	---
$\mathcal{F}_{i,j}$	scalar flux function of component i in column section j	---

$\tilde{\mathcal{F}}$	capacity vector function	---
g	function symbol	---
\mathbf{g}	function symbol	---
G	supplementary variable	[.]
h	function symbol	---
\mathbf{h}	function symbol	---
H	supplementary variable	[.]
i	index	[-]
\mathcal{I}	intersection of \mathcal{CH} and \mathcal{RH}_j	---
\mathbf{I}_N	identity matrix of dimension $N \times N$	---
j	index	[-]
\mathbf{J}	Jacobian matrix of the sorption isotherm $\mathbf{q}(\mathbf{c})$	---
k	index	[-]
K_{iN}	equilibrium constant of components i and N	[-]
\tilde{K}_{iN}	adjusted equilibrium constant of components i and N	[-]
$\bar{\mathbf{K}}$	matrix of mass transfer coefficients	[-]
\bar{k}_i	mass transfer coefficient of component i	[-]
l	index	[-]
\mathbf{l}_k	k th left eigenvector of $\frac{\partial \mathbf{q}}{\partial \mathbf{c}}$	---
$l_{k,i}$	i th entry of the k th left eigenvector	[.]
L	length of the column	[m]
L_j	length column section j	[m]
\mathcal{L}	set of all indices related to absent components \mathcal{CH}	---
m	index	[-]
m_j	flow-rate ratio in column section j	[-]
M	number of coinciding reversal hyperplanes	[-]
M_i	supplementary variable	[.]
n	index	[-]
N	number of components / index of N th component	[-]
N_L	number of absent components	[-]
N_t	number of grid points in coordinate t	[-]
N_z	number of grid points in coordinate z	[-]
\mathbf{p}	vector of steric factors	---
p_i	steric factor of component i	[-]
$\tilde{\mathbf{p}}$	vector of SMA related parameters	---
\mathcal{P}	parameter set of SMA parameter values	---
\mathbf{q}	solid phase concentration vector	---
q_i	solid phase concentration of component i	$\left[\frac{\text{mol}}{\text{m}^3}\right]$
$q_{N,\text{tot}}$	total solid phase concentration of component N	$\left[\frac{\text{mol}}{\text{m}^3}\right]$
q_{tot}	exchanger capacity	$\left[\frac{\text{mol}}{\text{m}^3}\right]$
\mathbf{q}_j	solid phase concentration vector in column section j	---
$q_{i,j}$	solid phase concentration of component i in column section j	$\left[\frac{\text{mol}}{\text{m}^3}\right]$
\mathbf{q}^0	hypothetical solid phase concentration vector	---

q^{sat}	SCI parameter	$[\frac{\text{mol}}{\text{m}^3}]$
q_i^0	hypothetical solid phase concentration of component i	$[\frac{\text{mol}}{\text{m}^3}]$
\bar{q}	actual solid phase concentration vector	---
Q^i	i th state (plateau) in the solid concentration phase space	---
\mathcal{QH}	hyperplane corresponding to \mathcal{CH}	---
\mathbf{r}_k	k th eigenvector of \mathbf{B} and $\frac{\partial \mathbf{q}}{\partial \mathbf{c}}$	---
$r_{k,i}$	i th entry of the k th eigenvector	[.]
\mathcal{R}	universal gas constant; 8.314	$[\frac{\text{J}}{\text{molK}}]$
\mathbf{R}	matrix of column eigenvectors	---
R_i	i th simple wave	---
\mathcal{RH}_{jk}	reversal hyperplane related to components j and k	---
s_k	shock wave velocity	[—]
\tilde{s}_k	physical shock wave velocity of family k	[.]
$\tilde{s}_{k,j}$	k th characteristic shock wave velocity in column section j	[.]
S_i	i th shock wave	---
t	dimensionless time coordinate	[—]
t^*	time coordinate	[s]
T	supplementary variable	[.]
\mathcal{T}	equilibrium temperature	[K]
u	mobile phase velocity	$[\frac{\text{m}}{\text{s}}]$
u_j	fluid phase velocity in column section j	$[\frac{\text{m}}{\text{s}}]$
u_s	solid phase velocity	$[\frac{\text{m}}{\text{s}}]$
U	supplementary variable	[.]
\mathbf{v}	joint capacity vector	---
v_i	joint capacity of component i	$[\frac{\text{mol}}{\text{m}^3}]$
\dot{V}	volumetric flow rate of the fluid phase	$[\frac{\text{m}^3}{\text{s}}]$
\dot{V}_j	volumetric flow rate of the fluid phase in column section j	$[\frac{\text{m}^3}{\text{s}}]$
$\dot{V}_{\text{desorbent}}$	volumetric flow rate of the inlet desorbent stream	$[\frac{\text{m}^3}{\text{s}}]$
\dot{V}_{extract}	volumetric flow rate of the outlet extract stream	$[\frac{\text{m}^3}{\text{s}}]$
\dot{V}_{feed}	volumetric flow rate of the inlet feed stream	$[\frac{\text{m}^3}{\text{s}}]$
$\dot{V}_{\text{raffinat}}$	volumetric flow rate of the outlet raffinat stream	$[\frac{\text{m}^3}{\text{s}}]$
\dot{V}_s	volumetric flow rate of the solid phase	$[\frac{\text{m}^3}{\text{s}}]$
\mathbf{w}	adjusted capacity vector	---
W	supplementary variable	[.]
\mathbf{x}	normalized fluid phase concentration vector	---
x_i	normalized fluid phase concentration of component i	[—]
\mathcal{X}	subset of normalized fluid concentration phase space	---
\mathbf{y}	normalized solid phase concentration vector	---
y_i	normalized solid phase concentration of component i	[—]
\mathcal{Y}	subset of normalized solid concentration phase space	---
z	dimensionless space coordinate	[—]
z^*	space coordinate	[m]
Z	supplementary variable	[.]

Greek letters

α	supplementary variable	[.]
β	supplementary variable	[.]
γ	supplementary variable	[.]
ϵ	total porosity	[-]
ϵ_e	interparticle voidage	[-]
ϵ_p	intraparticle voidage	[-]
ε	supplementary variable	[.]
ζ	supplementary variable	[.]
η	function symbol	--
Θ	supplementary variable	[.]
ϑ	SCI parameter	[-]
κ	adjusted phase ratio	[-]
\varkappa_{iN}	selectivity coefficient of components i and N	[-]
λ_k	k th eigenvalue of $\frac{\partial \mathbf{q}}{\partial \mathbf{c}}$	[-]
$\tilde{\lambda}_k$	characteristic velocity (k th eigenvalue of flux matrix)	[.]
$\tilde{\lambda}_{k,j}$	characteristic velocity in column section j	[.]
μ_i	reciprocal of the genuinely ionic charge of component i	[-]
μ_i^q	chemical potential of component i in the solid phase	$\left[\frac{J}{mol}\right]$
$\tilde{\mu}_i$	reciprocal of the genuinely ionic charge of component i	[-]
ν_i	reciprocal of the characteristic charge of component i	[-]
$\tilde{\nu}_i$	characteristic charge of component i	[-]
ξ_i	characteristic charge + steric factor of component i	[-]
π_i	surface potential of component i	$\left[\frac{mol}{m^3}\right]$
ρ	supplementary variable	[.]
ϱ_i	Langmuir isotherm parameter	[-]
σ	scalar for parametrization of curves i	[.]
θ_i	Langmuir isotherm parameter	$\left[\frac{m^3}{mol}\right]$
τ	supplementary variable	[.]
ϕ	function symbol	--
φ	function symbol	--
Φ	function symbol	--
χ_i	molar fraction of component i in solid phase	[-]
ψ	function symbol	--
Ψ	function symbol	--
ω	supplementary variable	[.]
Ω	function symbol	--

This page intentionally left blank.

Chapter 1

Introduction

1.1 Motivation and Scope

1.1.1 Chromatographic Processes

In many different areas of the industry such as chemical industry, pharmaceutical industry, or biotechnology exists a natural demand for high purity products. For this purpose many different separation technologies were developed. Some of the most applied technologies are distillation, extraction, and chromatography. The latter is used mostly for difficult separations that have only a small difference in specific physio-chemical properties regarding the involved target components. Main focus here is on liquid-solid phase chromatography since it is one of the most used phase combinations on the preparative scale, particularly in pharmaceutical and biotechnological processes. However, many results in this thesis can be directly applied to gas chromatography. Hence, the mobile phase is denoted more generally as fluid phase in the following.

In the following, the key idea of chromatography [1] is briefly explained using a single chromatographic column, the most basic but also most important process configuration, which is shown in Fig. 1.1. A mixture of two target components is injected into a chromatographic column using a suitable solvent. The fluid flows with a given velocity through the column, which contains a suitable stationary

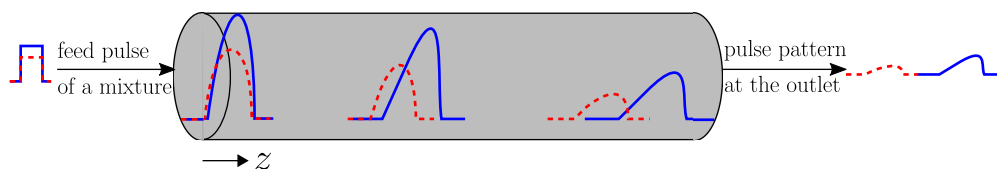


Figure 1.1: Pulse injection of a binary mixture into a column depicting a batch process. Transient pulse pattern at the column outlet indicates a complete separation.

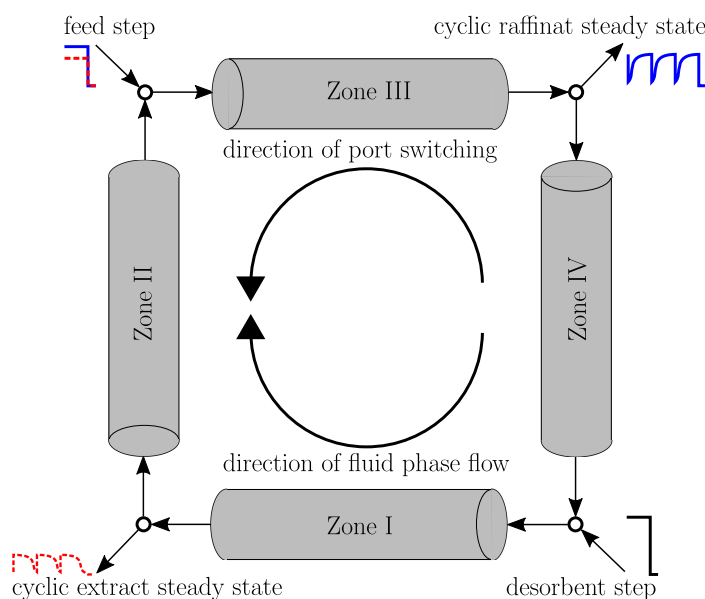


Figure 1.2: Step injection of a binary mixture into an SMB depicting a continuous process. Cyclic steady states of pure components at the two outlets indicate a continuous complete separation.

solid phase. 'Suitable' means, the interaction of target components in the fluid phase with the stationary phase admits a small difference between different target components. Even a slightly stronger interaction of one component leads in average to an increased number of binding states of short duration to the solid phase. This increased average number of binding states occurring during the transition from the column inlet to the outlet stronger retains in average the corresponding component in the column. As a result, the stronger sorbing component reaches in average the outlet of the column later. If in addition the column is long enough, then complete separation can be achieved as depicted in Fig. 1.1. With the configuration in Fig. 1.1, separation of target components requires pulse injections. Hence, single column chromatography can be only realized as a batch process.

In contrast to this, a realization of a continuous chromatographic process, the simulated moving bed (SMB) [2], is shown in Fig. 1.2. In this figure, the SMB consist of four single columns connected in series and forming a single loop. The cyclic switching of the input / output ports in the direction of the fluid phase 'simulates' a counter-current moving solid phase with respect to the flow direction of the fluid phase. In this configuration, a mixture is continuously injected resulting in a continuous output of pure stronger sorbing (extract) and weaker sorbing (raffinate) components.

Focus in this work is on single columns, since they are the most applied process configuration and represent the building blocks of more advanced separation technologies like SMB or two-dimensional chromatography [3], which all share the

same basic physical principles. A small part is specifically dedicated to the SMB configuration. This process realization is of interest due to its continuous operation, which admits the production of large quantities in less time and requires in addition less energy, less solvent, and also a smaller amount of solid phase media.

1.1.2 Model-based Design and Analysis

Independent of the specific process, chromatography significantly contributes to the cost of the overall process chain. Therefore, proper design of the process is economically important. Regarding their thermodynamic design, chromatographic processes generally admit the following degrees of freedom [4]. First, the choice of a suitable solid phase. For any given mixture this choice is limited to solid phases that interact with target components in the fluid phase in a desired way. Similarly, a suitable solvent is required to provide an appropriate fluid phase environment for the target components without compromising their sorption behavior. Column length is another crucial pre-operational degree of freedom that affects separation efficiency of the chromatographic process. In addition suitable operating parameters are required. In single column chromatography important operating parameters are the fluid flow rate and some gradients of additionally injected components [5]. A typical example are salt gradients in protein separation [6], where the sorbing behavior of the salt is used to efficiently elute proteins. Gradients are usually either step-wise or linearly injected. In this context it is important to find suitable or even optimal step sizes and slopes, respectively. Even so gradients can be also applied to SMB units, for example gradients of solvent modifiers [7]. Besides, the most important operating parameters for SMB processes are the flow rate ratios [8] in each zone of the process. They can be determined using the the so-called triangle theory [9], which is based on an analytical solution of an idealized column model assuming a true counter current movement of the fluid and the solid phase.

Two design methodologies are typically used, either an empirical or model-based design. In this thesis, only model-based design of chromatographic processes [1] is considered due to its efficiency, which is briefly described in the following. In order to account for a process under a large variety of conditions and different set-ups, an enormous amount of experimental data is required, which leads to a cost-intensive empirical design. The experimental effort can be reduced using mathematical models leading to a model-based design. A first, conceptual design can be based on analytical insight of some reasonably simplified models that admit such an analytical approach [10]. A typical example is the triangle theory for SMB processes mentioned above. In a second step, the analytical approach can be complemented with numerical simulations of some more detailed models [11]. Hence, simulations, which are obviously more cost efficient than time and material consuming experiments, can be used to predict the real process behavior more quantitatively. Further, numerically efficient simulations can be incorpo-

rated in advanced concepts such as optimization or control [12]. Both advanced concepts can improve the process performance significantly. If however neither useful analytical results nor numerically efficient simulations are available due to an increased complexity of the mathematical models, model-based design cannot be applied. Instead of going back to cost intensive empirical design methods, model-based design methods can be developed through advances in model-based analysis, which is the primary objective of this work. Especially, if the analysis eventually allows to obtain analytical results and / or numerically efficient simulations for chromatographic processes despite an increased complexity, a crucial step is taken for future advancement in design methods of these separation processes.

Model-based analysis requires mathematical representations of chromatographic processes. Mathematical modeling of these spatially distributed processes (see Figs. 1.1 and 1.2) leads to a system of partial differential equations (PDEs) [13]. There is a large variety of models with different complexity. In this work, the important class of equilibrium models [13] is considered since they account, despite numerous idealizations, for the most important principle, the sorption equilibrium of the chromatographic process. Main focus is on the ideal model [14, 15, 13]. It assumes a thermodynamic equilibrium between the fluid and solid phase, neglects all effects leading to band broadening, like axial dispersion for example, and therefore leads to a system of first-order quasi linear PDEs that can be solved semi-analytically using the methods of characteristics (MOC) [15]. In contrast, obtaining numerical solutions for hyperbolic PDE systems (efficiently) is in general challenging due to the formation of steep concentration fronts [16]. For equilibrium models, the sorption mechanism is mathematically represented in form of algebraic equations by so-called sorption isotherms, which result from the thermodynamic equilibrium of the two phases. Isotherms often represent the non-linearity of the PDE system of the ideal model. On one hand, finding a suitable isotherm is important to reflect the non-linear behavior and therefore possibly key features of the process. On the other hand, any suitable but also complex isotherm increases significantly the complexity of the mathematical problem formulation. Hence, mostly explicit isotherms [11, 15] are considered. Focus is here on the extension of model-based analysis to implicit isotherms. Such an extension allows to incorporate a large variety of more complex and thus possibly also of more suitable isotherms in model-based design methods. As a result, more challenging systems of partial differential algebraic equations (PDAEs) have to be solved analytically and / or numerically.

1.1.3 Implicit Sorption Isotherms

Focus of this thesis is on model-based analysis of chromatographic processes with implicit isotherms based on the ideal adsorbed solution theory (IAST) [17] and the law of mass action [18], respectively. The IAST is usually used for weaker sorption mechanisms, which are then often referred to as adsorption. Adsorption is based

on weaker electrostatic forces including ion-dipole interactions, hydrogen bonds, or hydrophobic interactions. The IAST is derived from thermodynamic principles. In contrast to the Langmuir isotherm, which is based on simple sorption kinetics [19], IAST allows for variable selectivities, and therefore it is able to account for additional phenomena such as selectivity reversals. In comparison with other sophisticated and thermodynamic consistent sorption principles like real adsorbed solution theory [20, 21] or vacancy solution theory [22], the IAST allows the prediction of multi-component adsorption based on single component isotherm (SCI) data, which is far easier to obtain [23]. IAST was successfully applied to gas [24] as well as liquid phase adsorption under dilute conditions [25]. Thus, the IAST formalism results not only in challenging implicit isotherms but also provides numerous relevant application examples in gas and liquid chromatography [26].

In contrast to adsorption, stronger physiosorption mechanisms are based on electrostatic forces of ionic charges. These mechanisms are referred to as ion exchange, which can be described by the mass action law. In its most elegant form, the ion exchange isotherm is derived from the concentration-based mass action law, which admits analytical treatment through application of the MOC. Classical analytical and numerical results were presented in [27, 28]. These results were helpful for applications involving small ions and a constant solution normality. These two aspects define the classical ion exchange (CIE), which is however limited regarding its real world applications such as sea water purification or separation of rare earths.

Separations in biotechnology, micro biology, and pharmaceutical industry heavily promoted the application of ion exchange processes since most relevant components are either differently charged amino acids or proteins. If separations involve large molecules like proteins, they incorporate new aspects like steric shielding and non-integer characteristic charges. In conjunction with a variable solution normality these aspects define the advanced ion exchange (AIE). In order to account for all three aspects in AIE, the steric mass action law (SMA) was developed [29], which is closely related to the mass action law used in CIE, thus motivating the application of the MOC also to the AIE formalism with SMA isotherm. Parameters of the SMA isotherm can be obtained from simple binary experiments [29]. Moreover, the SMA was applied successfully to many different bio separations [6, 30, 31, 32, 33]. Both, CIE and AIE introduce implicit isotherms. In addition of using an elegant but also challenging implicit isotherm, AIE allows to explore model-based analysis for the important class of bioseparations [34, 5, 35].

1.2 State of the Art

1.2.1 Numerical Approaches

Independent of the sorption principle, the PDE systems of equilibrium models can be solved by standard numerical methods such as full discretization methods

(FDM) [16] and method of lines (MOL) [36]. All of these methods rely on discretization techniques. The most important discretization schemes are finite differences (FD), finite elements (FE), finite volumes (FV) [13, 11]. Based on these, more sophisticated concepts including high resolution schemes [16] or adaptive grids [37] are also frequently used to improve the numerical performance.

In AIE, numerical solutions for equilibrium models are mostly obtained through FDM with FD [30, 38] or through MOL with FVM [39]. If the thermodynamic sorption equilibrium in AIE is described by the SMA, the implicit algebraic equations are either solved separately using iterative methods, such as Newton-type methods [40] in FDM [38] or simultaneously approximating them by corresponding ordinary differential equations (ODEs) that are based on a fast but finite mass-transfer [39] in order to achieve numerical efficiency of an MOL-based solution strategy. Note, the latter approach does not solve genuine equilibrium models. Consequently, there is a lack of numerical approaches that solve simultaneously the differential and algebraic equations (DAEs) efficiently.

In case of equilibrium model with IAST, FDM primarily in conjunction with FD or FVM [26] or MOL in conjunction with FD or FVM [41] is applied. Focus was particularly on efficiently solving the adsorption equilibrium provided by the IAST [17, 42, 43]. As a result, the modified FastIAS was developed [44]. It also uses Newton-type algorithms to solve the algebraic equations of the IAST formalism separately but improves these algorithms by exploiting the specific structure of the IAST equations. Despite being available already in 1985, it is the state-of-the-art IAST equilibrium solver still up to today and thus presents a useful benchmark. One of its more significant drawbacks is the limitation to analytically integrable and therefore explicit SCIs. More recently, other efficient but very limited approaches based on analytical solutions were proposed [45, 46] as well as an alternative approach [41]. It is based on a differential reformulation of the equilibrium conditions and applies numerical integration. This method is very powerful and avoids iteration at the expense of increased computational effort. Further computational effort is required to calculate the derivatives of the equilibrium concentrations of the solid phase, which are needed for packed bed adsorber simulation using a method of lines approach. Other limitations arise regarding classes of applicable SCIs. Numerical solution strategies that are comparable in efficiency with methods that use the modified FastIAS and also require only mild conditions on applicable SCIs are not available.

1.2.2 Analytical Approaches

Besides a numerical solution also an analytical solution is possible for hyperbolic conservation laws with piece-wise constant boundary and initial conditions - so called-Riemann problems - using the method of characteristics (MOC) [16]. The ideal model of chromatography together with standard modes of operation, such as the loading of an empty bed, or the regeneration of a fully loaded bed, or

the elution of a pulse, represents such a system [13]. In this context, the MOC is often called equilibrium theory. The requirement of hyperbolicity implies diagonalizability of the Jacobian that can be obtained from the sorption isotherm [15]. Consequently, application of the MOC to the ideal model depends on the choice of the isotherm. The MOC was applied successfully to Langmuir [15], Bi-Langmuir [47, 48], generalized Langmuir [49] isotherms. Beyond Langmuir-like isotherms, only a few other isotherms admit analytical insight into the properties of the sorption Jacobian.

Multi-component isotherms described by the IAST do admit under certain conditions for the SCIs analytical insight in form of the spectral properties regarding the sorption Jacobian [41]. The conditions are rather strong, but since the IAST provides a very challenging sorption equilibrium including integral equations, other analytical results regarding the IAST related Jacobian are not available.

In contrast, some analytical results regarding the CIE were already obtained by Tondeur [27]. A more comprehensive summary of classical results can be found in [28]. Based on these results, the MOC was successfully applied to CIE applications [50, 51] involving small ions. Since the field of application for ion exchange shifted to bioseparations involving very complex charged molecules, the AIE formalism is required to account for additional and some of the most significant properties like steric shielding and a variable solution normality [52] by using the SMA isotherm [29]. Some efforts to apply the MOC were made [6, 31, 53, 54, 55, 56] but in each case limited to specific applications introducing additional simplifying assumptions. Neither a rigorous application of the MOC to the AIE nor an extension of classical analytical results to the SMA isotherm is available.

Further, the MOC was successfully applied to binary SMB processes using linear or Langmuir isotherms [57] and was extended to isotherms with variable selectivity [58] including the IAST formalism. An extension of this so-called triangle theory to ion exchange processes was not presented.

1.3 Objectives

Main objective of this thesis is to develop new numerical and analytical methods for model-based analysis of chromatographic processes with implicit adsorption isotherms as introduced in the previous section.

The numerical solution strategy applied to equilibrium models with implicit isotherms aims to meet the following requirements. First, simultaneous solution of differential and algebraic equations, which allows to use DAE solvers that provide a number of advantages compared to methods that sequentially solve DAEs. Second, the methodology of the solution approach is independent of a specific isotherm, thus can be easily applied to the IAST and mass action-based AIE / CIE formalisms. Further, versatility of the approach allows also to apply different process configurations like single column or SMB with arbitrary initial and

boundary conditions. Third, efficiency of the approach can be demonstrated by using state-of-the art benchmarks. In particular, demonstration of numerical efficiency by comparison with modified FastIAS in conjunction with a variety of standard numerical methods for PDE systems. In order to demonstrate a genuine reduction of limitations, conditions of applicability and efficiency related to the developed numerical approach are significantly relaxed compared to the conditions of applicability related to methods using the modified FastIAS.

The analytical results obtained for the ideal model with isotherms based on the IAST or mass action-based AIE / CIE formalisms aim to meet the following requirements. First, validation of the simulation results provided by the numerical solution strategy applied to the ideal model in case of Riemann initial and boundary conditions. Second, properties of the Jacobian derived from the sorption equilibrium can be related to the differential index of the numerical approach in closed form, thus allowing to state sufficient conditions for the differential index to be equal to one a priori.

Further, the analytical results obtained for the ideal model with SMA isotherm used in the AIE formalism aim to meet the following additional requirements. First, success of a rigorous application of the MOC is known a priori based on analytically obtained eigenvalue and eigenvector representations of the sorption Jacobian. If strict hyperbolicity is concluded, these analytical results facilitate the MOC application since eigenvalues and eigenvectors are not required to be calculated numerically. Second, obtaining additional analytical results regarding topological properties of the concentration phase space with special emphasis on selectivity reversals that allow for a comparison with classical results. Therefore, the effect of variable solution normality and steric hindrance can be evaluated rigorously.

Finally, analytical results of idealized SMB processes using the mass action-based CIE formalism aim to extend the triangle theory to ion exchange processes.

Major results of this thesis as stated above were published* in advance in the following five articles:

- i) M. Fechtner, A. Kienle, *Efficient simulation and equilibrium theory for adsorption processes with implicit adsorption isotherms – mass action equilibria*, Chem. Eng. Sci. 171 (2017) 471–480.
- ii) M. Fechtner, A. Kienle, *Efficient simulation and equilibrium theory for adsorption processes with implicit adsorption isotherms – ideal adsorbed solution theory*, Chem. Eng. Sci. 177 (2018) 284–292.
- iii) M. Fechtner, M. Kasperit, A. Kienle, *Efficient simulation of ion exchange chromatography with application to bioseparations*, Computer Aided Chem. Eng. 43 (2018) 295–300.

*All five articles were published by Elsevier[®]. Articles from Elsevier[®] are allowed to be included in full or in part in a dissertation for non-commercial purposes. (<https://www.elsevier.com/about/policies/copyright/permissions>)

- iv) M. Fechtner, A. Kienle, *Equilibrium theory of ion exchange chromatography with variable solution normality and steric hindrance*, Chem. Eng. Sci. 199 (2019) 508–527.
- v) M. Fechtner, A. Kienle, *Rational design of ion exchange simulated moving bed processes*, Computer Aided Chem. Eng. 48 (2020), 733-738.

1.4 Outline

This thesis consists of seven chapters. The other six chapters cover the following content.

The second chapter introduces the relevant mathematical models and tools for their analysis. In particular, dynamical models with focus on equilibrium models and sorption isotherm models resulting from the IAST, CIE, and AIE formalism are explained in detail. Subsequently, the framework of the MOC is presented for hyperbolic systems. Finally, established numerical methods and standard discretization schemes are described.

In Chapter 3, the IAST in conjunction with equilibrium models is considered. Focus is on developing a numerical solution strategy for any implicit sorption isotherm, thus including the IAST. As a result, a numerical approach that allows for simultaneous solution of the DAE system, which results from discretization of the corresponding PDAE system, is presented. Particular focus is on the differential index of the DAE system. This index is shown to be equal to one if the Jacobian derived from the IAST-based isotherms has non-negative eigenvalues. A specific application example is used to benchmark the developed strategy against various numerical methods including the modified FastIAS, thus demonstrating its efficiency. Another application example shows that the solution strategy is applicable to any implicit SCI.

Chapter 4 covers the application of the numerical solution strategy to ion exchange applications described by the mass action-based CIE formalism and the ideal model. In addition, a complete picture of the equilibrium theory using the CIE formalism is presented. Numerous application examples using Riemann conditions are simulated. These results were validated by analytical results of the MOC. Particular focus was on selectivity reversals and their effect on process operation by analyzing full chromatographic cycles with boundary conditions in regions of different selectivity, wave interactions, and separability of target components. Additional phenomena resulting from multiple selectivity reversals are also presented. In case of the CIE formalism, the differential index of the numerical solution strategy is shown to be always equal to one based on spectral properties of the Jacobian derived from the mass action law.

Main focus in Chapter 5 is on analytical results regarding the ideal model using the SMA-based AIE formalism. Similar to the previous chapter, a complete picture of the equilibrium theory using now the SMA isotherm is presented. In addition, extended analytical results regarding selectivity reversals are compared

to classical results. New analytical results of the equilibrium theory and selectivity reversals are highlighted. These results are shown to predict the qualitative effects of a variable solution normality, which can affect the number and types of reversals, and the quantitative effect of steric factors, which shifts and scales the relevant domain in the concentration phase space. The effects of variable solution normality and steric factors are also thoroughly discussed and presented in three suitable case studies considering each AIE key feature separately and finally both key features jointly. The extension of the numerical solution strategy from CIE to AIE is straight forward and validated by comparing analytical and numerical solutions in all three case studies.

In Chapter 6, the extension of the triangle theory to ion exchange SMB processes is presented. In particular, the equations required to obtain the region of complete separation for ion exchange SMB processes are presented in closed form. The solution normality is shown to affect the region of complete separation significantly, hence it can be potentially used as additional design parameter. Similar to the previous chapter, the extension of the numerical solution strategy to SMB processes is straight forward and validated by using parameters close to semi-analytically obtained region of complete separation for a large number of related true moving bed (TMB) simulations and evaluating their separation efficiency.

The final chapter presents a summary of all results related to the analytical and the numerical approach is presented. An outlook to interesting future challenges regarding further extensions of ion exchange models is given. Special emphasis there is on a possible extension for variable pH. For this particular challenge, an extension of the AIE formalism is outlined.

The Appendix is mostly a collection of technical but essential (and for the most part new) proofs. For an improved understanding of the key ideas and messages, these proofs have been separated from the regular chapters. The last two appendices cover a non-strictly hyperbolic case and global properties of the AIE formalism with SMA isotherm, respectively. The last two appendices present entirely unpublished content. The second last appendix is concerned with the analytical investigation of a non-strictly hyperbolic case, where more than two selectivities coincide. The last Appendix presents a number of analytical results regarding global properties of the SMA-based AIE formalism including the boundary of relevant domains, which are here closed subsets in the concentration phase space.

Chapter 2

Theoretical Background

This chapter is concerned with the presentation of relevant mathematical models for packed column processes in liquid chromatography. In particular, the dynamic behavior of fixed-bed column sorption processes is shown to be mathematically described by partial differential equations (PDEs) that depend crucially on the sorption isotherm model. For a certain class of models, namely the ideal model, a well-known semi-analytical solution approach for so-called Riemann problems is described. It is based on the methods of characteristics (MOC) and is also referred to as equilibrium theory. Finally, well-established numerical solution methods for this relevant class of models are presented.

2.1 Model Equations

The required mathematical complexity of a chromatographic model depends on the number of significant process properties and their physio-chemical complexity. This leads to a large variety of models that can be used to describe the dynamics of different sorption-based packed column processes. A comprehensive summary of models can be found in [13]. In this thesis, main focus is on processes using a single tubular packed-bed column of length L and with a cross-sectional area A_c as shown in Fig. 2.1. This particular single-column process model is based on the following assumptions. The fluid is used as mobile phase by injecting it into the column with a feed concentration $\mathbf{c}_{\text{feed}}(t^*)$ of target components potentially varying with time t^* and a constant volumetric flow rate \dot{V} . The direction of the fluid flow along the column defines the direction of the spatial coordinate z^* . In the column, the fluid contains target components with concentration \mathbf{c} . Any effects that lead to radial gradients of \mathbf{c} are neglected, thus a spatially one dimensional process is considered. Moreover, no chemical reactions take place in the fluid phase. Based on a sorption mechanism between target components and solid phase, there is a mass transfer of target components from the fluid to the solid phase, which is assumed to be small compared to the convective transport in the fluid phase so that a constant interstitial velocity $u = \frac{\dot{V}}{\epsilon A_c}$ can be assumed. Effects that cause significant mass

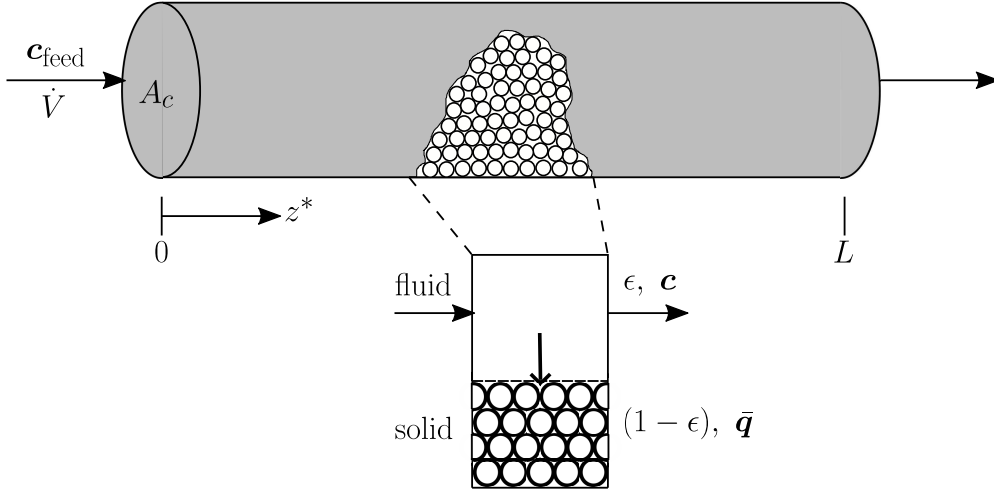


Figure 2.1: Single column chromatographic process that can be mathematically represented by a linear driving force model.

transfer resistance are assumed to be exclusively present in the solid phase. The concentration of target components sorbed to the solid phase is denoted by $\bar{\mathbf{q}}$. The solid phase itself consists of porous particles with total porosity ϵ , which accounts for the inter- and intraparticle volume. Note, a radial concentration distribution inside the particles is not considered. Porous particles are rigid, uniform in size, and uniformly packed. Consequently, the total bed porosity ϵ is constant. Further, the solid phase is assumed to be inert without chemical instabilities and degradation. Hence, there are no chemical reactions in the solid phase. Finally, the process is assumed to be operated isothermal. Consequently, energy balances can be omitted. With these assumptions the mathematical model of chromatographic column shown in Fig. 2.1 follows from the material balances of the solutes in the fluid and the solid phase according to

$$\epsilon \frac{\partial \mathbf{c}}{\partial t^*} + (1 - \epsilon) \frac{\partial \bar{\mathbf{q}}}{\partial t^*} + \epsilon u \frac{\partial \mathbf{c}}{\partial z^*} = \epsilon \mathbf{D}_a \frac{\partial^2 \mathbf{c}}{\partial (z^*)^2}, \quad \mathbf{c}, \bar{\mathbf{q}} \in \mathbb{R}^N, \quad (2.1a)$$

$$\frac{\partial \bar{\mathbf{q}}}{\partial t^*} = \frac{\bar{\mathbf{K}}}{1 - \epsilon} (\mathbf{q} - \bar{\mathbf{q}}), \quad \mathbf{q} \in \mathbb{R}^N. \quad (2.1b)$$

In this particular model the finite mass transfer is modeled using a linear driving force based on the difference of actual solid phase concentration $\bar{\mathbf{q}}$ and its equilibrium value \mathbf{q} , which can be determined from the thermodynamic equilibrium relation for given fluid phase concentration \mathbf{c} . Matrix $\bar{\mathbf{K}}$ contains the finite mass transfer coefficients that lump together the contributions of pore internal and external mass transfer resistance. Further, matrix $\mathbf{D}_a = \text{diag}(D_{a,1} \dots D_{a,N}) \in \mathbb{R}^{N \times N}$ is a constant diagonal matrix, where all entries $D_{a,i}$ on the diagonal are lumped parameters accounting for all dispersion effects that cause band broadening.

Model (2.1) is simplified by assuming infinite large mass transfer coefficients in $\bar{\mathbf{K}}$, which implies the equality $\bar{\mathbf{q}} = \mathbf{q}$, i.e. fluid and solid phase are immediately in a state of thermodynamic equilibrium. Due to the isothermal operation of the column, the equilibrium relation is described by a so-called sorption isotherm $\mathbf{q} = \mathbf{q}(\mathbf{c})$. As a result, we obtain the simpler equilibrium dispersive model

$$\frac{\partial \mathbf{c}}{\partial t^*} + F \frac{\partial \mathbf{q}(\mathbf{c})}{\partial t^*} + u \frac{\partial \mathbf{c}}{\partial z^*} = \mathbf{D}_a \frac{\partial^2 \mathbf{c}}{\partial (z^*)^2}, \quad \mathbf{c}, \mathbf{q} \in R^N. \quad (2.2)$$

Scalar $F = \frac{1-\epsilon}{\epsilon}$ denotes the phase ratio, which depends on the total porosity ϵ . The value of parameter F describes the ratio of the volume occupied by the solid phase with respect to the volume occupied by the fluid phase. Eq. (2.2) is a PDE system of first order in time coordinate t^* and of second order in spatial coordinate z^* . In order to solve Eq. (2.2), N initial and $2N$ boundary conditions are required.

If, in addition to the previous model assumptions also dispersion can be neglected, Eq. (2.2) can be further simplified to the ideal model

$$\frac{\partial \mathbf{c}}{\partial t^*} + F \frac{\partial \mathbf{q}(\mathbf{c})}{\partial t^*} + u \frac{\partial \mathbf{c}}{\partial z^*} = \mathbf{0}, \quad \mathbf{c}, \mathbf{q} \in R^N. \quad (2.3)$$

Eq. (2.3) is a system of N first-order PDEs in t^* and z^* requiring N initial and N boundary conditions. They are obtained from the initial loading of the column $\mathbf{c}(0, z^*) = \mathbf{c}_{\text{init}}$ and the feed values at the column inlet $\mathbf{c}(t^*, 0) = \mathbf{c}_{\text{feed}}$.

Main focus in this work is on the ideal model. Considering the numerous assumptions required for this model, its main purpose is the qualitative description of chromatographic processes, particularly in case of more complex chromatographic processes such as protein separation. In this case, size-related effects of large proteins, such as steric shielding [52, 29] and increased mass transfer resistance [5], are significant. Steric effects can be included directly in the sorption isotherm [29], which is included also in the ideal model. Thus, steric effects on sorption dynamics can be analyzed using Eq. (2.3). Since mass transfer resistance is neglected, quantitative predictions of the ideal model are likely to deviate from experimental data more significantly. For a quantitatively more accurate prediction, models that also account for mass transfer resistance, such as Eq. (2.1), are required. In contrast, if the separation involves only small molecules, the ideal model can be used for qualitative analysis as well as quantitatively more accurate predictions.

In this work, exclusively smooth isotherms $\mathbf{q}(\mathbf{c})$ are considered. The implied differentiability allows to rewrite Eq. (2.3) into the equivalent formulation

$$\frac{1}{u} \left(\mathbf{I}_N + F \frac{\partial \mathbf{q}}{\partial \mathbf{c}} \right) \frac{\partial \mathbf{c}}{\partial t^*} + \frac{\partial \mathbf{c}}{\partial z^*} = \mathbf{0}, \quad (2.4a)$$

$$\frac{\partial \tilde{\mathcal{F}}(\mathbf{c})}{\partial \mathbf{c}} \frac{\partial \mathbf{c}}{\partial t^*} + \frac{\partial \mathbf{c}}{\partial z^*} = \mathbf{0}, \quad (2.4b)$$

where $\mathbf{I}_N \in \mathbb{R}^{N \times N}$ is the identity matrix and $\tilde{\mathcal{F}}(\mathbf{c})$ denotes the vector-valued capacity function. This function is explicitly given by

$$\tilde{\mathcal{F}}(\mathbf{c}) = \frac{1}{u} (\mathbf{c} + F\mathbf{q}(\mathbf{c})). \quad (2.5)$$

Eq. (2.4) defines a system of N first-order quasi-linear PDEs. Alternatively, Eq. (2.4) can further be rewritten into

$$\frac{\partial \mathbf{c}}{\partial t^*} + u \left(\mathbf{I}_N + F \frac{\partial \mathbf{q}}{\partial \mathbf{c}} \right)^{-1} \frac{\partial \mathbf{c}}{\partial z^*} = \mathbf{0}, \quad (2.6a)$$

$$\frac{\partial \mathbf{c}}{\partial t^*} + \frac{\partial \mathcal{F}(\mathbf{c})}{\partial \mathbf{c}} \frac{\partial \mathbf{c}}{\partial z^*} = \mathbf{0}, \quad (2.6b)$$

where $\mathcal{F}(\mathbf{c})$ denotes the vector-valued flux of the PDE (2.6) that is only implicitly given by

$$\frac{\partial \mathcal{F}(\mathbf{c})}{\partial \mathbf{c}} = u \left(\mathbf{I}_N + F \frac{\partial \mathbf{q}}{\partial \mathbf{c}} \right)^{-1}. \quad (2.7)$$

Eq. (2.6b) represents the standard representation of quasi-linear conservation laws [16]. Hyperbolicity of the conservation law implies diagonalizability of matrix $u \left(\mathbf{I}_N + F \frac{\partial \mathbf{q}}{\partial \mathbf{c}} \right)$ [15]. Hence, existence of the matrix $u \left(\mathbf{I}_N + F \frac{\partial \mathbf{q}}{\partial \mathbf{c}} \right)^{-1}$ is guaranteed. For both conservation laws (2.4,2.6) the method of characteristics (MOC) can be applied to obtain semi-analytical solutions for so-called Riemann problems [14, 15], which are defined in the subsequent subsection. Application of the MOC to the ideal model is also referred to as equilibrium theory in context of equilibrium driven chromatographic processes.

The importance of the sorption isotherm $\mathbf{q}(\mathbf{c})$ is evident since it introduces the essential non-linearity to all models discussed so far. Semi-analytical solutions of the equilibrium theory allow for a preliminary, qualitative analysis of the chromatographic process revealing equilibrium-related key features without requiring numerous simulations or experiments. Results of this analytical approach enable a conceptual design, which can serve as an 'educated' starting point for further experimental and / or numerical process optimization. Moreover, efficient numerical solution methods that were successfully applied to the ideal model (2.3) can be usually extended to a larger class of models with additional differential operators in space, such as Eq. (2.2), in a straight forward manner by approximation through spatial discretization, which greatly increases the range of application for these methods.

In order to solve the ideal model (2.3), specific knowledge of the sorption isotherm $\mathbf{q}(\mathbf{c})$ is necessary. In this work, focus is on implicit isotherms. In particular, results will be obtained for two widely used implicit sorption isotherms, namely the ideal adsorbed solution theory (IAST) [17, 25, 24] and the stoichiometric ion exchange. The latter is described by the mass action law in classical

ion exchange (CIE) [27, 28] or by the steric mass action law (SMA) in advanced ion exchange (AIE) [29, 52].

First, essential equations and assumptions of the IAST are presented. Originally, this theory was developed for gas adsorption [17, 24]. Later, the IAST was extended to address also dilute liquid solutions [25]. The limitation to dilute solutions is required to predict multi-component behavior based on single component data, which obviously cannot account for interactions between the components in the fluid phase. Two phases are said to be in equilibrium if pressure, temperature, and chemical potential of every component is equal in both phases [59]. The IAST assumes an isobaric and isothermal operated adsorption process, thus the equilibrium condition can be formulated in terms of chemical potentials

$$\mu_i^c = \mu_i^q, \quad i = 1, \dots, N. \quad (2.8)$$

Here, μ_i^c and μ_i^q denote the chemical potentials of component i in the fluid and solid phase, respectively. For a dilute solution, μ_i^c is defined by [25]

$$\mu_i^c = \mu_i^* + \mathcal{R}\mathcal{T} \ln \left(\frac{c_i}{c_i^*} \right), \quad (2.9)$$

where μ_i^* and c_i^* denote reference state values for the chemical potential and corresponding fluid phase concentration, respectively, \mathcal{R} is the universal gas constant, \mathcal{T} is the equilibrium temperature, and c_i the fluid phase concentration of component i at equilibrium. An ideal adsorption is assumed, which neglects any surface heterogeneities of the solid phase. In this case μ_i^q is given by [17]

$$\mu_i^q = \mu_i^* + \mathcal{R}\mathcal{T} \ln \left(\frac{c_i^0(\pi, \mathcal{T})}{c_i^*} \right) + \mathcal{R}\mathcal{T} \ln(\chi_i). \quad (2.10)$$

Scalar χ_i is the molar fraction of component i in the solid phase at equilibrium, and c_i^0 is the so-called hypothetical fluid phase concentration of component i at equilibrium. The latter depends on equilibrium temperature \mathcal{T} and spreading pressure π at equilibrium. The fluid film that is in contact with the solid phase admits a certain surface tension, which is affected by adsorption. The difference in surface tension before and after adsorption is called spreading pressure. Eqs. (2.9) and (2.10) substituted into Eq. (2.8) results in

$$c_i = c_i^0(\pi, \mathcal{T})\chi_i, \quad i = 1, \dots, N, \quad (2.11)$$

which can be interpreted as an analogon to Raoult's law for adsorption [59]. A closure condition at equilibrium is defined by the sum of molar fractions in the solid phase

$$\sum_{i=1}^N \chi_i = \sum_{i=1}^N \frac{c_i}{c_i^0} = 1. \quad (2.12)$$

It relates actual and hypothetical fluid phase concentrations. In equilibrium, the multi-component mixture admits a specific surface potential π for given concentrations \mathbf{c} and temperature \mathcal{T} . The value of c_i^0 is defined by the requirement that the fluid phase hypothetically contains only component i and admits the same surface potential as the mixture at the same temperature \mathcal{T}

$$\pi_i(c_i^0, \mathcal{T}) = \pi(\mathbf{c}, \mathcal{T}), \quad i = 1, \dots, N. \quad (2.13)$$

As a result there are additional $N - 1$ independent equilibrium equations relating c_i^0 and π at temperature \mathcal{T} . In case of a single component and a constant volume of the solid phase, the Gibbs adsorption isotherm [59] relates the spreading pressure π_i to the chemical potential μ_i^q in the solid phase as follows

$$d\pi_i = \mathcal{A}^{-1} q_i^0 d\mu_i^q, \quad (2.14)$$

where \mathcal{A} denotes the specific surface area of the solid phase. The value of the hypothetical solid phase concentration q_i^0 of component i results from thermodynamic equilibrium of a single component in solid and fluid phase described by a single component isotherm (SCI). Hence, q_i^0 is obtained for given c_i^0 from

$$q_i^0 = q_i^0(c_i^0), \quad i = 1, \dots, N. \quad (2.15)$$

A key advantage of the IAST is that experimental data on SCIs can be easily obtained compared to data on multi-component isotherms [23]. If only a single component i is present, Eqs. (2.8) and (2.9) admit the following relation

$$\mu_i^q = \mu_i^c = \mu_i^* + \mathcal{R}\mathcal{T} \ln \left(\frac{c_i^0}{c_i^*} \right). \quad (2.16)$$

Eq. (2.16) allows to obtain differential $d\mu_i^q$ using the chain rule. The result can be substituted into Eq. (2.14).

$$d\pi_i(c_i^0, \mathcal{T}) = \frac{\mathcal{R}\mathcal{T}}{\mathcal{A}} \frac{q_i^0(c_i^0)}{c_i^0} dc_i^0. \quad (2.17)$$

Integration of Eq. (2.17) relates spreading pressure π_i at equilibrium to the equilibrium value of the hypothetical fluid phase concentration c_i^0 and equilibrium temperature \mathcal{T}

$$\int_{\pi_i(0, \mathcal{T})}^{\pi_i(c_i^0, \mathcal{T})} d\tilde{\pi}_i = \int_0^{c_i^0} \frac{\mathcal{R}\mathcal{T}}{\mathcal{A}} \frac{q_i^0(\sigma)}{\sigma} d\sigma \quad (2.18a)$$

$$\pi_i(c_i^0, \mathcal{T}) = \frac{\mathcal{R}\mathcal{T}}{\mathcal{A}} \int_0^{c_i^0} \frac{q_i^0(\sigma)}{\sigma} d\sigma. \quad (2.18b)$$

Substitution of Eq. (2.18b) into Eq. (2.13) and canceling factors $\frac{\mathcal{R}\mathcal{T}}{\mathcal{A}}$ results in $N - 1$ reformulated equilibrium relations

$$\int_0^{c_i^0} \frac{q_i^0(\sigma)}{\sigma} d\sigma = \int_0^{c_N^0} \frac{q_N^0(\sigma)}{\sigma} d\sigma, \quad i = 1, \dots, N - 1, \quad (2.19)$$

involving only hypothetical fluid concentrations c_i^0 . Finally, an ideal adsorbed solution satisfies the Lewis relationship [26]

$$\sum_{i=1}^N \frac{q_i}{q_i^0} = 1. \quad (2.20)$$

Division by q_{tot} and using the definition of mole fractions in the solid phase

$$q_i = q_{\text{tot}} \chi_i \quad (2.21)$$

leads to

$$\frac{1}{q_{\text{tot}}} = \sum_{i=1}^N \frac{q_i}{q_{\text{tot}}} \frac{1}{q_i^0} = \sum_{i=1}^N \frac{\chi_i}{q_i^0}, \quad (2.22)$$

which can be further rewritten using Eq. (2.11)

$$q_{\text{tot}} = \left(\sum_{i=1}^N \frac{1}{q_i^0} \frac{c_i}{c_i^0} \right)^{-1}. \quad (2.23)$$

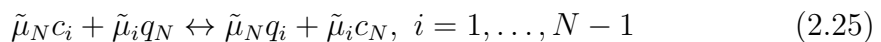
As a result, the solid phase concentrations q_i can be explicitly represented as adsorption isotherm functions of the fluid and hypothetical fluid phase concentrations by substituting Eqs. (2.11) and (2.23) into (2.21)

$$q_i(\mathbf{c}, \mathbf{c}^0) = \left(\sum_{i=1}^N \frac{1}{q_i^0(c_i^0)} \frac{c_i}{c_i^0} \right)^{-1} \frac{c_i}{c_i^0}, \quad i = 1, \dots, N. \quad (2.24)$$

The IAST has $3N$ unknown variables. The vector \mathbf{c}^0 with N entries is obtained implicitly from equilibrium relations (2.12) and (2.19). For all N entries of \mathbf{q}^0 there exists usually an explicit SCI (2.15). The remaining N entries of vector \mathbf{q} can be determined from Eq. (2.24) for given \mathbf{c} . Consequently, the IAST represents a set of $3N$ implicit equations. Note, in case of implicit SCI's the explicit equations in (2.15) are replaced by N implicit equations that are solved numerically for \mathbf{q}^0 .

A second important class of chromatographic processes to be considered in this thesis are ion exchange processes. We distinguish between the classical ion exchange (CIE) and advanced ion exchange (AIE). The former is used for processes involving exclusively smaller ions. Typical examples are sea water purification, which involves salt ions, and the separation of rare earths [28]. In contrast, AIE allows to consider large charged molecules like amino acids and especially proteins, which are the most important target components in bioseparations that are required for applications in biotechnology and microbiology [52, 60].

In CIE, the exchange of N ions can be modeled as a system of $N - 1$ reversible reactions



in chemical equilibrium also known as stoichiometric ion exchange. There are $N - 1$ target components i with fluid phase concentration c_i and solid phase concentration q_i . Component N is a suitable reference component, usually the counter-ions provided the solid phase. Likewise, c_N denotes the fluid and q_N the solid phase concentration of the counter-ions. Parameter $\tilde{\mu}_i$ is the charge of ion i . An alternative formulation of (2.25) can be obtained by multiplying it with $\frac{1}{\tilde{\mu}_i\tilde{\mu}_N}$

$$\frac{1}{\tilde{\mu}_i}c_i + \frac{1}{\tilde{\mu}_N}q_N \leftrightarrow \frac{1}{\tilde{\mu}_i}q_i + \frac{1}{\tilde{\mu}_N}c_N, \quad i = 1, \dots, N - 1, \quad (2.26a)$$

$$\mu_i c_i + \mu_N q_N \leftrightarrow \mu_i q_i + \mu_N c_N, \quad i = 1, \dots, N - 1 \quad (2.26b)$$

with μ_i denoting the reciprocal of the charge of component i . Assuming an isobar, isotherm process involving ideal fluid and solid phases, the mass action law [18] corresponding to Eq. (2.26b) reads

$$K_{iN} = \left(\frac{q_i}{c_i}\right)^{\mu_i} \left(\frac{c_N}{q_N}\right)^{\mu_N}, \quad i = 1, \dots, N - 1. \quad (2.27)$$

Eq. (2.27) states $N - 1$ equilibrium relations involving all fluid and solid phase concentrations. Parameters K_{iN} are binary equilibrium constants. Hence, any aggregation effects and interactions between sorbing components are not accounted for. Electroneutrality demands

$$q_{\text{tot}} = \sum_{i=1}^N \frac{q_i}{\mu_i} \quad (2.28)$$

for a fixed exchanger capacity q_{tot} . An additional restriction in CIE results from the assumption of a constant solution normality c_{tot} with

$$c_{\text{tot}} = \sum_{i=1}^N \frac{c_i}{\mu_i}. \quad (2.29)$$

Eq. (2.29) allows in conjunction with Eq. (2.28) to define normalized concentration variables

$$x_i = \frac{c_i}{\mu_i c_{\text{tot}}}, \quad i = 1, \dots, N - 1, \quad (2.30a)$$

$$y_i = \frac{q_i}{\mu_i q_{\text{tot}}}, \quad i = 1, \dots, N - 1, \quad (2.30b)$$

and therefore to obtain two corresponding closing conditions

$$\sum_{i=1}^N x_i = 1, \quad (2.31a)$$

$$\sum_{i=1}^N y_i = 1, \quad (2.31b)$$

and adjusted equilibrium relations

$$\tilde{K}_{iN} = \left(\frac{y_i}{x_i} \right)^{\mu_i} \left(\frac{x_N}{y_N} \right)^{\mu_N}, \quad i = 1, \dots, N-1, \quad (2.32a)$$

$$\tilde{K}_{iN} = K_{iN} \left(\frac{q_{\text{tot}}}{c_{\text{tot}}} \right)^{\mu_N - \mu_i}, \quad i = 1, \dots, N-1. \quad (2.32b)$$

Parameters \tilde{K}_{iN} are adjusted equilibrium constants. Both Eqs. (2.31a,2.31b) are used to explicitly represent some arbitrary reference component, e.g. component N . Thus the number of independent variables x_i and unknown variables y_i in Eq. (2.27) is reduced by one. Consequently, it is sufficient to solve (2.27) implicitly to obtain a vector $\mathbf{y}_{N-1} \in \mathbb{R}^{N-1}$ for a given vector $\mathbf{x}_{N-1} \in \mathbb{R}^{N-1}$.

The AIE is an extension of the CIE to account for important conditions in bioseparations [5]. In particular, the $N-1$ target components are usually macromolecules. Each target component $i < N$ has a characteristic charge (binding charge, effective charge) $\tilde{\nu}_i$. Since component N is usually a small ion, the characteristic charge $\tilde{\nu}_N$ coincides with the ionic charge $\tilde{\mu}_N$. The characteristic charge of component $i < N$ results from its dissociation into (poly-)ion i and (a) corresponding co-ion(s), and it is a constant, empirical parameter that is able to reflect the multi-pointed nature of the binding of larger molecules like proteins but without accounting for any variations in pH [52]. Hence, the characteristic charge allows to describe the equilibrium based on an extended mass action law similar to Eq. (2.27)

$$K_{iN} = \left(\frac{q_i}{c_i} \right)^{\nu_i} \left(\frac{c_N}{q_N} \right)^{\nu_N}, \quad i = 1, \dots, N-1, \quad (2.33)$$

where ν_i denotes the reciprocal of the characteristic charge of component i . Similar to the CIE, the $N-1$ equilibrium relations in Eq. (2.33) are completed by an N th equilibrium condition based on a closing condition for the fixed exchanger capacity q_{tot} , which is derived in the following. Large molecules can cause a steric hindrance, i.e. upon binding to the solid phase macromolecules shield some of the counter-ions on the solid phase from entering the fluid phase. These counter-ions are no longer available for the sorption process. This shielding is accounted for by a steric factor p_i that allows to determine the total concentration of counter-ions in the solid phase $q_{N,\text{tot}}$ with

$$q_{N,\text{tot}} = q_N + \sum_{i=1}^{N-1} p_i q_i = q_N + \sum_{i=1}^N p_i q_i, \quad (2.34)$$

where obviously $p_N = 0$ holds since ions related to small molecules do not have any steric effects. Note, variable q_N denotes the concentration of the counter-ions that are available for the interaction with macromolecules, which is consistent with the formulation in Eq.(2.33). Further, if the solid and fluid phase initially satisfy

electroneutrality and if the feed remains electroneutral, then the electroneutrality condition of the solid phase

$$q_{\text{tot}} = \frac{1}{\nu_N} q_N + \sum_{i=1}^{N-1} \left(\frac{1}{\nu_i} + p_i \right) q_i = \sum_{i=1}^N \xi_i q_i \quad (2.35)$$

based on a constant exchanger capacity q_{tot} , guarantees also the electroneutrality of the fluid phase. In contrast to the CIE restricted by Eq. (2.29), there is no such restriction for the AIE. Therefore, the solution normality c_{tot} can be variable, which is very important for many bioseparations that use salt gradients [31]. Eqs. (2.33) and (2.35) define the isotherm used in this work for AIE processes, and it is referred to as steric mass action law (SMA) [29]. As a final remark, the effect of co-ions is neglected [52]. The key aspect of this assumption is based on the fact that macro-molecules are considered to behave like neutral salts. Initially neutral, they dissociate into a so-called poly-ion and free co-ions. The poly-ion consists of the macro-molecule itself without any co-ions, i.e. with a characteristic charge of maximal absolute value, and co-ions that remain associated with it upon binding to the solid phase. Hence, the poly-ion has a characteristic charge with an absolute value smaller or equal to characteristic charge of the macro-molecule, thus accounting for the co-ions that remain in a certain neighborhood of the macro-molecule even after interaction with the solid phase. The free co-ions remain thermodynamically unchanged during the sorption process and therefore cancel out of the equilibrium relation [61]. It should be noted that the number of co-ions remaining close to the macro-molecule, which affects the value of the characteristic charge, depends on the local pH value. Consequently, the assumption of a constant pH is crucial for the applicability of the SMA. The SMA admits N algebraic equations (2.33,2.35) for the N unknown entries in \mathbf{q} . In general, the vector \mathbf{q} can be obtained from (2.33,2.35) for given \mathbf{c} only implicitly.

2.2 Equilibrium Theory

As described in the previous section, conservation laws in chromatography depend crucially on the thermodynamic equilibrium between the fluid and solid phase, which led to the expression of equilibrium theory for the analytical approach based on the method of characteristics (MOC). In particular, equilibrium theory is the application of the MOC to first-order hyperbolic conservation laws [15]. In this thesis focus is on so-called chromatographic cycles, which are of great importance in chromatography since they provide insight into the behavior of the of chromatographic processes [10]. In mathematical terms, these cycles define Riemann problems, i.e. a system of PDEs is solved in conjunction with piece-wise constant initial and boundary conditions. Application of the MOC provides analytical solutions for these type of problems [15]. As a result, first-order PDE systems (2.4,2.6) with piece-wise constant initial and boundary conditions can be

solved analytically in case of hyperbolicity [16, 62]. Without loss of generality, the equilibrium theory formalism is explained using representation (2.6) in standard conservation law formulation. PDE system (2.6) is said to be hyperbolic if matrix

$$\mathbf{B} = u \left(\mathbf{I}_N + F \frac{\partial \mathbf{q}}{\partial \mathbf{c}} \right)^{-1} \in \mathbb{R}^{N \times N} \quad (2.36)$$

has N linearly independent eigenvectors \mathbf{r}_k . If in addition all eigenvalues $\tilde{\lambda}_k$ of \mathbf{B} are real and distinct, the MOC can be applied in a straight forward manner for Riemann problems [16]. Additional difficulties of the application of the MOC may arise in case of non-strict hyperbolicity, which includes points where eigenvalues $\tilde{\lambda}_k$ have an algebraic multiplicity larger than one and a geometric multiplicity equal to one. Evaluating the effect of these so-called umbilic points [63] on Riemann problems and their solutions based on the MOC requires further investigation of the specific conservation law. PDE system (2.6) is assumed to be strictly hyperbolic if not stated otherwise. In general, the solution to a Riemann problem consists of $N + 1$ states connected by N transitions, where the initial state $C^N = \mathbf{c}_{\text{init}}$ and the final state $C^0 = \mathbf{c}_{\text{feed}}$ are known. The remaining states $C^i = \mathbf{c}_{i,\text{plateau}}$ have to be determined such that the related N transitions are all admissible. Note, the states connected by transitions are specific plateau values and therefore denoted with capital letters. Admissibility of all N transitions can be guaranteed only for sufficiently close C^0 and C^N [64]. Hence, general statements regarding solutions to Riemann problems are only local. However, for specific isotherms in (2.6) solutions admit global properties. This is shown to be the case for the SMA in Appendix I. Aside from hyperbolicity, genuine non-linearity defined by

$$\nabla \tilde{\lambda}_k \mathbf{r}_k \neq 0 \quad (2.37)$$

is an important property. If Eq. (2.37) is satisfied, the solution to Riemann problems is composed of shocks and simple waves only [16, 62]. Shocks are discontinuous solutions whereas simple waves are continuous solutions, which are differentiable almost everywhere [16]. Both types of solutions satisfy the integral formulation of Eqs. (2.6). Hence, they are so-called weak solutions of Eqs. (2.6). Knowing the image of both types of solutions in the concentration phase space of fluid concentrations \mathbf{c} , Riemann solutions can be constructed analytically.

The image of shocks is defined by the Rankine-Hugoniot jump conditions

$$\mathcal{F}(C^k) - \mathcal{F}(C^{k-1}) = \tilde{s}_k (C^k - C^{k-1}), \quad k = 1, \dots, N. \quad (2.38)$$

For fixed C^{k-1} , the set of all C^k that can be connected to C^{k-1} by a shock curve with some constant velocity \tilde{s}_k is determined from Eq. (2.38). Obviously, one parameter families of solutions are obtained [16, 62] since there are $N + 1$ unknowns $C^k \in \mathbb{R}^N$ as well as \tilde{s}_k and only N equations in (2.38). The flux $\mathcal{F}(\mathbf{c})$ cannot be determined in general, see Eq. (2.7). However, utilizing the equivalence of formulations (2.4) and (2.6), the known capacity vector function (2.5) can be

used instead. Note, compared to typically defined conservation laws, the roles of time and space coordinates in Eq. (2.4) are interchanged. As a result the corresponding jump conditions are defined by

$$\tilde{\mathcal{F}}(C^k) - \tilde{\mathcal{F}}(C^{k-1}) = \tilde{s}_k^{-1}(C^k - C^{k-1}), \quad (2.39a)$$

$$\Delta \tilde{\mathcal{F}}_k = \tilde{s}_k^{-1} \Delta C^k, \quad (2.39b)$$

$$\frac{1}{u} (\Delta C^k + F \Delta Q^k) = \tilde{s}_k^{-1} \Delta C^k, \quad (2.39c)$$

$$\frac{1}{u} (\Delta C^{k,i} + F \Delta Q^{k,i}) = \tilde{s}_k^{-1} \Delta C^{k,i}, \quad (2.39d)$$

$$k = 1, \dots, N, \quad i = 1, \dots, N.$$

Using Eqs. (2.39d), the Rankine-Hugoniot jump conditions (2.38) can be readily rewritten into the equivalent form

$$\tilde{s}_k = \frac{u}{1 + F \frac{\Delta q_{k,i}}{\Delta c_{k,i}}} = \frac{u}{1 + F s_k}, \quad k = 1, \dots, N, \quad i = 1, \dots, N. \quad (2.40)$$

Eq. (2.40) has the advantage of connecting the Rankine-Hugoniot jump conditions directly to the known isotherm $\mathbf{q}(\mathbf{c})$.

The image of simple waves, also called integral curve $\tilde{\mathbf{c}}$, connecting two states $C^k = \tilde{\mathbf{c}}_k(1)$ and $C^{k-1} = \tilde{\mathbf{c}}_k(0)$ is defined by

$$\frac{d\tilde{\mathbf{c}}_k(\sigma)}{d\sigma} = \phi(\sigma) \mathbf{r}_k, \quad \phi, \sigma \in \mathbb{R}, \quad \sigma \in [0, 1], \quad k = 1, \dots, N, \quad (2.41)$$

where $\phi(\sigma)$ is some scalar factor and σ is used to parameterize the integral curve. Eq. (2.41) allows to formally obtain a set on $N - 1$ non-trivial coupled ordinary differential equations with respect to some arbitrary reference component, here N

$$\frac{\frac{d\tilde{c}_{k,i}}{d\sigma}}{\frac{d\tilde{c}_{k,N}}{d\sigma}} = \frac{d\tilde{c}_{k,i}}{d\tilde{c}_{k,N}} = \frac{r_{k,i}}{r_{k,N}}, \quad i = 1, \dots, N \quad (2.42)$$

for each integral curve. There are N families of integral curves based on N linearly independent eigenvectors, which are implied by the assumption of strict hyperbolicity. Integral curves require knowledge of the (right) eigenvectors \mathbf{r}_k of matrix \mathbf{B} . However, the Jacobian $\frac{\partial \mathbf{q}}{\partial \mathbf{c}}$ has the same eigenvectors

$$\mathbf{R} = [\mathbf{r}_1 \ \mathbf{r}_2 \ \dots \ \mathbf{r}_N], \quad (2.43a)$$

$$\mathbf{R}^{-1} \mathbf{B} \mathbf{R} = \text{diag}(\mathbf{B}), \quad (2.43b)$$

$$\mathbf{R}^{-1} u \left(\mathbf{I}_N + F \frac{\partial \mathbf{q}}{\partial \mathbf{c}} \right)^{-1} \mathbf{R} = u \left(\mathbf{I}_N + F \mathbf{R}^{-1} \frac{\partial \mathbf{q}}{\partial \mathbf{c}} \mathbf{R} \right)^{-1} = \text{diag}(\mathbf{B}), \quad (2.43c)$$

$$\mathbf{R}^{-1} \frac{\partial \mathbf{q}}{\partial \mathbf{c}} \mathbf{R} = \text{diag} \left(\frac{\partial q}{\partial c} \right). \quad (2.43d)$$

Thus, integral curves are directly related to the isotherm $\mathbf{q}(\mathbf{c})$. Similarly, the velocity $\tilde{\lambda}_k$ of a k -simple wave is directly related to the isotherm $\mathbf{q}(\mathbf{c})$ through the eigenvalues λ_k of the Jacobian $\frac{\partial \mathbf{q}}{\partial \mathbf{c}}$. In particular, we obtain from the characteristic polynomial using standard determinant operations

$$\det \left(u \left(\mathbf{I}_N + F \frac{\partial \mathbf{q}}{\partial \mathbf{c}} \right)^{-1} - \tilde{\lambda} \mathbf{I}_N \right) = 0, \quad (2.44a)$$

$$\det \left(u \left(\mathbf{I}_N + F \frac{\partial \mathbf{q}}{\partial \mathbf{c}} \right)^{-1} - \tilde{\lambda} \mathbf{I}_N \right) = \det \left(\left(\mathbf{I}_N + F \frac{\partial \mathbf{q}}{\partial \mathbf{c}} \right) - \frac{u}{\tilde{\lambda}_k} \mathbf{I}_N \right), \quad (2.44b)$$

$$= \det \left(\frac{\partial \mathbf{q}}{\partial \mathbf{c}} - \frac{1}{F} \left(\frac{u}{\tilde{\lambda}_k} - 1 \right) \mathbf{I}_N \right) \quad (2.44c)$$

$$= \det \left(\frac{\partial \mathbf{q}}{\partial \mathbf{c}} - \lambda_k \mathbf{I}_N \right) \quad (2.44d)$$

the following relation

$$\tilde{\lambda}_k = \frac{u}{1 + F \lambda_k}, \quad (2.45)$$

which is similar in structure to Eq. (2.40).

If two states C^k and C^{k-1} lie on the same integral curve, they can be connected by a k -simple wave [62]. However, this transition is only admissible if also the inequality

$$\tilde{\lambda}_k(C^{k-1}) < \tilde{\lambda}_k(C^k) \quad (2.46)$$

holds. Due to genuine non-linearity (2.37), relation

$$\nabla \tilde{\lambda}_k \mathbf{r}_k > 0 \quad (2.47)$$

is satisfied along an integral curve. The relations in Eqs. (2.46) and (2.47) translate due to Eq. (2.45) to the equivalent formulations

$$\lambda_k(C^{k-1}) > \lambda_k(C^k), \quad (2.48a)$$

$$\nabla \lambda_k \mathbf{r}_k < 0. \quad (2.48b)$$

In contrast, if the two states C^k and C^{k-1} lie on the same shock curve, they can be connected by a k -shock. The transition is only admissible if also

$$\tilde{\lambda}_k(C^{k-1}) > \tilde{s}_k > \tilde{\lambda}_k(C^k) \quad (2.49)$$

holds. Eq. (2.49) is also called entropy condition, which was deduced in [64]. Using Eq. (2.40), the relation in Eq. (2.49) translates to

$$\lambda(C^{k-1}) < s_k < \lambda_k(C^k). \quad (2.50)$$

There is another type of transition that is frequently encountered, namely contact discontinuities [16]. The corresponding curves are characterized by their linear degeneracy, i.e.

$$\nabla \tilde{\lambda}_k \mathbf{r}_k = 0, \quad (2.51a)$$

$$\nabla \lambda_k \mathbf{r}_k = 0. \quad (2.51b)$$

Eq. (2.51b) implies a constant eigenvalue λ_k along the corresponding integral curve of family k , and the constant eigenvalue implies a constant velocity of the contact discontinuity. Consequently, the linear degenerate integral curve can be also identified as shock curve [62]. As a result the image of a k -contact discontinuity can be obtained from Eq. (2.38) or (2.41). Admissibility of the transition readily reduces to

$$\tilde{\lambda}_k(C^{k-1}) = \tilde{s}_k = \tilde{\lambda}_k(C^k), \quad (2.52a)$$

$$\lambda_k(C^{k-1}) = s_k = \lambda_k(C^k). \quad (2.52b)$$

In addition to these three fundamental types of transitions presented above more complex transitions are possible. If $\nabla \lambda_k \mathbf{r}_k = 0$ holds for isolated points such as inflection points in single-component systems [14], combined transition of simple waves and shocks occur. However, these combined transitions between two plateau values, where also Eqs. (2.48a) and (2.50) hold on parts of the transition, are not considered in this work.

A classical isotherm for which Riemann solutions as a sequence of shocks and simple waves can be constructed easily is the Langmuir isotherm. Shock curves and integral curves coincide since they are both straight lines that are required to be tangent in the initial state of each transition [64]. Hence, a single grid of shock and integral curves exists in the concentration phase space. This linear grid allows to construct Riemann solutions more easily. It can be orthogonalized by a change of coordinates further facilitating the construction of Riemann solutions [28, 15]. However, isotherms generally lead to a system of PDEs (2.4,2.6) where the shock and integral curves are neither straight lines nor do they coincide. In this case only the grid composed of integral curves is independent of operating conditions, i.e. initial and boundary conditions. In contrast, shock curves and intermediate plateaus depend on the initial and feed plateaus. Hence, the grid of shock curves is not known apriori, which increases the difficulty of constructing analytically Riemann solutions. However, the grid of integral curves is not only helpful to gain insight into simple wave transitions but also into shock transitions. This is certainly the case if integral curves vary only slightly from straight lines and almost coincide with shock curves. Even if corresponding integral and shock curves vary significantly, they have the same tangent in the initial state of the transition and the same curvature [64]. Therefore, the grid of integral curves can be used to gain qualitative knowledge of general Riemann problems. In context of chromatographic cycles, the grid of integral curves allows at least to gain qual-

itative knowledge regarding key features that are related to the given sorption isotherm.

2.3 Numerical Solution Methods

In this section, focus is again on the ideal model Eq. (2.3). Three numerical solution methods are relevant for this work, namely full discretization method (FDM), method of lines (MOL), and Method of Rothe (MOR) [36]. The first method requires discretization of both, time and space coordinate. The resulting system of algebraic equations can be rewritten more compactly into a matrix-vector representation. However, implementation, particularly of initial and boundary conditions can be more challenging compared to the other two methods. In contrast, the MOL and MOR require only one of the two coordinates to be discretized. For chromatographic models, only MOL is frequently used due to the straight forward application independent of spatial operators present in the PDEs, which is not the case for the MOR. If only one coordinate is discretized in Eq. (2.3), the resulting system of ordinary differential equations (ODEs) can then be solved using standard ODE solvers. For many applications, in particular in liquid chromatography, the implementation is very simple [65]. The solver uses some internal numerical discretization scheme for the other coordinate, thus providing variable order, variable step size, and error control of the internal scheme. Also the ODE systems allows for a compact matrix-vector representation. Furthermore, both methods allow for an efficient incorporation of additional algebraic equations. All three numerical solution methods can utilize a large variety of different discretization schemes. In chromatography widely used schemes are the finite differences (FD), finite elements (FE), and finite volumes (FV) [13, 11]. The choice of the specific discretization scheme depends on the properties that should be retained by the approximated solution, e.g. mass conservation, energy conservation, or characteristic curves [16]. For a proof of principle, first-order FD schemes are used in this thesis. Application of more elaborate schemes such as higher order schemes [16], orthogonal collocation [66, 67], or FV-schemes in conjunction with adaptive grids [37] is straight forward.

We distinguish between two cases. First, the sorption isotherm is assumed to be explicitly available $\mathbf{q} = \mathbf{f}(\mathbf{c})$. Typical examples of explicit isotherms are the linear and Langmuir isotherm [11]. In these cases, the Jacobian $\mathbf{J}(\mathbf{c}) = \frac{\partial \mathbf{q}}{\partial \mathbf{c}}$ can be easily obtained and representation (2.4a) of the ideal model is immediately available. In chromatography, forward differences in time and backward differences in space are usually applied in FDM [68, 13]. Denoting the number of grid points in space by N_z and the number of grid points in time by N_t , overall NN_zN_t algebraic

equations

$$(\mathbf{I}_N + F\mathbf{J}(\mathbf{c})) \frac{\mathbf{c}_j^{n+1} - \mathbf{c}_j^n}{\Delta t^*} + u \frac{\mathbf{c}_j^n - \mathbf{c}_{j-1}^n}{\Delta z^*} = \mathbf{0}, \quad (2.53)$$

$$n = 1, \dots, N_t, \quad j = 1, \dots, N_z$$

have to be solved. A necessary condition for the stability of the FD scheme in Eq. (2.53) is the so-called CFL-condition $u \frac{\Delta t^*}{\Delta z^*} < 1$ [13]. Applying the MOL or MOR to Eq. (2.4a) requires to solve NN_z or NN_t ODEs

$$(\mathbf{I}_N + F\mathbf{J}(\mathbf{c})) \frac{d\mathbf{c}}{dt^*} + u \frac{\mathbf{c}_j^n - \mathbf{c}_{j-1}^n}{\Delta z^*} = \mathbf{0}, \quad j = 1, \dots, N_z, \quad (2.54a)$$

$$(\mathbf{I}_N + F\mathbf{J}(\mathbf{c})) \frac{\mathbf{c}_j^n - \mathbf{c}_j^{n-1}}{\Delta t^*} + u \frac{d\mathbf{c}}{dz^*} = \mathbf{0}, \quad n = 1, \dots, N_t, \quad (2.54b)$$

respectively. Regarding the discretized coordinate, both methods use backward differences, and stability of the methods depends on the applied ODE solvers. The quantity Δt^* denotes a fixed time step, and Δz^* denotes a fixed space step. Eqs. (2.53) and (2.54) can be solved using standard software like Matlab[®] [69], which provides standard ODE solvers for Eqs. (2.54), such as ODE45 and ODE15s.

Second, the sorption isotherm is assumed to be implicitly available

$$\mathbf{0} = \mathbf{f}(\mathbf{q}, \mathbf{c}). \quad (2.55)$$

Typical examples are IAST-based isotherms and the SMA isotherm (see Section 2.1). In principle, the Jacobian can be obtained for any implicit isotherm using implicit differentiation

$$\mathbf{J}(\mathbf{q}, \mathbf{c}) = \frac{\partial \mathbf{q}}{\partial \mathbf{c}} = - \left(\frac{\partial \mathbf{f}}{\partial \mathbf{q}} \right)_c^{-1} \left(\frac{\partial \mathbf{f}}{\partial \mathbf{c}} \right)_q. \quad (2.56)$$

Eq. (2.56) allows to use again the formulation (2.4a) of the ideal model. However, the Jacobian depends now also on \mathbf{q} . Hence, Eq. (2.55) has to be solved anyway and (2.4a) provides no advantage compared to (2.3). In addition, analytical implicit differentiation may prove difficult, whereas numerical implicit differentiation may impair efficiency or even stability of the numerical solution method. As a result, the FDM can be applied to (2.3) avoiding the explicit calculation of the Jacobian. In this case $NN_z N_t$ algebraic equations are solved

$$\frac{\mathbf{c}_j^n - \mathbf{c}_j^{n-1}}{\Delta t^*} + F \frac{\mathbf{q}_j^n - \mathbf{q}_j^{n-1}}{\Delta t^*} + u \frac{\mathbf{c}_{j+1}^n - \mathbf{c}_j^n}{\Delta z^*} = \mathbf{0}, \quad (2.57)$$

$$n = 1, \dots, N_t, \quad j = 1, \dots, N_z,$$

in conjunction with N algebraic equations from Eq. (2.55). Since the value of \mathbf{q}_j^n can be obtained only by solving implicit Eq. (2.55) for \mathbf{c}_j^n , the numerically most efficient forward-backward differences scheme for conservation laws with implicit

isotherm [13] is applied in this work. Compared to finite differences used in Eq. (2.53), the discretization schemes of time and space coordinates are interchanged, and the corresponding CFL-condition reads $u \frac{\Delta t^*}{\Delta z^*} > 1$. This is possible in case of conservation laws since the 'roles' of time and space can be interchanged, which is indicated by the equivalence of Eqs. (2.4a) and (2.6a). Eq. (2.55) is solved for all pairs (n, j) in (2.57) separately by some iteration method, like Newton-type methods [40]. In case of the MOL (2.54a) and the MOR (2.54b), it possible to formulate the ODEs in conjunction with Eq. (2.55) as a single system consisting of NN_z or NN_t differential and N algebraic equations (DAEs). The DAE formulation allows for the simultaneous solution of (2.54a,2.55) for every j and (2.54b,2.55) for every n by using DAE solvers. In addition to the differential equations in (2.54), the algebraic equations in (2.55) also benefit from the numerical features provided by standard DAE solvers like ODE15s in Matlab[®], DASSL [70], LIMEX [71], or IDAS in SUNDIALS [72]. Note, the application of standard DAE software requires the differential index to be equal to one [73]. This property guarantees the existence of solutions as well as numerical efficiency of standard DAE solvers. Numerical efficiency also requires consistent initial values of dynamic and algebraic variables. This consistency is important for the initialization of the DAE solver [73, 69]. Initialization of the DAE is required only once and consistent initial values can be obtained in advance by solving Eq. (2.55) for $\mathbf{c} = \mathbf{c}_{\text{init}}$ using an arbitrary iterative method.

The IAST (2.12,2.15,2.19,2.24) in conjunction with Eq. (2.3) is typically solved by applying the FDM, thus approximating (2.3) with Eqs.(2.57). The remaining algebraic equations (2.12,2.15,2.19,2.24) are solved separately via some Newton-type algorithm [26, 43]. This general IAS method was further improved by solving only implicit Eqs. (2.12,2.19) through some Newton method [26, 44]. Compared to the general IAST method, the Jacobian related to the Newton method is sparse, which improves numerical efficiency. The improved IAS method is known as FastIAS. Later on, this particular method was further refined [26, 42] by rearranging the implicit Eqs. (2.12,2.19) such that the Jacobian of the Newton method is a sparse upper triangular matrix. This approach is also known as modified FastIAS. The efficient methods FastIAS and modified FastIAS require the SCIs (2.15) to be explicit and analytically integrable and also require very good initial guesses for the initialization of the Newton-type algorithms. Good estimates of initial guesses are available for applications in gas chromatography and liquid chromatography under dilute conditions [26]. An IAST-approach that avoids the usage of Newton-type methods, or any iterative method for that matter, was presented in [41]. Instead, a numerical integration is used based on a differential reformulation of the equilibrium conditions. It avoids iteration at the expense of increased computational effort, which is required to calculate the derivatives of the equilibrium concentrations of the solid phase. These derivatives are needed for packed bed adsorber simulation (2.4a) using the MOL approximation (2.54a). This IAST-

approach is restricted to explicit SCI with the particular structure

$$q_i^0 = f_i(c_i^0) = \frac{c_i^0 \frac{df_i}{dc_i^0}}{\tilde{f}_i(c_i^0)}, \quad i = 1, \dots, N. \quad (2.58)$$

Either the SMA isotherm of the AIE (2.33,2.35) or the mass action isotherm of the CIE (2.31,2.32) is solved in conjunction with Eq. (2.3) usually by applying the FDM [38, 6, 30, 31, 74]. The PDE system (2.3) is then approximated by a corresponding system of algebraic equations (2.57), where similar to the IAST, the implicit algebraic equations (2.33,2.35) or (2.31,2.32) are solved separately using iterative methods, such as the Newton-Raphson method [40]. Hence, the availability of good initial guesses is indispensable. It should be noted that compared to the IAST, neither the AIE nor the CIE assume generally dilute conditions, and good estimates on initial guesses for iterative methods might not be available.

Chapter 3

Ideal Adsorbed Solution Theory

This chapter including Appendix A was in parts published in Chemical Engineering Science, 177, M. Fechtner and A. Kienle, Efficient simulation and equilibrium theory for adsorption processes with implicit adsorption isotherms – Ideal adsorbed solution theory, 284–292 (2018).

3.1 Introduction

In this chapter, a solution strategy for the efficient simulation of equilibrium models (2.2,2.3) of packed bed adsorbers with an implicit sorption isotherm described by the IAST (2.12,2.15,2.19,2.24) is developed. It is based on a reformulation of the underlying partial differential equations, uses an MOL approach [36], avoids explicit differentiation of the adsorption isotherm and applies standard numerics for the simultaneous solution of the resulting differential and implicit algebraic equations.

The IAST was developed by Myers and Prausnitz [17] to predict the adsorption of multi-component mixtures from SCIs. The equations of the IAST (2.12,2.15,2.19,2.24) are implicit and include integral expressions (2.19) for the calculation of the spreading pressures (2.18b). Only in special cases an analytical calculation of the equilibrium composition of the adsorbed phase is possible [45, 46]. As stated in Section 2.3, a number of numerical approaches were proposed including the general IAS [17], the FastIAS [42] and the modified FastIAS [42, 26]. All of these methods are based on iterative solution of the IAST equations, therefore require good initial guesses and almost entirely apply to analytically integrable explicit single component isotherms. Therefore, an alternative approach was proposed recently by Landa et al. [41], which is very powerful and avoids iteration but at the expense of significantly increased computational effort. In addition this approach is limited to SCIs defined by Eq. (2.58)

The challenges and restrictions of those previous approaches are overcome by the solution strategy presented in the following. For this purpose, application of the strategy is demonstrated for two different benchmark problems with explicit

and implicit SCIs. Results for explicit SCIs are compared to previous numerical solution approaches based on the most efficient modified FastIAS. In contrast to this, results for implicit SCIs are new and cannot be obtained with any of the previous approaches. In addition, numerical results for explicit and implicit SCIs are validated with semi-analytical solution approaches from equilibrium theory.

3.2 Reformulation and Solution Strategy

Recalling Eq. (2.2), its solution requires the adsorption isotherms $\mathbf{q}(\mathbf{c})$ and, as describes in Section 2.3, usually also the Jacobian matrix of the derivatives of the adsorption isotherms $\frac{\partial \mathbf{q}}{\partial \mathbf{c}}$ according to the chain rule of differentiation. These derivatives however are difficult to obtain for complex adsorption isotherms. As already stated in Section 2.3, a method for the IAST based on some analytical formulas has been proposed in [41]. However, the method is tailored to the specific solution strategy in [41], which delivers a priori the hypothetical fluid phase concentrations c_i^0 as functions of the true fluid phase concentration c_i and is not directly applicable to other solutions strategies. This motivates the following reformulation. A new set of variables $\mathbf{v} \in \mathbb{R}^N$ is introduced according to

$$\mathbf{v} = F\mathbf{q}(\mathbf{c}) + \mathbf{c}. \quad (3.1)$$

It represents the joint capacity of the fluid and the adsorbed phase in Eq. (2.2) and is related to the capacity function in Eq. (2.5) by $\mathbf{v} = u\tilde{\mathcal{F}}$. In terms of the new variables, the model (2.2) reads

$$\frac{\partial \mathbf{v}}{\partial t^*} + u \frac{\partial \mathbf{c}}{\partial z^*} = \mathbf{D}_a \frac{\partial^2 \mathbf{c}}{\partial (z^*)^2}. \quad (3.2)$$

This equation is solved for \mathbf{v} . In addition, the following set of $2N$ implicit algebraic equations for \mathbf{c}^0 and \mathbf{c} is derived from Eqs. (2.12,2.15,2.19,2.24) and the definition of \mathbf{v} (3.1)

$$0 = f_i := \int_0^{c_i^0} \frac{q_i^0(\sigma)}{\sigma} d\sigma - \int_0^{c_i} \frac{q_i^0(\sigma)}{\sigma} d\sigma, \quad i = 1, \dots, N-1, \quad (3.3a)$$

$$0 = f_N := \sum_{j=1}^N \frac{c_j}{c_j^0} - 1, \quad (3.3b)$$

$$\begin{aligned} 0 &= g_i := Fq_i(\mathbf{c}) + c_i - v_i \\ &= F \left(\sum_{j=1}^N \frac{1}{q_j^0(c_j^0)} \frac{c_j}{c_j^0} \right)^{-1} \frac{c_i}{c_i^0} + c_i - v_i \quad i = 1, \dots, N. \end{aligned} \quad (3.3c)$$

In Eq. (3.3c), (2.24) was used to eliminate the q_i variables.

For the numerical solution, the partial differential equation (3.2) is discretized using a MOL approach [36]. For demonstration purposes the limiting case of

vanishing axial dispersion is considered in the remainder, and a simple scheme with first-order backward differences on an equidistant grid is used for the convection term. However, application of more efficient discretization methods using adaptive grids [37] and/or high resolution methods [16] is straight forward. The resulting system of ordinary differential equations (corresponding to (3.2)) for \mathbf{v} is solved simultaneously with algebraic equations (3.3a)-(3.3c) for \mathbf{c} and \mathbf{c}^0 using standard DAE numerics, in this work ODE15s in Matlab[69], provided that the differential index is equal to one [73]. The numerical solution of higher index systems is much more challenging [75] and not required here as will be shown subsequently. With the DAE approach, explicit differentiation of the adsorption isotherm is avoided.

In the following, it is shown that the differential index of the PDAE system (3.2, 3.3a-3.3c), or equivalently the DAE system resulting from its discretization, is always equal to one if the Jacobian $\frac{\partial \mathbf{g}}{\partial \mathbf{c}}$ has N real, positive eigenvalues. For thermodynamic reasons this should always be the case as shown by Kvaalen et al. [76] using displacement theory. Explicit proofs for Langmuir isotherms were given in [76], for Bi-Langmuir isotherms in [47] and for the IAS theory for a large class of pure component isotherms in [41]. In Appendix A these results are extended in two directions. First, it is shown that this spectral property holds for any thermodynamically consistent adsorption isotherm for mixtures of two adsorbable components. Second, it is shown that it may fail for multi-component mixtures that are not in the class defined by [41].

The PDAE system (3.2, 3.3a-3.3c), or equivalently the DAE system resulting from its discretization, has differential index one if the matrix of the derivatives of the algebraic equations (3.3a-3.3c) with respect to the algebraic variables \mathbf{c}^0, \mathbf{c} is nonsingular. From differentiation of Eqs. (3.3a-3.3c) and some elementary calculations we find

$$\begin{aligned} \det(\mathbf{J}) &= \det \begin{pmatrix} \left(\frac{\partial \mathbf{f}}{\partial \mathbf{c}^0} \right)_{\mathbf{c}} & \left(\frac{\partial \mathbf{f}}{\partial \mathbf{c}} \right)_{\mathbf{c}^0} \\ \left(\frac{\partial \mathbf{g}}{\partial \mathbf{c}^0} \right)_{\mathbf{c}, \mathbf{v}} & \left(\frac{\partial \mathbf{g}}{\partial \mathbf{c}} \right)_{\mathbf{c}^0, \mathbf{v}} \end{pmatrix} \\ &= \det \begin{pmatrix} \left(\frac{\partial \mathbf{f}}{\partial \mathbf{c}^0} \right)_{\mathbf{c}} & \left(\frac{\partial \mathbf{f}}{\partial \mathbf{c}} \right)_{\mathbf{c}^0} \\ \mathbf{0} & \left(\frac{\partial \mathbf{g}}{\partial \mathbf{c}} \right)_{\mathbf{c}^0, \mathbf{v}} - \left(\frac{\partial \mathbf{g}}{\partial \mathbf{c}^0} \right)_{\mathbf{c}, \mathbf{v}} \left(\frac{\partial \mathbf{f}}{\partial \mathbf{c}^0} \right)_{\mathbf{c}}^{-1} \left(\frac{\partial \mathbf{f}}{\partial \mathbf{c}} \right)_{\mathbf{c}^0} \end{pmatrix} \\ &= \det \left(\frac{\partial \mathbf{f}}{\partial \mathbf{c}^0} \right)_{\mathbf{c}} \det \left(\left(\frac{\partial \mathbf{g}}{\partial \mathbf{c}} \right)_{\mathbf{c}^0, \mathbf{v}} - \left(\frac{\partial \mathbf{g}}{\partial \mathbf{c}^0} \right)_{\mathbf{c}, \mathbf{v}} \left(\frac{\partial \mathbf{f}}{\partial \mathbf{c}^0} \right)_{\mathbf{c}}^{-1} \left(\frac{\partial \mathbf{f}}{\partial \mathbf{c}} \right)_{\mathbf{c}^0} \right). \end{aligned} \quad (3.4)$$

The indices at the brackets indicate which variable is constant during differentiation. From this equation, we find that regularity of matrix \mathbf{J} requires both determinants in the last row of this equation to be nonzero. The first determinant can be calculated explicitly using Gaussian elimination without row switching (see

also [26])

$$\begin{aligned} \det \left(\left(\frac{\partial \mathbf{f}}{\partial \mathbf{c}^0} \right)_{\mathbf{c}} \right) &= \prod_{j=1}^{N-1} \frac{q_j^0}{c_j^0} \left(-\frac{c_N}{(c_N^0)^2} - \sum_{j=1}^{N-1} \frac{-\frac{c_j}{(c_j^0)^2}}{\frac{q_j^0}{c_j^0}} \left(-\frac{q_N^0}{c_N^0} \right) \right) \\ &= -q_{\text{tot}}^{-1} \prod_{j=1}^{N-1} \frac{q_j^0}{c_j^0}. \end{aligned} \quad (3.5)$$

It is nonzero for nonzero concentrations.

The matrix in the second determinant is equal to $\left(\frac{\partial \mathbf{g}}{\partial \mathbf{c}} \right)_{\mathbf{v}}$, which is obtained by differentiation of (3.3c), when \mathbf{c}^0 is interpreted as a function of \mathbf{c} according to Eqs. (3.3a,3.3b)

$$\left(\frac{\partial \mathbf{g}}{\partial \mathbf{c}} \right)_{\mathbf{v}} = \left(\frac{\partial \mathbf{g}}{\partial \mathbf{c}} \right)_{\mathbf{c}^0, \mathbf{v}} + \left(\frac{\partial \mathbf{g}}{\partial \mathbf{c}^0} \right)_{\mathbf{c}, \mathbf{v}} \frac{\partial \mathbf{c}^0}{\partial \mathbf{c}}. \quad (3.6)$$

The derivative of \mathbf{c}^0 with respect to \mathbf{c} is obtained by implicit differentiation of Eqs. (3.3a,3.3b) according to

$$\frac{\partial \mathbf{c}^0}{\partial \mathbf{c}} = - \left(\frac{\partial \mathbf{f}}{\partial \mathbf{c}^0} \right)_{\mathbf{c}}^{-1} \left(\frac{\partial \mathbf{f}}{\partial \mathbf{c}} \right)_{\mathbf{c}^0}. \quad (3.7)$$

Alternatively, $\left(\frac{\partial \mathbf{g}}{\partial \mathbf{c}} \right)_{\mathbf{v}}$ can be calculated by differentiation of the first line of Eq. (3.3c)

$$\left(\frac{\partial \mathbf{g}}{\partial \mathbf{c}} \right)_{\mathbf{v}} = F \frac{\partial \mathbf{q}}{\partial \mathbf{c}} + \mathbf{I}_N. \quad (3.8)$$

Hence, the second determinant in Eq. (3.4) yields

$$\det \left(\frac{\partial \mathbf{g}}{\partial \mathbf{c}} \right)_{\mathbf{v}} = \prod_{i=1}^N (F \lambda_i + 1), \quad (3.9)$$

where the λ_i 's are the eigenvalues of the matrix $\frac{\partial \mathbf{q}}{\partial \mathbf{c}}$. Consequently, the second determinant is also nonzero if these eigenvalues are positive, which completes the proof.

Remarks:

1. A crucial aspect of the DAE formulations are consistent initial values $\mathbf{v}_{\text{init}}(z)$, $\mathbf{c}_{\text{init}}^0(z)$. They can be easily calculated by solving (3.3a-3.3c) offline for given initial conditions $\mathbf{c}_{\text{init}}(z)$.

2. So far, explicit SCIs have been assumed according to equation (2.15). However, it is worth noting that also implicit SCIs according to

$$0 = h_i(c_i^0, q_i^0), \quad i = 1, \dots, N, \quad (3.10)$$

can be handled using the new method. For implicit SCI, equations (3.10) have to be solved for every $\sigma \in [0, c_i^0]$, in order to evaluate the integral expressions in (2.19). Since the hypothetical fluid phase concentrations c_i^0 depend on z^* and t^* , this can be done in two different ways. Either the SCIs are re-evaluated at every point in space and time according to the present values of c_i^0 , or they are calculated a priori only once for estimated upper bounds on c_i^0 , which is of course much more efficient. Using these function values, the integral expressions in (2.19) are then evaluated using some numerical quadrature.

The iterative calculation of the implicit SCIs requires good starting values, which are often not available. Therefore, the following approach based on integration according to Davidenko's method [77] with trivial initial conditions is used in this chapter

$$\frac{dq_i^0}{d\sigma_i} = - \left(\frac{\partial h_i}{\partial q_i^0} \right)^{-1} \frac{\partial h_i}{\partial \sigma_i}, \quad q_i^0(0) = 0, \quad i = 1, \dots, N. \quad (3.11)$$

3. In the limit of vanishing axial dispersion, an alternative reformulation of the partial differential equation (2.2) can be found. For this purpose Eqs. (2.15) and (2.24) are inserted into the partial differential equation (2.2) with $\mathbf{D}_a = 0_N$ leading to

$$\frac{\partial \mathbf{c}}{\partial z} + u^{-1} \frac{\partial}{\partial t} \left(\mathbf{c} + F \left(\sum_{j=1}^N \frac{1}{q_j^0(c_j^0)} \frac{c_j}{c_j^0} \right) \mathbf{c} * \tilde{\mathbf{c}}^0 \right) = \mathbf{0}, \quad (3.12)$$

$$\mathbf{c}(0, z) = \mathbf{c}_0(z), \quad \mathbf{c}(t, 0) = \mathbf{c}_{\text{feed}}(t).$$

Note, 0_N is a $N \times N$ matrix where all entries are equal to zero.

In this equation the '*' symbol denotes the element-wise multiplication of \mathbf{c} and $\tilde{\mathbf{c}}^0 = \left[\frac{1}{c_1^0}, \dots, \frac{1}{c_N^0} \right]^T$. System (3.12) together with (3.3a) and (3.3b) forms a PDAE system that is equivalent to the previous system (3.2), and (3.3a-3.3c). It can be solved efficiently using the MOR [78] instead of a MOL approach. In the MOR, first the temporal instead of the spatial coordinate is discretized leading to a system of ordinary differential equations in space, which are then integrated together with the algebraic equations using a DAE method. In this case, \mathbf{c} is the dynamic variable and \mathbf{c}^0 is the only algebraic variable. This reformulation seems attractive because it requires

only N additional algebraic variables per grid point. In view of Eq. (3.5) the differential index of this alternative reformulation is also always equal to one for arbitrary N . Hence, the MOR-based DAE formulation is applicable to any SCIs, especially also to those resulting in non-hyperbolic systems. This allows to retain the advantages of a DAE formulation (numerical stability, usage of flow-sheet simulation) also for cases where the MOL-based DAE formulation is not applicable.

4. If the single component isotherms are implicit, parallelization of the solution to these algebraic equations within the present DAE approach seems appealing. Formally, the corresponding vector of algebraic variables extended by \mathbf{q}^0 becomes

$$\begin{aligned} \mathbf{c}_{\text{ext}} &= [\mathbf{c}, \mathbf{q}^0, \mathbf{c}^0]^T, \\ \mathbf{q}_{\text{ext}}(\mathbf{c}, \mathbf{q}^0, \mathbf{c}^0) &= [\mathbf{g}(\mathbf{c}, \mathbf{c}^0, \mathbf{q}^0), \mathbf{h}(\mathbf{c}, \mathbf{c}^0, \mathbf{q}^0), \mathbf{f}(\mathbf{c}, \mathbf{c}^0, \mathbf{q}^0)]. \end{aligned} \quad (3.13)$$

In order for the differential index to be equal to one, the matrix

$$\frac{\partial \mathbf{q}_{\text{ext}}}{\partial \mathbf{c}_{\text{ext}}} = \begin{bmatrix} \frac{\partial \mathbf{g}}{\partial \mathbf{c}} & \frac{\partial \mathbf{g}}{\partial \mathbf{q}^0} & \frac{\partial \mathbf{g}}{\partial \mathbf{c}^0} \\ \frac{\partial \mathbf{h}}{\partial \mathbf{c}} & \frac{\partial \mathbf{h}}{\partial \mathbf{q}^0} & \frac{\partial \mathbf{h}}{\partial \mathbf{c}^0} \\ \frac{\partial \mathbf{f}}{\partial \mathbf{c}} & \frac{\partial \mathbf{f}}{\partial \mathbf{q}^0} & \frac{\partial \mathbf{f}}{\partial \mathbf{c}^0} \end{bmatrix} \in \mathbb{R}^{3N \times 3N}, \quad (3.14)$$

similar to the one in (3.4), has to be regular. However, some partial derivatives with respect to \mathbf{q}^0 do not exist since the integral

$$\left(\frac{\partial f_i}{\partial q_i^0} \right)_{\mathbf{c}, \mathbf{c}^0, \mathbf{q}^0 \setminus \{q_i^0\}} = \pm \int_0^{c_i^0} \frac{1}{\sigma} d\sigma, \quad i = 1, \dots, N \quad (3.15)$$

does not converge. Hence, defining \mathbf{q}^0 as algebraic variable is not feasible.

3.3 Applications

In this section, the methods introduced in the previous section are evaluated and compared to established solution approaches for two different benchmark problems with explicit and implicit SCIs, respectively. For a simple and efficient validation with the equilibrium theory, binary examples are considered. However, based on the formulation and results in the previous chapter, application of the developed numerical solution approaches to multi-component systems is straight forward.

The numerical results in this section were obtained using a standard desktop computer with intel[®] core[™]i7-4790 3.6 GHz and 16 GB RAM. Matlab[®] [69] was used to perform the numerical simulations. In particular, ODE15s was used to solve the DAEs resulting from the discretization of the partial differential equations using first-order backward differences, ODE45 to solve the ODEs resulting from Davidenko's method in Eq. (3.11) and the Matlab function 'trapz' for numerical evaluation of the integrals in Eq. (2.19). In addition to ODE15s the

parameter	value	description
L [cm]	5	column length
N_z [$-$]	100	number of grid points
u [$\frac{cm}{min}$]	7.9556	interstitial velocity
ϵ [$-$]	0.745	void fraction
q_{11}^{sat} [$\frac{mmol}{l}$]	147.2	isotherm parameter
q_{12}^{sat} [$\frac{mmol}{l}$]	6.0	isotherm parameter
b_{11} [$\frac{l}{mmol}$]	0.087	isotherm parameter
b_{12} [$\frac{l^2}{mmol^2}$]	0.01	isotherm parameter
b_{13} [$\frac{l}{mmol}$]	1.69	isotherm parameter
q_{21}^{sat} [$\frac{mmol}{l}$]	122.4	isotherm parameter
q_{22}^{sat} [$\frac{mmol}{l}$]	17.0	isotherm parameter
b_{21} [$\frac{l}{mmol}$]	0.103	isotherm parameter
b_{22} [$\frac{l^2}{mmol^2}$]	0.032	isotherm parameter
b_{23} [$\frac{l}{mmol}$]	1.78	isotherm parameter

Table 3.1: Parameters of the first IAST example with explicit combined quadratic plus Langmuir SCIs.

open source solver IDAS was tested as an alternative. This solver was incorporated into the Matlab[®] environment using SUNDIALS, a suite of nonlinear and differential/algebraic equation solvers [72].

3.3.1 Example with Explicit SCIs

The first example was taken from [41]. It is concerned with the adsorption of phenyl-n-decane (abbreviation 'C10') and phenyl-n-undecane (abbreviation 'C11') in acetonitrile on graphitized carbon. Adsorption of individual components is described by explicit SCIs using a combined quadratic plus Langmuir model

$$q_i^0 = q_{i1}^{sat} \frac{c_i^0(b_{i1} + 2b_{i2}c_i^0)}{1 + b_{i1}c_i^0 + b_{i2}(c_i^0)^2} + q_{i2}^{sat} \frac{c_i^0 b_{i3}}{1 + b_{i3}c_i^0}, \quad i = 1, \dots, N. \quad (3.16)$$

Parameter values were taken from [41] and can be found in Tab. 3.1. The SCIs are shown in Fig. 3.1. Since this is a system with two adsorbable components, requirements for a differential index of 1 as discussed in the previous section and Appendix A are satisfied.

For a rigorous evaluation, the new MOL-based and MOR-based DAE approaches are compared to two different implementations of the modified FastIAS by Do [26], which was originally developed by [42]. The modified FastIAS solves efficiently the equilibrium equations (3.3a,3.3b) using the Newton method. The first implementation is a mixed DAE-FastIAS approach that uses the reformulation (3.2), (3.3c) in combination with a MOL approach and the modified FastIAS

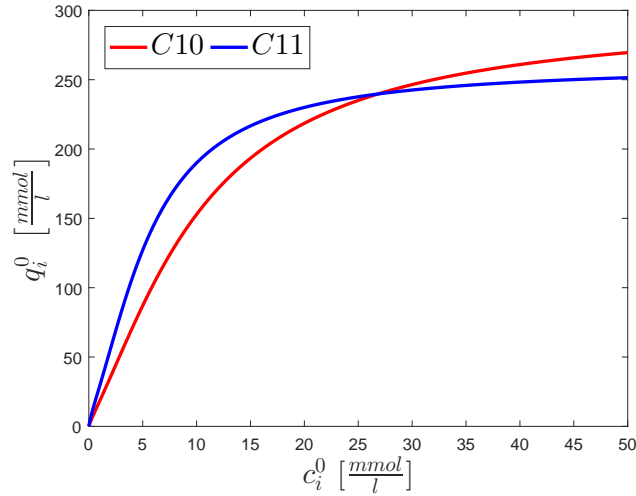


Figure 3.1: SCIs of phenyl-n-decane (C10) and phenyl-n-undecane (C11) computed with the combined quadratic plus Langmuir model.

for the calculation of the hypothetical fluid phase concentrations c_i^0 . Thus, solving simultaneously equations (3.2),(3.3c) for \mathbf{v} , \mathbf{c} , while the equations (3.3a,3.3b) are solved separately for each spatial grid point at any given time for \mathbf{c}^0 . Again, in light of Eq. (3.9) the differential index of this DAE approach is also equal to one. It is worth pointing out that in the new DAE approaches, all algebraic equations are solved simultaneously with the differential equations using DAE numerics, whereas in the modified FastIAS approaches Eqs. (3.3c) are solved separately by iteration. Therefore the new MOL- and MOR-based approaches are expected to be more efficient and stable.

For the second implementation of the modified FastIAS method, total discretization of the model (2.2) is applied using simple backward differences for the spatial derivatives and forward differences for the time derivatives. Again the modified FastIAS method is used at any point in time and space. In all cases axial dispersion is neglected with $\mathbf{D}_a = 0_N$.

In the remainder, focus is on the following scenario. An empty column is injected with a pulse feed of $5.4 \left[\frac{\text{mmol}}{\text{l}}\right]$ phenyl-n-decane and $5.0 \left[\frac{\text{mmol}}{\text{l}}\right]$ phenyl-n-undecane starting at 0 min and ending at 10 min . The resulting breakthrough curves at the end of the column obtained with the different approaches over a time interval of $[0, 20] \text{ min}$ are shown in Fig. 3.2. Results are in good agreement with Fig. 8.4 in [41]. Corresponding computation times are given in Tab. 3.2.

Numerical parameters of the different approaches were selected in such a way that the accuracy of all approaches is similar and therefore allows a fair comparison of computation times. For the MOL-based DAE approach backward differences with $N_z = 100$ equidistant space grid points were used. It was found that a four times higher number of equidistant time grid points was required

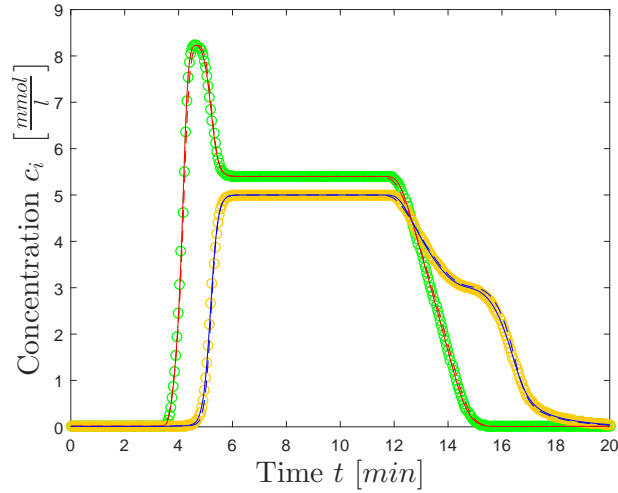


Figure 3.2: Calculated breakthrough curves for the first example. Solid lines - MOL-based (ODE15s and IDAS) and MOR-Based DAE approach (ODE15s), circles - mixed DAE-FastIAS approach (ODE15s with Newton), dashed lines - modified FastIAS with total discretization (Newton).

formulation	solver	average execution time
MOL-based DAE	IDAS	5.2 s
	ODE15s	11.0 s
full discretization & modified FastIAS	Newton-Raphson [26]	12.0 s
mixed DAE-FastIAS	ODE15s & Newton-Raphson [26]	36.0 s
MOR-based DAE	ODE15s	92.1 s

Table 3.2: Comparison of the execution times of the different numerical approaches for the first IAST application example.

for the MOR-based DAE approach to achieve similar accuracy. Although the MOR-based PDAE formulation (3.12,3.3a,3.3b) has only $2N$ variables compared to $3N$ variables for the MOL-based PDAE formulation (3.2,3.3a-3.3c), the computation time reported in Tab. 3.2 is higher due to the increased number of grid points. Further differences may be attributed to different structural properties of the different formulations. It is concluded that the MOR-based approach is less attractive compared to the MOL approach and therefore not further considered in this chapter.

From Tab. 3.2 it is also confirmed that the MOL-based DAE approach is much faster than the mixed DAE-FastIAS approach. The reasons have been discussed above.

Despite minor differences in accuracy, the total discretization in combination with the modified FastIAS is almost as efficient as the MOL-based DAE approach. For the total discretization, 400 time steps and 1250 space steps were used. The high number of space steps was required to satisfy the CFL condition for numerical stability [16], which is a crucial issue for the type of total discretization applied here. Main advantage of the MOL-based DAE approach compared to the total discretization approach are seen in two facts: (i) In the DAE approach, more sophisticated methods for time integration including variable order, variable step size in combination with error control can be applied without extra effort by using corresponding standard software. This may lead to improved numerical accuracy and stability. In case of the used IDAS solver, an improved efficiency is clearly visible, see Tab. 3.2. (ii) As stated above, the MOL-based DAE approach is particular well suited for the simulation of multi-column processes using standard software for equation oriented dynamic flow-sheet simulation. Such tools support flexible configuration of complex plants from elementary modeling and/or process units and therefore reduce the implementation effort.

For validation purposes, the numerical solution of the MOL-based method is finally compared to the predictions of equilibrium theory in Fig. 3.3 [15]. Fig. 3.3a represents the solution of the scenario in Fig. 3.2 in the concentration phase space of the eigenvectors of the Jacobian $\frac{\partial \mathbf{q}}{\partial \mathbf{c}}$. Eigenvalues and eigenvectors have been calculated with the formulas in Appendix A. The lower diagram represents an improved simulation with an increased number of $N_z = 1000$ grid points to reduce the numerical dispersion. Agreement between theoretical and numerical results in Fig. 3.3a is excellent. The plateau values in Fig. 3.3b also coincide visibly with the corners of the trajectory in Fig. 3.3a.

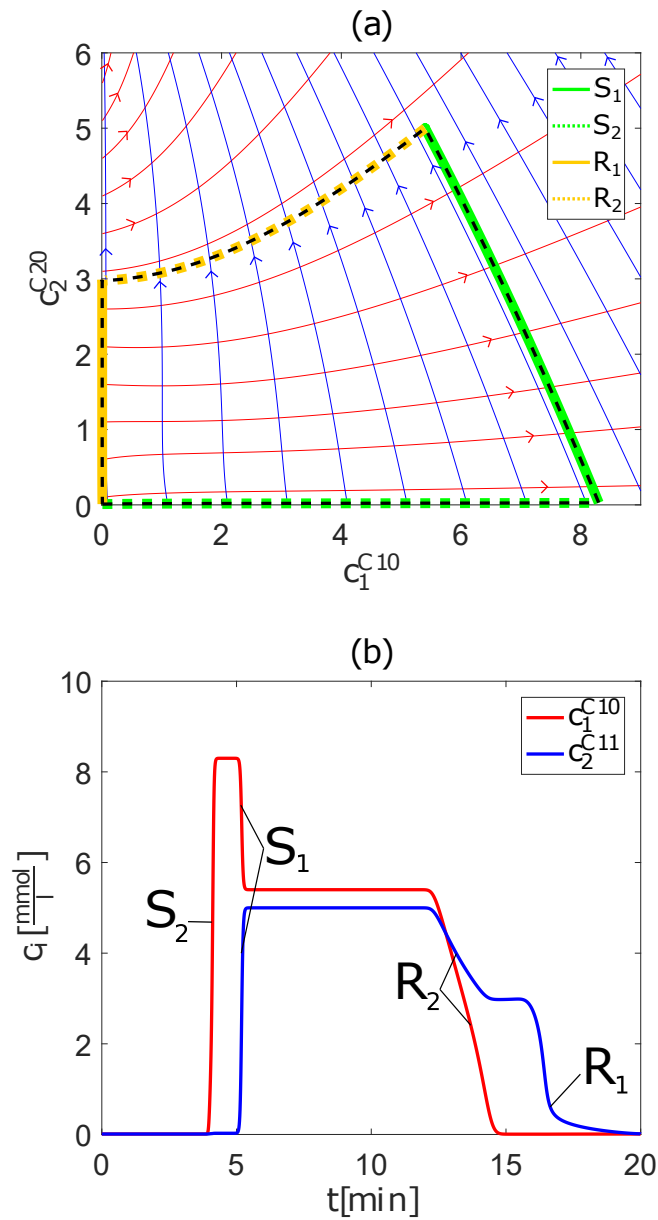


Figure 3.3: Validation of numerical results for the first example: (a) Trajectories in the concentration phase space calculated with equilibrium theory (bold lines) overlaid with the numerical solution (dashed line). (b) Elution profiles of the numerical solution for $Nz = 1000$ grid points.

parameter	value	description
L [m]	0.1	column length
N_z [-]	100	number of grid points
u [$\frac{m}{s}$]	0.0012	interstitial velocity
ϵ [-]	0.8	void fraction
q_1^{sat} [$\frac{mg}{ml}$]	75.0	isotherm parameter
q_2^{sat} [$\frac{mg}{ml}$]	316.0	isotherm parameter
b_1 [$\frac{ml}{mg}$]	0.03047	isotherm parameter
b_2 [$\frac{ml}{mg}$]	0.0153	isotherm parameter
ϑ_1 [-]	0.6434	isotherm parameter
ϑ_2 [-]	-2.037	isotherm parameter

Table 3.3: Parameters of the second IAST example with implicit Fowler-Guggenheim SCIs.

3.3.2 Example with Implicit SCIs

Next, application of the MOL-based DAE formulation is demonstrated for a second benchmark problem with implicit SCIs. Since the modified FastIAS needs integrable and explicit SCIs, it cannot be applied to this second example.

The example system was taken from [66]. It is concerned with the adsorption of 2-phenylethanol (component '1') and 3-phenylpropanol (component '2') in methanol-water on octadecyl-silica, where an implicit multi-component Fowler-Guggenheim isotherm is used. In this section, IAST based on the implicit SCIs obtained as limiting cases from the multi-component Fowler-Guggenheim isotherm is used

$$0 = h_i(c_i^0, q_i^0) = b_i c_i^0 \exp\left(-\vartheta_i \frac{q_i^0}{q_i^{\text{sat}}}\right) + \frac{q_i^0}{q_i^0 - q_i^{\text{sat}}}, \quad i = 1, 2. \quad (3.17)$$

Therefore, only a qualitative comparison with [66] is possible. Using the Davidenko procedure [77], equations (3.17) are replaced by the equivalent initial value problem

$$\begin{aligned} \frac{dq_i^0}{d\sigma} &= \left(\vartheta_i b_i \frac{\sigma}{q_i^{\text{sat}}} \exp\left(-\vartheta_i \frac{q_i^0}{q_i^{\text{sat}}}\right) + \frac{q_i^{\text{sat}}}{(q_i^0 - q_i^{\text{sat}})^2} \right)^{-1} b_i \exp\left(-\vartheta_i \frac{q_i^0}{q_i^{\text{sat}}}\right), \\ q_i(0) &= 0, \quad i = 1, 2, \end{aligned} \quad (3.18)$$

to calculate the SCIs. The parameters for this example can be found in Tab. 3.3 and are taken from [66]. Results are shown in Fig. 3.4. Since the calculation of the SCIs can be separated from the simulation, the same arguments for the differential index can be applied as in the previous section and Appendix A. Again, the

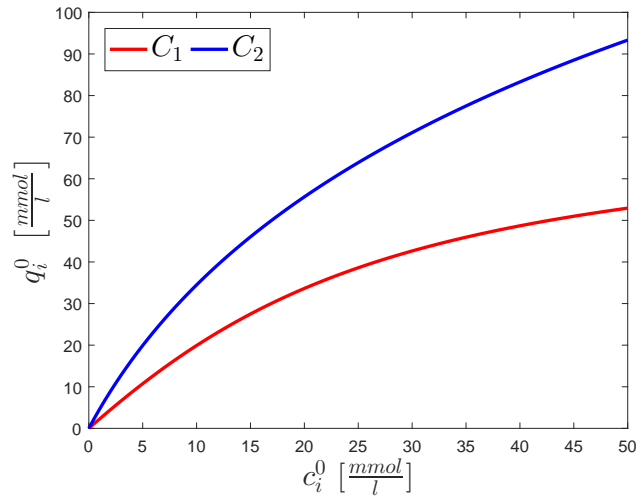


Figure 3.4: SCIs of 2-phenylethanol (C_1) and 3-phenylpropanol (C_2) computed with the Fowler-Guggenheim model.

differential index is equal to one for the present system with two adsorbable components and the MOL-based DAE approach can be applied. For demonstration purposes axial dispersion is again neglected corresponding to $\mathbf{D}_a = \mathbf{0}_N$.

A similar set-up like the previous example is considered, where an empty column is injected with a feed pulse of $6.0 \frac{mg}{ml}$ 2-phenylethanol and $6.0 \frac{mg}{ml}$ 3-phenylpropanol starting at $t^* = 0.0$ s and ending at $t^* = 10.0$ s. Corresponding breakthrough curves are shown in Fig. 3.5 for the time interval $[0, 300]$ s. Due to the different multi-component isotherms, the results in Fig. 3.5 are only in qualitative agreement with Fig. 3.4 in [66]. Main difference is a shift of profiles by 25 s. Nevertheless, the example in Fig. 3.5 demonstrates the applicability of the new MOL-based DAE approach also for non-integrable and implicit single component adsorption isotherms.

In a second step, the numerical solution is also validated with the semi-analytical solution obtained from equilibrium theory. For this purpose a chromatographic cycle consisting of the loading of an empty bed followed by the regeneration is considered. The solution trajectory in the concentration phase space obtained from equilibrium theory is shown in Fig. 3.6a. Corresponding concentration profiles calculated numerically with the MOL-based DAE approach using an increased number of $N_z = 1000$ grid points is shown in Fig. 3.6b. Additionally, the injection interval is increased to $[0, 100]$ s for an improved visibility of the plateau values. Again, agreement between theoretical and numerical results in Fig. 3.6a is excellent. In the concentration range considered in this figure, the system is almost linear decoupled. This is reflected by the almost orthogonal patch grid of the eigenvectors in Fig. 3.6a and by the decoupled transitions as well as the 'symmetry' between adsorption and desorption fronts in Fig. 3.6b.

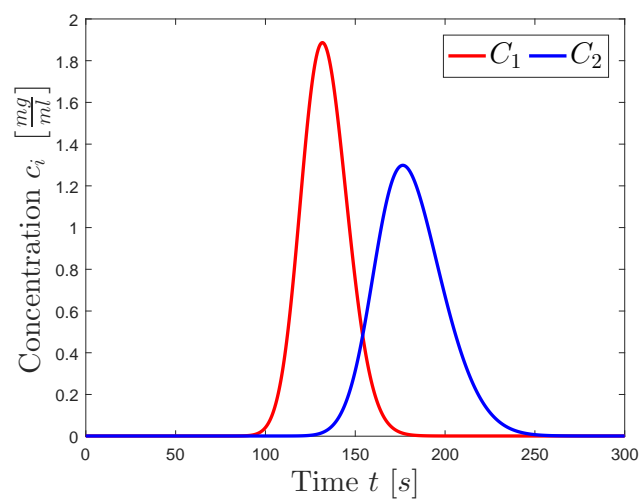


Figure 3.5: Calculated eluted peaks for the second example.

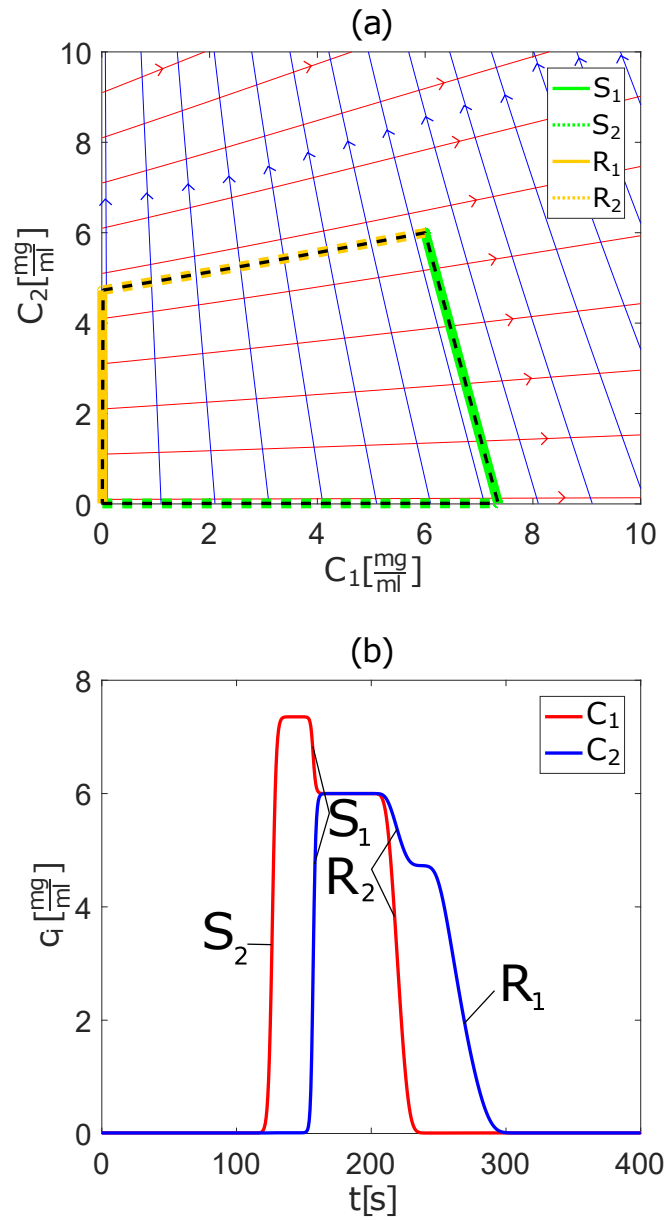


Figure 3.6: Validation of numerical results for the second example: (a) Trajectories in the concentration phase space calculated with equilibrium theory (bold lines) overlaid with the numerical solution (dashed line). (b) Elution profiles of the numerical solution for $N_z = 1000$ grid points and an injection interval of $[0, 100]$ s.

3.4 Summary

Two different DAE-based methods were developed for the numerical solution of equilibrium models of fixed bed adsorbers using IAST for an arbitrary number of components, namely an MOL- and a MOR-based approach. It was shown that the first is clearly superior to the second. Further, the efficiency of the MOL-based approach was verified by comparison with different implementations of the popular modified FastIAS method. Restrictions of (modified) FastIAS concerning the single component isotherms could be relaxed. It was shown that the DAE methods can be applied to a large class of SCIs including non-integrable and even implicit equations. Applicability of the DAE approaches was justified by proving a differential index of one for all types of isotherms leading to a Jacobian of the derivatives of the adsorption isotherms with only real and positive eigenvalues. This applies to all binary and a large class of multi-component mixtures. However, for multi-component mixtures also cases with complex eigenvalues can be found, which are not suitable from the thermodynamic as well as the numerical point of view and need revision.

Chapter 4

Classical Ion Exchange (CIE)

This chapter including (Appendix B) was in parts published in Chemical Engineering Science, 171, M. Fechtner and A. Kienle, Efficient simulation and equilibrium theory for adsorption processes with implicit adsorption isotherms – Mass action equilibria, 471–480 (2017).

4.1 Introduction

In this chapter, a solution strategy for the efficient simulation of equilibrium models (2.2,2.3) of packed bed sorbers with an implicit sorption isotherm described by the CIE (2.31,2.32) is developed. The resulting PDAE system is computationally much more difficult to treat due to the implicit phase equilibrium. Usually some challenging implicit analytical or numerical differentiation of the equilibrium relations is required to calculate the capacity matrix $\frac{\partial \mathcal{F}(\mathbf{c})}{\partial \mathbf{c}}$ (see Eq. (2.4b)) of the model equations [66, 41].

A much easier alternative approach is proposed here. It uses MOL and a reformulation of the underlying sorber model equations in the form of a DAE system with differential index 1. It can be solved with available standard software for DAEs and thereby avoids explicit differentiation of the sorption isotherm.

A characteristic feature of the CIE are potential selectivity reversals predicted by the ideal model. It also admits an analytical approach using the equilibrium theory. Classical equilibrium theory is for Langmuir isotherms [15] or ion exchange with constant separation factors [28]. More recently, extensions were given to Bi-Langmuir [79, 47], generalized Langmuir [49], generalized Bi-Langmuir [48], and also to reactive systems with simultaneous phase and reaction equilibrium [80, 81, 82]. In the present chapter, results regarding the CIE in [27, 50, 28] are further extended to provide a full picture of possible transitions.

First the numerical approach is introduced. Afterwards, a rigorous analysis is given based on equilibrium theory. Focus is on selectivity reversals and their impact on operability and uniqueness of solutions. Theoretical findings are validated with numerical simulations.

4.2 Reformulation and Solution Strategy

The following is based on the well known equilibrium dispersive model Eq. (2.2) of a packed bed sorber. In dimensionless form the model reads

$$\frac{\partial}{\partial t} (\mathbf{c} + F\mathbf{q}(\mathbf{c})) + \frac{\partial \mathbf{c}}{\partial z} = \mathbf{D}_a \frac{\partial^2 \mathbf{c}}{\partial z^2}, \quad \mathbf{c}, \mathbf{q} \in \mathbb{R}^N \quad (4.1)$$

with dimensionless time and space coordinates

$$z = z^*/L, \quad t = t^*u/L. \quad (4.2)$$

Again, the ideal equilibrium model is included for negligible axial dispersion corresponding to $\mathbf{D}_a = 0$. Focus in the present chapter is on stoichiometric ion exchange with mass action equilibrium and constant solution normality (in short CIE), see e.g.[28]. However, the solution strategy can also be applied to any other implicit sorption equilibria that can be represented by Eq. (2.55). In CIE, as mentioned in Section 2.1, a constant solution normality (2.29) and a fixed exchanger capacity (2.28) are assumed, which reduces the degrees of freedom of Eq. (4.1) by one and normalized concentrations (2.30) can be introduced. In normalized concentrations the model equations without physical dispersion read

$$\frac{\partial}{\partial t} (\mathbf{x} + \kappa\mathbf{y}(\mathbf{x})) + \frac{\partial \mathbf{x}}{\partial z} = 0, \quad \mathbf{x}, \mathbf{y} \in \mathbb{R}^{N-1} \quad (4.3)$$

with $\kappa = Fq_{\text{tot}}/c_{\text{tot}}$. For the sake of readability, the dimensional reference $N - 1$ of \mathbf{x}_{N-1} and \mathbf{y}_{N-1} is dropped. Recalling the summation conditions (2.31) for the \mathbf{x} and \mathbf{y} variables, only $N - 1$ equations of (4.3) are required. The equilibrium relations have to be reformulated accordingly. For CIE, we find $N - 1$ algebraic equations for $N - 1$ independent variables in \mathbf{x} and \mathbf{y} , respectively

$$\tilde{K}_{iN} = \left(\frac{y_i}{x_i} \right)^{\mu_i} \left(\frac{x_N}{y_N} \right)^{\mu_N} = \text{const}, \quad i = 1, \dots, N - 1. \quad (4.4)$$

for any reference component 'N'.

For equal $\mu_i = \mu_N = \mu$ for all $i = 1, \dots, N - 1$ we obtain constant separation factors \varkappa_{iN} according to

$$\varkappa_{iN} = \left(\frac{y_i}{x_i} \right) \left(\frac{x_N}{y_N} \right) = \tilde{K}_{iN}^{\frac{1}{\mu}} = \text{const}, \quad (4.5)$$

and Eq. (4.4) can be solved explicitly for

$$y_i = \frac{\varkappa_{iN} x_i}{1 + \sum_{k=1}^{N-1} (\varkappa_{kN} - 1) x_k}. \quad (4.6)$$

If the genuine ionic charges of the different species are not equal, the separation factors are no longer constant and Eqs. (4.4) represents a set of $N - 1$ implicit

algebraic equations to calculate the y_i 's from the x_i 's. These equations can be put to the form

$$0 = f_i(\mathbf{y}, \mathbf{x}) = 1 - \frac{1}{\tilde{K}_{iN}} \cdot \left(\frac{y_i}{x_i}\right)^{\mu_i} \left(\frac{x_N}{y_N}\right)^{\mu_N}, \quad i = 1, \dots, N-1. \quad (4.7)$$

Alternatively, we may reformulate Eqs. (2.27,2.28) as a single implicit equation and a set of $N-1$ explicit equations [83]. However, in view of applicability to other implicit sorption equilibria, formulation (4.7) is used in the remainder.

For an efficient numerical solution of the model equations (4.3) for the packed bed sorber, the dimensionless quantity

$$\mathbf{w} = \mathbf{x} + \kappa \mathbf{y}(\mathbf{x}), \quad (4.8)$$

which reflects the joint capacity of the fluid and the sorbed phase in Eq. (4.3) (similar to Eq. (3.1)), is introduced. Note, that \mathbf{w} could be normalized by division with $1 + \kappa$, which however has no effect on the general procedure and is therefore not considered here. In terms of \mathbf{w} and \mathbf{x} the model equations can now be reformulated as

$$\frac{\partial \mathbf{w}}{\partial t} + \frac{\partial \mathbf{x}}{\partial z} = \mathbf{0}, \quad (4.9a)$$

$$\mathbf{0} = \mathbf{f} \left(\mathbf{x}, \mathbf{y} = \frac{\mathbf{w} - \mathbf{x}}{\kappa} \right), \quad (4.9b)$$

which are solved simultaneously for \mathbf{w} and \mathbf{x} using MOL, which leads to a system of differential equations and implicit algebraic equations with differential index one allowing application of ODE15s in Matlab[69]. For a discussion of the differential index, the reader is referred to Appendix B.

Since focus is on Riemann problems with piece-wise constant initial and boundary conditions, consistent initial conditions are easily calculated with an offline evaluation of the sorption equilibrium (4.7) for given fluid phase composition \mathbf{x} .

Similar to the solution strategy in Section 3.2, main advantage of the present solution strategy is that we avoid explicit differentiation of the sorption isotherm in formulation (4.9a), (4.9b) compared to the standard formulations (4.1), (2.55).

4.3 Equilibrium Theory

As well as Eq. (2.3), Eq. (4.3) represents a system of first-order quasilinear partial differential equations, which is shown to be strictly hyperbolic. Therefore, it can also be solved (semi-) analytically for piece-wise constant initial and boundary conditions using the MOC. For this purpose Eq. (4.3) is rewritten as

$$\frac{\partial \mathbf{x}}{\partial t} + \left(\mathbf{I}_{N-1} + \kappa \frac{\partial \mathbf{y}}{\partial \mathbf{x}} \right)^{-1} \frac{\partial \mathbf{x}}{\partial z} = \mathbf{0}, \quad (4.10)$$

similar to Eq. (2.6). Here, \mathbf{I}_{N-1} is the $(N-1) \times (N-1)$ identity matrix. In contrast to previous work [83, 27, 50, 28] so called 'adjusted' times and velocities are omitted in this model formulation for the clarity of presentation.

In the remainder it will be shown that the solution of system (4.3) and (4.10) in conjunction with Riemann boundary and initial conditions consist of simple waves, shocks, or contact discontinuities.

Recalling Eq. (2.45), any concentration of a smooth transition is traveling with characteristic velocity $\tilde{\lambda}_k$ corresponding to the eigenvalues of matrix $(\mathbf{I}_{N-1} + \kappa \frac{\partial \mathbf{y}}{\partial \mathbf{x}})^{-1}$ in Eq. (4.10)

$$\tilde{\lambda}_k = \frac{1}{1 + \kappa \lambda_k}, \quad (4.11)$$

where the λ 's are the eigenvalues of $\frac{\partial \mathbf{y}}{\partial \mathbf{x}}$.

From implicit differentiation of Eq. (4.7) we obtain similar to Eq. (2.56)

$$\frac{\partial \mathbf{y}}{\partial \mathbf{x}} = - \left(\frac{\partial \mathbf{f}}{\partial \mathbf{y}} \right)^{-1} \frac{\partial \mathbf{f}}{\partial \mathbf{x}}, \quad (4.12)$$

with

$$- \frac{\partial \mathbf{f}}{\partial \mathbf{y}} = \text{diag}_{N-1} \left(\frac{\mu_i}{y_i} \right) + \mathbf{1}_{N-1} \frac{\mu_N}{y_N}, \quad (4.13a)$$

$$\frac{\partial \mathbf{f}}{\partial \mathbf{x}} = \text{diag}_{N-1} \left(\frac{\mu_i}{x_i} \right) + \mathbf{1}_{N-1} \frac{\mu_N}{x_N}, \quad (4.13b)$$

where $\text{diag}_{N-1}(z_i)$ stands for the $(N-1) \times (N-1)$ diagonal matrix with elements z_i , $\forall i = 1, \dots, N-1$ and $\mathbf{1}_{N-1}$ is a $(N-1) \times (N-1)$ matrix where all entries are equal to one. With this, the characteristic equation for the calculation of the eigenvalues λ_k can be written as

$$0 = \det \left(\frac{\partial \mathbf{y}}{\partial \mathbf{x}} - \lambda_k \mathbf{I}_{N-1} \right) \quad (4.14a)$$

$$= \det \left(- \frac{\partial \mathbf{f}}{\partial \mathbf{x}} - \lambda_k \frac{\partial \mathbf{f}}{\partial \mathbf{y}} \right) \quad (4.14b)$$

$$= \det \left(\text{diag}_{N-1} \left(\frac{\mu_i}{x_i} - \lambda_k \frac{\mu_i}{y_i} \right) + \mathbf{1}_{N-1} \left(\frac{\mu_N}{x_N} - \lambda_k \frac{\mu_N}{y_N} \right) \right) \quad (4.14c)$$

For $\lambda_k \neq \frac{y_i}{x_i}$ the characteristic equation can be expanded into

$$0 = \sum_{i=1}^N \frac{1}{x_i - \lambda_k \frac{y_i}{x_i}}, \quad (4.15)$$

which has $N-1$ real and distinct roots in the intervals

$$\frac{y_1}{x_1} > \lambda_1 > \frac{y_2}{x_2} > \dots > \frac{y_k}{x_k} > \lambda_k > \frac{y_{k+1}}{x_{k+1}} > \dots > \frac{y_{N-1}}{x_{N-1}} > \lambda_{N-1} > \frac{y_N}{x_N} \quad (4.16)$$

if the components are ordered in decreasing selectivity for the solid phase.

For $\lambda_k = \frac{y_i}{x_i}$ we find from Eq. (4.14c) $\lambda_k = \frac{y_i}{x_i} = \frac{y_N}{x_N}$ for any reference component 'N'. If the above ordering of components is applied, this is only possible between neighboring components undergoing a selectivity reversal with indices i, N being equal to $k, k+1$. In view of Eq. (4.7) we find that the characteristic velocity is constant along the selectivity reversal according to

$$\lambda_k = \frac{y_k}{x_k} = \frac{y_{k+1}}{x_{k+1}} = \tilde{K}_{k,k+1}^{\frac{1}{\mu_k - \mu_{k+1}}} \quad (4.17)$$

giving rise to a contact discontinuity, see Eq. (2.51b).

The image of the smooth transitions in the concentration phase space is given by the corresponding (right) eigenvectors \mathbf{r}_k . For $\lambda_k \neq \frac{y_k}{x_k}$ the eigenvectors follow from

$$0 = \left(\frac{\mu_i}{x_i} - \lambda_k \frac{\mu_i}{y_i} \right) r_{k,i} + \left(\frac{\mu_N}{x_N} - \lambda_k \frac{\mu_N}{y_N} \right) \sum_{m=1}^{N-1} r_{k,m}, \quad \forall i = 1, \dots, N-1. \quad (4.18)$$

In view of the characteristic equation (4.15) an obvious choice to satisfy this equation is

$$\mathbf{r}_k = \left[\frac{1}{\frac{\mu_1}{x_1} - \lambda_k \frac{\mu_1}{y_1}}, \dots, \frac{1}{\frac{\mu_{N-1}}{x_{N-1}} - \lambda_k \frac{\mu_{N-1}}{y_{N-1}}} \right]^T. \quad (4.19)$$

For the selectivity reversal with $\lambda_k = \frac{y_k}{x_k}$ we find

$$\mathbf{r}_k = [0, \dots, 0, r_{k,k} = 1, r_{k,k+1} = -1, 0, \dots, 0]^T, \quad k = 1, \dots, N-1 \quad (4.20)$$

corresponding to a straight line along which all concentrations are constant except for components 'k' and 'k+1'. In case of a ternary system, the two possible selectivity reversal lines defined by $[1, -1]$ and $[0, 1]$ are parallel to the $x_3 = 1 - x_1 - x_2 = 0$ -line and the x_2 -axis, respectively.

Using the above expressions for λ_k and \mathbf{r}_k , it can be proven that the characteristic velocity along the k-th characteristic is changing monotonically for $\lambda_k \neq \frac{y_k}{x_k}$ according to

$$\nabla \lambda_k \mathbf{r}_k \neq 0. \quad (4.21)$$

Note, the proof of Eq. (4.21) is merely a special case of the proof presented in Appendix C. Similar results were reported by [84] for stoichiometric ion exchange without selectivity reversals.

Related to the spatial coordinate z , for simple waves the characteristic velocity $\tilde{\lambda}_k$ is monotonically increasing in the direction of increasing z (see Eq. (2.46,2.47)), whereas for shock waves the velocity \tilde{s}_k is monotonically decreasing in the direction of increasing z (see Eq. (2.49)). The shock velocity \tilde{s}_k follows from the integral

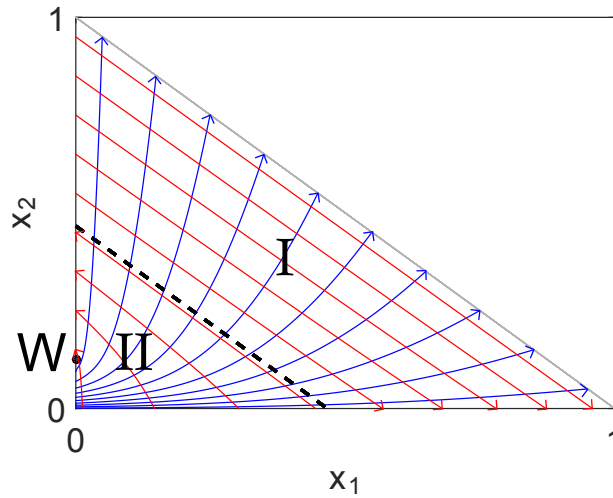


Figure 4.1: Concentration phase space of the first example system with one selectivity reversal.

material balances across the shock also known as the Rankine Hugoniot conditions (2.39), which is in similar form to Eq. (4.11)

$$\tilde{s}_k = \frac{1}{1 + \kappa \frac{\Delta y_i}{\Delta x_i}}, \forall i = 1, \dots, N - 1. \quad (4.22)$$

These equations also define the image of the shock waves in the concentration phase space, similar to the eigenvectors introduced above. In general, eigenvectors and shock curves are tangent to each other. For $\mu_i = \mu_N$ for all $i = 1, \dots, N - 1$, corresponding to the case of constant separation factors, both types of curves are straight lines and coincide. For $\mu_i \neq \mu_N$ they are curved and therefore different, but still close in the cases to be discussed subsequently, so that the following qualitative discussion will be based on the path grid of the eigenvectors only. However, existence of the different wave solutions was also checked on a rigorous basis using entropy conditions (2.50).

4.4 Results

A ternary example, with one selectivity reversal indicated by the dashed line is shown in Fig. 4.1. Corresponding parameters are given in Tab. 4.1. In Region I component 1 is stronger sorbed, whereas in Region II component 2 is stronger sorbed. The red curves were calculated from the eigenvector \mathbf{r}_1 corresponding to the eigenvalue λ_1 , which satisfies $\lambda_1 > \lambda_2$. Since the characteristic speed in Eq. (4.11) depends on the reciprocal of the λ 's, the eigenvector \mathbf{r}_1 represents the family of slow waves. The arrows are pointing in the direction of increasing characteristic

parameter	value	description
L	15.0	column length
N_z	750	number of grid points
u	1.0	interstitial velocity
ϵ	0.5	void fraction
c_{tot}	1.0	solution normality
q_{tot}	2.0	exchanger capacity
K_{13}	4.0	equilibrium constant
K_{23}	2.67	equilibrium constant
μ_1	2	stoichiometric factor
μ_2	1	stoichiometric factor
μ_3	1	stoichiometric factor

Table 4.1: Parameters of the first example system with one selectivity reversal.

velocity. The orientation of the red curves is reverted from Region I to Region II, whereas the orientation of the blue curves is uniform in the whole composition space. The characteristic velocity along the selectivity reversal is constant as discussed in the previous section. Point W represents a watershed point where the eigenvalues coincide. According to Appendix I this can only happen on the boundary of the concentration triangle.

In the remainder different characteristic scenarios are discussed. For all loading and regeneration scenarios, the numerical plateau values in the profiles are identical with equilibrium theory solutions in the concentration phase. Wave profiles depend on the number of grid points but show very similar behavior as predicted by the equilibrium theory. First focus is on the loading of an empty bed with a feed in Region I as shown in Fig. 4.2. Feed and initial composition are represented by points C^F and C^i in Fig. 4.2a. The solution consists of a shock wave S_1 corresponding to the path C^F - C^{P_1} in Fig. 4.2a and a shock wave S_2 corresponding to the path C^{P_1} - C^i in Fig. 4.2a. Corresponding simulation results using backward differences with 750 equidistant grid points are shown in Fig. 4.2b. The behavior shown in Fig. 4.2 is similar to a system with constant separation factors or a Langmuirian system with component 1 being the stronger sorbed component. It shows the characteristic intermediate plateau for the weaker sorbed component with increased composition compared to the adjacent plateaus of the feed and the initial conditions.

The situation is reverted for a loading of an empty bed with feed in Region II as illustrated in Fig. 4.3. Here, the behavior is similar to a system with constant separation factors or a Langmuirian system with component 2 being the stronger sorbed component and is therefore some sort of mirror image of the situation in Fig. 4.2.

The limiting case with a feed composition on the selectivity reversal is shown

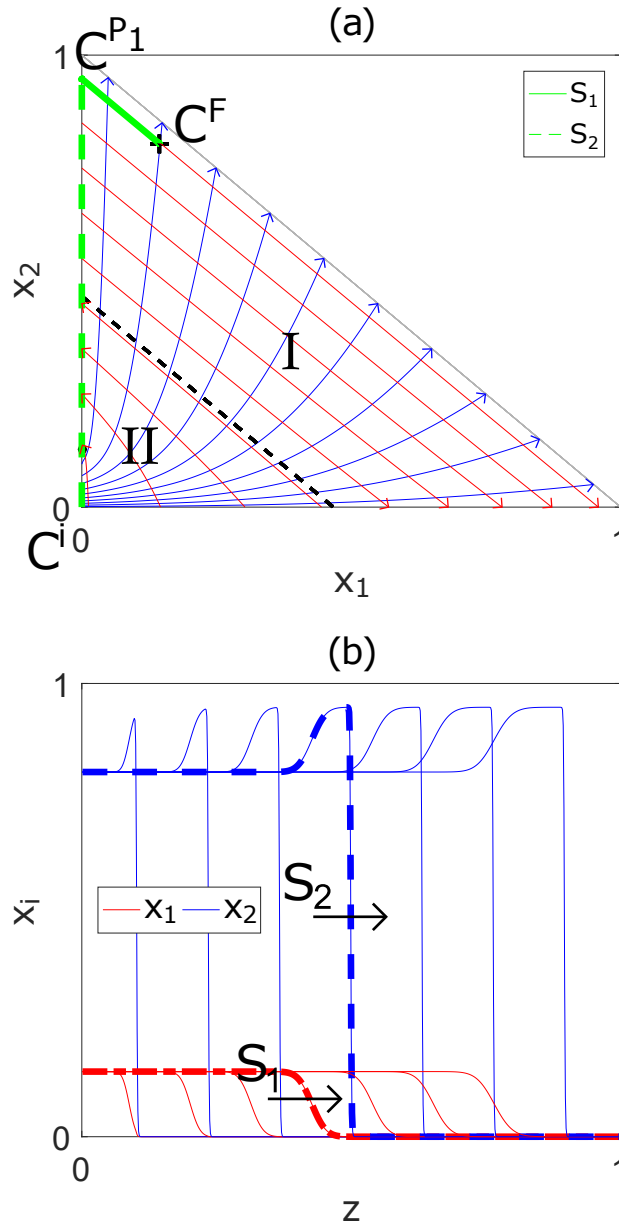


Figure 4.2: (a) Solution in the concentration phase space for the loading of an empty bed with point C^F defined by $\mathbf{c}_{\text{feed}} = [0.1437, 0.8046]^T$ in I. (b) Corresponding spatial profiles $x_i(z)$ at different time points with.

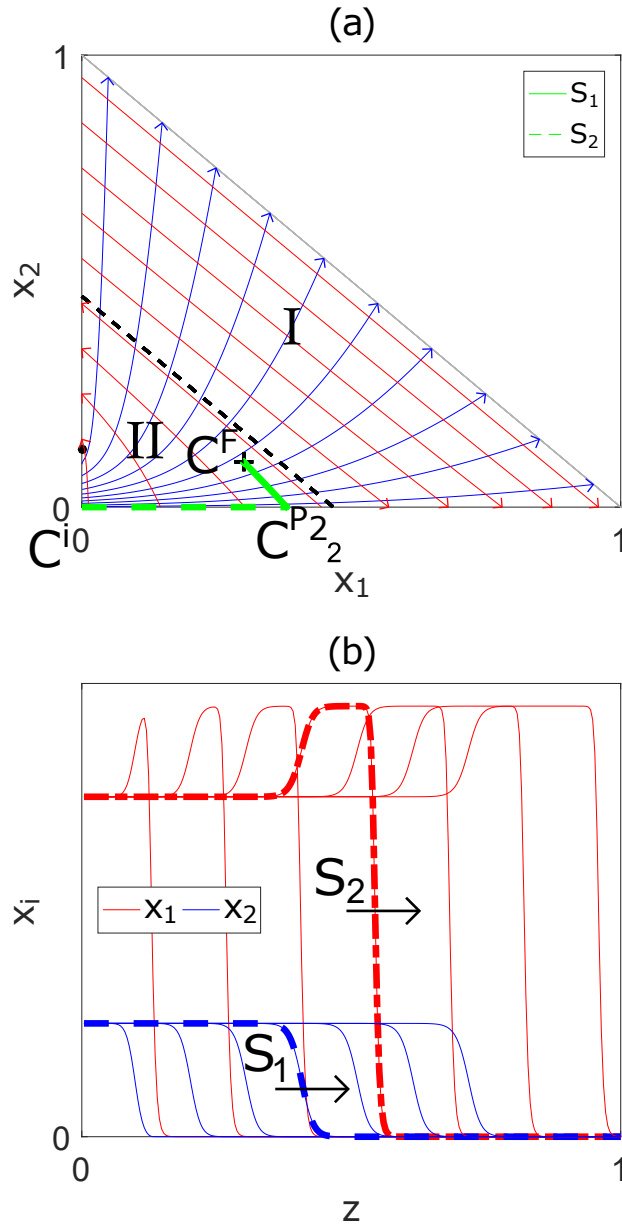


Figure 4.3: (a) Solution in the concentration phase space for the loading of an empty bed with point C^F defined by $\mathbf{c}_{\text{feed}} = [0.3, 0.1]^T$ in II. (b) Corresponding spatial profiles $x_i(z)$ at different time points.

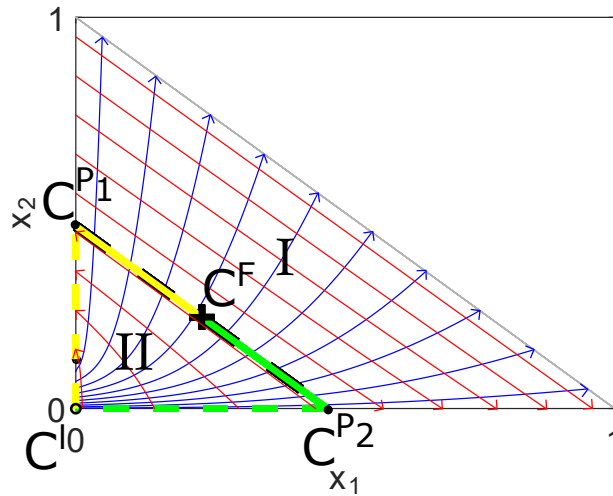


Figure 4.4: Two possible solutions in the concentration phase space for the loading of an empty bed with point C^F defined by $\mathbf{c}_{\text{feed}} = [7/30, 7/30]^T$ on the selectivity reversal.

in Fig. 4.4. Here, the shock velocities for the shocks $C^{P1}-C^i$ and $C^{P2}-C^i$ along the x_1 and the x_2 axis coincide with the constant characteristic velocity along the selectivity reversal. Hence, both solutions $C^F-C^{P1}-C^i$ and $C^F-C^{P2}-C^i$ are feasible in the sense of Eq. (2.52). It can be further shown, that any other point on the selectivity reversal is connected to the origin by a shock wave with the same velocity like the shocks $C^{P1}-C^i$, and $C^{P2}-C^i$ leading to a whole spectrum of possible solutions. For this singular case, uniqueness cannot be obtained through entropy conditions alone. Similar phenomena were reported in [85, 51] for distillation processes. Which one of these solutions is obtained in simulation depends on the intrinsic stability of the different wave solutions and on numerical dispersion, which is introduced by discretization. A simulation example with 200 and 2000 grid points is shown in Fig. 4.5. A rigorous mathematical stability analysis of the underlying partial differential equations with dispersion is challenging and clearly beyond the scope of this work.

From the practical point of view, Fig. 4.4 represents a singular situation which nicely explains the transition between the two different patterns in Figs. 4.2 and 4.3 but can not be observed as such in practice due to fluctuations.

Next focus is on chromatographic cycles, which were also not addressed in the classical literature [27, 50, 28]. The chromatographic cycle corresponds to a pulse disturbance, consisting of the loading of an empty bed in the front followed by the regeneration of the loaded bed in the rear.

A first scenario with a feed in Region I is shown in Figure 4.6a. The loading in the front corresponds to Fig. 4.2. It consists of two shocks, with a band of pure component 2 in the front, which is the weaker sorbed component in Region

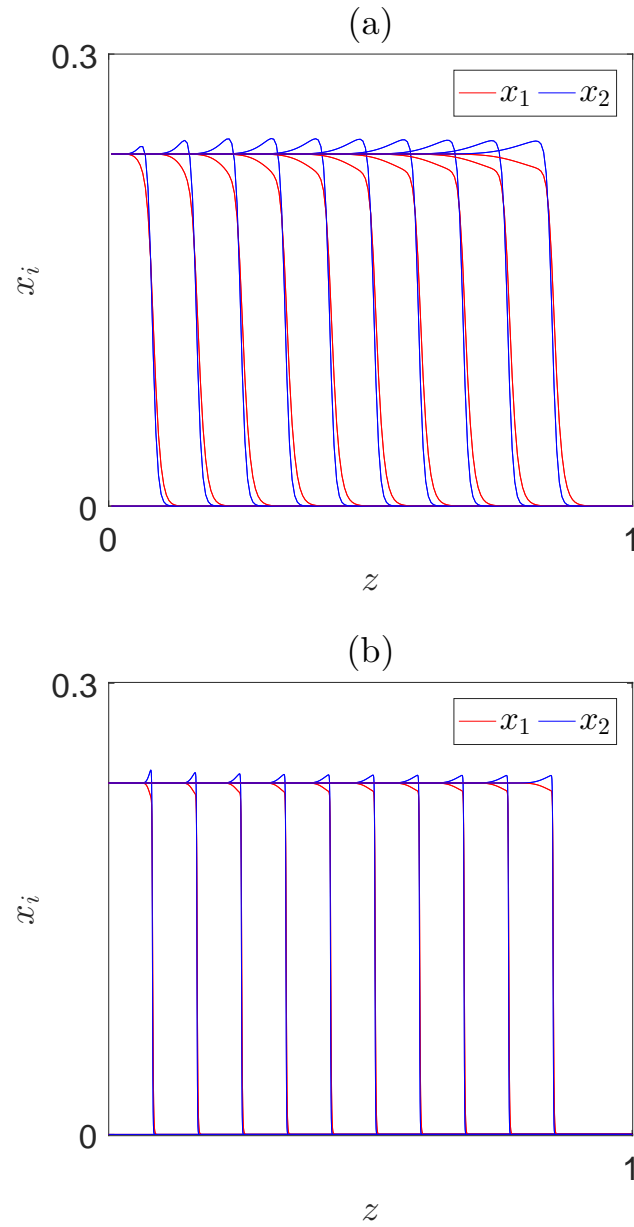


Figure 4.5: Numerical simulation with (a) 200 and (b) 2000 grid points for a feed on the selectivity reversal at C^F defined by $\mathbf{c}_{\text{feed}} = [7/30, 7/30]^T$ corresponding to Fig. 4.4

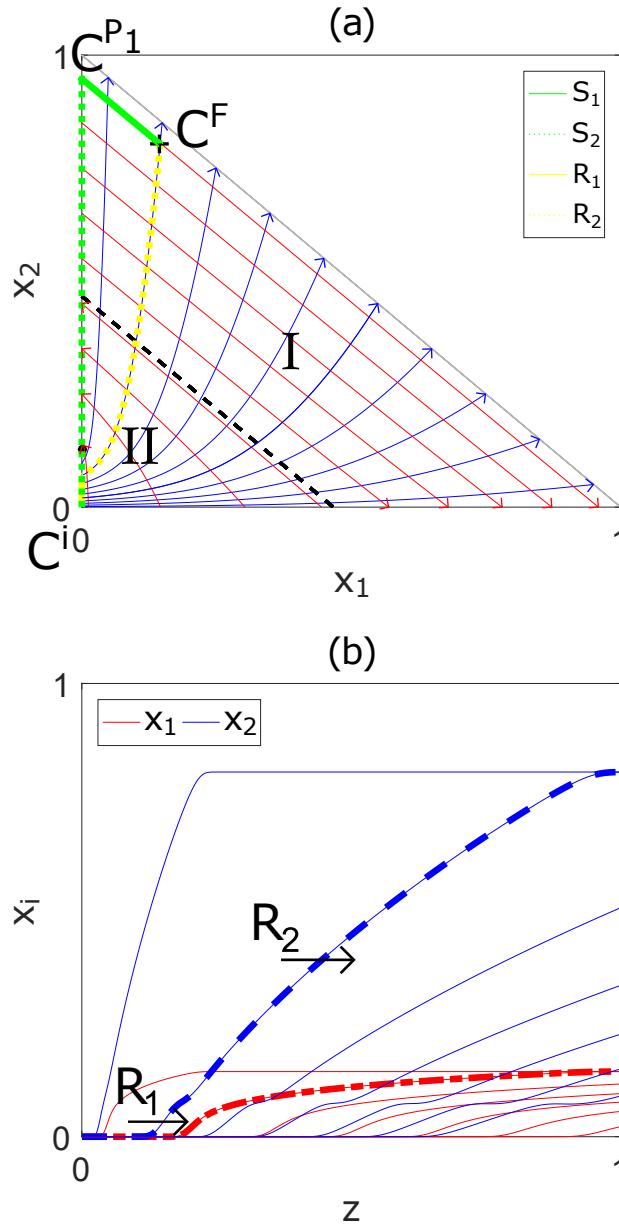


Figure 4.6: (a) Chromatographic cycle in the concentration phase space for C^F defined by $\mathbf{c}_{\text{feed}} = [0.1437, 0.8046]^T$ in I. (b) Corresponding spatial regeneration profiles $x_i(z)$ at different time points.

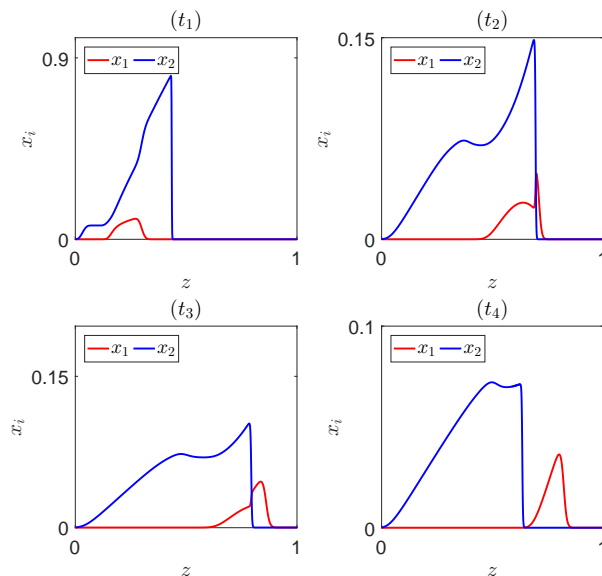


Figure 4.7: Spatial profiles at different time points for a pulse injection with plateau at C^F defined by $\mathbf{c}_{\text{feed}} = [0.1437, 0.8046]^T$ in I (see also Fig. 4.6a).

I. The regeneration consists two simple waves R_1 and R_2 illustrated in yellow in Fig. 4.6a. Due to the special topology of the path grid R_1 coincides with the x_2 axis generating also a band of pure component 2 in the rear. Corresponding simulation results for the regeneration are shown in Fig. 4.6b. Together with the corresponding loading profiles in Fig 4.2b, the complete cycle can be reconstructed. After interaction of the different fronts the pattern will be resolved in two pure component pulses with pure component 1 in the front and pure component 2 in the rear as shown in Fig. 4.7. This is due to the fact that during wave interactions the selectivity reversal is crossed and the final resolution is taking place in Region II, where component 1 is the weaker sorbed component.

This is also confirmed with a second scenario with feed in Region II, which is illustrated in Figure 4.8. Loading in the front corresponds to the previous Fig. 4.3 consisting of two shock waves with a band of pure component 1 in the front which is the weaker sorbing component in Region II. Regeneration in the rear consists of two simple waves R_1 and R_2 illustrated in yellow in Fig. 4.8a. Again, simulation results for the regeneration that are shown in Fig. 4.8b can be used to obtain the complete cycle with the loading profiles of Fig. 4.3b. The topology of the concentration phase in II is simpler than in I and more similar to a Langmuirian system, leading to a band of pure component 2 in the rear. After elementary interaction of the different fronts the pattern will be resolved in two pure component pulses, as shown in Fig. 4.9, with pure component 1 in the front and pure component 2 in the rear like in the previous case. This clearly shows that

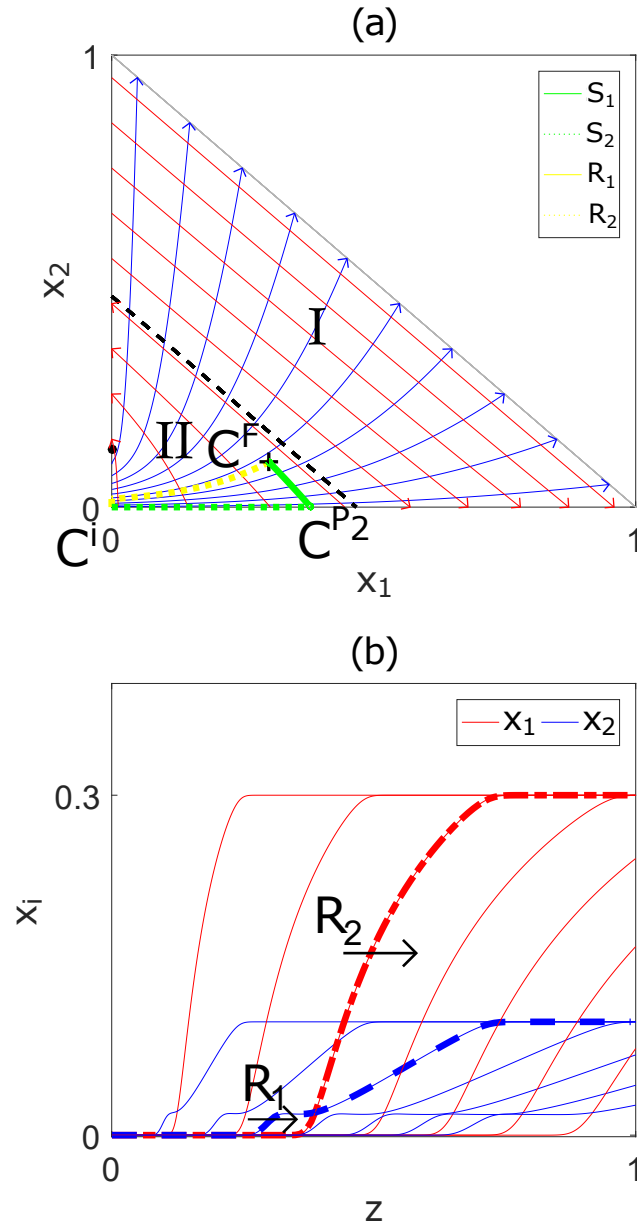


Figure 4.8: (a) Chromatographic cycle in the concentration phase space for C^F defined by $c_{\text{fed}} = [0.3, 0.1]^T$ in II. (b) Corresponding spatial regeneration profiles $x_i(z)$ at different time points.

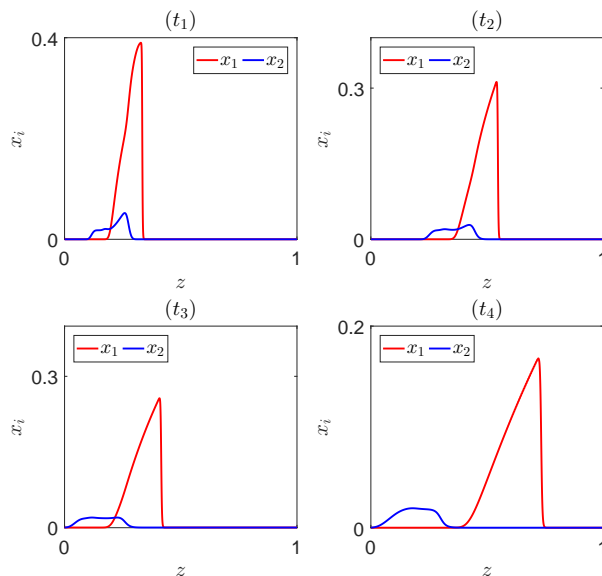


Figure 4.9: Spatial profiles at different time points for a pulse injection with plateau at C^F defined by $\mathbf{c}_{\text{feed}} = [0.3, 0.1]^T$ in II (see also Fig. 4.8a).

the influence of the selectivity reversal strongly depends on the mode of operation. For the step inputs in Figs. 4.2 and 4.3 qualitatively different final patterns were obtained, whereas for the pulse inputs only the transients were different but those were then resolved in similar final patterns.

Like in Fig. 4.4 multiple solutions with respect to Eq. (2.52) are also possible for the chromatographic cycle if the feed composition is located on the selectivity reversal as shown in Fig. 4.10. Following the argumentation above any solution will be resolved in the same final pattern.

Additional features can occur in systems with multiple selectivity reversals as illustrated with an example in Fig. 4.11. Parameters are given in Tab. 4.2. Like in the previous case, a selectivity reversal between components 1 and 2 is observed at the boundary between Regions I and II. In addition, a selectivity reversal between components 2 and 3 occurs at the boundary between Regions I and III. An interesting feature which was also reported by [27, 50] is the occurrence of wave patterns with more than $N - 1$ wave fronts as illustrated in Fig. 4.11, which is not the case if C^F and C^i are interchanged. This theoretical prediction could also be validated with the new numerical approach presented in this chapter as illustrated in Fig. 4.11b. For better resolution 1000 equidistant grid points were used in Fig. 4.11b.

Finally, it should be mentioned that generally the existence theorem for simple wave, shock, or contact discontinuity solutions is confined to local situations [62], where points C^F and C^i would be required to be sufficiently close. However in

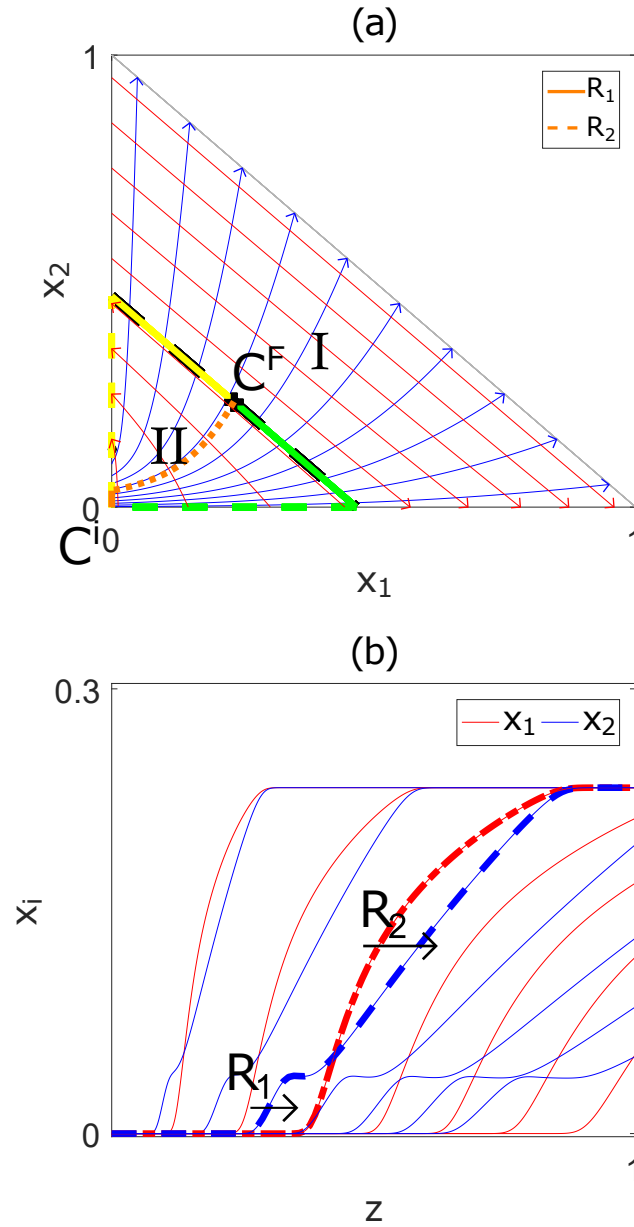


Figure 4.10: (a) Two possible chromatographic cycles in the concentration phase space for C^F defined by $\mathbf{c}_{\text{feed}} = [7/30, 7/30]^T$ on the selectivity reversal. (b) Corresponding spatial regeneration profiles $x_i(z)$ at different time points.

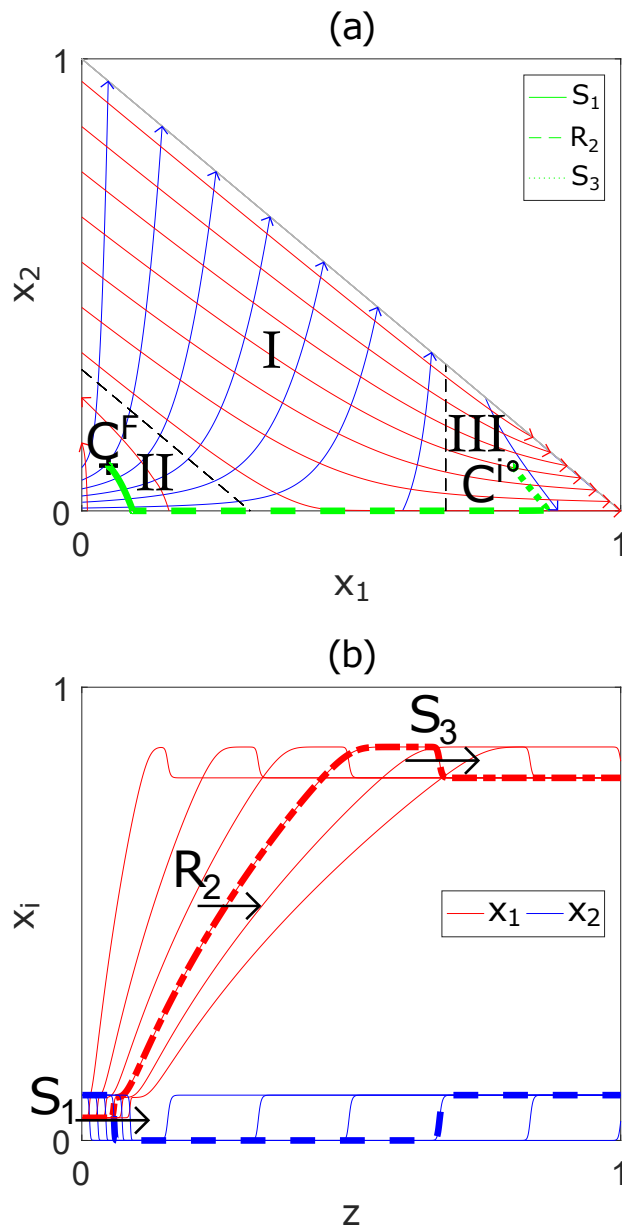


Figure 4.11: (a) Concentration phase space of the second example system with two selectivity reversals including a path from C^F defined by $\mathbf{c}_{\text{feed}} = [0.05, 0.1]^T$ to C^i defined by $\mathbf{c}_{\text{init}} = [0.8, 0.1]^T$. (b) Corresponding spatial profiles $x_i(z)$ at different time points.

parameter	value	description
L	20.0	column length
N_z	1000	number of grid points
u	1.0	interstitial velocity
ϵ	0.5	void fraction
c_{tot}	0.01	solution normality
q_{tot}	2.0	exchanger capacity
K_{13}	100.0	equilibrium constant
K_{23}	14.88	equilibrium constant
μ_1	4	stoichiometric factor
μ_2	1	stoichiometric factor
μ_3	4	stoichiometric factor

Table 4.2: Parameters of the second example system with two selectivity reversals.

this case, limitations due to the local restriction of the implicit function theorem are not present. For details, the reader is referred to Appendix I.

4.5 Summary

An efficient method for the numerical solution of equilibrium models of fixed bed sorbers with implicit sorption isotherms was presented. Application was demonstrated using the CIE with possible selectivity reversals. The effect of selectivity reversals on process operation was studied systematically using a combined numerical, analytical approach. Besides the validation of the new numerical approach also interesting patterns of behavior were found complementing previous studies for this particular kind of system.

This page intentionally left blank.

Chapter 5

Advanced Ion Exchange (AIE)

This chapter including Appendix C-Appendix G was in parts published in Chemical Engineering Science, 199, M. Fechtner and A. Kienle, Equilibrium theory of ion exchange chromatography with variable solution normality and steric hindrance, 508–527 (2019).

5.1 Introduction

In this chapter, the equilibrium theory to the ideal model (2.4 or 2.6) of packed bed sorbers is extended to a more general class of advanced ion exchange (AIE) processes with an implicit sorption isotherm described by the SMA (2.33,2.35). As stated in the preceding chapter, CIE [27, 50, 28] assumes constant ionic strength and neglects steric effects. However, variable ionic strength plays an important role in gradient and displacement chromatography, which are frequently applied to enhance the separation of molecules with similar properties [6, 38, 32]. Further, steric effects play an important role for larger molecules such as proteins encountered in many bio separations [5, 60]. Therefore, the objective of the present chapter is to extend equilibrium theory for CIE to processes with variable ionic strength and to account for steric effects by using the well known SMA. Consequently, the extension in this chapter inherits also the limiting assumptions of the SMA, most notably the lack of accounting for a variation in pH or a variable exchanger capacity based on the dissociation of weak acid functional groups in the solid phase. Contributions that provide a local equilibrium model for these cases, which are not considered here, are for example [56] and [55], respectively.

Past attempts to apply the method of characteristics in ion exchange chromatography using the SMA were performed in [6] for binary mixtures and isocratic elution as well as in [31] for binary mixtures and linear salt gradients. Further extensions of the equilibrium theory to ternary systems for monovalent species [53] or related to step gradient conditions [54] for binary mixtures were also presented. However, past contributions do not provide the rigorous application of the equilibrium theory to arbitrary N component systems using the SMA with

variable solution normality.

In the following, the theory is developed step by step, and the relation to the previous findings for the CIE is established. For illustration purposes of the different effects, three different application examples are considered afterwards. Analytical results are validated through comparison with numerical simulation. For this purpose, the solution strategy introduced in Section 4.2 is extended to the SMA, which is briefly discussed in the subsequent section. In order to demonstrate further the flexibility of the numerical solution approach, it is also shown to be applicable to arbitrary boundary conditions.

5.2 Extension of the Solution Strategy

The following is based on the ideal model (2.3) of chromatography

$$\frac{\partial}{\partial t} (\mathbf{c} + F\mathbf{q}(\mathbf{c})) + \frac{\partial \mathbf{c}}{\partial z} = 0, \quad \mathbf{c}, \mathbf{q} \in R^N, \quad (5.1)$$

again with dimensionless time $t = t^*u/L$ and space $z = z^*/L$ coordinate.

The sorption isotherm of stoichiometric ion exchange follows from the mass action law according to Eq. (2.33). In general component 'N' is usually a simple ionic component. However it can be any kind of reference ion. In order to emphasize its special role in the present chapter, component 'N' is denoted as the salt, which is used to change the sorption behavior of all other components. For constant solution normality \tilde{c}_{tot} , the salt concentration is not independent anymore but follows from $c_N = \tilde{c}_{\text{tot}} - \sum_{i=1}^{N-1} \frac{c_i}{\nu_i}$, which is not the case in this chapter. Thus, the solution normality can change. Typically, ν_N is equal to one. However, for generality the following development is not restricted to this case. Accordingly, q_N is the salt load of the solid phase or the free accessible salt load of the solid phase in case of steric hindrance by the other molecules. For fixed ion exchanger capacity q_{tot} , the salt load q_N follows from Eq. (2.35). For negligible steric effects $p_i = 0$, the corresponding generalized factor ξ_i defined in Eq. (2.35) reduces to $\xi_i = 1/\nu_i$. This applies in particular to the salt, i.e. $p_N = 0$, also in the presence of steric hindrance by the other molecules.

In the general case of unequal characteristic charges of the different ions, Eqs. (2.33), (2.35) represent a system of implicit algebraic equations, which will be denoted

$$0 = f_i(\mathbf{q}, \mathbf{c}) = \frac{1}{K_{iN}} \cdot \left(\frac{q_i}{c_i} \right)^{\nu_i} \left(\frac{c_N}{q_N} \right)^{\nu_N} - 1, \quad \forall i = 1, \dots, N-1, \quad (5.2a)$$

$$0 = f_N(\mathbf{q}) = \sum_{i=1}^N \xi_i q_i - q_{\text{tot}} \quad (5.2b)$$

in the following.

For an efficient numerical solution of the model equations, Eqs. (5.1) and (5.2) are used in combination with the solution strategy introduced in Section 4.2. The extension of the solution strategy to the SMA is straight forward. Again, this strategy comprises a reformulation of the model equations by introducing variable $\mathbf{v} = \mathbf{c} + F\mathbf{q}(\mathbf{c})$, a discretization of the resulting equations using MOL with finite differences and a subsequent simultaneous solution of the resulting DAE system applying standard DAE numerics. Note, vector $\mathbf{v} \in \mathbb{R}^N$ includes the joint capacities of all components. For demonstration purposes, simple first-order backward differences based on an equidistant grid with $N_z = 1000$ spatial grid points are used here as well. The corresponding DAE system is solved with ODE15s in MATLAB[®] [69].

Utilizing the same line of arguments as introduced in Section 4.2 and the spectral properties to be discussed in the next section, it can be shown that the differential index of the resulting DAE system is always equal to one, which, as we already know, alleviates the numerical solution considerably. The proof is almost identical to the one presented in Appendix B and therefore omitted.

One of the additional advantages of the numerical solution strategy from Section 4.2 is its flexibility and simplicity of implementation. In particular, it is straight forward to implement any type of boundary conditions. This is important since many applications use (linear) gradient elution. For a proof of principle, the results reported in [6] Fig. 5.1b with parameters in Tab. 2 are reproduced. The objective of this example is the separation of three proteins. For this purpose, a column is equilibrated with 30 *mM* of the salt (NaCl). A feed is injected containing 30 *mM* sodium and 0.2 *mM* of each protein (chymotrypsinogen A, cytochrome c, lysozyme) for 254.47 *s*. The feed is then changed to contain sodium only. In addition to the 30 *mM* NaCl, a linear gradient of 0.19649 $\frac{mM}{s}$ further increases its feed concentration over time. The separation result, which is in very good agreement with the results in [6], is shown in Fig. 5.1.

Finally, it is important to note that instead of the N component material balances of Eq. (5.1) we may also use only $N - 1$ component material balances together with some sort of total material balance that is obtained through multiplication of the component material balances with factors ξ_i and summation over all components. Introducing

$$c_{\text{tot}} = \sum_{i=1}^N \xi_i c_i, \quad (5.3)$$

we find in view of Eq. (2.35)

$$\frac{\partial c_{\text{tot}}}{\partial t} + \frac{\partial c_{\text{tot}}}{\partial z} = \mathbf{0}. \quad (5.4)$$

It should be noted that c_{tot} is generally *not* the total solution normality, which would be $\sum_{i=1}^N c_i/\nu_i$, but some formal equivalent to q_{tot} in Eq. (2.35). In the

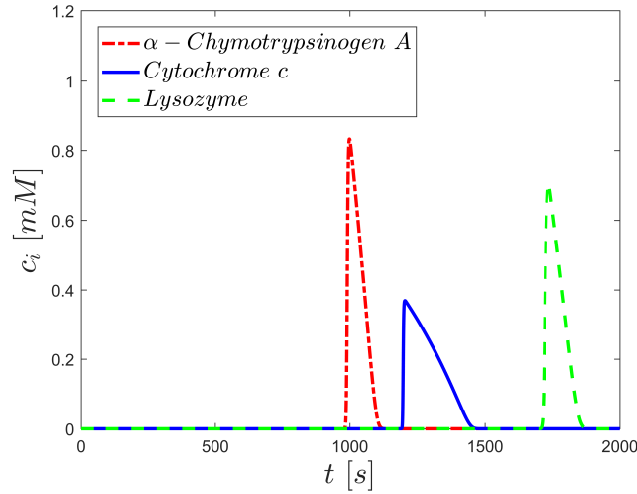


Figure 5.1: Protein separation with linear salt gradient $0.19649 \frac{mM}{s}$.

remainder of this chapter, c_{tot} is called the modified solution normality. Modification is due to factors p_i as in (2.35) accounting for steric hindrance. If this steric hindrance is absent, the modified solution normality coincides with the total solution normality, i.e. the latter is simply a special case included in the modified solution normality.

Eq. (5.4) represents a linear transport equation. Since Eq. (5.4) is decoupled from the component material balances (5.1), c_{tot} depends only on the given boundary and initial conditions but not the component material balances, which proves to be numerically slightly more efficient. In contrast to this, the component material balances depend on the value of c_{tot} through the equilibrium relations (5.2), because of

$$c_N = \frac{c_{\text{tot}} - \sum_{i=1}^{N-1} \xi_i c_i}{\xi_N}. \quad (5.5)$$

The alternative model formulation (5.4) provides useful insight into the solution structures to be discussed in the next section. In view of Eqs. (5.1) and (5.4), any step change of the concentrations at the inlet are shown to be resolved into $N - 1$ transitions with $c_{\text{tot}} = \text{const}$ and a single transition ' N ' with variable c_{tot} . In other words the k th transitions with $k < N$ takes place on a specific c_{tot} hyperplane defined by (5.3). Further details will be discussed in the next section.

5.3 Equilibrium Theory

In the remainder we will develop the analytical solution of Eqs. (5.1,5.2) with Riemann conditions. In particular, we show that the system (5.1,5.2) is strictly

hyperbolic and either genuinely or linear degenerate except a special case of non-strict hyperbolicity, which is analyzed in Appendix H. Eq. (5.1) is rewritten in the following form

$$\frac{\partial \mathbf{c}}{\partial t} + \left(\mathbf{I}_N + F \frac{\partial \mathbf{q}}{\partial \mathbf{c}} \right)^{-1} \frac{\partial \mathbf{c}}{\partial z} = 0, \quad \mathbf{c}, \mathbf{q} \in R^N, \quad (5.6)$$

similar to Eq. (2.6a).

In the following, it will also be shown that contact discontinuities are either related to a selectivity reversal or a change of the solution normality. In contrast, simple waves and shocks will be shown to occur elsewhere on c_{tot} hyperplanes defined by Eq. (5.3) in the concentration phase space.

Similar to Eq. (2.45), the characteristic velocity $\tilde{\lambda}_k$ of a smooth transition follows from the eigenvalues of matrix $(\mathbf{I}_N + F \frac{\partial \mathbf{q}}{\partial \mathbf{c}})^{-1}$ in (5.6) according to

$$\tilde{\lambda}_k = \frac{1}{1 + F \lambda_k}. \quad (5.7)$$

Therein, the λ_k 's are the eigenvalues of the Jacobian matrix $\frac{\partial \mathbf{q}}{\partial \mathbf{c}}$. By implicit differentiation of Eq. (5.2) we find Eq. (2.56) with

$$-\frac{\partial \mathbf{f}}{\partial \mathbf{q}} = \begin{bmatrix} \text{diag}_{N-1} \left(-\frac{\nu_i}{q_i} \right) & \begin{matrix} \frac{\nu_N}{q_N} \\ \vdots \\ \frac{\nu_N}{q_N} \end{matrix} \\ -\xi_1 & -\xi_2 & \dots & -\xi_{N-1} & -\xi_N \end{bmatrix}, \quad (5.8a)$$

$$-\frac{\partial \mathbf{f}}{\partial \mathbf{c}} = \begin{bmatrix} \text{diag}_{N-1} \left(\frac{\nu_i}{c_i} \right) & \begin{matrix} -\frac{\nu_N}{c_N} \\ \vdots \\ -\frac{\nu_N}{c_N} \end{matrix} \\ 0 & \dots & \dots & \dots & 0 \end{bmatrix}, \quad (5.8b)$$

where diag_{N-1} denotes a $(N-1) \times (N-1)$ dimensional diagonal matrix with index $i = 1, \dots, N-1$. Hence, the eigenvalues λ_k follow from the characteristic equation

$$0 = \det \left(\frac{\partial \mathbf{q}}{\partial \mathbf{c}} - \lambda_k \mathbf{I}_N \right) \quad (5.9a)$$

$$= \det \left(-\frac{\partial \mathbf{f}}{\partial \mathbf{c}} - \lambda_k \frac{\partial \mathbf{f}}{\partial \mathbf{q}} \right) \quad (5.9b)$$

$$= \det \left(\begin{bmatrix} \text{diag}_{N-1} \left(\frac{\nu_i}{c_i} - \lambda_k \frac{\nu_i}{q_i} \right) & \begin{matrix} -\frac{\nu_N}{c_N} + \lambda_k \frac{\nu_N}{q_N} \\ \vdots \\ -\frac{\nu_N}{c_N} + \lambda_k \frac{\nu_N}{q_N} \end{matrix} \\ -\lambda_k \xi_1 & -\lambda_k \xi_2 & \dots & -\lambda_k \xi_{N-1} & -\lambda_k \xi_N \end{bmatrix} \right) \quad (5.9c)$$

For $\lambda_k \neq \frac{q_i}{c_i}$, the characteristic equation yields

$$0 = \left(\prod_{j=1}^{N-1} \frac{\nu_j}{c_j} - \lambda_k \frac{\nu_j}{q_j} \right) \left(-\lambda_k \xi_N - \sum_{i=1}^{N-1} -\frac{\lambda_k \xi_i}{\frac{\nu_i}{c_i} - \lambda_k \frac{\nu_i}{q_i}} \left(-\frac{\nu_N}{c_N} + \lambda_k \frac{\nu_N}{q_N} \right) \right) \quad (5.10)$$

or equivalently

$$0 = \lambda_k \sum_{i=1}^N \frac{\xi_i}{\frac{\nu_i}{c_i} - \lambda_k \frac{\nu_i}{q_i}}, \quad (5.11)$$

which has N non-negative and distinct roots

$$\frac{q_1}{c_1} > \lambda_1 > \frac{q_2}{c_2} > \dots > \frac{q_k}{c_k} > \lambda_k > \frac{q_{k+1}}{c_{k+1}} > \dots > \frac{q_{N-1}}{c_{N-1}} > \lambda_{N-1} > \frac{q_N}{c_N} > \lambda_N = 0 \quad (5.12)$$

implying hyperbolicity. In (5.12), the components are again ordered in decreasing affinity to the solid phase. Note, the selectivity order in (5.12) is valid only until the occurrence of a so-called reversal, which is discussed next.

For $\lambda_k = \frac{q_k}{c_k}$, we find from Eq. (5.9c) in view of the ordering introduced in Eq. (5.12) that λ_k also has to be equal to $\frac{q_{k+1}}{c_{k+1}}$ corresponding to a selectivity reversal $\frac{q_k}{c_k} = \frac{q_{k+1}}{c_{k+1}}$ for any $i = 1, \dots, N-1$. Even so two selectivities are equal, the eigenvalues in Eq. (5.12) remain obviously distinct, thus preserving the hyperbolicity also on the reversal. The existence and topology of such selectivity reversals in CIE was studied intensively in Section 4.3. In this section, results will be extended to variable solution normality and/or ion exchange with steric hindrance. In particular it is shown that changes in the modified solution normality may also introduce selectivity reversals.

Along the selectivity reversal, the characteristic velocity is constant according to

$$\lambda_k = \frac{q_k}{c_k} = \frac{q_{k+1}}{c_{k+1}} = K_{k,k+1}^{\frac{1}{\nu_k - \nu_{k+1}}}, \quad (5.13)$$

corresponding to a contact discontinuity. From (5.13) it is clear that $\nu_k \neq \nu_{k+1}$ is a necessary condition for the existence of a selectivity reversal.

Another contact discontinuity occurs along the N th characteristic field corresponding to $\lambda_N = 0$, i.e. $\tilde{\lambda}_N = 1$. According to the discussion in the previous section regarding (5.4), we find that the modified solution normality will only change along the N th characteristic field but stays constant along the others. Changes of the modified solution normality propagate with the normalized interstitial velocity of one prior to all other transitions. In contrast, concentrations c_1, \dots, c_N can change along each characteristic field.

The image of simple waves in the concentration phase space for fluid phase concentrations c_i is given by the corresponding (right) eigenvectors \mathbf{r}_k . Based on Eq. (5.9c), the eigenvectors follow from

$$0 = \left(\frac{\nu_i}{c_i} - \lambda_k \frac{\nu_i}{q_i} \right) r_{k,i} + \left(-\frac{\nu_N}{c_N} + \lambda_k \frac{\nu_N}{q_N} \right) r_{k,N}, \quad (5.14a)$$

$$0 = -\lambda_k \sum_{i=1}^N \xi_i r_{k,i}. \quad (5.14b)$$

Recalling the characteristic equations (5.9b), Eq. (5.14) are readily satisfied for

$$\mathbf{r}_k = \left[\frac{1}{\frac{\nu_1}{c_1} - \lambda_k \frac{\nu_1}{q_1}}, \dots, \frac{1}{\frac{\nu_N}{c_N} - \lambda_k \frac{\nu_N}{q_N}} \right]^T \quad (5.15)$$

if $\lambda_k \neq \frac{q_k}{c_k}$. Using the characteristic equation (5.11) for λ_k , equilibrium formulation (5.2) and (5.15) for \mathbf{r}_k , it can be proven that the characteristic velocity $\tilde{\lambda}_k$ along the k th characteristic is monotonically increasing for $\lambda_k \neq \frac{q_k}{c_k}$ and $k < N$ because of the genuine non-linearity (2.47) and (2.48b). Details can be found in Appendix C.

The shock velocity \tilde{s}_k follows from the principles that lead to Eq. (2.40), which are in similar form to Eq. (5.7)

$$\tilde{s}^k = \frac{1}{1 + F \frac{\Delta q_i}{\Delta c_i}}, \quad i = 1, \dots, N. \quad (5.16)$$

These equations also define the image of the shock waves in the concentration phase space. If $\nu_i \neq \nu_j$ for some $i \neq j$ the image of the shock waves in the concentration phase space is curved and tangent at the beginning to the integral curves, which are defined by the eigenvectors \mathbf{r}_k , otherwise they coincide (see Section 4.2 and [15]). For $\lambda_k = \frac{q_k}{c_k} = \text{const}$, $k < N$ or $k = N$ we find

$$\nabla \lambda_k \mathbf{r}_k = 0 \quad (5.17)$$

corresponding to a contact discontinuity. According to (5.13) $\lambda_k = \frac{q_k}{c_k}$ corresponds to a selectivity reversal. Based on Eq. (5.14), the related eigenvector is

$$\mathbf{r}_k = [0, \dots, 0, r_{k,k} = \xi_k^{-1}, r_{k,k+1} = -\xi_{k+1}^{-1}, 0, \dots, 0]^T, \quad k < N. \quad (5.18)$$

This represents a straight line in the concentration phase space. Due to the tangency mentioned above, the jump conditions of the corresponding contact discontinuity are also satisfied along this line and therefore it coincides with the corresponding shock curve. Remember, all previously investigated types of transitions ($k < N$) take place on some c_{tot} hyperplane (5.3).

In contrast, c_{tot} changes along the remaining N th transition. The image of the contact discontinuity of the N th characteristic field follows from the jump conditions (5.16) for $\tilde{s}^N = 1$, which results in

$$\Delta q_i / \Delta c_i = 0, \quad (5.19)$$

and is equivalent to

$$q_i = q_i(\mathbf{c}) = q_i(\mathbf{c}^*) = q_i^*. \quad (5.20)$$

Therein, \mathbf{c}^* represent the states before the contact discontinuity occurs, and \mathbf{c} represents the states after the contact discontinuity occurs. Since the contact discontinuity corresponding to λ_N is always traveling first in time, the state before as well as c_{tot} before and after the occurrence of the contact discontinuity follow from the given boundary and initial conditions. Depending on these quantities the state after the occurrence of the contact discontinuity can be calculated from the jump conditions (5.20) and the equilibrium relations (2.33) according to

$$q_i = c_i K_{iN}^{\frac{1}{\nu_i}} \left(\frac{q_N}{c_N} \right)^{\frac{\nu_N}{\nu_i}} = c_i^* K_{iN}^{\frac{1}{\nu_i}} \left(\frac{q_N^*}{c_N^*} \right)^{\frac{\nu_N}{\nu_i}} = q_i^*, \quad (5.21a)$$

$$c_i \left(\frac{q_N}{c_N} \right)^{\frac{\nu_N}{\nu_i}} = c_i^* \left(\frac{q_N^*}{c_N^*} \right)^{\frac{\nu_N}{\nu_i}}, \quad (5.21b)$$

$$c_i = c_i^* \left(\frac{c_N}{c_N^*} \right)^{\frac{\nu_N}{\nu_i}}. \quad (5.21c)$$

The unknown variable c_N in the curves (5.21c) for c_i depend on c_{tot} . For any given c_{tot} value, (5.21c) reduces to a point due to the intersection with the corresponding c_{tot} hyperplane (5.3), which results in

$$0 = \Phi(c_N) = \sum_{i=1}^N \xi_i c_i^* \left(\frac{c_N}{c_N^*} \right)^{\frac{\nu_N}{\nu_i}} - c_{\text{tot}}. \quad (5.22)$$

Thus, the remaining components c_i can be obtained from (5.21c).

It is worth noting that the representation of the jump conditions of the contact discontinuity (5.20) in the concentration phase space are curved but coincide with the integral curves of the corresponding simple wave solution, which is shown in the following. Recalling Eq. (2.42), the relation between integral curves and eigenvectors corresponding to λ_N is

$$\frac{dc_i}{dc_N} = \frac{r_{N,i}}{r_{N,N}} = \frac{\nu_N}{\nu_i} \frac{c_i}{c_N}. \quad (5.23)$$

Eq. (5.23) can be easily integrated between two states \mathbf{c}^* , \mathbf{c} reversing the chain rule of differentiation, thus separating the variables c_i and c_N

$$\nu_i \int_{c_i^*}^{c_i} \frac{d\tilde{c}_i}{\tilde{c}_i} = \nu_N \int_{c_N^*}^{c_N} \frac{d\tilde{c}_N}{\tilde{c}_N}, \quad (5.24a)$$

$$\nu_i \ln \left(\frac{c_i}{c_i^*} \right) = \nu_N \ln \left(\frac{c_N}{c_N^*} \right), \quad (5.24b)$$

$$\hookrightarrow c_i = c_i^* \left(\frac{c_N}{c_N^*} \right)^{\frac{\nu_N}{\nu_i}}, \quad (5.24c)$$

which is identical to the curves in (5.21c).

5.4 Selectivity Reversals

One of the most significant features of the sorption based on the stoichiometric mass action law is the possible existence of selectivity reversals, which were first investigated in detail by Tondeur [27] and Helfferich & Klein [28] for the CIE (constant solution normality and no steric hindrance). Focus in [28, 27] was on loading behavior. The role of selectivity reversals for chromatographic cycles and pulse development was discussed in Section 4.4. Since the SMA is an extension of CIE, the question arises how this extension affects the properties of the selectivity reversals. Based on the results for the equilibrium theory in Section 5.3, the spectral results of the SMA related to a selectivity reversal

$$\lambda_j = \frac{q_j}{c_j} = \frac{q_k}{c_k}, \quad (5.25)$$

are similar to the ones for the stoichiometric mass action law in Section 4.3. In particular, the related contact discontinuity is described by a straight line parallel to the eigenvector \mathbf{r}_j of the form (5.18), where only the two reversal participating components 'j' and 'k' change. However if steric factors p_i are non-zero, they readily affect (5.18) through (2.35). Note, the components 'j' and 'k' do not necessarily need to satisfy $|j - k| = 1$ since the possibility that another selectivity reversal has already occurred changes the initial order in (5.12) accordingly.

In the following, a topological representation of the selectivity reversals accounting for steric effects and the variable solution normality is derived. For this purpose, Eq. (5.25) is assumed to be satisfied in conjunction with Eqs. (5.2). Together they form a set of N equations allowing for the elimination of N variables q_i in (2.35). Hence, the corresponding region in the concentration phase space is represented by the 'jk' reversal hyperplane

$$0 = \sum_{i \neq j,k} \xi_i c_i \left(K_{ij} K_{jk}^{\frac{\nu_j}{\nu_j - \nu_k}} \right)^{\frac{1}{\nu_i}} + (\xi_j c_j + \xi_k c_k) K_{jk}^{\frac{1}{\nu_j - \nu_k}} - q_{\text{tot}}, \quad (5.26)$$

or equivalently

$$0 = \sum_{i=1}^N \xi_i c_i \left(K_{ij} K_{jk}^{\frac{\nu_j}{\nu_j - \nu_k}} \right)^{\frac{1}{\nu_i}} - q_{\text{tot}}, \quad (5.27)$$

using $K_{jj} = 1$ and $K_{kj} = K_{jk}^{-1}$. Compared to the selectivity reversal described in Chapter 4, the dimension of the reversal hyperplane is increased by one to $N - 1$, which is a direct consequence of the missing closing condition for the fluid phase concentrations due to the variability of the solution normality. Furthermore, the reversal hyperplane (5.26,5.27) depends not only on the parameters q_{tot} , K_{ij} , K_{jk} and ν_i but also on ξ_i , which can contain non-vanishing steric factors p_i .

Physically meaningful results are obtained from equation (5.27) if the 'jk' hyperplane intersects exclusively the edges of the positive orthant, i.e. $c_i > 0$

for all $i = 1, \dots, N$. In other words, these intersections define the condition of the existence of the ' jk ' reversal hyperplane, and they are characterized by the fact that only a single component c_i in (5.27) is non-zero. This gives rise to the following criteria for the existence of a ' jk ' reversal hyperplane

$$0 = \xi_i c_i \left(K_{ij} K_{jk}^{\frac{\nu_j}{\nu_j - \nu_k}} \right)^{\frac{1}{\nu_i}} - q_{\text{tot}}, \quad \forall i = 1, \dots, N. \quad (5.28)$$

Since all concentrations and parameters are greater than zero, both conditions are satisfied for some $c_i > 0$ independently of all q_{tot} , K_{ij} , K_{jk} and ξ_i parameter values if and only if

$$\nu_j \neq \nu_k. \quad (5.29)$$

Eq. (5.29) represents the only necessary and sufficient condition for the existence of a reversal hyperplane.

It can be shown that reversal hyperplanes have no proper intersection but can be identical. Details regarding both properties can be found in Appendix D and Appendix H.

The selectivity reversal in CIE assumes a constant value for c_{tot} as well as no steric hindrance. Therefore, a classical ' jk ' selectivity reversal is the intersection of the corresponding c_{tot} hyperplane (5.3) and the ' jk ' reversal hyperplane (5.26,5.27) with $\xi_i = \frac{1}{\nu_i}$. The requirement of a constant solution normality is an additional restriction, which explains the relaxed condition (5.29) compared to the conditions in [28].

The generalized intersection of a ' jk ' reversal hyperplane with a c_{tot} hyperplane of constant modified solution normality is best represented rewriting (5.3) into

$$\xi_j c_j + \xi_k c_k = c_{\text{tot}} - \sum_{i \neq k, j} \xi_i c_i, \quad (5.30)$$

and applying (5.30) to (5.26)

$$0 = \sum_{i \neq j, k} \xi_i c_i \left[\left(K_{ij} K_{jk}^{\frac{\nu_j}{\nu_j - \nu_k}} \right)^{\frac{1}{\nu_i}} - K_{jk}^{\frac{1}{\nu_j - \nu_k}} \right] + K_{jk}^{\frac{1}{\nu_j - \nu_k}} c_{\text{tot}} - q_{\text{tot}}. \quad (5.31)$$

Eq. (5.31) describes a $N - 2$ dimensional reversal hyperplane with variables c_i , $i \neq \{j, k\}$ and c_{tot} . Moving along trajectories with $c_{\text{tot}} = \text{const}$ and $c_i = \text{const}$ for all $i \neq j, k$, the right-hand side of Eq. (5.30) is constant, which is equivalent to the result (5.18). Representation (5.31) describes the selectivity reversal in CIE if additionally $\xi_i = \frac{1}{\nu_i}$ holds. Another crucial difference of (5.31) and its representation in [28] is the absence of the normalization factor $\frac{c_{\text{tot}}}{q_{\text{tot}}}$ in the equilibrium constants, which are independent of c_{tot} and q_{tot} in the present case.

In the next section, focus is on chromatographic cycles. They were also discussed in Section 4.4 for CIE. A chromatographic cycle consists of two phases,

the loading and the regeneration. In case of Riemann conditions and a variable (modified) solution normality, both phases allow for two different c_{tot} hyperplanes (5.3). Only one of these two c_{tot} hyperplanes need to intersect an arbitrary ' jk ' reversal hyperplane in order to admit a classical ' jk ' selectivity reversal. Thus, the likelihood of the chromatographic cycle to be affected by a selectivity reversal is increased compared to cycles in Section 4.4. Moreover, one of these two c_{tot} hyperplanes does not require to assume a specific c_{tot} value but to be only in a certain interval, which further relaxes the conditions of the chromatographic cycle to be affected by a selectivity reversal. For more details, the reader is referred to Appendix E.

In case of a variable (modified) solution normality, there is an additional possibility for the intersection of a reversal hyperplane realized through the contact discontinuity of the N th characteristic field corresponding to $\lambda_N = 0$. Such an intersection with an arbitrary ' jk ' reversal hyperplane exists if the following equation

$$\begin{aligned} 0 &= \Psi(c_N) \\ &= \sum_{i=1}^N \xi_i c_i^* \left(\left(\frac{c_N}{c_N^*} \right)^{\nu_N} K_{ij} K_{jk}^{\frac{\nu_j}{\nu_j - \nu_k}} \right)^{\frac{1}{\nu_i}} - q_{\text{tot}}, \end{aligned} \quad (5.32)$$

admits a physically meaningful solution $c_N > 0$. In (5.32), the state \mathbf{c}^* denotes the state before the occurrence of the contact discontinuity as in (5.20). Again, all other components can be determined from Eq. (5.21c). Further details can also be found in Appendix E. Eq. (5.32) includes the special case of CIE with $\xi_i = \frac{1}{\nu_i}$ referring to a genuine ionic charge. Hence, a change in the solution normality itself increases the potential of a chromatographic cycle to be affected by a selectivity reversal even further.

5.5 Application Examples

In this section, the additional features of the SMA compared to the CIE are studied through simulations of a single chromatographic column to verify the theoretical results of previous sections. In particular, the effects of a variable solution normality and the steric factors are considered separately in the first two subsections, respectively, whereas joint effects and their relation to the first two cases are studied in a third subsection. In all cases Riemann experiments are performed for three component systems with constant initial conditions and piece-wise constant boundary conditions, where two components c_1 , c_2 are target components. The third component c_3 (the 'salt') can be used to affect the sorption behavior of the other two components, thus allowing for an additional degree of freedom in process design. For a complete picture containing effects on the loading and regeneration behavior, so called chromatographic cycles are considered. They are realized via injection of pulses with a sufficient pulse width that guarantees no overlap of the

parameter	value	description
L [m]	5.0	column length
N_z [-]	1000	number of grid points
u [$\frac{m}{s}$]	1.0	interstitial velocity
ϵ [-]	0.5	void fraction
q_{tot} [$\frac{\text{mol}}{\text{m}^3}$]	2.0	exchanger capacity
K_{13} [-]	8.0	equilibrium constant
K_{23} [-]	2.67	equilibrium constant

Table 5.1: Basic parameters used in all application example studies of Section 5.5.

parameter	value	description
ν_1 [-]	2	stoichiometric coefficient
ν_2 [-]	1	stoichiometric coefficient
ν_3 [-]	1	stoichiometric coefficient
p_1 [-]	0	steric factor
p_2 [-]	0	steric factor
p_3 [-]	0	steric factor

Table 5.2: Specific parameters of the CIE-based sorption model.

two involved Riemann problems. The basic simulations parameters applied to any application example independently of the specific set-up can be found in Tab.5.1. Simulation results are obtained through the approach described in Section 4.2. Note, the set-up specific parameters in the following subsections are chosen such that all significant features can be illustrated step-by-step in a compact manner. However, for a proof of principle, an example based on experimentally derived parameters is briefly presented in Appendix G.

5.5.1 Effect of the Variable Solution Normality

Specific parameters are listed in Tab.5.2. First, we consider a classical stoichiometric set-up without steric hindrance $p_i = 0$ and with constant solution normality $c_{\text{tot}} = 2 \frac{\text{mol}}{\text{m}^3}$. The column is equilibrated with $\mathbf{c}_{\text{init}} = [0, 0, 2]^T \frac{\text{mol}}{\text{m}^3}$, the third component only. At time unit 0 starts the injection also of the two other components with $\mathbf{c}_{\text{feed}} = [0.4, 0.6, 1.2] \frac{\text{mol}}{\text{m}^3}$. After 10 time units the feed changes back to $\mathbf{c}_{\text{feed}} = [0, 0, 2]^T \frac{\text{mol}}{\text{m}^3}$ for regeneration purposes of the first two components. The values of third component is specifically chosen to guarantee a constant solution normality c_{tot} . The results consisting of two shocks S_1, S_2 and two simple waves R_1, R_2 are presented in Fig. 5.2. Note, no selectivity reversal occurs.

In order to investigate the effect of the variable solution normality, a similar set-up to the previous one is considered. In this case, a variable solution normality is

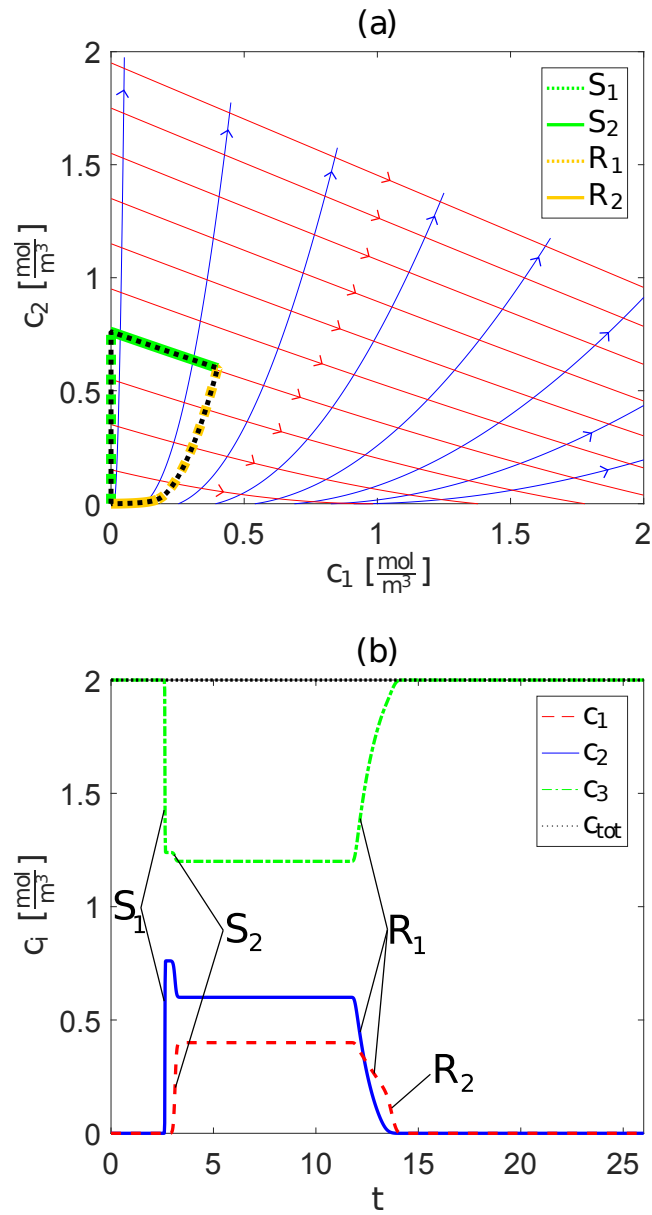


Figure 5.2: (a) Chromatographic cycle in the concentration phase space realized by a pulse experiment of the classical stoichiometric ion exchange with constant solution normality c_{tot} . Numerical results (black dashed line) overlap solution predicted by the equilibrium theory (green and orange lines). (b) Corresponding elution profiles $c_i(z)$ indicate two shocks S_1 , S_2 and two simple waves R_1 , R_2 .

realized through different initial conditions. In particular, a column equilibrated with c_3 only, i.e. $\mathbf{c}_{\text{init}} = [0, 0, 0.1]^T \frac{\text{mol}}{\text{m}^3}$ is injected with the same feed pulse of $\mathbf{c}_{\text{feed}} = [0.4, 0.6, 1.2]^T \frac{\text{mol}}{\text{m}^3}$ starting at $t = 0$ and ending at $t = 10$ as in the previous set-up, which again introduces components c_1 and c_2 into the column. After 10 time units the feed is changed to $\mathbf{c}_{\text{feed}} = [0, 0, 0.5]^T \frac{\text{mol}}{\text{m}^3}$ in order to regenerate the bed. The relevant topology is shown in Fig. 5.3a. There are two c_{tot} planes of interest corresponding to the values $c_{\text{tot}} = 0.5 \frac{\text{mol}}{\text{m}^3}$ and $c_{\text{tot}} = 2 \frac{\text{mol}}{\text{m}^3}$, respectively. Note, that the latter c_{tot} value is identical to the one in Fig. 5.2a. There are also two reversal planes (grey), but only the intermediate one between $c_{\text{tot}} = 0.5 \frac{\text{mol}}{\text{m}^3}$ and $c_{\text{tot}} = 2 \frac{\text{mol}}{\text{m}^3}$ is relevant. Corresponding numerical results are shown in Fig. 5.3b but are also plotted into Fig. 5.3a (black dashed line) showing that only the two c_{tot} planes and the two eigenvectors corresponding to $\lambda_3 = 0$ are relevant.

Considering the two contact discontinuities CD_1 , CD_2 regarding $\lambda_N = 0$, their prediction based on the equilibrium theory (green) in Fig. 5.3a obviously match the numerical results very well. These two transitions are also highlighted in Fig. 5.3b. As mentioned in Section 5.3, c_{tot} changes only along those contact discontinuities allowing for a second relevant c_{tot} plane with $c_{\text{tot}} = 0.5 \frac{\text{mol}}{\text{m}^3}$ besides the one with $c_{\text{tot}} = 2 \frac{\text{mol}}{\text{m}^3}$. This is clearly visible in Fig. 5.3. For the same reason they are not present in Fig. 5.2 with $c_{\text{tot}} = \text{const} = 2 \frac{\text{mol}}{\text{m}^3}$. Note, the initial loading of the column corresponds to a $c_{\text{tot}} = 0.1 \frac{\text{mol}}{\text{m}^3}$ plane. As already explained in Section 5.3, only c_3 changes along the first contact discontinuity CD_1 with the trivial intersection $[0, 0, 2]^T \frac{\text{mol}}{\text{m}^3}$, which coincides with the initial condition in Fig. 5.2. Hence, the $c_{\text{tot}} = 0.1 \frac{\text{mol}}{\text{m}^3}$ plane does not provide more insight and is neglected here. The intersection of the second contact discontinuity CD_2 , however, has to be determined from (5.22) and (5.21c) with $\mathbf{c}^* = \mathbf{c}_{\text{feed}}$ and yields $\mathbf{c} = [0.1898, 0.1350, 0.2701]^T \frac{\text{mol}}{\text{m}^3}$.

Investigating the remaining transitions it is sufficient to consider the projections of the two c_{tot} planes in the (c_1, c_2) space. The loading behavior on the $c_{\text{tot}} = 2 \frac{\text{mol}}{\text{m}^3}$ plane with two shocks S_1 , S_2 in Fig. 5.4 for the two target components c_1 , c_2 is identical to the one in Fig. 5.2 since the c_{tot} planes and initial conditions on this plane are identical. The regeneration behavior on the $c_{\text{tot}} = 0.5 \frac{\text{mol}}{\text{m}^3}$ plane in Fig. 5.5a consists also of two simple waves R_1 , R_2 but it is obviously different from the regeneration in Fig. 5.2a. Neither of the two c_{tot} planes Fig. 5.4a, Fig. 5.5a shows the existence of a selectivity reversal. However, in Fig. 5.5b component c_1 is obviously stronger sorbing in the regeneration phase, whereas in Fig. 5.2b the second component c_2 is stronger sorbing during the regeneration of c_1 and c_2 . This selectivity reversal can be easily explained by means of Fig. 5.3a. It shows that the contact discontinuity CD_2 crosses the '1, 2' reversal plane, which explains the reversed regeneration behavior on the $c_{\text{tot}} = 2 \frac{\text{mol}}{\text{m}^3}$ plane in Fig. 5.2 compared to the $c_{\text{tot}} = 0.5 \frac{\text{mol}}{\text{m}^3}$ plane in Fig. 5.5. The intersection can be calculated from (5.32), (5.21c) and yields $\mathbf{c}^R = [0.2829, 0.3001, 0.6002]^T \frac{\text{mol}}{\text{m}^3}$. Since this contact discontinuity admits a change in c_{tot} , this variability in c_{tot} based on different initial conditions is directly connected to the presence of the '1, 2' selectivity reversal

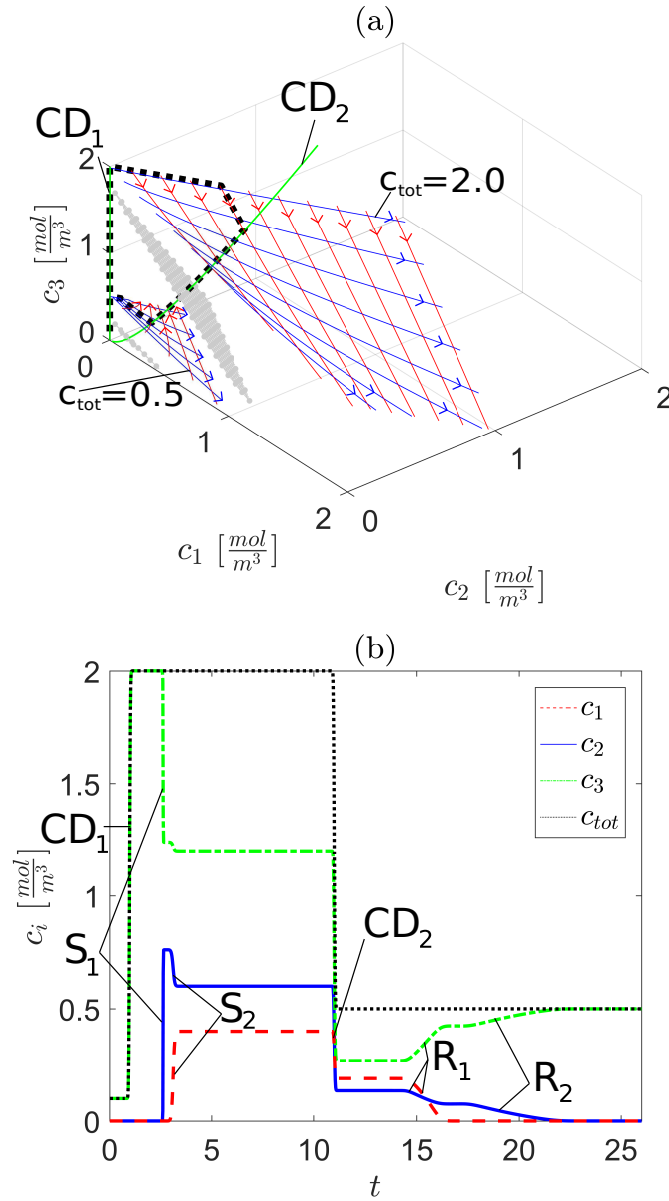


Figure 5.3: (a) Chromatographic cycle in the concentration phase space realized by a pulse experiment of the classical stoichiometric ion exchange with variable solution normality c_{tot} . Grey planes indicate reversal planes '1,2' and '1,3'. Numerical results (black dashed line) overlap two contact discontinuities CD_1 , CD_2 (solid green lines) while the remaining transitions are located in two different planes $c_{\text{tot}} = 0.5 \frac{\text{mol}}{\text{m}^3}$, $c_{\text{tot}} = 2 \frac{\text{mol}}{\text{m}^3}$, which are all predicted by the equilibrium theory. (b) Corresponding elution profiles $c_i(z)$ indicate two additional contact discontinuities CD_1 , CD_2 compared to Fig. 5.2.

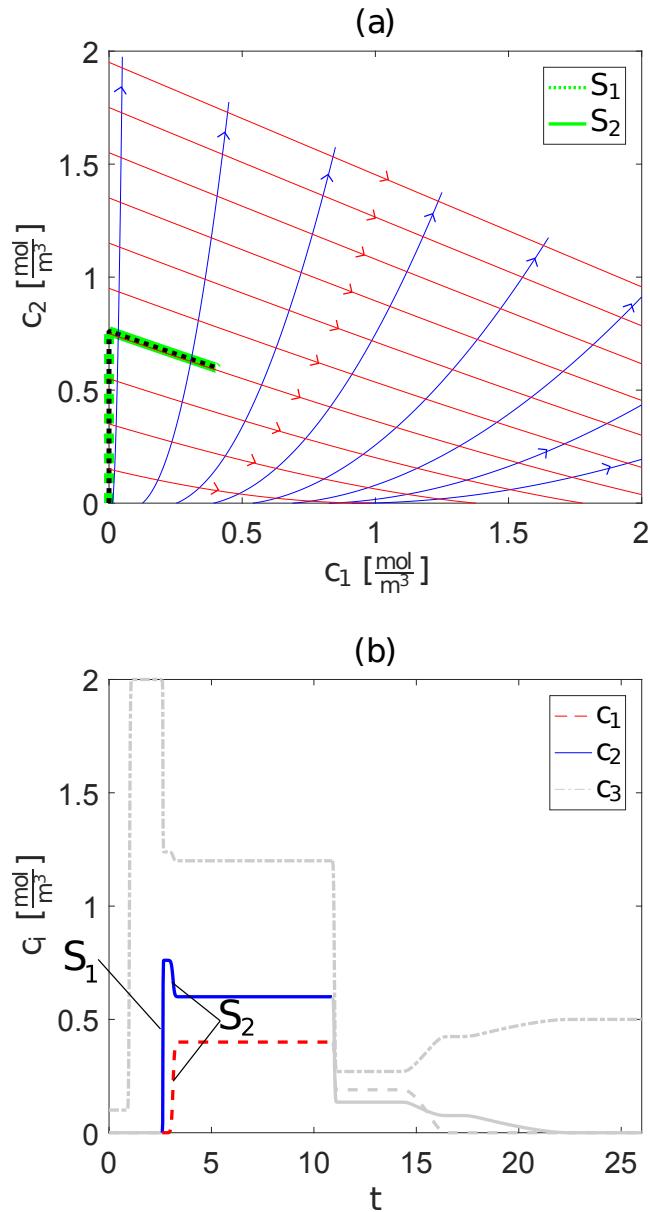


Figure 5.4: (a) Projection of the loading phase of the chromatographic cycle on the $c_{\text{tot}} = 2 \frac{\text{mol}}{\text{m}^3}$ plane into the (c_1, c_2) space. Numerical results (black dashed line) overlap the two shocks predicted by the equilibrium theory (green lines) and are identical to the corresponding ones in Fig. 5.2a. (b) Corresponding elution profiles $c_i(t)$ indicate the two occurring shocks S_1, S_2 during the loading phase, which are identical to Fig. 5.2b.

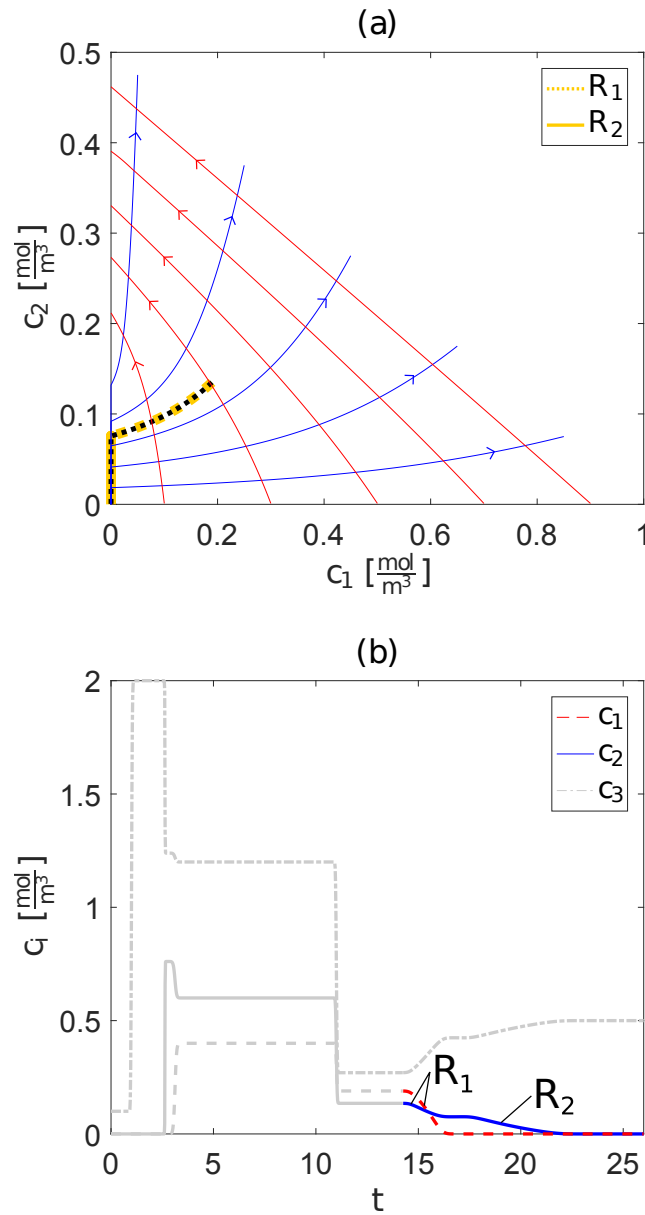


Figure 5.5: (a) Projection of the regeneration phase of the chromatographic cycle on the $c_{tot} = 0.5 \frac{\text{mol}}{\text{m}^3}$ plane into the (c_1, c_2) space. Numerical results (black dashed line) overlap the two simple waves predicted by the equilibrium theory (orange lines). (b) Corresponding elution profiles $c_i(t)$ during regeneration indicate two occurring simple waves R_1, R_2 that show reversed selectivity compared to Fig. 5.2b.

parameter	value	description
ν_1 [-]	2	stoichiometric coefficient
ν_2 [-]	1	stoichiometric coefficient
ν_3 [-]	1	stoichiometric coefficient
p_1 [-]	2	steric factor
p_2 [-]	1	steric factor
p_3 [-]	0	steric factor

Table 5.3: Specific parameters of the SMA-based sorption model.

in the chromatographic cycle. Again, the two shocks highlighted in Fig. 5.4b and two simple waves highlighted in Fig. 5.5b are also plotted (black dashed lines) into the respective (c_1, c_2) space Fig. 5.4a, 5.5a, and they are readily predicted by the equilibrium theory (green lines).

A comparison of Fig. 5.4a and Fig. 5.5a shows that the monotonicity of the eigenvalues on the red integral curves reversed but the watershed changed also its position significantly from the c_1 -axis to the c_2 -axis. Hence, a variable solution normality allows in general for significant topological changes of the path grid on the c_{tot} hyperplanes.

The reversal zones introduced in Appendix E yield for this specific example $[c_{\text{tot}}^{\text{low}}, c_{\text{tot}}^{\text{upp}}]_{1,2} = \frac{1}{9}[6, 16] \frac{\text{mol}}{\text{m}^3}$ and $[c_{\text{tot}}^{\text{low}}, c_{\text{tot}}^{\text{upp}}]_{1,3} = \frac{1}{32}[3, 8] \frac{\text{mol}}{\text{m}^3}$. For the relevant '1, 2' reversal plane and the two cycle participating c_{tot} planes holds $\bar{c}_{\text{tot}} = \frac{1}{9}[4.5, 18]$ and therefore $[c_{\text{tot}}^{\text{low}}, c_{\text{tot}}^{\text{upp}}]_{1,2} \subset \bar{c}_{\text{tot}}$, which by itself guarantees the '1, 2' selectivity reversal to occur during the chromatographic cycle. Note, this prediction can be purely based on theoretical results and requires neither simulation nor experimental data.

5.5.2 Effect of the Steric Factors

Parameters required for the examples in this section are listed in Tab.5.2 and 5.3. In order to avoid any confusion with the effect of the variable solution normality, the following set-ups are designed such that $c_{\text{tot}}^I = c_{\text{tot}}^{II} = c_{\text{tot}} = \text{const} = 0.5 \frac{\text{mol}}{\text{m}^3}$ hold for a CIE model 'I' and a SMA model 'II', respectively. Thus, only the effect of the steric factors is considered, and it also allows to consider the relevant projections into the (c_1, c_2) space for a simpler presentation.

Fig. 5.6 allows for an efficient comparison. Their quantitative difference is apparent, but also their qualitative similarity can be conjectured, which is consistent with the results in Appendix F. Therein, a bijective coordinate transformation is shown to exist between sorption models differing only in their steric factors if they are subject to an identical (modified) solution normality as in the present case with $c_{\text{tot}} = \text{const} = 0.5 \frac{\text{mol}}{\text{m}^3}$.

In order to quantify this similarity, a chromatographic cycle on the c_{tot} plane of the CIE (Fig. 5.7) is compared with a chromatographic cycle having corresponding

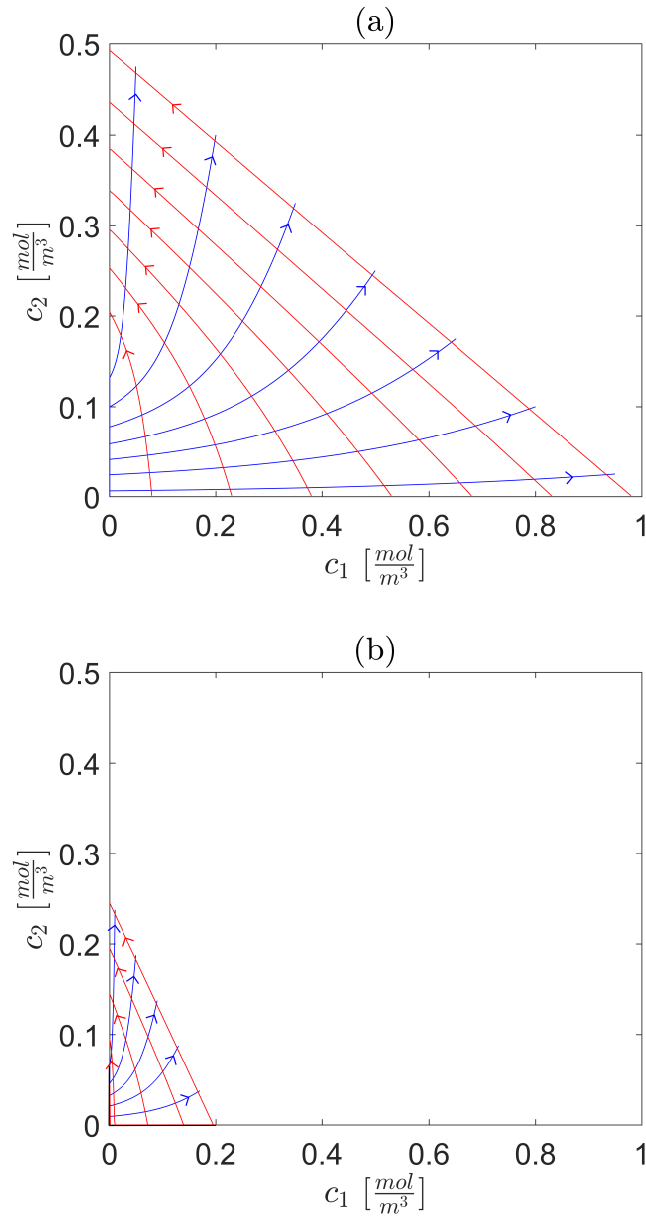


Figure 5.6: (a) Projection of the CIE-based c_{tot}^I plane into the (c_1, c_2) space, which is identical to Fig. 5.5a. (b) Projection of the SMA-based c_{tot}^{II} plane into the (c_1, c_2) space using the same domain as in (a).

scaled initial and boundary conditions (Fig. 5.8) subject to (F.1). In the CIE case, the column is equilibrated with $\mathbf{c}_{\text{init}} = [0, 0, 0.5]^T \frac{\text{mol}}{\text{m}^3}$. A pulse feed is injected at time unit 0 with $\mathbf{c}_{\text{feed}}^I = [0.3, 0.3, 0.05]^T \frac{\text{mol}}{\text{m}^3}$ and changed back to $\mathbf{c}_{\text{feed}} = [0, 0, 0.5]^T \frac{\text{mol}}{\text{m}^3}$ at 10 time units. In the SMA case, the column is also equilibrated with $\mathbf{c}_{\text{init}} = [0, 0, 0.5]^T \frac{\text{mol}}{\text{m}^3}$. Similarly, a pulse feed is injected at $t = 0$ with $\mathbf{c}_{\text{feed}}^{II} = [0.06, 0.15, 0.05]^T \frac{\text{mol}}{\text{m}^3}$ and changed back to $\mathbf{c}_{\text{feed}} = [0, 0, 0.5]^T \frac{\text{mol}}{\text{m}^3}$ at $t = 10$. Comparing the profiles in Fig. 5.7b and Fig. 5.8b, the quantitative difference is again evident as is their qualitative similarity. Both showing two shocks S_1, S_2 and two simple waves R_1, R_2 in the same order at identical time units. Moreover, the selectivity of the components is identical. Applying the transformation (F.1) to the SMA-based solution in 5.8b results in concentration profiles identical to the CIE-based ones in 5.7b. Hence, the information of the stoichiometric and steric c_{tot} plane are redundant. As shown in Appendix F, the complete concentration phase space are redundant for both cases.

The demonstrated example is representative for the general effect of steric factors on all results derived in previous sections. Steric factors can have a significant quantitative impact but do not affect any result qualitatively.

5.5.3 Joint Effects of Steric Factors and Variable Solution Normality

The additionally required parameters related to this subsection are listed in Tabs. 5.2 and 5.3. The following set-up considers again two c_{tot} planes but now with different values $c_{\text{tot}}^I \neq c_{\text{tot}}^{II}$. Similar to the previous subsection, a CIE-based case is considered ($\xi_i^I = \frac{1}{\nu_i}$) as well as a SMA-based case ($\xi_i^{II} = \frac{1}{\nu_i} + p_i$) with the same change of steric factors from $\mathbf{p}^I = [0, 0, 0]^T$ to $\mathbf{p}^{II} = [2, 1, 0]^T$, while all other parameters are again identical. However, instead of scaling the boundary and initial condition to keep the solution normality c_{tot}^I and modified solution normality c_{tot}^{II} on both planes identical, the feed is kept constant $\mathbf{c}_{\text{feed}}^I = \mathbf{c}_{\text{feed}}^{II} = \mathbf{c}_{\text{feed}}$. This set-up reflects the situation of changing one or more components with different steric factors while keeping all other experimental conditions identical.

A CIE-based case with $c_{\text{tot}}^I = 0.5 \frac{\text{mol}}{\text{m}^3}$ and a SMA-based case with $c_{\text{tot}}^{II} = 1.2 \frac{\text{mol}}{\text{m}^3}$ are considered. Due to the definition of the set-up with an identical feed \mathbf{c}_{feed} , their intersection includes the point $\mathbf{c}_{\text{feed}} = [0.2, 0.3, 0.1]^T \frac{\text{mol}}{\text{m}^3}$ itself. As before steric factors affect positioning and orientation in the concentration phase space. Since their c_{tot} values are different, the transformation (F.1) does not exist for this case. However, both c_{tot} are constant realized through an specific choice of c_3 values, which again allows for a simplified and effective comparison involving only the (c_1, c_2) space in the remainder.

In the CIE-based case, the column is equilibrated initially with $\mathbf{c}_{\text{init}}^I = [0, 0, 0.5]^T \frac{\text{mol}}{\text{m}^3}$. A pulse that introduces components c_1 and c_2 starts with $\mathbf{c}_{\text{feed}} = [0.2, 0.3, 0.1]^T \frac{\text{mol}}{\text{m}^3}$ at $t = 0$ and changes back to $\mathbf{c}_{\text{feed}}^I = [0, 0, 0.5]^T \frac{\text{mol}}{\text{m}^3}$ at $t = 10$ for the regeneration of the first two components. The third component is changed such that

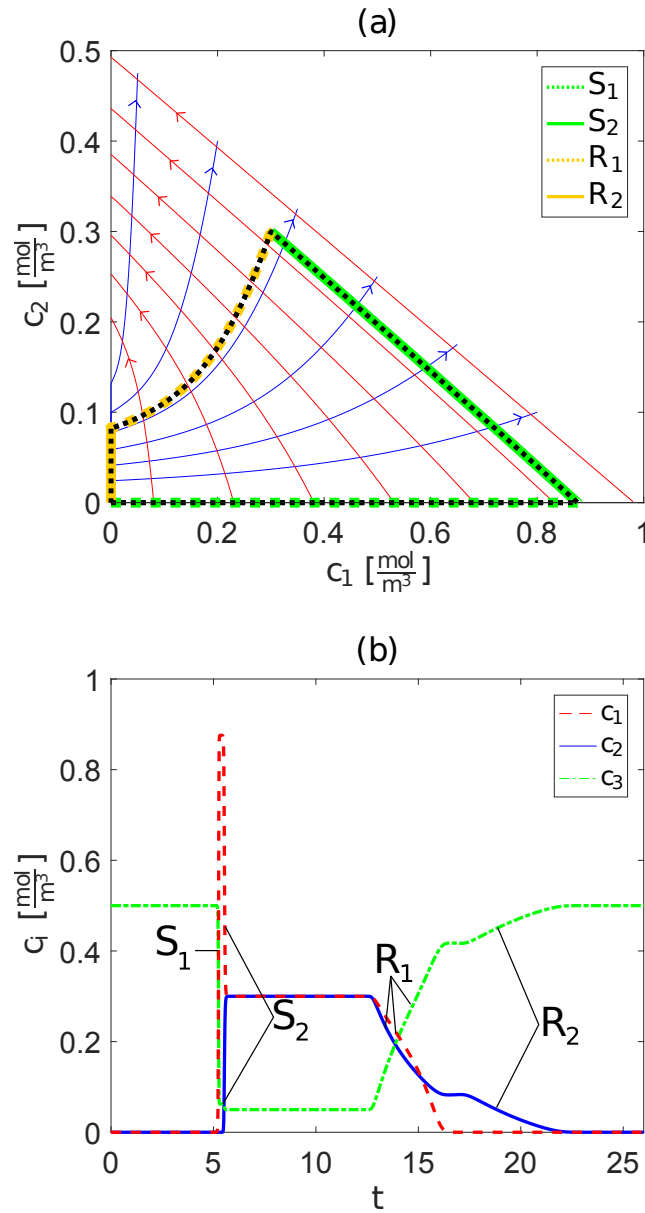


Figure 5.7: (a) Projection of the chromatographic cycle on the c_{tot}^I plane into the (c_1, c_2) space realized by a pulse experiment of the CIE with c_{tot}^I . Numerical results (black dashed line) overlap solution predicted by the equilibrium theory (green and orange lines). (b) Corresponding elution profiles $c_i(z)$ indicate two shocks S_1, S_2 and two simple waves R_1, R_2 .

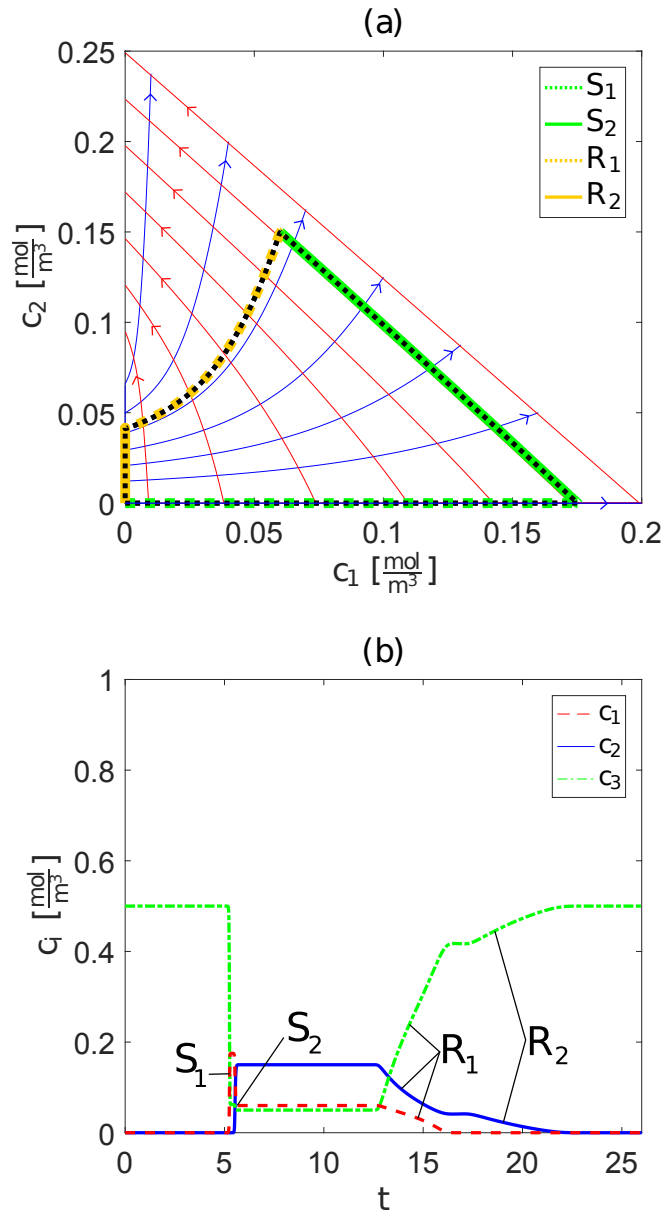


Figure 5.8: (a) Projection of the chromatographic cycle on the c_{tot}^{II} plane into the (c_1, c_2) space realized by a pulse experiment of the ion exchange based on the SMA with a constant modified solution normality c_{tot}^{II} . Numerical results (black dashed line) overlap solution predicted by the equilibrium theory (green and orange lines). (b) Corresponding elution profiles $c_i(z)$ indicate two shocks S_1, S_2 and two simple waves R_1, R_2 qualitatively identical to Fig. 5.7b.

$c_{\text{tot}}^I = 0.5 \frac{\text{mol}}{\text{m}^3}$ is kept constant. The c_{tot}^I plane including the validation of numerical results (black dashed line) with equilibrium theory prediction (green and orange) as well as the numerically obtained profiles are shown in Fig. 5.9.

These results can be compared with the corresponding ones on the c_{tot}^{II} plane in Fig. 5.10. A similar pulse set-up was performed here starting with an equilibrated column $\mathbf{c}_{\text{init}}^{II} = [0, 0, 1.2]^T \frac{\text{mol}}{\text{m}^3}$ and a pulse at time unit 0 with the same $\mathbf{c}_{\text{feed}} = [0.2, 0.3, 0.1]^T \frac{\text{mol}}{\text{m}^3}$ that is changed back at 10 time units to $\mathbf{c}_{\text{feed}}^{II} = [0, 0, 1.2]^T \frac{\text{mol}}{\text{m}^3}$. The different ξ_i^{II} values in this case lead to the different $c_{\text{tot}}^{II} = 1.2 \frac{\text{mol}}{\text{m}^3}$ and the corresponding adjustment of the third component to keep it constant, i.e. different initial and regeneration conditions. Again, numerical results and equilibrium theory prediction are in excellent agreement.

Comparing Fig. 5.9a and Fig. 5.10a, apart from the fact that both show two shocks S_1, S_2 during the loading and two simple waves R_1, R_2 during the regeneration, two apparent distinction can be readily identified. First, only in Fig. 5.10a a selectivity reversal (grey) can be observed. Second, the chromatographic cycles are reversed in the sense that in Fig. 5.9, component c_1 is stronger adsorbing during the loading phase of the pulse, whereas in Fig. 5.10 component c_2 is stronger sorbing in the same phase. A similar situation occurs if we operated on the c_{tot}^{II} plane in Fig. 5.10a with a \mathbf{c}_{feed} on different sites of the selectivity reversal, which has been presented in Section 4.4.

For both sorption models 'I' and 'II', the fixed \mathbf{c}_{feed} introduces a difference in c_{tot} values due to different steric factors. This results in significant topological differences between the two c_{tot} planes in Fig. 5.9a and Fig. 5.10a that can be predicted by the equilibrium theory only if applied to case 'I' and 'II' separately.

In the present case, two chromatographic cycles are considered separately. However, using the results from the preceding subsection, the concentration phase space corresponding to 'II' contains a \tilde{c}_{tot} plane that is similar to the c_{tot}^I plane in Fig. 5.9a in the sense of (F.1). If also $\mathbf{c}_{\text{feed}}^{II} = \mathbf{c}_{\text{feed}}^I$ holds, the chromatographic cycle for 'II' will consist of the two relevant \tilde{c}_{tot} and c_{tot}^{II} planes, which are connected by a contact discontinuity corresponding to $\lambda_3 = 0$. Thus, two significantly different c_{tot} planes are present in a single chromatic cycle, which is then similar to the result in Subsection 5.5.1 with constant steric factors. In particular, if the inverse mapping of (F.1) is applied to the solution in Fig. 5.3, a similar result with the same qualitative behavior in the concentrations phase space of 'II' is obtained. Consequently, also in case of a variable solution normality, the effect of steric factors is quantitative only, which is again consistent with the results in Appendix F.

Since the joint effect is a straight forward extension of the results in the previous subsections and does not yield any additional insight, the corresponding simulations in a three dimensional concentration state space are omitted.

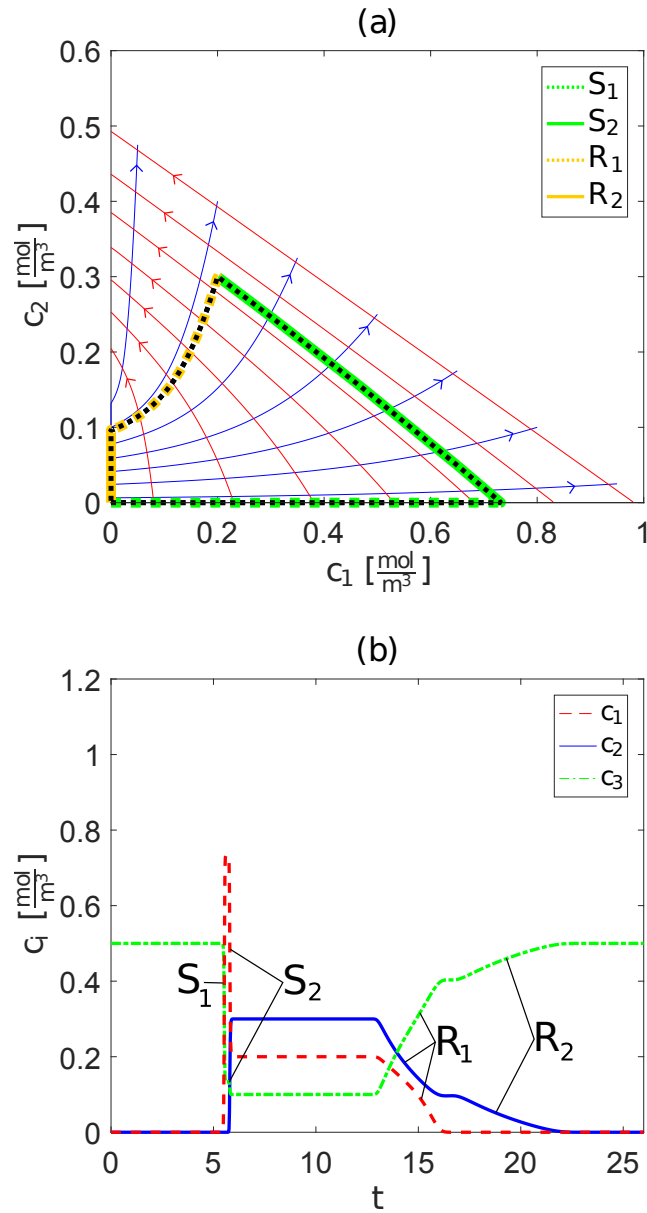


Figure 5.9: (a) Projection of the chromatographic cycle on the $c_{\text{tot}}^I = 0.5 \frac{\text{mol}}{\text{m}^3}$ plane into the (c_1, c_2) space realized by a pulse experiment of the CIE with c_{tot}^I . Numerical results (black dashed line) overlap solution predicted by the equilibrium theory (green and orange lines). (b) Corresponding elution profiles $c_i(z)$ indicate two shocks S_1, S_2 and two simple waves R_1, R_2 similar to Fig. 5.7b.

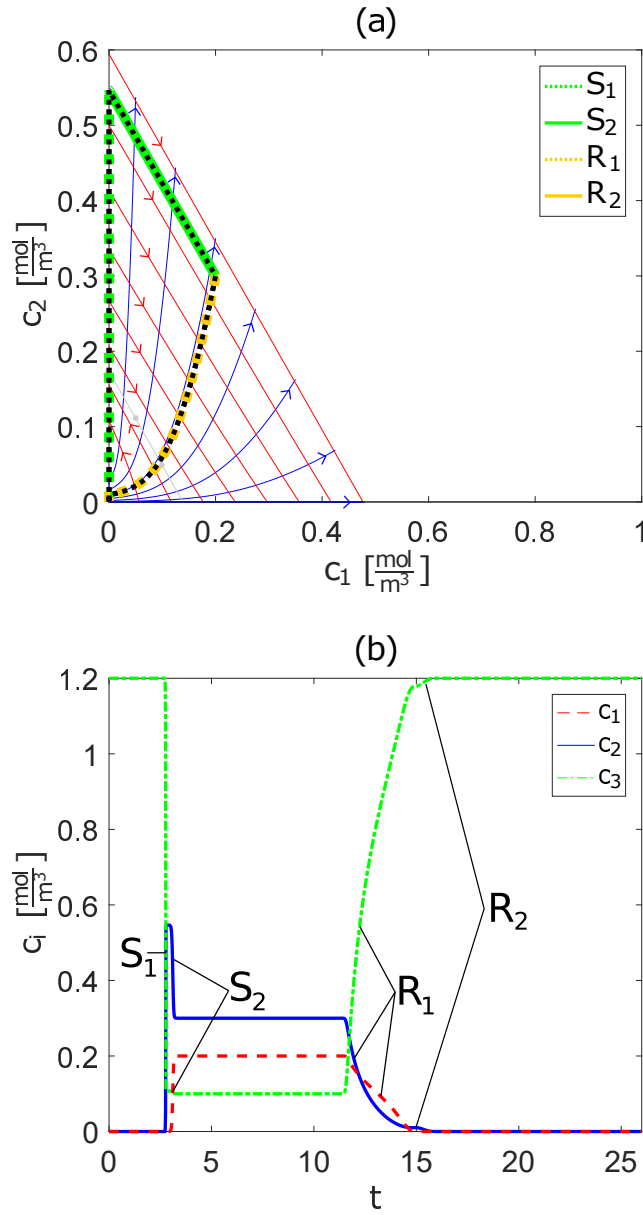


Figure 5.10: (a) Projection of the chromatographic cycle on the $c_{\text{tot}}^{II} = 1.2 \frac{\text{mol}}{\text{m}^3}$ plane into the (c_1, c_2) space realized by a pulse experiment of the SMA-based ion exchange with constant modified solution normality c_{tot}^{II} . The grey line indicates a 1,2 selectivity reversal. Numerical results (black dashed line) overlap solution predicted by the equilibrium theory (green and orange lines). (b) Corresponding elution profiles $c_i(z)$ indicate two shocks S_1, S_2 and two simple waves R_1, R_2 with reversed selectivity of the two components compared to Fig. 5.9b.

5.6 Summary

The numerical solution strategy introduced in Section 4.2 was extended to the SMA for arbitrary boundary conditions. These results were used to validate the extension of the equilibrium theory to AIE accounting for variable solution normality and steric hindrance. Possible fields of application are separation of proteins [29] where often salt gradients are applied [30] and also amino acids [86, 87]. Important findings are: that variable solution normality may introduce selectivity reversals and may thereby change the solution qualitatively (order of elution, types of transitions etc.). It was proven that in contrast to this, steric hindrance affects the solution only quantitatively (plateau values, propagation velocities etc.). This chapter provides methods and tools for the prediction of column dynamics and therefore builds an important basis for future work on conceptual design and control of single- and multi-column systems. Limitations for protein separations are due to the limitations of the SMA isotherm used in this work. In particular, the assumption of a constant pH. For Systems with variable pH additional effects may arise, which are not covered by the present theory. For such systems, at the moment only a numerical approach is possible [56].

Chapter 6

Continuous Separation Processes

This chapter was in parts published in Computer Aided Chemical Engineering, 48, M. Fechtner and A. Kienle, Rational design of ion exchange simulated moving bed processes, 733-738 (2020).

6.1 Introduction

Simulated moving bed (SMB) processes represent a powerful technology for continuous chromatographic separations. Triangle theory as introduced by [88] can be used for the rational design of SMB processes. The theory is based on an idealized mathematical model that allows an analytical solution using the MOC for certain types of explicit sorption isotherms including linear and Langmuir isotherms [9].

In a first step, the theory is extended to the CIE, and sorption is described by implicit isotherms. Therefore, an analytical approach is not possible anymore. Using the theoretical results for a single column from Sections 4.3 as well as 5.3 and following the ideas presented by [58], a corresponding semi-analytical approach is proposed. The approach allows to determine the region of complete separation in the space of the design parameters. Results are validated by rigorous numerical solution of the full blown model realized through the extension of the numerical solution strategy (4.2). Further, the present approach is shown to be superior to a simplified approach, where the ion-exchange equilibrium is fitted with a Langmuir isotherm, a frequently applied concept in practice. Finally, use of the solution normality as additional design parameter is discussed.

6.2 Triangle Theory

Triangle theory was developed for the ideal true moving bed (TMB) [9] as depicted in Fig. 6.1. Aside from the fluid phase, the solid phase is also moving allowing for continuous separation at steady state operation. In addition, two inlets - feed and desorbent - and two outlets - extract and raffinat - are used in order to realize

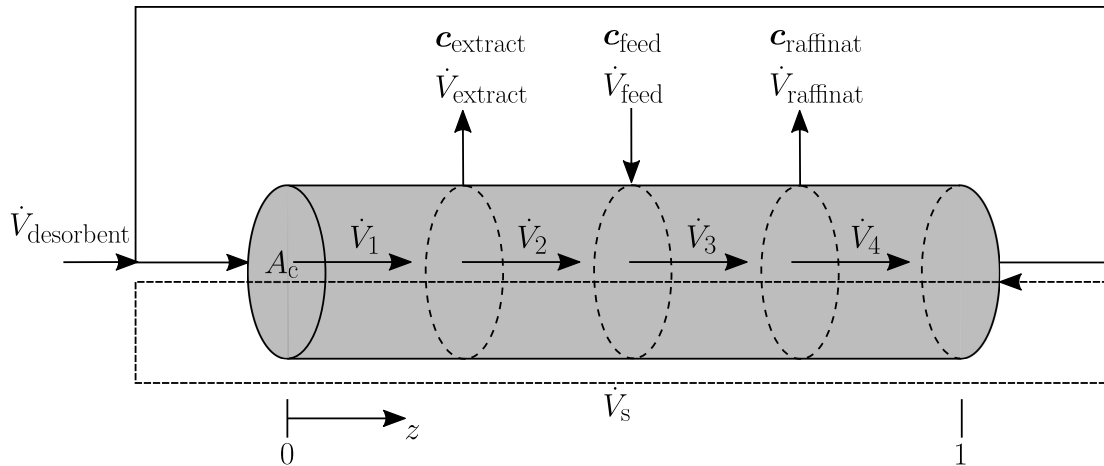


Figure 6.1: TMB process unit consisting of four CS resulting from two inlet and two outlet streams.

a complete separation of mixtures with two target components $i = 1, 2$. As a result, the process is divided into four section $j = 1, \dots, 4$. Note, a third sorbing component $i = 3$ - the counter ions - is added to keep the solution normality c_{tot} constant, thus realizing application of the CIE formalism. In contrast, the solvent is also injected with \dot{V}_{des} as non-sorbable desorbent. This flow rate is used to adjust the flow in Column section (CS) 1. For this particular configuration, the corresponding model reads [89]

$$\begin{aligned} \frac{\partial}{\partial t}(c_{i,j} + Fq_{i,j}) + Fu_s \frac{\partial}{\partial z}(m_j c_{i,j} - q_{i,j}) &= 0, \\ \mathbf{c}_j, \mathbf{q}_j &\in \mathbb{R}^N, \quad j = 1, \dots, 4 \end{aligned} \quad (6.1)$$

The practical realization of the process in Fig. 6.1 - the SMB - is shown in Fig. 1.2. The design procedure for the SMB first introduced by [88] is based on the analytical solution of the ideal TMB model Eq. (6.1) using the MOC. A solution of Eq. (6.1) requires initial conditions $\mathbf{c}_j(0, z) = \mathbf{c}_{j,init}$ and boundary conditions $\mathbf{c}_j(t, 0) = \mathbf{c}_{j,feed}$ as well as $\mathbf{q}_j(t, 1) = \mathbf{q}_{j,feed}$ for each column section. Note, the process is initially equilibrated and the thermodynamic equilibrium between the fluid phase with \mathbf{c} and the solid phase with \mathbf{q} represented by some isotherm $\mathbf{q}(\mathbf{c})$ holds, i.e. $\mathbf{q}_j(0, z) = \mathbf{q}_j(\mathbf{c}_{j,init})$. The fluid phase velocity for each CS is denoted by $u_j = \frac{\dot{V}_j}{\epsilon A_c}$, while the counter-current velocity of the solid phase, which is constant everywhere, is denoted by $u_s = \frac{\dot{V}_s}{(1-\epsilon)A_c}$. Variable $t = t^*u_s/L$ and $z = z^*/L_j$ denote dimensionless time and space coordinates, respectively, for each CS. The parameters $m_j = \frac{u_j}{Fu_s}$ denotes the dimensionless flow-rate ratio in CS j . The spatial distribution of the components is determined by their net fluxes in fluid and solid phase. The flux of component i in CS j is readily obtained from Eq.

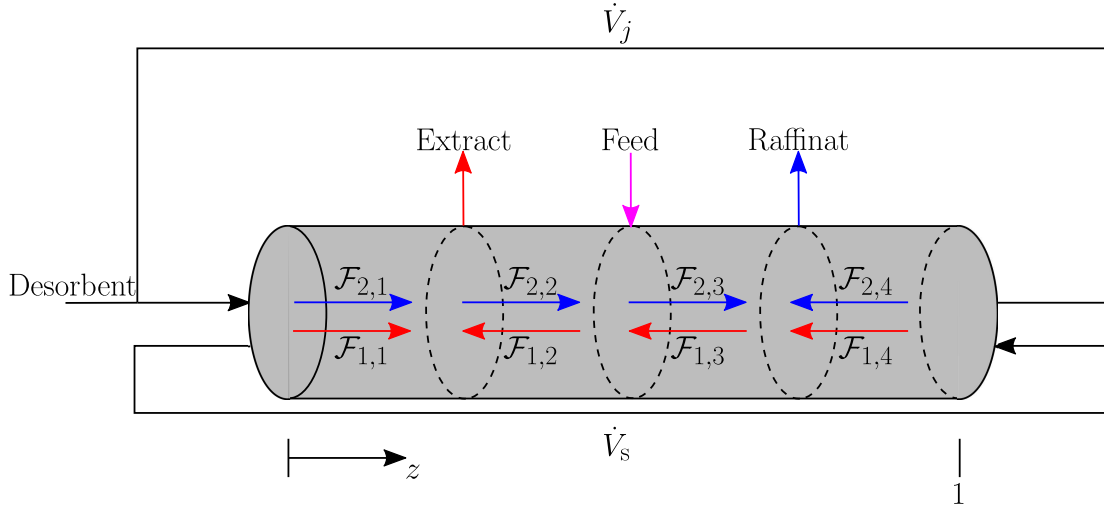


Figure 6.2: TMB with required fluxes of the target components $i = 1, 2$ to achieve their complete separation.

(6.1) as

$$\mathcal{F}_{i,j} = Fu_s(m_j c_{i,j} - q_{i,j}). \quad (6.2)$$

The objective of the process in Fig. 6.1 is the complete separation of target components $i = 1, 2$. The key idea depicted in Fig. 6.2 is based on the exploitation of the different sorption strengths such that in relation to the feed location the flux of the stronger sorbing component 1 is counter-current to the fluid flow ($\mathcal{F}_{1,2} \leq 0, \mathcal{F}_{1,3} \leq 0$) while the flux of the weaker component 2 is in fluid flow direction ($\mathcal{F}_{2,2} \geq 0, \mathcal{F}_{2,3} \geq 0$). In order to allow eventually for a continuous separation process, a closed-loop configuration is used in addition. It allows for regions of regeneration in addition to regions of loading, thus realizing the presence of front and rear waves for each component without discontinuing the feed of target components. Due to the closed loop configuration the flux orientations of each target component $i = 1, 2$ have to be reversed in two locations. In particular, component 1 and component 2 fluxes are reversed at the extract ($\mathcal{F}_{1,1} \geq 0$) and raffinat outlet ($\mathcal{F}_{2,4} \leq 0$), respectively. Hence, each target component flux 'converges' at the respective outlet. In contrast, both target components 'diverge' at the desorbent inlet due to the second reversal of the flux orientation ($\mathcal{F}_{1,4} \leq 0, \mathcal{F}_{2,1} \geq 0$). Thus, CS 2 and the extract stream contain all components but component 2 ($\mathbf{c}_{\text{extract}} = [c_1, 0, c_3]^T$), CS 3 and the raffinat stream contain all components but component 1 ($\mathbf{c}_{\text{raffinat}} = [0, c_2, c_3]^T$), and CS 1 and 4 contain only component 3 such that the fluid and solid phase are completely regenerated regarding the target components $i = 1, 2$. Based on Eq. (6.2), the previous considerations and assuming the absence of a selectivity reversal, the direction of the flux determined by the sign of $(m_j c_{i,j} - q_{i,j})$ results in the following conditions for the flow-rate

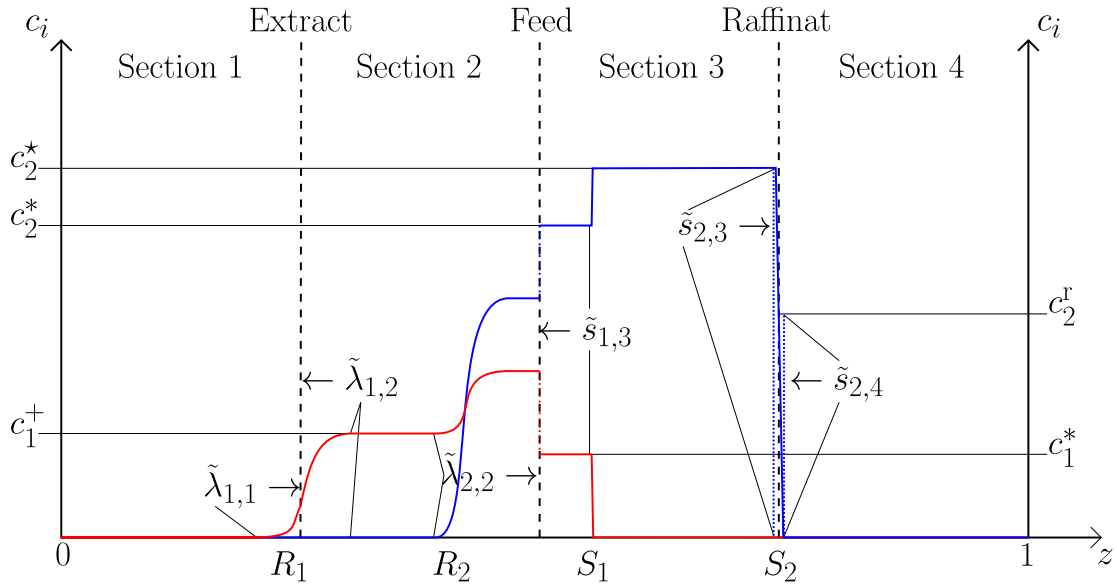


Figure 6.3: Transient concentration profile of two components approaching steady state solution of the TMB.

ratios m_j to realize a complete separation of the target components

$$\text{CS 1: } m_1 \geq \frac{q_{1,1}}{c_{1,1}} \geq \frac{q_{2,1}}{c_{2,1}}, \quad (6.3a)$$

$$\text{CS 2: } \frac{q_{2,2}}{c_{2,2}} \leq m_2 \leq \frac{q_{1,2}}{c_{1,2}}, \quad (6.3b)$$

$$\text{CS 3: } \frac{q_{2,3}}{c_{2,3}} \leq m_3 \leq \frac{q_{1,3}}{c_{1,3}}, \quad (6.3c)$$

$$\text{CS 4: } m_4 \leq \frac{q_{2,4}}{c_{2,4}} \leq \frac{q_{1,4}}{c_{1,4}}. \quad (6.3d)$$

The MOC-based steady state solution of the quasi-linear PDE system in Eq. (6.1) resulting from a single Riemann problem is assumed to be composed of simple waves and shock waves for both components, which is the case for Langmuir-like isotherms [15]. In general, this assumption has to be verified. Specifically, all transitions related to CS 1 and 3 are assumed to be simple waves, whereas transitions related to CS 3 and 4 are assumed to be shock waves as depicted in Fig. 6.3. These assumptions are required for the application of the triangle theory [89]. The constant steady state velocities of these waves are related to the m_j values by [58]

$$\tilde{\lambda}_{k,j} = \frac{Fu_s(m_j - \lambda_k)}{1 + F\lambda_k}, \quad k = 1, 2, j = 1, \dots, 4, \quad (6.4a)$$

$$\tilde{s}_{k,j} = \frac{Fu_s(m_j - s_k)}{1 + Fs_k}, \quad k = 1, 2, j = 1, \dots, 4. \quad (6.4b)$$

In Eq. (6.4), the sign of the wave velocities depends on $m_j - \lambda_k$ and $m_j - s_k$, respectively. In agreement with Eq. (6.3) and Fig. 6.3, the following bounds on the flow-rate ratios m_j are obtained [58]

$$\text{CS 1: } m_1 \geq \lambda_1|_{c_1=0, c_2=0}, \quad (6.5a)$$

$$\text{CS 2: } \lambda_2|_{c_1^+, c_2=0} \leq m_2 \leq \lambda_1|_{c_1^+, c_2=0}, \quad (6.5b)$$

$$\text{CS 3: } s_2|_{c_1=0, c_1^*=0, c_2^* \rightarrow 0} \leq m_3 \leq s_1|_{c_1^* \rightarrow c_1^*=0, c_2^* \rightarrow c_2^*}, \quad (6.5c)$$

$$\text{CS 4: } m_4 \leq s_2|_{c_1=0, c_2^* \rightarrow 0}. \quad (6.5d)$$

In this chapter, the CIE is used to define the thermodynamic equilibrium, thus using Eqs. (2.27), (2.28) and (2.29) the following equations for two independent variables c_1 , c_2 are obtained

$$K_{i3} = \left(\frac{q_i}{c_i}\right)^{\mu_i} \left(\frac{c_3}{q_3}\right)^{\mu_3} = \text{const}, \quad i = 1, 2, \quad (6.6a)$$

$$c_3 = \mu_3 \left(c_{\text{tot}} - \frac{c_1}{\mu_1} - \frac{c_2}{\mu_2} \right), \quad q_3 = \mu_3 \left(q_{\text{tot}} - \frac{q_1}{\mu_1} - \frac{q_2}{\mu_2} \right). \quad (6.6b)$$

Here, component 3, which is used to keep the solution normality constant, is used as dependent variable. Using the general approach of [89] described in [58], Eq. (6.6) can be used to obtain constraints on every m_j such that complete separation of components 1 and 2 can be achieved.

6.3 Results

First, the conditions on the flow-rate ratios are specified for CIE applications with two target components $i = 1, 2$

$$\text{CS 1: } m_1 \geq \frac{q_1}{c_1} \Big|_{c_1=0, c_2=0}, \quad (6.7a)$$

$$\text{CS 2: } \min \left\{ \frac{q_2}{c_2}, \frac{\alpha \frac{q_3}{c_3} + \beta \frac{q_1}{c_1}}{\alpha + \beta} \right\} \Big|_{c_2=0} \leq m_2 \leq \max \left\{ \frac{q_2}{c_2}, \frac{\alpha \frac{q_3}{c_3} + \beta \frac{q_1}{c_1}}{\alpha + \beta} \right\} \Big|_{c_2=0}, \quad (6.7b)$$

$$\alpha = \frac{\mu_3}{\mu_1} q_1, \quad \beta = \frac{\mu_1}{\mu_3} q_3,$$

$$\text{CS 3: } \frac{q_2^* - q_2}{c_2^* - c_2} \Big|_{c_1=0, c_2=0, c_1^*=0} \leq m_3 \leq \frac{q_1^* - q_1}{c_1^* - c_1} \Big|_{c_1^*=0} = \frac{q_2^* - q_2}{c_2^* - c_2} \Big|_{c_1^*=0}, \quad (6.7c)$$

$$\text{CS 4: } m_4 \leq \frac{q_2^r - q_2}{c_2^r - c_2} \Big|_{c_1=0, c_2=0}. \quad (6.7d)$$

In Eq. (6.5a) concentrations of both components are zero. According to the results in Appendix I (I.18, I.19) the eigenvalues satisfy $\lambda_1 = \frac{q_1}{c_1}$ and $\lambda_2 = \frac{q_2}{c_2}$ resulting in Eq. (6.7a). Similarly, $c_2 = 0$ holds in Eq. (6.5b). Therefore, at least on of the two

eigenvalues can be identified with $\frac{q_2}{c_2}$ (see Eq. (I.41)). The other eigenvalue follows from the characteristic equation (5.11) with $c_2 = q_2 = 0$. Hence, inequality (6.7b) is obtained for arbitrary CIE applications with two target components. The shock velocities in Eqs. (6.5c) and (6.5d) are obtained through application of the jump conditions (2.40). Eventually, we obtain for the flow-rate ratio m_1 the following constant lower bound

$$m_1 \geq \frac{q_1}{c_1} \Big|_{c_1=0, c_2=0} = K_{13}^{\frac{1}{\mu_1}} \left(\frac{q_{\text{tot}}}{c_{\text{tot}}} \right)^{\frac{\mu_3}{\mu_1}} = \text{const}, \quad (6.8)$$

which guarantees complete regeneration of the solid phase in CS 1. The following bounds on m_4 guarantee the complete regeneration of the fluid phase in CS 4

$$-\frac{1}{F} \leq m_4 \leq \frac{q_2(c_2^r)}{c_2^r} = K_{23}^{\frac{1}{\mu_2}} \left(\frac{q_{\text{tot}} - \frac{q_2(c_2^r)}{\mu_2}}{c_{\text{tot}} - \frac{c_2^r}{\mu_2}} \right)^{\frac{\mu_3}{\mu_2}}, \quad (6.9a)$$

$$(m_3 - m_2)c_{2,\text{feed}} = \left(m_3 - \frac{q_2(c_2^r)}{c_2^r} \right) c_2^r. \quad (6.9b)$$

The left-hand side in Eq. (6.9a) is obtained for the minimal desorbent inlet $\dot{V}_{\text{desorbent}} = 0$ [90]. Scalar c_2^r denotes the raffinate concentration of component 2, and the value of c_2^r is obtained from Eq. (6.9b) - the overall mass balance of component 2 in process unit 6.1 under the assumption of total regeneration in CS 4 - for given values of m_2 and m_3 . The maximal value of m_4 in Eq. (6.9a) allows the shock front of component 2 to be standing in CS 4 [14]. The value of $q_2(c_2^r)$ is obtained by solving Eq. (6.6) for $\mathbf{c} = [0, c_2^r, c_{\text{tot}} - \frac{c_2^r}{\mu_2}]$. Assuming the variables m_1 and m_4 to satisfy Eqs. (6.8) and (6.9), complete separation depends only on the choice of m_2 and m_3 [58]. Therefore, a corresponding region of complete separation can be projected into the (m_2, m_3) plane, see the triangular shaped set in Fig. 6.4. The bounds of the triangular-like set defined by the minimal and maximal values of m_2 and m_3 , respectively, are obtained by following the procedure in [58]. The black curve in Fig. 6.4 results from the overall mass balance of component 2 in CS 2 and 3 under the assumption of complete separation

$$(m_3 - m_2)c_{2,\text{feed}} = m_3c_2 - q_2 \quad (6.10)$$

and the minimal value of m_3 in Eq. (6.7c). In this case, the right-hand side in Eq. (6.10) is zero and implies $m_3 = m_2$, which is the black curve in Fig. 6.4. For the minimal and maximal value of m_2 in Eq. (6.7b), we obtain the following two functions $m_2(c_1)$

$$m_2(c_1) = \frac{q_2}{c_2} \Big|_{c_2=0} = K_{23}^{\frac{1}{\mu_2}} \left(\frac{q_{\text{tot}} - \frac{q_1(c_1)}{\mu_1}}{c_{\text{tot}} - \frac{c_1}{\mu_1}} \right)^{\frac{\mu_3}{\mu_2}}, \quad (6.11a)$$

$$m_2(c_1) = \frac{\frac{\mu_3}{\mu_1} q_1(c_1) \frac{q_{\text{tot}} - \frac{q_1(c_1)}{\mu_1}}{c_{\text{tot}} - \frac{c_1}{\mu_1}} + \frac{\mu_1}{\mu_3} \left(q_{\text{tot}} - \frac{q_1(c_1)}{\mu_1} \right) \frac{q_1(c_1)}{c_1}}{\frac{\mu_3}{\mu_1} q_1(c_1) + \frac{\mu_1}{\mu_3} \left(q_{\text{tot}} - \frac{q_1(c_1)}{c_1} \right)}, \quad (6.11b)$$

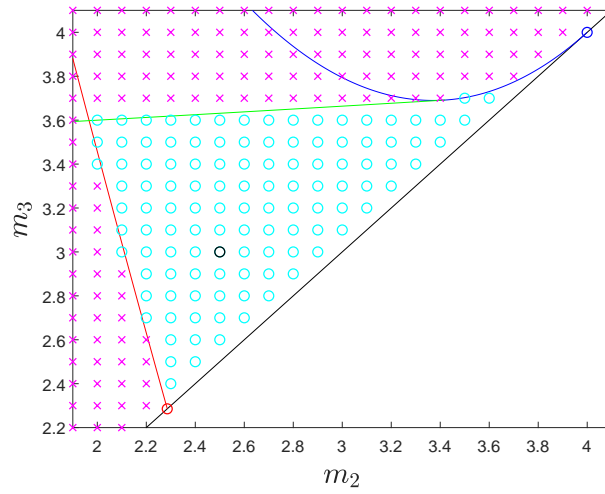


Figure 6.4: TMB triangle showing predicted region of complete separation. Circles indicate complete separation and crosses incomplete separation. Corresponding steady states obtained from dynamical simulation.

Using the overall mass balance of component 1 in CS 2 and 3 under the assumption of complete separation

$$(m_3 - m_2)c_{1,\text{feed}} = q_1 - m_2c_1 \quad (6.12)$$

the value of m_3 can be obtained as a function of m_2 . Using a sufficiently large interval for c_1 , two curves $m_3(m_2(c_1))$ are obtained; the red curve in Fig. 6.4 by combining Eqs. (6.11a,6.12) and the blue curve in Fig. 6.4 by combining Eqs. (6.11b,6.12). Note, depending on the specific parameters (for details see Tab. 6.1) in Eq. (6.6), the functions in Eq. (6.11), which define the red and blue curve, can be interchanged. Finally, calculation of the green curve in Fig. 6.4 is demonstrated. The parameters in Tab. 6.1 are chosen such that the CIE example admits for the maximal value of m_3 in Eq. (6.7c) a steady state solution to the Riemann problem composed of the four plateau states $C^0 = (0, 0)$, $C^1 = (c_1^+, 0)$, $C^2 = (c_1^*, c_2^*)$, and $C^3 = (0, c_2^*)$ that are connected by two shocks and two simple waves similar to Fig. 6.3 but without discontinuity at the feed inlet. In particular, C^1 and C^2 are connected by a 2-simple wave, therefore they lie on the same integral curve \tilde{c}_2 corresponding to eigenvalue λ_2 . Variable c_2^* is used for parametrization of the green curve. Thus, the remaining variables c_1^+ , c_1^* , c_2^* , m_2 , and m_3 have to

parameter	value	description
L [m]	0.5	column length
L_j [m]	0.125	j th CS length
A_c [m ²]	0.2	column cross sectional area
N_z [-]	800	number of spatial grid points
u_s [$\frac{m}{s}$]	0.1	solid phase velocity
ϵ [-]	0.5	void fraction
q_{tot} [$\frac{\text{mol}}{l}$]	2.0	exchanger capacity
c_{tot} [$\frac{\text{mol}}{l}$]	1.0	solution normality
K_{13} [-]	8.0	equilibrium constant
K_{23} [-]	1.143	equilibrium constant
μ_1 [-]	2	stoichiometric factor
μ_2 [-]	1	stoichiometric factor
μ_3 [-]	1	stoichiometric factor
$c_{1,\text{feed}}$ [$\frac{\text{mol}}{l}$]	0.3	feed of component 1
$c_{2,\text{feed}}$ [$\frac{\text{mol}}{l}$]	0.4	feed of component 2

Table 6.1: TMB process and simulation parameters.

be determined. For this purpose, the following set of equations is solved

$$m_2 = \frac{\frac{q_1^+}{c_{1,\text{feed}}}(c_{2,\text{feed}} - c_2^*) + q_2^*}{\frac{c_1^+}{c_{1,\text{feed}}}(c_{2,\text{feed}} - c_2^*) + c_2^*}, \quad (6.13a)$$

$$m_3 = \frac{q_1^+ - m_2 c_1^+}{c_{1,\text{feed}}} + m_2, \quad (6.13b)$$

$$0 = K_{13}^{\frac{1}{\mu_1}} \left(\frac{q_{\text{tot}} - \frac{q_1^*}{\mu_1} - \frac{q_2^*}{\mu_2}}{c_{\text{tot}} - \frac{c_1^*}{\mu_1} - \frac{c_2^*}{\mu_2}} \right)^{\frac{\mu_3}{\mu_1}} - m_3, \quad (6.13c)$$

$$0 = q_2^* - q_2^* - m_3(c_2^* - c_2^*), \quad (6.13d)$$

$$\tilde{c}_1^+ = \int_{c_2^*}^{c_2^*} \frac{q_1}{q_2} \frac{\mu_2}{\mu_1} \frac{q_2}{c_2} - \lambda_2 dc_2 + c_1^*, \quad (6.13e)$$

where q_1^+ and q_2^* are obtained by solving Eq. (6.6) for $c_2 = 0$ and $c_1 = 0$, respectively. Similarly, q^* is obtained by solving Eq. (6.6) for c^* . Note, equations (6.13a,6.13b), which result from reformulating the mass balances (6.10) and (6.12), are easily solved for m_2 and m_3 . However, they require some initial guess for c_1^+ . Subsequently, equations (6.13c,6.13d), which result from rewriting the right-hand side in Eq. (6.7c) and using Eq. (6.6), are solved for c_1^* , c_2^* . Finally, Eq. (6.13e) is used to obtain a \tilde{c}_1^+ that lies on the same integral curve \tilde{c}_1 as c_1^* does. Thus, the set of equations in Eq. (6.13) has to be solved iteratively until $|\tilde{c}_1^+ - c_1^+| < \epsilon$ for a sufficiently small $\epsilon \ll 1$. Note, the integrand in Eq. (6.13) is obtained from

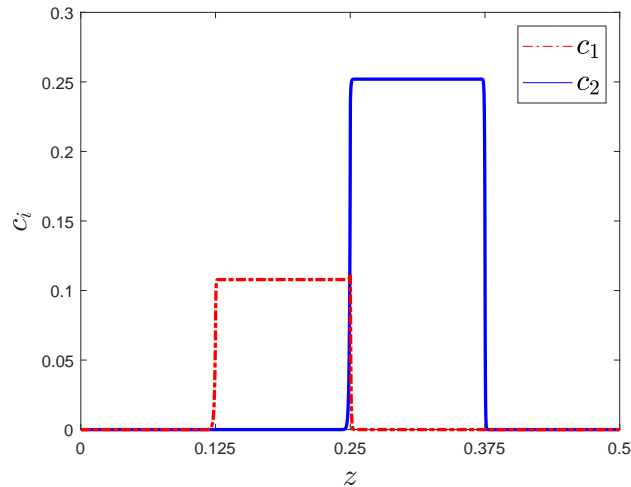


Figure 6.5: Steady state concentration profile for $m_2 = 2.5$ and $m_3 = 3.0$ (indicated by black circle in Fig. 6.4) obtained through dynamical simulation of the TMB.

substitution of Eq. (5.15) into Eq. (2.42).

The triangle-like set in Fig. 6.4 is verified by performing numerical simulations of the TMB (6.1) for different combinations (m_2, m_3) . For this purpose, the numerical approach for a single column presented in Section 4.3 was extended to solve also the continuous true counter-current model (6.1). Since the same sorption isotherm is applied as in Section 4.3, the differential index is one. Hence, standard solvers to efficiently solve the DAE system, which results again from application of the MOL to the corresponding PDAE system, can be used providing known advantages. Additionally, the Riemann set-up is used for initializing the dynamic problem to the steady state solution. It easily allows to obtain consistent initial conditions by solving Eq. (6.6) for piece-wise constant initial values just once. A particular simulation with $(m_2 = 2.5, m_3 = 3.0)$ is shown in Fig. 6.5. It clearly shows the complete separation of the target components as predicted by the triangle theory.

The Langmuir isotherm

$$q_i = \frac{\varrho_i c_i}{1 + \sum_j \theta_j c_j} \quad (6.14)$$

is one of the most popular sorption isotherms. Beside the flexibility to reproduce many sorption mechanisms [11], it provides also many mathematical features that simplify an analysis, in particular related to equilibrium theory [15] and therefore also for the triangle theory [9]. If Eq. (6.14) is fitted to Eq. (6.6), the corresponding sets of complete separation predicted by the two different models can be compared. Fig. 6.6 shows that the Langmuir-related triangular set is a subset

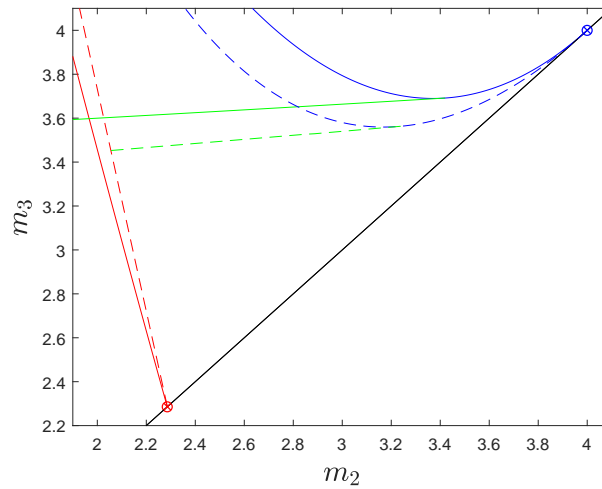


Figure 6.6: Comparison of predicted TMB triangles using CIE (solid lines) and Langmuir isotherm (dashed lines), respectively. Fitted Langmuir parameters: $\varrho_1 = 4.0$, $\theta_1 = 0.413$, $\varrho_2 = 2.286$, $\theta_2 = 0.095$

of the one related to the CIE. There is a distinct difference particularly close to the optimal operating point [89], i.e. the intersection of the red and green lines. Hence, a design based on Langmuir isotherm can lead to suboptimal operating conditions.

The results presented so far, allow also an investigation of the effect of the solution normality c_{tot} , which can be used as a process design parameter. For this purpose, three scenarios with different but fixed solution normalities are considered. Further, the values of c_{tot} do not lie within a reversal zone (Appendix E), i.e. $c_{\text{tot}} \notin [0.286, 0.327] \frac{\text{mol}}{\text{l}}$. The corresponding triangular-shaped sets can be seen in Fig. 6.7. From this figure it is clear that, at least in the range of these cases, differences in c_{tot} have only a minor effect on the shape of the three sets. However, there is a significant change of their position in the (m_2, m_3) plane. Thus, significantly different regions for the sets of complete separation are available through variation of c_{tot} .

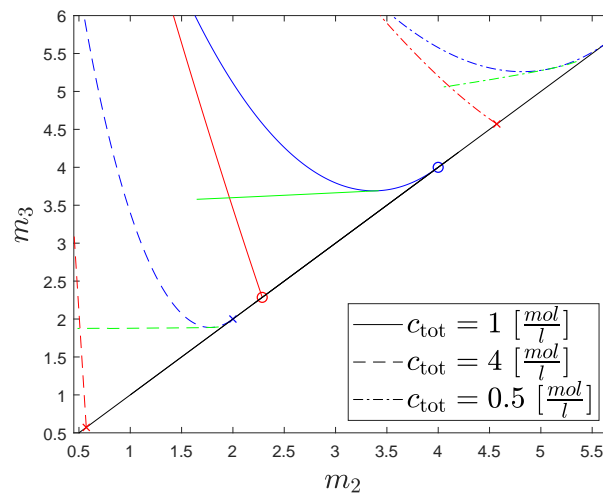


Figure 6.7: Effect of different but constant solution normalities on the predicted TMB triangle. All three cases $c_{tot} = 1$ (solid lines), $c_{tot} = 4$ (dashed lines), and $c_{tot} = 0.5$ (dash-dot lines) without selectivity reversal.

6.4 Summary

In this chapter, the triangle theory was applied to the CIE, which allows the rational design of ion exchange simulated moving bed processes. This can also be done by using the Langmuir isotherm, which however is shown to lead to regions of suboptimal process conditions. In a first step, the potential of the solution normality as additional design parameter was investigated. It provides a greater flexibility for the choice of (m_2, m_3) values, which then can be used to accommodate other process aspects in order to increase the performance. Further, the efficient numerical approach for implicit adsorption isotherms presented in Section 4.2 was successfully extended to TMB processes. Thus, simulations of the TMB were used to validate theoretical results.

Chapter 7

Concluding Remarks

The model-based analysis of chromatographic processes with implicit sorption isotherms was demonstrated for the AIE, including the CIE as special case, and the IAST. Our model-based analysis can be categorized in an analytic and numerical approach. The analytical approach is based on the analysis of an ideal column model, which assumes thermodynamic equilibrium between fluid and solid phase and neglects actual dispersion, among others. The non-linearity is introduced by the sorption isotherm. Characteristic patterns of behavior are analyzed and discussed step by step for different implicit sorption isotherms and compared to numerical solutions, which were obtained efficiently with a new DAE approach. Main results are summarized in the following.

7.1 Analytical Approach

First, focus is on ion exchange. If not stated otherwise, results are related to AIE. Obtaining the boundaries on the eigenvalues of the Jacobian, which is based on an analytical representation of the corresponding characteristic equation, allowed to deduce hyperbolicity. In addition, it was possible to obtain analytical representations of the corresponding eigenvectors. This allowed to easily apply the MOC for system with an arbitrary number of components. In case of the IAST it was at least possible to derive generalized spectral properties for binary systems. The MOC allowed to semi-analytically obtain results for so-called Riemann problems. In particular, the type of transitions that connect states related to different plateaus could be identified. Moreover, the topology for all simple wave solutions became available through the grid composed of integral curves. This grid is also closely related to the shock curves, and it can be used at least qualitatively to predict the behavior in case of shock wave solutions. Knowledge on the eigenvalues also allowed to use entropy conditions that help to predict which sequence of transitions connecting initial, boundary, and intermediate states is admissible. It was possible to include this information also as a topological property into the path grid through the proof of genuine non-linearity everywhere except for some

linear degenerate paths. These linear degenerate paths were also analyzed and can be categorized in two types. Regarding the first type, these are contact discontinuities that are the only path along which the solution normality changes. In fact, the related left eigenvector is shown to be the normal vector to hyperplanes with constant solution normality. Hence, they are shown to be a so-called Riemann invariant. In other words, every transition not related to this type of linear degenerate field is shown to exist only on a hyperplane of constant solution normality. This is a key property of the concentration phase space. It was also possible to show that steric factors have only a quantitative but not qualitative effect on such hyper planes since there exists a linear transformation between isotherms that differ only in their steric factors. The second type of linear degenerate paths defines so-called reversal hyperplanes. Since these paths are invariant to the hyper planes of constant solution normality, they exist in the intersection of the two hyperplane types. The existence of reversal hyperplanes was shown to be more relaxed compared to classical selectivity reversals in [28]. The reversal planes can be intersected by either a hyperplane of constant solution normality or the linear degenerate paths on which the solution normality changes. Hence, the reversal hyperplanes are another key property of the concentration phase space allowing to predict reversals. In particular, it was possible to define reversal zones, which allows to distinguish between guaranteed occurrence of reversals, guaranteed absence of reversals, or potential occurrence of reversals during a sequence of transitions. In addition, different reversal hyperplanes are shown to be usually separated from each other since there is no proper intersection between them. However, the case of coinciding reversal hyperplanes was investigated. This case is an interesting example for a loss of strict hyperbolicity but remains hyperbolic and is proven to admit also a unique solution with a reduced number of required transitions. Generally, all analytical results are local requiring sufficiently close initial and boundary states. However, it was also possible to prove that hyperplanes of constant solution normality are

- i) hyperbolic everywhere with the exception uncritical of water shed points
- ii) genuinely nonlinear everywhere with the exception of contact discontinuities, which however do not affect uniqueness of solutions
- iii) domains for which the SMA sorption isotherm admits a global inverse.

These three properties ensure the global character for the existence of unique Riemann solutions on these hyperplanes since none of these three properties is valid only locally as assumed by general theorems. Note, in Section 5.3 the first type of linear degenerate paths that connects these domains admits also a unique solution for any two points on different hyperplanes and is therefore extending the global character to the complete positive orthant. Consequently, any sequence in the complete concentration phase space \mathbb{R}^N based on Riemann problems remains global in character. The existence of a global inverse is shown in two different ways. One of them, the 'global inverse function theorem' requires detailed knowledge

of the Jacobian including the boundary of the domain, which can be particularly difficult. In obtaining the required results even more properties were revealed, e.g. an analytic representation of water shed curves or the existence of the continuation of the eigenvector representations on the boundary.

All the mathematical properties mentioned above allow clearly for a deeper understanding without requiring any simulation or experimental results. Hence, they allow for a qualitatively efficient first process design reducing the required amount of time, resources, and therefore money. This first design can then be used iteratively to design the real world behavior of the process. In case the real world set-up uses step gradients, the quantitative results based on Riemann problem solutions further improve the predictability of the real world behavior. However, even in different set-ups like gradient elution, analytical results can be used either as initial guess or to define favorable conditions improving the subsequent experimental design and/or numerical optimization of the sorption process.

7.2 Numerical Approach

For both, AIE (including CIE) and IAST, analytical results are used to validate the numerical solution strategy. The solution strategy itself however, is not limited to conservation laws. It is applicable to any equilibrium model since all of these models allow for the presented reformulation. In addition, any sorption isotherm that can be represented by $\mathbf{0} = \mathbf{f}(\mathbf{c}, \mathbf{q})$ (e.g. AIE) or $\mathbf{0} = \mathbf{f}(\mathbf{c}, \mathbf{c}^0, \mathbf{q})$ (e.g. IAST) is admissible. The main purpose of the PDAE formulation is to provide numerical efficiency by avoiding explicit (numerical) differentiation of the Jacobian. The efficiency depends on the differential index. In the best case, it is equal to one. It was possible to guarantee this property for any sorption admitting a Jacobian with only non-negative eigenvalues. If the MOL is applied, the resulting DAE system also has a differential index of one and can be efficiently solved by choosing one of the many available advanced DAE solvers with many features like variable step size or error control among others. The solution strategy is also independent of any manual discretization scheme, which is required for the MOL. The efficiency of the approach was shown for the more complex IAST. In this case, there exists even a numerical solution approach that is specifically tailored to the structure of algebraic equations admitted by the IAST [42]. Despite its age, the modified FastIAS approach is still a state of the art solution approach. However, the example presented in Subsection 3.3.1 clearly demonstrates that the presented numerical approach can outperform the FastIAS. There are in addition numerous other advantages: Consistent initial guesses need to be calculated only once separately before the simulation, accessibility to flow-sheet simulation, admissibility of any time dependent boundary conditions, or simplicity of implementation that allows for straight forward extension (e.g. to counter-current continuous separation processes).

Considering the advantages above, the numerical solution strategy is applicable to a large variety of complex sorption processes providing numerical efficiency. This allows for an efficient simulation-based process design, complex numerical optimization, and potentially simulation during online monitoring, e.g. fault diagnosis, model predictive control.

7.3 Future Research

Certainly, there are many interesting challenges for future research like further development of theoretical and numerical results related to multi-column SMB processes with varying solution normality [91, 92]. However, this last section is dedicated to one particular challenge of great interest in ion exchange chromatography. Considering the results summarized in the two preceding subsections, profound insight through analytical results was gained supported also by simulations. The model-based analysis seems to be quite 'successful'. However, the analysis is also bounded by the limitations of model assumptions. The AIE, though using the mechanistic SMA, does not cover one very important aspect; pH dependency. In ion exchange chromatography, very important applications are bioseparations. These bioseparations primarily involve proteins. Even though the SMA was specifically developed for protein separation by allowing for steric effects and variable solution normality, it does not account for pH variations. 'Unfortunately' in many protein separations, a variation in pH cannot always be prevented through the use of specific buffers if the range of process conditions is large [5, 93]. Hence, pH effects cannot be neglected anymore [94]. In fact, variations of pH in form of internally induced [56, 95] or externally controlled pH gradients [96, 97] are even desired since they can often improve the separation performance. Accounting for the pH dependence has been one of the most discussed topics in recent years [5].

There are basically three approaches that have been used to account for pH dependencies. First, there exists an extension of the SMA that tries to account for pH dependence indirectly through variable charges of the proteins [98, 99, 100]. However, the connection to the pH could not be established based on rigorous physical principles. In addition, the model is enormously complex. As a consequence this approach admits no analytical insight. Even numerical solutions are difficult to obtain, and its predictability considering the pH dependency is limited to the case studies and not applicable more generally. It is of no surprise that this SMA extension was almost not pursued any further. The second approach is motivated by the use of easy or at least well-established isotherms, e.g. linear, Langmuir, SMA among others [101, 102, 103, 104]. These isotherms are simply extended to an empirical version by incorporating the pH dependency directly to previously constant parameters such that they can at least reproduce the experimental data used for modeling. In the limit of no pH variation these models admit their well-known behavior. This approach can already be regarded as surrogate modeling, which in this particular realization is limited to the specific case

studies at hand. Such an approach does also not admit any analytical insight, in particular related to pH variations. In addition, limiting the structure of the isotherm model to a specific well-known isotherm also restricts its applicability. Compared to the first approach, it at least allows for efficient numerical solutions. This approach is usually used, when focus is more on the specific process and the data is already restricted to a specific set-up so that it might be sufficient to use a simple chromatographic surrogate isotherm model. A more rigorous application of the approach is clearly out of question. The third approach is genuine surrogate modeling in ion exchange chromatography [105, 34, 106, 35, 107]. This principle is applied for a large variety of applications [108]. Developed in the 1950s, it became more popular with the advances in computer technology, especially during the last two decades when artificial intelligence and big data became a popular topic throughout engineering and natural sciences as well as mathematics and informatics. As the name implies, surrogate models also do not provide analytical insight, but are rigorously applicable to very large variety of different processes. The methods and tools developed for surrogate model enable often efficient numerical solutions. Therefore, the third option seems to be superior to the other two. At least numerically, especially regarding numerical optimization, it is the most efficient and universally applicable approach. Accordingly, surrogate modeling is applied most frequently. All three approaches mentioned above do not admit any analytical insight. This work however, is an example that it is worth investigating the possibility of a mechanistic model accounting for the pH dependence while retaining analytical accessibility at least to some degree. For this purpose, the following idea is briefly presented. Based on the results obtained for the AIE in this work, it is well worth investigating a suitable extension to account for pH variations. The key idea is the introduction of modes for each component defined by different but constant SMA parameters. In particular, each component is assumed to affect the pH through chemical reaction with water thus changing the concentration of H_3O^+ (or OH^-). Each reaction results in a new mode of a component. The concentration of these modes are identified as additional states in the concentration phase space. This extended state (or phase) space needs to be limited only to relevant modes in order to limit its dimension. Therefore, identifying the relevant modes with their respective SMA parameters (characteristic charge, equilibrium constant, and steric factor) and modeling their chemical reaction is the main challenge of this approach. If the approach is indeed realizable, concentration of the components do not only depend on sorption but also on the reactions in the fluid phase. In a next step, generalized concentrations states are used as in [80, 81, 82] in order to obtain again a conservation law that can be subjected to a profound mathematical analysis. Hopefully, this will amount to some theoretical insight into the (original) concentration phase space and its topological key features, which would be a very important tool in the efficient design for protein separation processes.

This page intentionally left blank.

Appendix

Appendix A IAST: Spectral properties

The results for the differential index in Chapter 3 depend on the eigenvalues λ_i of the Jacobian matrix $\frac{\partial \mathbf{q}}{\partial \mathbf{c}}$. It has been shown in [41] that these eigenvalues are always real and positive for IAST isotherms provided the SCIs $q_i^0(c_i^0)$ are strictly monotonically increasing and have the structure defined by Eq. (2.58). This structural requirement is met by many but not all SCIs. A counter example using the Tóth isotherm is considered at the end of this appendix.

The monotonicity requirement

$$\frac{dq_i^0(c_i^0)}{dc_i^0} > 0, \quad c_i^0 \neq 0 \quad i = 1, \dots, N, \quad (\text{A.1})$$

is a direct consequence of phase stability. Any non-monotonic SCI will give rise to two different fluid concentrations in equilibrium with the same adsorbed phase concentration indicating a phase split of the fluid phase.

It is worth noting that the above eigenvalue result implies hyperbolicity of the ideal equilibrium model without axial dispersion if the corresponding eigenvectors are linearly independent. Remember, hyperbolicity is the basic requirement for the equilibrium theory [10].

In this appendix the results from [41] will be extended in two directions. First, the result will be generalized to mixtures with two adsorbable components with *any* strictly monotonically increasing SCIs, no matter whether explicit or implicit. Therefore the structural requirement (2.58) is relaxed. Afterwards, it is shown that such general statement is not possible in the multicomponent case with more than two adsorbable components.

First focus is on binary mixtures. The Jacobian of the IAST takes with \mathbf{c} being the only independent variable, i.e. $\mathbf{q} = \mathbf{q}(\mathbf{c}, \mathbf{c}^0(\mathbf{c}, \mathbf{q}^0(\mathbf{c}^0(\mathbf{c}))))$, the generalized form

$$\frac{\partial \mathbf{q}}{\partial \mathbf{c}} = \left(\frac{\partial \mathbf{q}}{\partial \mathbf{c}} \right)_{\mathbf{c}^0} + \left(\frac{\partial \mathbf{q}}{\partial \mathbf{c}^0} \right)_{\mathbf{c}} \frac{\partial \mathbf{c}^0}{\partial \mathbf{c}}, \quad (\text{A.2a})$$

$$\left(\frac{\partial \mathbf{q}}{\partial \mathbf{c}^0} \right)_{\mathbf{c}} = \left(\frac{\partial \mathbf{q}}{\partial \mathbf{c}^0} \right)_{\mathbf{c}, q^0} + \left(\frac{\partial \mathbf{q}}{\partial \mathbf{q}^0} \right)_{\mathbf{c}, \mathbf{c}^0} \frac{\partial \mathbf{q}^0}{\partial \mathbf{c}^0}, \quad (\text{A.2b})$$

$$\frac{\partial \mathbf{c}^0}{\partial \mathbf{c}} = - \left(\frac{\partial \mathbf{f}}{\partial \mathbf{c}^0} \right)_{\mathbf{c}}^{-1} \left(\frac{\partial \mathbf{f}}{\partial \mathbf{c}} \right)_{\mathbf{c}^0}. \quad (\text{A.2c})$$

Note, in (A.2) we require the values of q_i^0 to be explicitly available for each c_i^0 , but no further information on the functional structure of the q_i^0 is required, i.e. it does not matter if $q_i^0 = q_i^0(c_i^0)$ or $0 = h(q_i^0, c_i^0)$ is solved intermediately. A unique solution of the latter is guaranteed due to the strict monotonicity of the SCIs.

For $N = 2$, the analytical formula of the Jacobian reads accordingly

$$\mathbf{J} = \frac{\partial \mathbf{q}}{\partial \mathbf{c}} = q_{\text{tot}}^2 \begin{bmatrix} \frac{\chi_2}{c_1^0 q_2^0} + M_1 & -\frac{\chi_1}{c_2^0 q_2^0} + \frac{c_1^0}{c_2^0} M_1 \\ -\frac{\chi_2}{c_1^0 q_1^0} + \frac{c_2^0}{c_1^0} M_2 & \frac{\chi_1}{c_2^0 q_1^0} + M_2 \end{bmatrix}, \quad (\text{A.3a})$$

$$M_1 = \chi_1 \frac{q_{\text{tot}}}{c_1^0 q_1^0} \left(\frac{\chi_1}{q_1^0} \frac{c_1^0}{q_1^0} \frac{dq_1^0}{dc_1^0} + \frac{q_1^0}{q_2^0} \frac{\chi_2}{q_2^0} \frac{c_2^0}{q_2^0} \frac{dq_2^0}{dc_2^0} + \frac{q_1^0}{q_2^0} \frac{\chi_2}{q_2^0} - \frac{\chi_2}{q_2^0} \right), \quad (\text{A.3b})$$

$$M_2 = \chi_2 \frac{q_{\text{tot}}}{c_2^0 q_2^0} \left(\frac{\chi_2}{q_2^0} \frac{c_2^0}{q_2^0} \frac{dq_2^0}{dc_2^0} + \frac{q_2^0}{q_1^0} \frac{\chi_1}{q_1^0} \frac{c_1^0}{q_1^0} \frac{dq_1^0}{dc_1^0} + \frac{q_2^0}{q_1^0} \frac{\chi_1}{q_1^0} - \frac{\chi_1}{q_1^0} \right), \quad (\text{A.3c})$$

with molar fractions $\chi_i = \frac{c_i}{c_i^0}$ as defined in Eq. (2.12). The eigenvalues of Jacobian in (A.3a) can be derived from the characteristic equation $\det(\mathbf{J} - \lambda I)$ resulting in the following quadratic equation

$$a\lambda^2 - b\lambda + c = 0, \quad (\text{A.4a})$$

$$a = q_{\text{tot}}^{-4}, \quad (\text{A.4b})$$

$$b = q_{\text{tot}}^{-2} \left(\frac{1}{c_1^0} \frac{1}{q_2^0} \chi_2 + \frac{1}{c_2^0} \frac{1}{q_1^0} \chi_1 + M_1 + M_2 \right), \quad (\text{A.4c})$$

$$c = \frac{1}{c_2^0} \frac{1}{q_1^0} M_1 + \frac{1}{c_1^0} \frac{1}{q_2^0} M_2, \quad (\text{A.4d})$$

where the two possible eigenvalues can be readily derived

$$\lambda_i = \frac{b \pm \sqrt{b^2 - 4ac}}{2a}. \quad (\text{A.5})$$

In order to obtain spectral properties that guarantee a differential index of one for any pair of monotonic increasing SCIs, both eigenvalues have to be real and positive. In (A.4b), the inequality $a > 0$ is obviously satisfied since all concentrations are positive. Based on (A.5), the inequalities

$$b > 0, \quad (\text{A.6a})$$

$$c > 0, \quad (\text{A.6b})$$

$$b^2 - 4ac \geq 0, \quad (\text{A.6c})$$

have to be additionally verified to realize the required spectral properties.

Using relation (A.1), one can derive for both coefficients a , b lower limits a_l , b_{low} from their definition in (A.4b,A.4c) by applying $\frac{dq_i^0}{dc_i^0} = 0$ to M_1 and M_2 resulting in

$$b_{\text{low}} = q_{\text{tot}}^{-1} \left(\frac{1}{c_1^0 q_2^0} \frac{\chi_2}{q_2^0} + \frac{1}{c_2^0 q_1^0} \frac{\chi_1}{q_1^0} \right) > 0, \quad (\text{A.7a})$$

$$b > b_{\text{low}} > 0, \quad (\text{A.7b})$$

$$c_{\text{low}} = \frac{q_{\text{tot}}}{c_1^0 c_2^0} \left(\frac{\chi_1 \chi_2}{q_1^0 q_2^0} - \frac{\chi_1 \chi_2}{(q_1^0)^2 q_2^0} + \frac{\chi_1 \chi_2}{(q_1^0)^2 q_2^0} - \frac{\chi_1 \chi_2}{q_1^0 q_2^0} \right) = 0, \quad (\text{A.7c})$$

$$c > c_{\text{low}} = 0. \quad (\text{A.7d})$$

The term $b^2 - 4ac$ can be reformulated such that it readily satisfies the inequality in (A.6c)

$$b^2 - 4ac = q_{\text{tot}}^{-2} ((\gamma - \alpha - \beta)^2 + 4(\rho - \tau)^2 \zeta) \geq 0, \quad (\text{A.8a})$$

$$\alpha = \frac{1}{c_1^0 q_1^0} \chi_1 \left(\frac{\chi_1 c_1^0}{q_1^0 q_1^0} \frac{dq_1^0}{dc_1^0} + \frac{q_1^0 \chi_2}{q_2^0 q_2^0} \frac{c_2^0}{q_2^0} \frac{dq_2^0}{dc_2^0} \right) > 0, \quad (\text{A.8b})$$

$$\beta = \frac{1}{c_2^0 q_2^0} \chi_2 \left(\frac{\chi_2 c_2^0}{q_2^0 q_2^0} \frac{dq_2^0}{dc_2^0} + \frac{q_2^0 \chi_1}{q_1^0 q_1^0} \frac{c_1^0}{q_1^0} \frac{dq_1^0}{dc_1^0} \right) > 0, \quad (\text{A.8c})$$

$$\gamma = \frac{1}{c_1^0 q_2^0} \frac{\chi_2}{q_2^0} + \frac{1}{c_2^0 q_1^0} \frac{\chi_1}{q_1^0} > 0, \quad (\text{A.8d})$$

$$\rho = \frac{1}{c_2^0 q_1^0} > 0, \quad (\text{A.8e})$$

$$\tau = \frac{1}{c_1^0 q_2^0} > 0, \quad (\text{A.8f})$$

$$\zeta = \frac{\chi_1 \chi_2}{q_1^0 q_2^0} \left(\chi_1 \frac{c_1^0 q_2^0}{q_1^0 q_1^0} \frac{dq_1^0}{dc_1^0} + \chi_2 \frac{c_2^0 q_1^0}{q_2^0 q_2^0} \frac{dq_2^0}{dc_2^0} \right) > 0, \quad (\text{A.8g})$$

thus concluding the proof of $\lambda_i \in \mathbb{R}_{>0}$ with $i \in \{1, 2\}$ for binary mixtures. If additionally the following is satisfied

$$\int_0^{c_1^0} \frac{q_1^0(\sigma)}{\sigma} d\sigma = \int_0^{c_2^0} \frac{q_2^0(\sigma)}{\sigma} d\sigma \quad \rightarrow \quad \frac{q_1^0}{c_1^0} \neq \frac{q_2^0}{c_2^0}, \quad (\text{A.9})$$

which is a negligible restriction for the choice of the SCIs, the relation in (A.6c) becomes a strict inequality since $(\rho - \tau)^2 > 0$ holds. Hence, both eigenvalues are also distinct and the Jacobian is strictly hyperbolic for non-vanishing concentrations.

The previous result of real and positive eigenvalues using only the assumption (A.1) cannot be extended to systems with more than two components, which is similar to the spectral results in [47]. For this purpose, a simple three component counter example using the Tóth isotherm

$$q_i^0 = q_i^{\text{sat}} b_i c_i^0 (1 + (b_i c_i^0)^{\theta_i})^{-\frac{1}{\theta_i}}, \quad i \in \{1, 2, 3\}, \quad (\text{A.10})$$

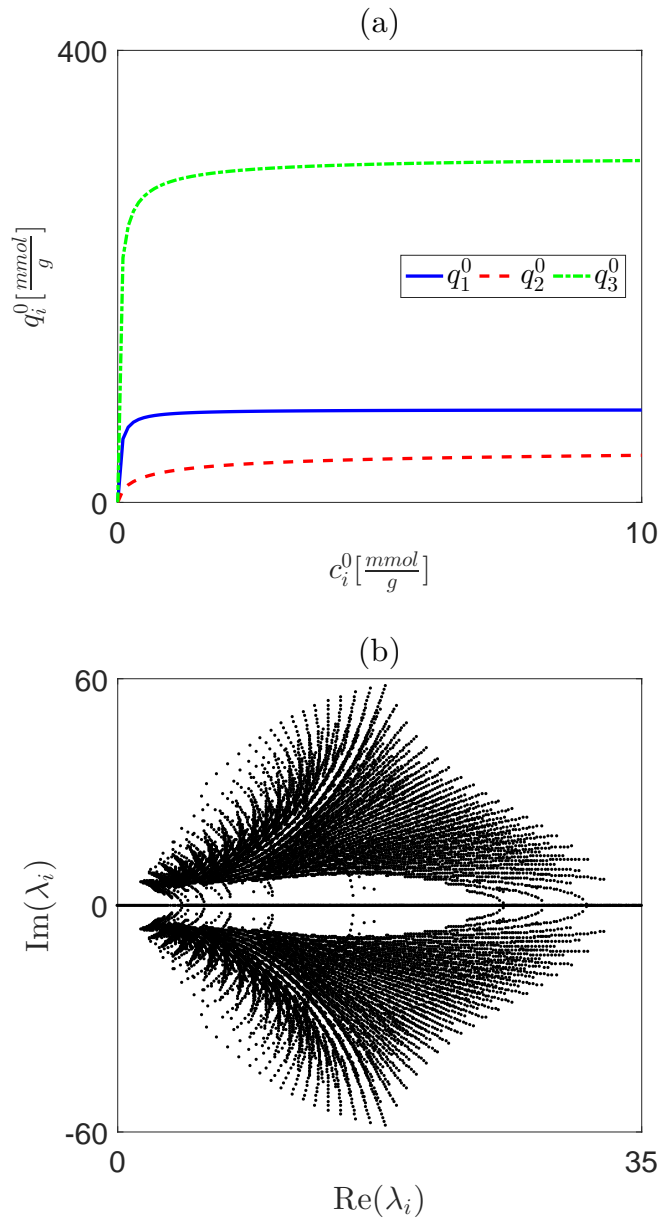


Figure Appendix A.1: (a) SCIs of toluene (component 1), dichloromethane (component 2) and trichloroethylene (component 3) computed with the Tóth model. (b) Complex right half-plane of all three eigenvalues for 100^3 concentration combinations $c_i \in [0, 10] \frac{\text{mmol}}{\text{g}}$.

parameter	$i = 1$	$i = 2$	$i = 3$
$q_i^{\text{sat}} [\frac{\text{mmol}}{\text{g}}]$	82.135	51.683	307.89
$b_i [-]$	22.476	6.894	307.89
$\vartheta_i [-]$	0.98	0.509	0.675

Table Appendix A.1: Parameters of the Tóth isotherm in Appendix A.

which satisfies (A.1) for all physically relevant concentrations, as shown in Fig. Appendix A.1a, is considered. Parameter values in Tab. Appendix A.1 are taken from [109]. A reasonable range of $[0.1 : 0.1 : 10] \frac{\text{mmol}}{\text{g}}$ for the concentrations c_i of all three components allows for 100^3 different vector valued concentrations $\mathbf{c} = [c_1, c_2, c_3]^T$. Exploiting the general definition (A.2) of the Jacobian, every eigenvalue that corresponds to a particular value of \mathbf{c} can be calculated numerically using standard software, e.g. MATLAB[®] [69]. The results are shown in Fig. Appendix A.1b, where the location of the eigenvalues $\lambda_i(\mathbf{c})$ in the complex right half-plane is shown. Since the existence of complex eigenvalues can be easily concluded from Fig. Appendix A.1b, the Jacobian of this counter example is indeed not hyperbolic. As a consequence, the Jacobian does admit neither strict hyperbolicity nor exclusively real, positive eigenvalues.

Appendix B CIE: Differential Index

In the remainder of this appendix, it is shown that the PDAE system (4.9), or the corresponding DAE system resulting from the discretization of (4.9), using the MOL approach, respectively, is of differential index 1, whenever the Jacobian $\frac{\partial \mathbf{y}}{\partial \mathbf{x}}$ has $N-1$ real, positive eigenvalues λ_i . As stated in Section 3.2, for thermodynamic reasons this should always be the case [76]. Hence, the result of this appendix does not only apply to mass action equilibria but is valid for any thermodynamically reasonable sorption equilibrium.

The PDAE system (4.9) is of differential index 1 when the matrix of the derivatives of the algebraic equations (4.9b) with respect to the algebraic variable \mathbf{x} is nonsingular. From differentiation of Eq. (4.9b) we find

$$\left(\frac{\partial \mathbf{f}}{\partial \mathbf{x}}\right)_{\mathbf{w}} = \left(\frac{\partial \mathbf{f}}{\partial \mathbf{x}}\right)_{\mathbf{y}} - \frac{1}{\kappa} \left(\frac{\partial \mathbf{f}}{\partial \mathbf{y}}\right)_{\mathbf{x}}. \quad (\text{B.1})$$

Therein, the indices at the brackets indicate which variable is constant during differentiation.

For the calculation of the Jacobian $\frac{\partial \mathbf{y}}{\partial \mathbf{x}}$, the equilibrium composition of the solid phase \mathbf{y} is interpreted as a function of the fluid phase composition \mathbf{x} . From implicit differentiation of the equilibrium relation

$$\mathbf{0} = \mathbf{f}(\mathbf{x}, \mathbf{y}(\mathbf{x})) \quad (\text{B.2})$$

we find

$$\frac{\partial \mathbf{y}}{\partial \mathbf{x}} = - \left(\frac{\partial \mathbf{f}}{\partial \mathbf{y}}\right)_{\mathbf{x}}^{-1} \left(\frac{\partial \mathbf{f}}{\partial \mathbf{x}}\right)_{\mathbf{y}} \quad (\text{B.3})$$

Since $\frac{\partial \mathbf{y}}{\partial \mathbf{x}}$ has $N-1$ positive eigenvalues λ_i , it is regular, i.e. its determinant is nonzero. Further, due to the product rule for determinants both matrices on the right hand side of the above equation also have to be regular. Substitution of Eq. (B.3) into Eq. (B.1) yields

$$\left(\frac{\partial \mathbf{f}}{\partial \mathbf{x}}\right)_{\mathbf{w}} = - \left(\frac{\partial \mathbf{f}}{\partial \mathbf{y}}\right)_{\mathbf{x}} \left(\frac{\partial \mathbf{y}}{\partial \mathbf{x}} + \frac{1}{\kappa} \mathbf{I}_{N-1}\right). \quad (\text{B.4})$$

The eigenvalues of

$$\left(\frac{\partial \mathbf{y}}{\partial \mathbf{x}} + \frac{1}{\kappa} \mathbf{I}_{N-1}\right) \quad (\text{B.5})$$

are equal to $\lambda_i + 1/\kappa$ and are therefore also positive and the corresponding matrix is regular. Hence, the matrix on the left hand side of Eq. (B.4) is a product of two regular matrices and therefore also regular, which completes the proof.

Finally, the DAE system resulting from the discretization of (4.9) using a MOL approach is also of differential index 1, if the above is satisfied at any spatial position in the reactor. This however, is trivial since the above results are valid for any concentrations.

Appendix C AIE: Genuine Non-linearity

The following considerations in this appendix exclude $\lambda_k = 0$ and $\lambda_k = \frac{q_k}{c_k}$ for any k . Both cases are shown to be linear degenerate in Section 5.3. In the remainder the k th field is shown to be genuinely non-linear for a certain subset \mathcal{C} of $\mathbb{R}_{\geq 0}^N$ according to

$$\nabla \lambda_k(\mathbf{c}) \mathbf{r}_k(\mathbf{c}) \neq 0, \quad \forall \mathbf{c} \in \mathcal{C}. \quad (\text{C.1})$$

The gradient of λ_k can be obtained through implicit differentiation of the characteristic equation (5.11)

$$\varphi(\mathbf{c}, \mathbf{q}, \lambda_k) = 0 = \lambda_k \sum_{i=1}^N \frac{\xi_i \nu_i}{\frac{1}{c_i} - \lambda_k \frac{1}{q_i}}, \quad (\text{C.2})$$

which results in

$$\frac{\partial \lambda_k}{\partial c_j} = - \left(\frac{\partial \varphi}{\partial \lambda_k} \right)_{\mathbf{c}, \mathbf{q}}^{-1} \left(\left(\frac{\partial \varphi}{\partial c_j} \right)_{\mathbf{c} \setminus c_j, \mathbf{q}, \lambda_k} + \sum_{l=1}^N \left(\frac{\partial \varphi}{\partial q_l} \right)_{\mathbf{c}, \mathbf{q} \setminus q_l, \lambda_k} \frac{\partial q_l}{\partial c_j} \right). \quad (\text{C.3})$$

Hereafter, constant held variables will be omitted for clarity of presentation. Results for the derivatives in (C.3) are summarized in the following

$$\frac{\partial \varphi}{\partial \lambda_k} = \lambda_k \sum_{i=1}^N \frac{\xi_i \frac{1}{q_i}}{\left(\frac{1}{c_i} - \lambda_k \frac{1}{q_i} \right)^2}, \quad (\text{C.4a})$$

$$\frac{\partial \varphi}{\partial c_j} = \frac{\lambda_k}{c_j^2} \frac{\xi_j \nu_j}{\left(\frac{1}{c_j} - \lambda_k \frac{1}{q_j} \right)^2}, \quad (\text{C.4b})$$

$$\frac{\partial \varphi}{\partial q_l} = - \frac{\lambda_k^2}{q_l^2} \frac{\xi_l \nu_l}{\left(\frac{1}{c_l} - \lambda_k \frac{1}{q_l} \right)^2}, \quad (\text{C.4c})$$

$$\frac{\partial q_l}{\partial c_j} = \frac{\nu_N}{\nu_l} \frac{q_l}{q_N} \left(\frac{\partial q_N}{\partial c_j} - \frac{q_N}{c_N} \delta_{jN} \right) + \frac{q_j}{c_j} \delta_{jl}, \quad (\text{C.4d})$$

$\forall k, j, l.$

Here, δ denotes the Kronecker delta. Eq. (C.4d) contains $\frac{\partial q_N}{\partial c_j}$, which can also be obtained through implicit differentiation of (5.2b) when substituting all components q_m with $m \neq N$ by (5.2a)

$$\psi(\mathbf{c}, q_N) = 0 = q_{\text{tot}} - \sum_{m=1}^N \xi_m c_m K_{mN}^{\frac{1}{\nu_m}} \left(\frac{q_N}{c_N} \right)^{\frac{\nu_N}{\nu_m}}, \quad (\text{C.5})$$

resulting in

$$\begin{aligned}\frac{\partial q_N}{\partial c_j} &= - \left(\frac{\partial \psi}{\partial q_N} \right)_c^{-1} \left(\frac{\partial \psi}{\partial c_j} \right)_{c \setminus c_j, q_N}, \\ &= - \frac{q_N}{\nu_N} \left(\sum_{m=1}^N \frac{\xi_m}{\nu_m} q_m \right)^{-1} \xi_j \frac{q_j}{c_j} + \frac{q_N}{c_N} \delta_{jN},\end{aligned}\tag{C.6}$$

which allows us to write

$$\frac{\partial q_l}{\partial c_j} = - \frac{q_l}{\nu_l} \left(\sum_{m=1}^N \frac{\xi_m}{\nu_m} q_m \right)^{-1} \xi_j \frac{q_j}{c_j} + \frac{q_l}{c_j} \delta_{jl}.\tag{C.7}$$

Therefore, an element of the gradient of any λ_k can be written as follows

$$\frac{\partial \lambda_k}{\partial c_j} = -G(H_j + W_j),\tag{C.8a}$$

$$G = \left(\sum_{i=1}^N \frac{\frac{\xi_i}{\nu_i} \frac{1}{q_i}}{\left(\frac{1}{c_i} - \lambda_k \frac{1}{q_i} \right)^2} \right)^{-1} > 0,\tag{C.8b}$$

$$H_j = \frac{\frac{\xi_j}{\nu_j} \frac{1}{c_j}}{\left(\frac{1}{c_j} - \lambda_k \frac{1}{q_j} \right)},\tag{C.8c}$$

$$W_j = \lambda_k \sum_{l=1}^N \frac{\frac{\xi_l}{\nu_l} \frac{1}{q_l}}{\left(\frac{1}{c_l} - \lambda_k \frac{1}{q_l} \right)^2} \left(\sum_{m=1}^N \frac{\xi_m}{\nu_m} q_m \right)^{-1} \xi_j \frac{q_j}{c_j} = W \xi_j \frac{q_j}{c_j} > 0,\tag{C.8d}$$

$\forall k, j$.

Using the derived representation of $\nabla \lambda_k$ and the definition of the corresponding non-trivial eigenvector \mathbf{r}_k in (5.15), the following arithmetic expression is obtained

$$\nabla \lambda_k(\mathbf{c}) \mathbf{r}_k(\mathbf{c}) = -G(H + WZ) < 0,\tag{C.9a}$$

$$H = \sum_{j=1}^N \frac{H_j^2}{\frac{\xi_j}{c_j}} > 0,\tag{C.9b}$$

$$Z = \sum_{j=1}^N \frac{q_j}{c_j} \frac{\frac{\xi_j}{\nu_j}}{\frac{1}{c_j} - \lambda_k \frac{1}{q_j}} > 0.\tag{C.9c}$$

Since all parameters, present concentrations and all eigenvalues ($\lambda_N = 0$ already excluded) are greater than zero, the inequalities for G , H , W in (C.8b,C.9b,C.8d)

are obviously satisfied. The inequality for Z in (C.9c) is deduced from a lower bound that is derived in the following

$$Z = T + U, \quad (\text{C.10a})$$

$$T = \sum_{j=1}^k \frac{q_j}{c_j} \frac{\frac{\xi_j}{\nu_j}}{\frac{1}{c_j} - \lambda_k \frac{1}{q_j}}, \quad \frac{q_j}{c_j} \geq \frac{q_k}{c_k} > \lambda_k, \quad (\text{C.10b})$$

$$U = \sum_{j=k+1}^N \frac{q_j}{c_j} \frac{\frac{\xi_j}{\nu_j}}{\frac{1}{c_j} - \lambda_k \frac{1}{q_j}}, \quad \frac{q_j}{c_j} < \lambda_k < \frac{q_k}{c_k}, \quad (\text{C.10c})$$

$$T \geq \frac{q_k}{c_k} \sum_{j=1}^k \frac{\frac{\xi_j}{\nu_j}}{\frac{1}{c_j} - \lambda_k \frac{1}{q_j}}, \quad (\text{C.10d})$$

$$U > \frac{q_k}{c_k} \sum_{j=k+1}^N \frac{\frac{\xi_j}{\nu_j}}{\frac{1}{c_j} - \lambda_k \frac{1}{q_j}}, \quad (\text{C.10e})$$

$$Z > \frac{q_k}{c_k} \sum_{j=1}^N \frac{\frac{\xi_j}{\nu_j}}{\frac{1}{c_j} - \lambda_k \frac{1}{q_j}} = 0, \quad (\text{C.10f})$$

where the equality in (C.10f) can be easily deduced from (5.11) for positive eigenvalues. Hence, all characteristic fields of a family $k < N$ and with $\lambda_k \neq \frac{q_k}{c_k}$ are genuinely non-linear for all $\mathbf{c} \in \mathcal{C} = \mathbb{R}_{\geq 0}^N$, i.e. no negative concentrations. The fact that the results in this appendix are also valid on the boundary, i.e. an arbitrary number (but not all) of arbitrary components is not present, is demonstrated in Appendix I.

Note, the entries of the Jacobian $\frac{\partial \mathbf{q}}{\partial \mathbf{c}}$ are defined by (C.7). Therefore, it is possible to determine the left eigenvectors \mathbf{l}_k that correspond to some eigenvalue λ_k by solving the following equations

$$\mathbf{l}_k \left(\frac{\partial \mathbf{q}}{\partial \mathbf{c}} - \lambda_k \mathbf{I}_N \right) = \mathbf{0}, \quad (\text{C.11a})$$

$$\sum_{i=1}^N l_{k,i} \frac{\partial q_i}{\partial c_j} - \lambda_k l_{k,j} = 0 \quad (\text{C.11b})$$

$$l_{k,j} = \frac{\frac{\xi_j}{c_j}}{\frac{1}{c_j} - \lambda_k \frac{1}{q_j}} \left(\sum_{m=1}^N \frac{\xi_m}{\nu_m} q_m \right)^{-1} \sum_{i=1}^N l_{k,i} \frac{q_i}{\nu_i}, \quad (\text{C.11c})$$

$\forall k, j = 1, \dots, N.$

The Eqs. in (C.11) are satisfied by choosing

$$\mathbf{l}_k = \left[\frac{\frac{\xi_1}{c_1}}{\frac{1}{c_1} - \lambda_k \frac{1}{q_1}}, \dots, \frac{\frac{\xi_N}{c_N}}{\frac{1}{c_N} - \lambda_k \frac{1}{q_N}} \right], \quad (\text{C.12})$$

which can be validated using (5.11) to obtain the identity

$$\begin{aligned}
\sum_{i=1}^N \frac{\xi_i}{\nu_i} q_i &= \sum_{i=1}^N \frac{\xi_i}{\nu_i} q_i + \sum_{i=1}^N \frac{\lambda_k \frac{\xi_i}{\nu_i}}{\frac{1}{c_i} - \lambda_k \frac{1}{q_i}}, \\
&= \sum_{i=1}^N \frac{\frac{\xi_i}{\nu_i} q_i \left(\frac{1}{c_i} - \lambda_k \frac{1}{q_i} \right) + \lambda_k \frac{\xi_i}{\nu_i}}{\frac{1}{c_i} - \lambda_k \frac{1}{q_i}}, \\
&= \sum_{i=1}^N \frac{\frac{\xi_i}{\nu_i} \frac{q_i}{c_i}}{\frac{1}{c_i} - \lambda_k \frac{1}{q_i}} = \sum_{i=1}^N l_{k,i} \frac{q_i}{\nu_i}
\end{aligned} \tag{C.13}$$

in conjunction with the results in (C.11). In contrast to the right eigenvectors in (5.15), the left eigenvectors depend on the ξ but not directly on the ν parameters (only indirectly through ξ). The left eigenvector corresponding to $\lambda_N = 0$ becomes

$$\mathbf{l}_N = [\xi_1, \dots, \xi_N]. \tag{C.14}$$

Due to the special structure of Eq. (C.14)

$$\mathbf{l}_N \mathbf{r}_k = 0 \quad \forall k < N \tag{C.15}$$

holds, which is also implied by (5.14). Further, the following relations can be formulated

$$\mathbf{l}_N \mathbf{r}_N = \sum_{i=1}^N \frac{\xi_i}{\nu_i} c_i > 0, \tag{C.16a}$$

$$\mathbf{l}_N = \nabla_{c_{\text{tot}}}. \tag{C.16b}$$

Consequently c_{tot} hyperplanes defined by (5.3) are Riemann invariants [63] corresponding to λ_N since

$$\nabla_{c_{\text{tot}}} \mathbf{r}_k = \begin{cases} 0 & k = 1, \dots, N \\ \sum_{i=1}^N \frac{\xi_i}{\nu_i} c_i & k = N \end{cases}. \tag{C.17}$$

Appendix D AIE: Reversal Intersections

In the following it is shown that different reversal hyperplanes do not intersect each other. More precisely, the intersection of two arbitrary reversal hyperplanes are either the hyperplanes itself or empty but no proper intersection exists. For this purpose, two arbitrary reversal hyperplanes ' jk ' and ' mn ' that differ in at least one of their indices are considered. From the respective representation based on (5.27), their intersection is defined by

$$0 = \sum_{i=1}^N \xi_i c_i \omega_i, \quad (\text{D.1a})$$

$$\omega_i = \left(K_{ij} K_{jk}^{\frac{\nu_j}{\nu_j - \nu_k}} \right)^{\frac{1}{\nu_i}} - \left(K_{im} K_{mn}^{\frac{\nu_m}{\nu_m - \nu_n}} \right)^{\frac{1}{\nu_i}}. \quad (\text{D.1b})$$

The trivial case, where all components are absent yields no relevance and is therefore not considered. It can be deduced that the ω_i 's have the same sign. In particular the following relations hold

$$K_{jk}^{\frac{\nu_j}{\nu_j - \nu_k}} > K_{jm} K_{mn}^{\frac{\nu_m}{\nu_m - \nu_n}} \rightarrow \omega_i > 0, \quad i = 1, \dots, N, \quad (\text{D.2a})$$

$$K_{jk}^{\frac{\nu_j}{\nu_j - \nu_k}} < K_{jm} K_{mn}^{\frac{\nu_m}{\nu_m - \nu_n}} \rightarrow \omega_i < 0, \quad i = 1, \dots, N. \quad (\text{D.2b})$$

In case of any given ' jk ' and ' mn ' reversal hyperplane, the parameters in (D.2) are fixed for all ω_i . Hence, either $\omega_i > 0$ or $\omega_i < 0$ holds. In addition, all ξ_i are positive, consequently Eq. (D.1a) requires that the c_i do not all have the same sign. In other words, it is necessary that there exists at least a single component ' l ' with $c_l < 0$. Therefore, a proper intersection does not exist in the positive orthant, where $c_i \geq 0$ for all i .

For conditions (D.2), the intersection of two arbitrary reversal hyperplanes for physically meaningful c_i is always empty. However, if

$$\begin{aligned} K_{jk}^{\frac{\nu_j}{\nu_j - \nu_k}} &= K_{jm} K_{mn}^{\frac{\nu_m}{\nu_m - \nu_n}} \rightarrow \omega_i = 0, \\ i &= 1, \dots, N, \end{aligned} \quad (\text{D.3})$$

we can easily conclude that both reversal hyperplanes are identical. A detailed discussion of this case can be found in Appendix H.

Appendix E AIE: Reversal Zones

In this appendix, an interval for c_{tot} , the so-called reversal zone, is defined. A corresponding c_{tot} hyperplane with a value of c_{tot} in this interval is guaranteed to intersect some ' jk ' reversal hyperplane for physically meaningful c_i . For this purpose we consider the equation for the intersection (5.31) of these two types of hyperplanes and apply the same reasoning used prior to Eq. (5.28). Eq. (5.31) can be reformulated into

$$c_{\text{tot}} - q_{\text{tot}} K_{jk}^{-\frac{1}{\nu_j - \nu_k}} = \sum_{i \neq j, k} \xi_i c_i \left(K_{jk}^{\frac{1}{\nu_j - \nu_k}} - \left(K_{ij} K_{jk}^{\frac{\nu_j}{\nu_j - \nu_k}} \right)^{\frac{1}{\nu_i}} \right) K_{jk}^{-\frac{1}{\nu_j - \nu_k}}. \quad (\text{E.1})$$

Therefore, the conditions for solutions that satisfy $c_i > 0$ yield

$$c_{\text{tot}} - q_{\text{tot}} K_{jk}^{-\frac{1}{\nu_j - \nu_k}} = \xi_i c_i \left(K_{jk}^{\frac{1}{\nu_j - \nu_k}} - \left(K_{ij} K_{jk}^{\frac{\nu_j}{\nu_j - \nu_k}} \right)^{\frac{1}{\nu_i}} \right) K_{jk}^{-\frac{1}{\nu_j - \nu_k}}, \quad (\text{E.2a})$$

$$\text{sign} \left(c_{\text{tot}} - q_{\text{tot}} K_{jk}^{-\frac{1}{\nu_j - \nu_k}} \right) = \text{sign} \left(K_{jk}^{\frac{1}{\nu_j - \nu_k}} - \left(K_{ij} K_{jk}^{\frac{\nu_j}{\nu_j - \nu_k}} \right)^{\frac{1}{\nu_i}} \right), \quad (\text{E.2b})$$

$$\forall i \neq j, k.$$

There are two possible cases. First,

$$K_{jk}^{\frac{1}{\nu_j - \nu_k}} \geq \left(K_{ij} K_{jk}^{\frac{\nu_j}{\nu_j - \nu_k}} \right)^{\frac{1}{\nu_i}}, \quad \forall i \neq j, k, \quad (\text{E.3a})$$

$$K_{jk}^{-\frac{1}{\nu_j - \nu_k}} \leq \left(K_{ij} K_{jk}^{\frac{\nu_j}{\nu_j - \nu_k}} \right)^{-\frac{1}{\nu_i}}, \quad \forall i \neq j, k. \quad (\text{E.3b})$$

Based on (E.2)

$$c_{\text{tot}} \geq q_{\text{tot}} K_{jk}^{-\frac{1}{\nu_j - \nu_k}}, \quad (\text{E.4})$$

has to be satisfied in this case, which defines a minimum value for c_{tot} . If further

$$c_{\text{tot}} \leq q_{\text{tot}} \min_{i \neq j, k} \left[\left(K_{ij} K_{jk}^{\frac{\nu_j}{\nu_j - \nu_k}} \right)^{-\frac{1}{\nu_i}} \right], \quad (\text{E.5})$$

holds, (E.3) is guaranteed to be satisfied due to (E.4). Thus, (E.5) defines a maximum value for c_{tot} . In this case the reversal zone in which all c_{tot} planes are guaranteed to intersect some ' jk ' reversal hyperplane is given by

$$c_{\text{tot}} \in [c_{\text{tot}}^{\text{low}}, c_{\text{tot}}^{\text{upp}}] = q_{\text{tot}} \left[K_{jk}^{-\frac{1}{\nu_j - \nu_k}}, \min_{i \neq j, k} \left[\left(K_{ij} K_{jk}^{\frac{\nu_j}{\nu_j - \nu_k}} \right)^{-\frac{1}{\nu_i}} \right] \right]. \quad (\text{E.6})$$

In contrast to the first case, the second one assumes

$$K_{jk}^{\frac{1}{\nu_j - \nu_k}} \leq \left(K_{ij} K_{jk}^{\frac{\nu_j}{\nu_j - \nu_k}} \right)^{\frac{1}{\nu_i}}, \quad \forall i \neq j, k, \quad (\text{E.7a})$$

$$K_{jk}^{-\frac{1}{\nu_j - \nu_k}} \geq \left(K_{ij} K_{jk}^{\frac{\nu_j}{\nu_j - \nu_k}} \right)^{\frac{-1}{\nu_i}}, \quad \forall i \neq j, k. \quad (\text{E.7b})$$

By the same line of argument as in the first case, we readily obtain an analog reversal zone with

$$c_{\text{tot}} \in [c_{\text{tot}}^{\text{low}}, c_{\text{tot}}^{\text{upp}}] = q_{\text{tot}} \left[\max_{i \neq j, k} \left[\left(K_{ij} K_{jk}^{\frac{\nu_j}{\nu_j - \nu_k}} \right)^{-\frac{1}{\nu_i}} \right], K_{jk}^{-\frac{1}{\nu_j - \nu_k}} \right]. \quad (\text{E.8})$$

All c_{tot} hyperplanes with $c_{\text{tot}} \in [c_{\text{tot}}^{\text{low}}, c_{\text{tot}}^{\text{upp}}]$ yield an intersection with the ' jk ' reversal hyperplane, i.e. they admit a classical selectivity reversal (5.31).

Compared to [28] where a process requires to be operated on the same c_{tot} hyperplane within the reversal zone described by (E.6) or (E.8), the chromatographic cycle with variable c_{tot} is operated on two c_{tot} hyperplanes requiring only one of them to be within the reversal zone in order to admit a classical ' jk ' selectivity reversal. However, if $c_{\text{tot}} \notin [c_{\text{tot}}^{\text{low}}, c_{\text{tot}}^{\text{upp}}]$ for all relevant c_{tot} , no classical selectivity reversal will be present on corresponding c_{tot} hyperplanes.

The second type of interaction with any ' jk ' reversal hyperplane can be realized through its intersection with a contact discontinuity corresponding to λ_N . This transition connects c_{tot} hyperplanes over a certain range $\bar{c}_{\text{tot}} = [c_{\text{tot}}^*, c_{\text{tot}}]$, see notation in (5.20). There are three possible scenarios. First, if $[c_{\text{tot}}^{\text{low}}, c_{\text{tot}}^{\text{upp}}] \cap \bar{c}_{\text{tot}} = \emptyset$, the N th transition does not intersect the ' jk ' reversal hyperplane for physically meaningful c_i and (5.32) admits definitely a solution $c_N < 0$. Second, if $[c_{\text{tot}}^{\text{low}}, c_{\text{tot}}^{\text{upp}}] \cap \bar{c}_{\text{tot}} \neq \emptyset$, the contact discontinuity might intersect the ' jk ' reversal hyperplane and (5.32) has to be checked whether it admits $c_N > 0$ or $c_N < 0$. Finally, they guaranteed to intersect each other in the third case if $[c_{\text{tot}}^{\text{low}}, c_{\text{tot}}^{\text{upp}}] \subseteq \bar{c}_{\text{tot}}$ holds, and (5.32) admits a solution $c_N > 0$ accordingly.

Appendix F AIE: Steric Factors

In order to understand the effect that is related exclusively to steric hindrance, two models are considered that differ only in their respective steric factors. Without loss of generality, two cases are considered where the sorption equilibrium is described by either the CIE without steric effects ('I') or by the AIE with steric effects ('II'). In case of model 'I' $p_i = 0$ holds for all i , i.e. $\xi_i^I = \frac{1}{\nu_i}$. In contrast, model 'II' satisfies $p_i > 0$ for at least one i . Thus, the second model accounts for the steric hindrance of at least one component with $\xi_i^{II} = \frac{1}{\nu_i} + p_i$. Note, that all other parameters (K_{iN} , ν_i and q_{tot}) of the two models are identical. These two models are investigated using two different sorption set-ups on a single column.

In the first set-up, the feed and initial loading of the column are specifically chosen to equate the solution normality of model 'I' with the modified solution normality of model 'II', i.e. $c_{\text{tot}}^I = c_{\text{tot}}^{II} = c_{\text{tot}}$. In this case, there exists a simple linear and bijective transformation from concentration phase space II into the concentration phase space I

$$\mathbf{c}^I = \text{diag}_N(\nu_i \xi_i) \mathbf{c}^{II} = \text{diag}_N(1 + \nu_i p_i) \mathbf{c}^{II}, \quad (\text{F.1a})$$

$$\mathbf{q}^I = \text{diag}_N(\nu_i \xi_i) \mathbf{q}^{II} = \text{diag}_N(1 + \nu_i p_i) \mathbf{q}^{II}. \quad (\text{F.1b})$$

Equation (F.1) can be derived from the corresponding equilibrium relation and the electro-neutrality condition of each model

$$f_i(\mathbf{q}^I, \mathbf{c}^I) = \frac{1}{K_{iN}} \left(\frac{q_i^I}{c_i^I} \right)^{\nu_i} \left(\frac{c_N^I}{q_N^I} \right)^{\nu_N} - 1 = 0, \quad (\text{F.2a})$$

$$q_{\text{tot}} = \sum_{i=1}^N \frac{q_i^I}{\nu_i}, \quad c_{\text{tot}}^I = \sum_{i=1}^N \frac{c_i^I}{\nu_i}, \quad (\text{F.2b})$$

as well as

$$f_i(\mathbf{q}^{II}, \mathbf{c}^{II}) = \frac{1}{K_{iN}} \left(\frac{q_i^{II}}{c_i^{II}} \right)^{\nu_i} \left(\frac{c_N^{II}}{q_N^{II}} \right)^{\nu_N} - 1 = 0, \quad (\text{F.3a})$$

$$q_{\text{tot}} = \sum_{i=1}^N \xi_i q_i^{II}, \quad c_{\text{tot}}^{II} = \sum_{i=1}^N \xi_i c_i^{II}. \quad (\text{F.3b})$$

Eqs. (F.2) can be readily transferred to Eqs. (F.3) using (F.1) if and only if $c_{\text{tot}}^I = c_{\text{tot}}^{II} = c_{\text{tot}}$ holds, thus resulting in the same algebraic equations. Consequently, the Jacobian of model 'I' is identical to the one of model 'II' after transformation. Therefore, it is only necessary to obtain the concentration phase topology based on integral curves for all $c_{\text{tot}} > 0$ of only one model since the other one can be directly derived using (F.1).

The second set-up uses the same Riemann conditions, i.e. the same feed $\mathbf{c}_{\text{feed}}^I = \mathbf{c}_{\text{feed}}^{II} = \mathbf{c}_{\text{feed}}$ and initial loading $\mathbf{c}_{\text{init}}^I = \mathbf{c}_{\text{init}}^{II} = \mathbf{c}_{\text{init}}$ for both models. Normalities

c_{tot}^I and c_{tot}^{II} in (F.2,F.3) have obviously different weighting factors, while the components c_i^I , c_i^{II} are subject to the same initial and boundary conditions. In particular, at least at the beginning of the process and once the feed conditions are established $c_i^I = c_i^{II}$ is satisfied for all i everywhere in the column. Due to the different weighting factors

$$\frac{1}{\nu_i} < \frac{1}{\nu_i} + p_i = \xi_i, \quad (\text{F.4})$$

the corresponding solution normality and modified solution normality do not coincide in general. If $c_{\text{tot}}^I = c_{\text{tot}}^{II}$ does not hold for the complete process, the above simple coordinate transformation cannot be applied.

Note that in both set-ups the orientation and positioning of the c_{tot}^I and c_{tot}^{II} hyperplanes are different due to the different weighting factors already mentioned. In both set-ups, for every c_{tot}^I hyperplane in the complete concentration phase space of 'I' there exists a similar c_{tot}^{II} hyperplane with $c_{\text{tot}}^{II} = c_{\text{tot}}^I$ somewhere in the concentration phase space of 'II' based on the similarity in (F.2,F.3). However, only in the first set-up, the boundary and initial conditions are specifically scaled for both models so that all process participating c_{tot}^I and c_{tot}^{II} hyperplanes are also similar in the sense of (F.1). In case of the second set-up, the process participating c_{tot}^I and c_{tot}^{II} hyperplanes can differ arbitrarily. Note, this difference in solution normalities is introduced due different steric factors, hence representing the case where a change in solution normality between two set-ups is related exclusively to different steric factors. The most significant differences can be the intersection with different reversal hyperplanes and different locations and/or number of watershed points.

All results presented here demonstrate the quantitative effect for steric hindrance. Consequently, the results in Section 5.3 as well as the results for selectivity reversals in Section 5.4 and the ones in appendices Appendix C, Appendix D, Appendix E, Appendix H, and Appendix I are affected by steric factors quantitatively but not qualitatively.

Appendix G AIE: Experimental Test System

In this appendix, application of the theory developed in Section 5.5 and illustrated there with an academic benchmark problem is demonstrated for an experimental test system. The specific values of the considered Riemann set-up as well as parameter values taken from [30], are listed in Tab. Appendix G.1.

parameter	value	description
L [mm]	54.0	column length
N_z [-]	1000	number of grid points
u [$\frac{mm}{s}$]	0.4244	interstitial velocity
ϵ [-]	0.73	void fraction
q_{tot} [mM]	525.0	exchanger capacity
K_{31} [-]	0.0135	equilibrium constant
K_{32} [-]	0.045	equilibrium constant
ν_1^{-1} [-]	5.03	characteristic charge
ν_2^{-1} [-]	5.67	characteristic charge
ν_3^{-1} [-]	1.0	characteristic charge
p_1 [-]	7.43	steric factor
p_2 [-]	27.4	steric factor
p_3 [-]	0.0	steric factor

Table Appendix G.1: Experimental parameters.

Note, the numerical strategy was already verified by reproducing partially the results from [30] in Section 5.2.

In this particular case only two proteins α -Chymotrypsinogen A and Cytochrome c are considered. The strong cation-exchanger column is initially equilibrated with 30 mM sodium phosphate and the solution pH is assumed to be 6.0 at all times. At time unit 0, a buffer with 0.2 mM of both proteins and 213 mM sodium phosphate is injected for 3.114 dimensionless time units, which allows for the development of the intermediate feed plateaus. Thereafter, the feed is changed to contain again only sodium phosphate, but in addition it still contains a high concentration of 183 mM sodium phosphate for an efficient elution of the two proteins, which especially compresses simple wave R_1 .

As a result of this Riemann experiment, a chromatographic cycle in Fig. Appendix G.1 is obtained similar to the one in Fig. 5.3. For clarity of presentation, Fig. Appendix G.1a shows only the relevant integral curves in the concentration phase space that predict the numerical solution to illustrate the validity of the applied equilibrium theory. The basic principles discussed in Section 5.5 can be immediately seen in Fig. Appendix G.1b. The first contact discontinuity CD_1 only affects the sodium ion concentration. Reaching then the value of $c_{tot} = 215.1$ mM , two shocks S_1 and S_2 follow affecting the two proteins and

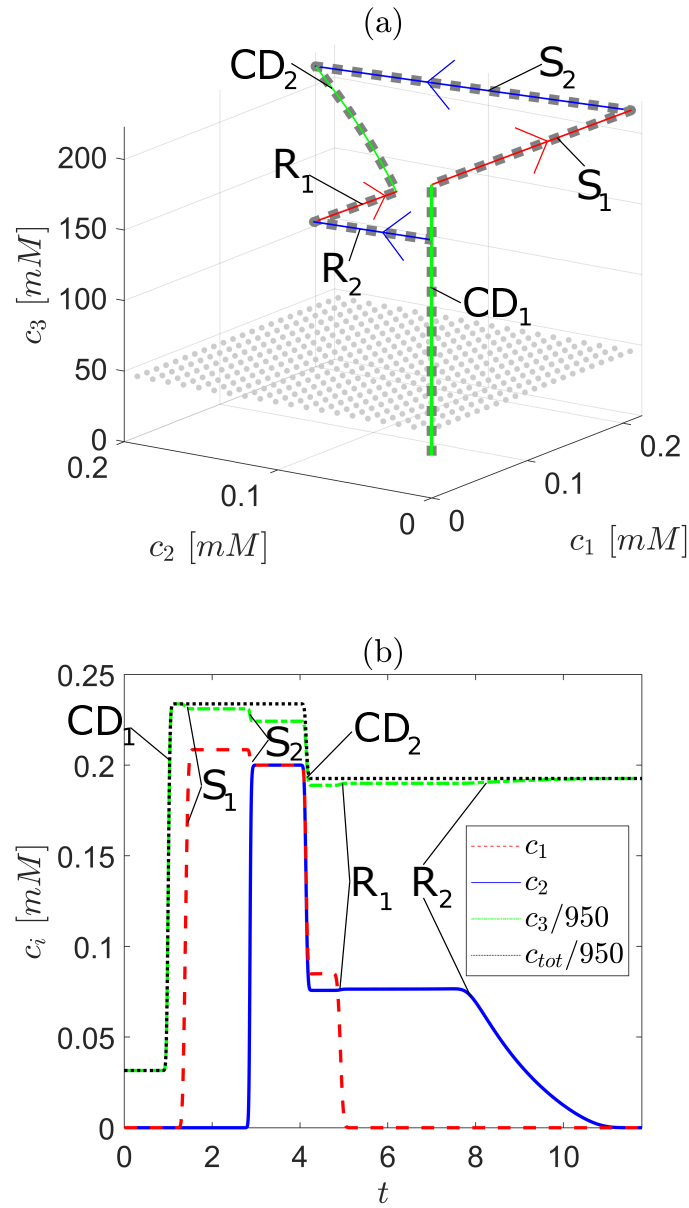


Figure Appendix G.1: (a) Chromatographic cycle in the concentration phase space realized by a pulse experiment for two proteins (α -Chymotrypsinogen A, Cytochrome c) and sodium phosphate. Gray plane indicates reversal plane '1, 2'. Numerical results (grey dashed line) overlap two contact discontinuities, two shock curves and two integral curves, which are all predicted by the equilibrium theory (colored). (b) Corresponding elution profiles $c_i(z)$ indicate that shocks and simple waves occur for different but constant c_{tot} values. The values for c_3 and c_{tot} are scaled by a factor of $\frac{1}{950}$.

sodium ions but not c_{tot} . Subsequently, another contact discontinuity CD_2 follows affecting not only all components but again changing the value of c_{tot} to 183 mM . The elution of the two proteins proceeds by admitting two simple waves. Again, these two transitions do not affect the value of c_{tot} . Consequently, the chromatographic cycle of this example operates on two relevant c_{tot} planes connected by CD_2 , and the analogy of the present real world example to the one discussed in Section 5.5 can be easily established. The same analysis can be applied here. The arrows in Fig. Appendix G.1a point in the direction of increasing characteristic velocity $\tilde{\lambda}_k$, therefore predicting the type of transition correctly. In case of the shocks, the integral curves are almost straight, thus nearly coinciding with the corresponding shock curves. For all other cases, the integral curves match the exact solution path in the concentration phase space. In this particular case, no selectivity reversal is present since the order of elution in Fig. Appendix G.1b is preserved during the complete cycle. This can also be seen in from Fig. Appendix G.1a, where the corresponding '1, 2' reversal plane is below all transitions that follow after CD_1 . Based on this topological property it can be easily predicted that there is indeed no '1, 2' reversal involved between the two relevant c_{tot} values. This concludes the proof of principle.

Appendix H AIE: Non-strict Hyperbolicity

Appendix H.1 The $j, j + 1$ selectivity reversal

In this appendix the singular case of coinciding reversal hyperplanes, which was already mentioned in Appendix D, is discussed. First, recall Eq. (5.11), which implies that the eigenvalues are located between the poles of the characteristic equation with the exception of $\lambda_N = 0$. As we already know, in the presence of a $j(j + 1)$ reversal hyperplane two corresponding poles coincide, i.e. $\frac{q_j}{c_j} = \frac{q_{j+1}}{c_{j+1}}$. However, the system remains strictly hyperbolic, in particular also on the reversal hyperplane itself, with

$$\frac{q_1}{c_1} > \lambda_1 > \frac{q_2}{c_2} > \dots > \frac{q_j}{c_j} = \lambda_j = \frac{q_{j+1}}{c_{j+1}} > \dots > \frac{q_{N-1}}{c_{N-1}} > \lambda_{N-1} > \frac{q_N}{c_N} > \lambda_N = 0. \quad (\text{H.1})$$

In general, the eigenvectors follow from Eq. (5.14). In case of $\lambda_j = \frac{q_j}{c_j} = K_{j,j+1}^{\frac{1}{\nu_j - \nu_{j+1}}} = \text{const}$, the eigenvector is constant and coincided with the reversal hyperplane according to

$$\mathbf{r}_j = [0, \dots, 0, r_{j,j} = \xi_j^{-1}, r_{j,j+1} = -\xi_{j+1}^{-1}, 0, \dots, 0]^T, \quad j < N, \quad (\text{H.2})$$

which is consistent with Eq. (5.18). Remember, any transition on a reversal hyperplane is a contact discontinuity for which the integral and shock curves coincide. Further, Eq. (H.2) shows that only the reversal participating components j and $j + 1$ change on a reversal hyperplane, while all other components are constant. As shown in Section 5.4, such a reversal hyperplane always exists in the positive orthant of the concentration phase space if not all components have the same characteristic charges $\frac{1}{\nu_i}$. Note, due to Eq. (H.1) the contact discontinuity corresponding to $\lambda_N = 0$ is obviously not related to any reversal condition of identical selectivities and is therefore excluded from (H.2). Finally, the $j(j + 1)$ hyperplane itself is defined by the following two equivalent representations

$$\begin{aligned} &\mathcal{RH}_{j(j+1)} : \\ 0 &= \sum_{i \neq j, j+1} \xi_i c_i \left(K_{ij} K_{j(j+1)}^{\frac{\nu_j}{\nu_j - \nu_{j+1}}} \right)^{\frac{1}{\nu_i}} + (\xi_j c_j + \xi_{j+1} c_{j+1}) K_{j(j+1)}^{\frac{1}{\nu_j - \nu_{j+1}}} - q_{\text{tot}} \end{aligned} \quad (\text{H.3})$$

and

$$\begin{aligned} &\mathcal{RH}_{j(j+1)} : \\ 0 &= \sum_{i=1}^N \xi_i c_i \left(K_{ij} K_{j(j+1)}^{\frac{\nu_j}{\nu_j - \nu_{j+1}}} \right)^{\frac{1}{\nu_i}} - q_{\text{tot}}, \quad K_{jj} = 1, \quad K_{(j+1)j} = K_{j(j+1)}^{-1}, \end{aligned} \quad (\text{H.4})$$

consistent with Eqs. (5.26,5.27).

Appendix H.2 Two Coinciding Reversal Hyperplanes

Main focus is on two coinciding reversal hyperplanes. The ordering of selectivities in (H.1) holds at least for some non-empty subset in the positive orthant of the concentration phase space. If two reversal planes exist and both coincide, then it is obvious from (H.1) that three neighboring selectivities are involved. In the following, the corresponding neighboring indices are denoted by j , $j+1$ and $j+2$. For these three indices it is possible to define also three different reversal hyperplanes that could possibly coincide. Due to the fact that these indices can be arbitrarily interchanged, we consider without loss of generality the two reversal hyperplanes related to $j(j+1)$ and $j(j+2)$ and define the common reversal hyperplane accordingly by $\mathcal{RH}_j = \mathcal{RH}_{j(j+1)} = \mathcal{RH}_{j(j+2)}$. On \mathcal{RH}_j the corresponding two reversal equations

$$\frac{q_j}{c_j} = \frac{q_{j+1}}{c_{j+1}}, \quad \frac{q_j}{c_j} = \frac{q_{j+2}}{c_{j+2}} \quad (\text{H.5})$$

hold. They define the sole feature of \mathcal{RH}_j on which the proof in this section is based.

Using Eq. (H.4), the intersection of the reversal hyperplanes $j(j+1)$ as well as $j(j+2)$ has to satisfy

$$0 = \sum_{i=1}^N \xi_i c_i \omega_i, \quad (\text{H.6a})$$

$$\omega_i = \left(K_{ij} K_{j(j+1)}^{\frac{\nu_j}{\nu_j - \nu_{j+1}}} \right)^{\frac{1}{\nu_i}} - \left(K_{ij} K_{j(j+2)}^{\frac{\nu_j}{\nu_j - \nu_{j+2}}} \right)^{\frac{1}{\nu_i}}. \quad (\text{H.6b})$$

As shown in Appendix D, the intersection is nonempty if and only if

$$K_{j(j+1)}^{\frac{1}{\nu_j - \nu_{j+1}}} = K_{j(j+2)}^{\frac{1}{\nu_j - \nu_{j+2}}} \quad (\text{H.7})$$

holds. In this case $\omega_i = 0$ for all $i = 1, \dots, N$, therefore (H.6) is satisfied for all $\mathbf{c} \in \mathbb{R}_{>0}^N$, i.e. the reversal hyperplanes $j(j+1)$ and $j(j+2)$ coincide classifying (H.7) as corresponding necessary and sufficient condition. From a practical point of view, condition (H.7) seems rather restrictive. However, since the parameters $\tilde{\mathbf{p}} = [K_{j(j+1)}, K_{j(j+2)}\nu_j, \nu_{j+1}, \nu_{j+2}]^T$ rely on experimental data they are subjected to parameter uncertainty. In particular, there potentially exist parameter sets $\tilde{\mathcal{P}}$ including on the one hand parameter values that satisfy

$$\tilde{\mathbf{p}} \in \tilde{\mathcal{P}} : K_{j(j+1)}^{\frac{1}{\nu_j - \nu_{j+1}}} > K_{j(j+2)}^{\frac{1}{\nu_j - \nu_{j+2}}}, \quad (\text{H.8})$$

and on the other hand also parameter values that satisfy

$$\tilde{\mathbf{p}} \in \tilde{\mathcal{P}} : K_{j(j+1)}^{\frac{1}{\nu_j - \nu_{j+1}}} < K_{j(j+2)}^{\frac{1}{\nu_j - \nu_{j+2}}}. \quad (\text{H.9})$$

Hence, case (H.7) is satisfied for some $\tilde{\mathbf{p}}^* \in \tilde{\mathcal{P}}$ and cannot be disregarded. As a result, the Riemann solution based on (H.7) may further proof to admit a reasonable approximation in practice assuming that $\max_{\tilde{\mathbf{p}} \in \tilde{\mathcal{P}}} \|\tilde{\mathbf{p}} - \tilde{\mathbf{p}}^*\|$ is sufficiently small.

The theoretical analysis of the Riemann solution related to (H.7) is presented in the following starting with a summary of the main results in

Theorem Appendix H.1. *Assume (H.7) to be satisfied for the given parameters of system Θ (5.2,5.6). Then Θ is non-strictly hyperbolic on \mathcal{RH}_j with exactly one eigenvalue equal to (H.5) that has an algebraic and geometrical multiplicity of two. All other eigenvalues have an algebraic multiplicity of one. Assume further Θ to be subjected to the following Riemann experiment. Let the constant boundary condition $C^j = \mathbf{c}_{\text{feed}}$ satisfy $C^j \in \mathcal{RH}_j$. If the constant initial condition $C^N = \mathbf{c}_{\text{init}}$ is chosen such that C^j does not lie on an integral or shock curve corresponding to a eigenvalue λ_i or shock speed s_i with $N \geq i \geq j+2$ and therefore the intermediate state $C^{j+2} \in \mathcal{RH}_j$ satisfies $C^{j+2} \neq C^j$, then the two points C^{j+2} and C^j are connected by a single contact discontinuity that can be uniquely identified.*

Note, the origin of the concentration phase space is excluded to be a viable initial condition in Theorem Appendix H.1 since it is connected to any point on any reversal hyperplane, in fact to any point in the positive orthant by an integral curve related to λ_N , which is described in Section 5.3. Further, points on the c_N axis is excluded as well. Each point on the c_N is related to a different solution normality. Further, there might exist reversal hyperplanes that admit points of the same solution normality. As a result, these points can be connected to the one point on the c_N axis with the same solution normality by a single shock curve, which is discussed in Section 4.4. Knowing that strict hyperbolicity is maintained everywhere except on \mathcal{RH}_j based on (H.1), all transitions related to λ_i with $N \geq i \geq j+2$, which are required to reach some intermediate state $C^{j+2} \in \mathcal{RH}_j$ from any admissible initial condition C^N , are unique. Further due to the specific choice of $C^j \in \mathcal{RH}_j$, all transitions corresponding to $\lambda_k > \lambda_j$ with $1 \leq k < j$ are obviously not required. Hence, it remains to proof that $\lambda_j = \lambda_{j+1}$ has the algebraic multiplicity of two and in addition that both corresponding transitions admit a unique solution connecting C^j with any distinct C^{j+2} by means of a single contact discontinuity.

Proof of Theorem Appendix H.1. In a first step, it is shown that the algebraic multiplicity of multiple eigenvalues is equal to two if two hyperplanes coincide. For this purpose Eq. (5.11) is rewritten into the equivalent form

$$0 = \lambda_j \sum_{i=1}^N \xi_i \prod_{k \neq i} \left(\frac{\nu_k}{c_k} - \lambda_j \frac{\nu_k}{q_k} \right). \quad (\text{H.10})$$

In light of condition (H.5) on \mathcal{RH}_j , the equation

$$\frac{q_j}{c_j} = \lambda_j = \frac{q_{j+1}}{c_{j+1}} = \lambda_{j+1} = \frac{q_{j+2}}{c_{j+2}} \quad (\text{H.11})$$

holds. Indeed Eq. (H.11) does satisfy (H.10), and it becomes evident that in this case the smallest number of factors equal to zero in each summand in (H.10) is equal to two. Hence, the algebraic multiplicity has to be equal to two excluding the following cases on \mathcal{RH}_j

$$\cdots > \lambda_{j-1} = \frac{q_j}{c_j} = \lambda_j = \frac{q_{j+1}}{c_{j+1}} = \lambda_{j+1} = \frac{q_{j+2}}{c_{j+2}}, \quad (\text{H.12a})$$

$$\frac{q_j}{c_j} = \lambda_j = \frac{q_{j+1}}{c_{j+1}} = \lambda_{j+1} = \frac{q_{j+2}}{c_{j+2}} = \lambda_{j+2} > \cdots \quad (\text{H.12b})$$

that are also consistent with (H.5) but imply an algebraic multiplicity of three, which is obviously a contradiction. As a result, the complete order of selectivities and eigenvalues on \mathcal{RH}_j satisfies

$$\begin{aligned} \frac{q_1}{c_1} > \lambda_1 > \frac{q_2}{c_2} > \lambda_2 > \cdots \\ \cdots > \lambda_{j-1} > \frac{q_j}{c_j} = \lambda_j = \frac{q_{j+1}}{c_{j+1}} = \lambda_{j+1} = \frac{q_{j+2}}{c_{j+2}} > \lambda_{j+2} > \cdots \\ \cdots > \lambda_{N-1} > \frac{q_N}{c_N} > \lambda_N = 0. \end{aligned} \quad (\text{H.13})$$

Based on (H.13), the system Θ is non-strictly hyperbolic on \mathcal{RH}_j . Further, transitions related to (H.11) can only be located on \mathcal{RH}_j , where they are admitting the connection of the plateau states C^{j+2} and C^j .

In order to proof that there always exists a unique solution that connects C^{j+2} and C^j , Eq. (5.14) is solved for (H.11). It is readily possible to obtain two linearly independent eigenvectors with respect to λ_j and λ_{j+1} , e.g. \mathbf{r}_j and \mathbf{r}_{j+1} as formulated in (H.2)

$$\mathbf{r}_j = [0, \dots, 0, r_{j,j} = \xi_j^{-1}, r_{j,j+1} = -\xi_{j+1}^{-1}, 0, \dots, 0]^T, \quad (\text{H.14a})$$

$$\mathbf{r}_{j+1} = [0, \dots, 0, r_{j+1,j+1} = \xi_{j+1}^{-1}, r_{j+1,j+2} = -\xi_{j+2}^{-1}, 0, \dots, 0]^T. \quad (\text{H.14b})$$

As a result, system Θ is still hyperbolic on \mathcal{RH}_j . Further, both eigenvalues are constant, which can be obtained by using (5.2) in conjunction with (H.5) resulting in

$$q_i = c_i \left(K_{ij} K_{j(j+1)}^{\frac{\nu_j}{\nu_j - \nu_{j+1}}} \right)^{\frac{1}{\nu_i}}, \quad i \neq j, j+1, j+2, \quad (\text{H.15a})$$

$$q_m = c_m K_{j(j+1)}^{\frac{1}{\nu_j - \nu_{j+1}}}, \quad m = j, j+1, j+2 \quad (\text{H.15b})$$

allowing to identify the eigenvalues using (H.11) with

$$\frac{q_j}{c_j} = \lambda_j = \frac{q_{j+1}}{c_{j+1}} = \lambda_{j+1} = \frac{q_{j+2}}{c_{j+2}} = K_{j(j+1)}^{\frac{1}{\nu_j - \nu_{j+1}}} = K_{j(j+2)}^{\frac{1}{\nu_j - \nu_{j+2}}} = \text{const.} \quad (\text{H.16})$$

Eq. (H.15) also allows to define a representation for \mathcal{RH}_j similar to (H.3)

$$\mathcal{RH}_j : 0 = \sum_{i \neq j, j+1, j+2} \xi_i c_i \left(K_{ij} K_{j(j+1)}^{\frac{\nu_j}{\nu_j - \nu_{j+1}}} \right)^{\frac{1}{\nu_i}} + K_{j(j+1)}^{\frac{1}{\nu_j - \nu_{j+1}}} \sum_{m=j}^{j+2} \xi_m c_m - q_{\text{tot}} \quad (\text{H.17})$$

The connection of C^{j+2} and C^j is realized on the linear degenerate hyperplane \mathcal{RH}_j . Therefore, it involves only transitions related to the constant eigenvalues λ_j and λ_{j+1} . As demonstrated in [16] for linear hyperbolic regions, the difference of C^{j+2} and C^j can be formulated as sum of weighted eigenvectors

$$C^j - C^{j+2} = \alpha_j \mathbf{r}_j + \alpha_{j+1} \mathbf{r}_{j+1}. \quad (\text{H.18})$$

For the specific case investigated here, the unknown weights are defined by

$$C_j^j - C_{j+2}^{j+2} = \alpha_j \xi_j^{-1}, \quad C_{j+2}^j - C_{j+2}^{j+2} = \alpha_{j+1} \xi_{j+2}^{-1}. \quad (\text{H.19})$$

Note, there are indeed only two equations in (H.19) for the two unknowns α_j and α_{j+1} . All C_i^j with $i \neq j, j+1, j+2$ remain constant, i.e. $C_i^j = C_i^{j+2}$ and provide no additional constraint. Moreover, the eigenvectors in (H.14) are invariant with respect to hyperplanes

$$\mathcal{CH} : 0 = \sum_{i=1}^N \xi_i c_i - c_{\text{tot}} \quad (\text{H.20})$$

of constant solution normality c_{tot} , which is shown in Section 5.3. In this particular case along any linear combination of \mathbf{r}_j and \mathbf{r}_{j+1} , we have

$$\begin{aligned} \Delta c_{\text{tot}} = 0 &= \sum_{i=j}^{j+2} \xi_i (C_i^j - C_i^{j+2}) \\ &= \xi_j \alpha_j \xi_j^{-1} + \xi_{j+1} (-\alpha_j + \alpha_{j+1}) \xi_{j+1}^{-1} + \xi_{j+2} (-\alpha_{j+1}) \xi_{j+2}^{-1} = 0. \end{aligned} \quad (\text{H.21})$$

Therefore

$$C_{j+1}^j - C_{j+1}^{j+2} = (-\alpha_j + \alpha_{j+1}) \xi_{j+1}^{-1} \quad (\text{H.22})$$

is guaranteed to satisfy (H.20) for any α_j as well as α_{j+1} , and therefore (H.22) does not provide an additional constraint on those two coefficients. The invariance of the transitions related to λ_j and λ_{j+1} also means that they are limited to the intersection of the reversal hyperplane defined by (H.17) with hyperplane of constant solution normality defined by (H.20)

$\mathcal{I} :$

$$0 = \sum_{i \neq j, j+1, j+2} \xi_i c_i \left(\left(K_{ij} K_{j(j+1)}^{\frac{\nu_j}{\nu_j - \nu_{j+1}}} \right)^{\frac{1}{\nu_i}} - K_{j(j+1)}^{\frac{1}{\nu_j - \nu_{j+1}}} \right) + K_{j(j+1)}^{\frac{1}{\nu_j - \nu_{j+1}}} c_{\text{tot}}^j - q_{\text{tot}}, \quad (\text{H.23})$$

where the value of c_{tot}^j is fixed and given by the boundary condition C^j . The intersection \mathcal{I} is nonempty if (H.20) is within a reversal zone, i.e. the solution normality satisfies

$$c_{\text{tot}}^j \in [c_{\text{tot}}^{j,\text{low}}, c_{\text{tot}}^{j,\text{upp}}] = \begin{cases} q_{\text{tot}} \left[\gamma, \min_{i \neq j, (j+1)} \beta_i \right], & \gamma \leq \beta_i \quad i \neq j, j+1 \\ q_{\text{tot}} \left[\max_{i \neq j, (j+1)} \beta_i, \gamma \right], & \gamma \geq \beta_i \quad i \neq j, j+1 \end{cases}, \quad (\text{H.24a})$$

$$\beta_i = \left(K_{ij} K_{j(j+1)}^{\frac{\nu_j}{\nu_j - \nu_{j+1}}} \right)^{-\frac{1}{\nu_i}}, \quad \gamma = K_{j(j+1)}^{-\frac{1}{\nu_j - \nu_{j+1}}}. \quad (\text{H.24b})$$

Details regarding reversal zones can be found in Appendix E.

Since $\lambda_j = \lambda_{j+1}$, the difference or transition (H.18,H.19) is not described by a sequence of two linear transitions where we need to find an intermediate state. Instead (H.18,H.19) directly defines the transition, which is a superposition of two linear transitions resulting in a single linear transition, i.e. a single straight line connecting C^j and C^{j+2} . This straight line is uniquely defined by these two points in the concentration state phase, which also means that C^j can be connected by a corresponding straight line to any $C^{j+2} \in \mathcal{RH}_j$ for any fixed c_{tot}^j . Consequently, the straight line directly depends on the choice of boundary conditions C^j , which defines the relevant c_{tot}^j , and initial conditions C^N , which is obviously related to C^{j+2} . This is an interesting distinction from the linear degenerate transition in unique reversal hyperplanes since they are fixed for certain parameters independently of boundary and initial conditions, see (H.2).

In other words, a single contact discontinuity is obtained that results from the superposition of two contact discontinuities on the linearly degenerate hyperplane \mathcal{RH}_j . It is uniquely defined by (H.18,H.19) and satisfies the jump conditions (5.16) with $\tilde{s}_j = \tilde{\lambda}_j$ between any two distinct points in \mathcal{I} . The previous statement holds for any two distinct points on \mathcal{RH}_j since Eq. (H.24) is satisfied for any c_{tot}^j resulting from $C^j \in \mathcal{RH}_j$ by definition. \square

For illustration purposes, simulation of a four component example is shown in Fig. Appendix H.1. Corresponding simulation parameters can be found in Tab. Appendix H.1. The parameters satisfy Eq. (H.7) such that the '1,2' and '1,3' reversal hyperplanes coincide. From Eq. (H.23) a suitable $c_{4,\text{feed}}$ is determined for given values of the other three reversal participating components resulting in $\mathbf{c}_{\text{feed}} = \frac{1}{60}[36, 12, 20, 55] \frac{\text{mol}}{\text{m}^3}$. In addition, initial conditions are $\mathbf{c}_{\text{init}} = 10^{-3}[1, 1, 1, 100] \frac{\text{mol}}{\text{m}^3}$. Since the boundary condition lies on the coinciding reversal hyperplanes and the initial condition does not lie on the c_4 -axis, the regeneration should consist of four transitions compared to the three transitions during the loading, where the transition connected to the feed plateau has to be a contact discontinuity. These predictions are verified by simulation results shown in Fig. Appendix H.1.

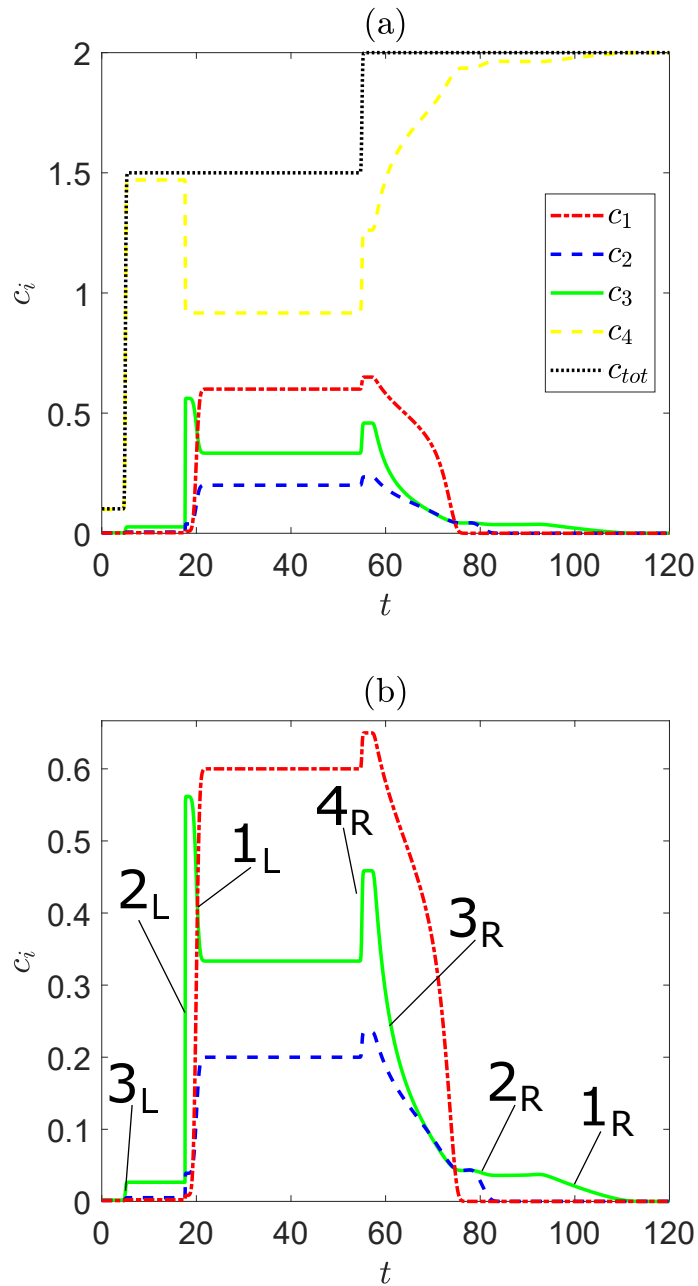


Figure Appendix H.1: (a) Concentration profiles of all four components c_i and c_{tot} show four transitions during regeneration but only three transitions during loading. (b) Section of the concentration profile (a) that shows particularly well the four transitions (1_R, 2_R, 3_R, 4_R) after the feed value and three transitions before the feed value (1_L, 2_L, 3_L), where 1_L denotes the contact discontinuity of interest.

parameter	value	description
L [m]	5.0	column length
N_z [-]	1500	number of grid points
u [$\frac{m}{s}$]	1.0	interstitial velocity
ϵ [-]	0.5	void fraction
q_{tot} [$\frac{\text{mol}}{\text{m}^3}$]	2.0	exchanger capacity
K_{14} [-]	297.0	equilibrium constant
K_{24} [-]	33.0	equilibrium constant
K_{24} [-]	11.0	equilibrium constant
ν_1 [-]	4	equilibrium constant
ν_2 [-]	2	equilibrium constant
ν_3 [-]	1	equilibrium constant
ν_4 [-]	1	equilibrium constant

Table Appendix H.1: Parameters used in simulation example for a non-strictly hyperbolic case.

Appendix H.3 Multiple Coinciding Reversal Hyperplanes

Using the reasoning above, the case of two coinciding reversal hyperplanes can be extended to $M > 2$ coinciding reversal hyperplanes. This extension is straight forward, therefore only the most important results are summarized in the following. The maximal number of coinciding reversal hyperplanes is $\frac{(N-1)N}{2}$. However, in this appendix the results are limited to $2 \leq M < N$. This is reasonable due to the fact that the maximal number of reversal equations is $N - 1$ since there are only N selectivities $\frac{q_i}{c_i}$ that can be equal. Consequently if $M \geq N$ no additional reversal equations will be present, which means that the all results based on this key feature do not change further. As in the previous section, the case of the component j to participate in all occurring reversals is considered. Any other case follows the same reasoning requiring only the corresponding indices to be considered.

First it is obvious that now $M - 1$ equations

$$K_{j(j+1)}^{\frac{1}{\nu_j - \nu_{j+1}}} = \dots = K_{j(j+M)}^{\frac{1}{\nu_j - \nu_{j+M}}} \quad (\text{H.25})$$

have to be satisfied on a reversal hyperplane \mathcal{RH}_j , which becomes decreasingly probable with increasing M . Note, Eq. (H.25) is the only condition with an increasing number of equations even for $M \geq N$. However, the degree of freedom defined by $2M + 1 - (M - 1)$ has a maximum value of $N + 1$ since every equation that is introduced when $M \geq N$ adds only one new parameter. As a result the degree of freedom is $N + 1$ for all $M \geq N - 1$. Finally, the following order is satisfied on \mathcal{RH}_j

$$\begin{aligned} \frac{q_1}{c_1} > \lambda_1 > \frac{q_2}{c_2} > \lambda_2 > \dots \\ \dots > \lambda_{j-1} > \frac{q_j}{c_j} = \lambda_j = \dots = \lambda_{j+M-1} = \frac{q_{j+M}}{c_{j+M}} > \lambda_{j+M} > \dots \\ \dots > \lambda_{N-1} > \frac{q_N}{c_N} > \lambda_N = 0. \end{aligned} \quad (\text{H.26})$$

In (H.26), the eigenvalue with algebraic multiplicity of M is constant and equal to the value defined by (H.25). The system Θ is therefore non-strictly hyperbolic on \mathcal{RH}_j but remains linear hyperbolic with

$$\mathbf{r}_{j+i} = [0, \dots, 0, r_{j+i, j+i} = \xi_{j+i}^{-1}, 0, \dots, 0, r_{j+i, j+M} = -\xi_{j+M}^{-1}, 0, \dots, 0]^T. \quad (\text{H.27})$$

Similar to (H.18,H.19), the transition between any two points C^j and C^{j+M} on \mathcal{RH}_j is uniquely defined by

$$C^j - C^{j+M} = \sum_{i=0}^{M-1} \alpha_{j+i} \mathbf{r}_{j+i}, \quad (\text{H.28a})$$

$$C_{j+i}^j - C_{j+i}^{j+M} = \alpha_{j+i} \xi_{j+i}^{-1}, \quad i = 0, \dots, M - 1. \quad (\text{H.28b})$$

Note, as before, the point C^{j+M} is reached through the transitions related to λ_i with $N \geq i \geq j + M$, while C^j is connected by an unique contact discontinuity to C^{j+M} resulting from a superposition of M simultaneously occurring contact discontinuities. Similar to (H.17), \mathcal{RH}_j is represented by

$\mathcal{RH}_j :$

$$0 = \sum_{i \neq j, \dots, j+M} \xi_i c_i \left(K_{ij} K_{j(j+1)}^{\frac{\nu_j}{\nu_j - \nu_{j+1}}} \right)^{\frac{1}{\nu_i}} + K_{j(j+1)}^{\frac{1}{\nu_j - \nu_{j+1}}} \sum_{m=j}^{j+M} \xi_m c_m - q_{\text{tot}}, \quad (\text{H.29a})$$

$\mathcal{I} :$

$$0 = \sum_{i \neq j, \dots, j+M} \xi_i c_i \left(\left(K_{ij} K_{j(j+1)}^{\frac{\nu_j}{\nu_j - \nu_{j+1}}} \right)^{\frac{1}{\nu_i}} - K_{j(j+1)}^{\frac{1}{\nu_j - \nu_{j+1}}} \right) + K_{j(j+1)}^{\frac{1}{\nu_j - \nu_{j+1}}} c_{\text{tot}}^j - q_{\text{tot}}. \quad (\text{H.29b})$$

Eq. (H.29) admits the following special case if all N components participate on \mathcal{RH}_j , i.e. if at least $M = N - 1$ reversal hyperplanes coincide

$$\mathcal{RH}_j : 0 = K_{j(j+1)}^{\frac{1}{\nu_j - \nu_{j+1}}} \sum_{m=1}^N \xi_m c_m - q_{\text{tot}}, \quad (\text{H.30a})$$

$$\mathcal{I} : 0 = K_{j(j+1)}^{\frac{1}{\nu_j - \nu_{j+1}}} c_{\text{tot}}^j - q_{\text{tot}}. \quad (\text{H.30b})$$

Since \mathcal{RH}_j has the same normal vector as all hyperplanes \mathcal{CH} as defined in (H.20), \mathcal{I} is non-empty only for one particular hyperplane \mathcal{CH}_j with (H.24) reducing to a single point c_{tot}^j that satisfies (H.30).

Appendix I AIE: Global Properties on \mathcal{CH} hyperplanes

This appendix demonstrates that the isotherm of the AIE is invertible on any c_{tot} hyperplane \mathcal{CH} (Eq. (H.20)). In a first step, the isotherm of the CIE is shown to be bijective in a convex subset \mathcal{X}_{N-1} of the positive orthant. Subsequently, an equivalence of this result with the existence of a bijective AIE isotherm function on any \mathcal{CH} is established. In addition, a stronger version of global invertibility is shown by application of the global inverse theorem by Hadamard [110]. For this purpose, eigenvalue and eigenvector results are obtained for the entire domain \mathcal{X}_{N-1} . Particular focus is on the boundary of $\partial\mathcal{X}_{N-1}$. In addition, strict hyperbolicity and genuine non-linearity are shown to be satisfied almost everywhere on \mathcal{X}_{N-1} with the exception of isolated points and selectivity reversals, respectively. Based on the equivalence of the AIE isotherm with \mathcal{CH} and the CIE isotherm with \mathcal{X}_{N-1} , it is conjectured that in case of the AIE an uniqueness theorem regarding Riemann solutions (including shocks, simple waves, and contact discontinuities) can be derived more globally for any \mathcal{CH} . In contrast, general theorems, e.g. Theorem 17.18 in [62] hold only locally, specifically due to the application of the implicit function theorem.

Appendix I.1 Existence of a Bijective Function

For a constant solution normality, the equilibrium relations (5.2,5.3) can be formulated in normalized coordinates $\mathbf{x}_N, \mathbf{y}_N \in \mathbb{R}^N$ with an additional closing condition as follows

$$0 = f_i(\mathbf{x}_N, \mathbf{y}_N) = \frac{1}{\tilde{K}_{iN}} \left(\frac{y_i}{x_i} \right)^{\nu_i} \left(\frac{x_N}{y_N} \right)^{\nu_N} - 1, \quad i = 1, \dots, N-1, \quad (\text{I.1a})$$

$$0 = f_N(\mathbf{y}_N) = \sum_{i=1}^N y_i - 1, \quad (\text{I.1b})$$

$$0 = f_{N+1}(\mathbf{x}_N) = \sum_{i=1}^N x_i - 1, \quad (\text{I.1c})$$

$$x_i = \xi_i \frac{c_i}{c_{\text{tot}}}, \quad y_i = \xi_i \frac{q_i}{q_{\text{tot}}}, \quad \tilde{K}_{iN} = K_{iN} \left(\frac{q_{\text{tot}}}{c_{\text{tot}}} \right)^{\nu_N - \nu_i}, \quad i = 1, \dots, N. \quad (\text{I.1d})$$

Due to the two closing conditions (I.1b,I.1c), the degree of freedom of the implicit function $\mathbf{\Omega}(\mathbf{x}_N, \mathbf{y}_N) = 0$ defined by Eqs. (I.1a-I.1c) is equal to $N-1$ and does not depend on the choice of independent variables, either the normalized fluid phase concentrations x_i or the normalized solid phase concentrations y_i . Therefore we can identify the equivalence of $\mathbf{\Omega}(\mathbf{x}_N, \mathbf{y}_N) = 0$ with a special case of $\mathbf{\Omega}(\mathbf{c}, \mathbf{q}) = 0$ denoted by $\mathbf{\Omega}_{\mathcal{CH}}(\mathbf{c}, \mathbf{q}) = \mathbf{\Omega}(\mathbf{x}_N, \mathbf{y}_N) = 0$ in order to account for the constant solution normality that defines the hyperplane \mathcal{CH} .

First, $N - 1$ of the fluid phase concentrations x_i are chosen to be the independent variables. Here x_N is the dependent reference variable, but it could be interchanged with any other independent variable. Eqs. (I.1a) and (I.1b) can be equivalently formulated as

$$y_i = x_i \tilde{K}_{iN}^{\frac{1}{\nu_i}} \left(\frac{y_N}{x_N} \right)^{\frac{\nu_N}{\nu_i}}, \quad i = 1, \dots, N - 1, \quad (\text{I.2a})$$

$$0 = \sum_{i=1}^N x_i \tilde{K}_{iN}^{\frac{1}{\nu_i}} \left(\frac{y_N}{x_N} \right)^{\frac{\nu_N}{\nu_i}} - 1. \quad (\text{I.2b})$$

Obviously, Eq. (I.2a) substituted into Eq. (I.1b) results in Eq. (I.2b). Hence, Eq. (I.2b) alone can be used to equivalently replace Eqs. (I.1a) and (I.1b). Introducing the variable $\tilde{y} = \frac{y_N}{x_N} > 0$, Eq. (I.2b) can be rewritten into

$$0 = \sum_{i=1}^N x_i \tilde{K}_{iN}^{\frac{1}{\nu_i}} \left(\frac{y_N}{x_N} \right)^{\frac{\nu_N}{\nu_i}} - 1 = \sum_{i=1}^N \alpha_i \tilde{y}^{\frac{\nu_N}{\nu_i}} - 1 = \eta(\tilde{y}). \quad (\text{I.3})$$

Note that due to Eq. (I.2b) there exists at least one non-vanishing component $m \in \{1, \dots, N\}$. As a results from Eq. (I.2a), the ratio $\frac{y_N}{x_N} > 0$ remains well-defined. Eq. (I.3) can be interpreted as a function of \tilde{y} with constant factors α_i for arbitrary but fixed x_i 's. Note, at least $\alpha_m = 1$ is non-zero. Further, if any factor α_i is non-zero, then it is also greater than zero due to its definition in Eq. (I.3). Since $\tilde{y} = \frac{y_N}{x_N} > 0$, we are only interested in solutions $\tilde{y} \in (0, \infty)$. The following properties of $\eta(\tilde{y})$ guarantee a unique solution \tilde{y} in the interval $(0, \infty)$

$$\eta(0) = -1, \quad (\text{I.4a})$$

$$\lim_{\tilde{y} \rightarrow \infty} \eta(\tilde{y}) = \sum_{i=1}^N \alpha_i \tilde{y}^{\frac{\nu_N}{\nu_i}} - 1 > \sum_{i=1}^N x_i - 1 = 0. \quad (\text{I.4b})$$

Considering the derivative

$$\frac{d\eta(\tilde{y})}{d\tilde{y}} = \sum_{i=1}^N \alpha_i \frac{\nu_N}{\nu_i} \tilde{y}^{\frac{\nu_N}{\nu_i} - 1} > 0, \quad (\text{I.5})$$

it clearly shows that $\eta(\tilde{y})$ is strictly monotonically increasing in $(0, \infty)$ allowing only for single solution \tilde{y} in this interval, thus indicating its uniqueness. The dependent variable x_N results uniquely from Eq. (I.1c) for any given composition, i.e. $x_N = 1 - \sum_{i=1}^{N-1} x_i$. Recalling the explicit relations for all other components in I.2a, one obtains

$$y_i = x_i \tilde{K}_{iN}^{\frac{1}{\nu_i}} \tilde{y}^{\frac{\nu_N}{\nu_i}}, \quad i \in \{1, \dots, N - 1\}. \quad (\text{I.6})$$

The uniqueness of \tilde{y} carries readily over to all remaining components y_i for any given composition defined by the x_i 's. Moreover, the remaining dependent solid

phase concentration of component N can be also calculated uniquely from $y_N = 1 - \sum_{i=1}^{N-1} y_i$. Consequently, we find for every $\mathbf{x}_N \in \mathcal{X}_N$ a unique point $\mathbf{y}_N \in \mathcal{Y}_N$. Hence, $\Omega(\mathbf{x}_N, \mathbf{y}_N)$ implies the existence of a function

$$\begin{aligned} \mathbf{y}_N(\mathbf{x}_N) : \mathcal{X}_N &\rightarrow \mathcal{Y}_N, \\ \mathcal{X}_N \subset \mathbb{R}^N, \mathcal{Y}_N &\subset \mathbb{R}^N. \end{aligned} \quad (\text{I.7})$$

Note, in case of the fluid phase concentrations, the dimension can be decreased by using f_{N+1} to obtain for example explicitly x_N beforehand. Further, in case of the solid phase concentrations, the dimension can be decreased by using f_N to calculate for example explicitly y_N independently of the x_i 's. Considering the reduced system $\Omega(\mathbf{x}_{N-1}, \mathbf{y}_{N-1})$

$$0 = f_i(\mathbf{x}_{N-1}, \mathbf{y}_{N-1}) = \frac{1}{\tilde{K}_{iN}} \left(\frac{y_i}{x_i} \right)^{\nu_i} \left(\frac{x_N}{y_N} \right)^{\nu_N} - 1, \quad (\text{I.8a})$$

$$y_N = 1 - \sum_{i=1}^{N-1} y_i, \quad x_N = 1 - \sum_{i=1}^{N-1} x_i, \quad (\text{I.8b})$$

it is obvious that $\Omega(\mathbf{x}_{N-1}, \mathbf{y}_{N-1})$ is equivalent to $\Omega(\mathbf{x}_N, \mathbf{y}_N)$. Therefore, the function $\mathbf{y}_N(\mathbf{x}_N)$ is also implied by $\Omega(\mathbf{x}_{N-1}, \mathbf{y}_{N-1})$. However, the variables x_N and y_N can be replaced directly by the corresponding closing condition as shown in Eq. (I.8b), such that we find for any $\mathbf{x}_{N-1} \in \mathcal{X}_{N-1}$ a unique $\mathbf{y}_{N-1} \in \mathcal{Y}_{N-1}$. As a result both systems $\Omega(\mathbf{x}_{N-1}, \mathbf{y}_{N-1})$ and $\Omega(\mathbf{x}_N, \mathbf{y}_N)$ also imply the existence of the function

$$\begin{aligned} \mathbf{y}_{N-1}(\mathbf{x}_{N-1}) : \mathcal{X}_{N-1} &\rightarrow \mathcal{Y}_{N-1}, \\ \mathcal{X}_{N-1} \subset \mathbb{R}^{N-1}, \mathcal{Y}_{N-1} &\subset \mathbb{R}^{N-1}. \end{aligned} \quad (\text{I.9})$$

Deduction of Eq. (I.9) is straight forward. For this particular case however, a simple verification is provided. Assume function $\mathbf{y}_{N-1}(\mathbf{x}_{N-1})$ does not exist, i.e. there exists a \mathbf{x}_{N-1}^* with $\mathbf{y}(\mathbf{x}_{N-1}^*) = \{\mathbf{y}_{N-1}^*, \mathbf{y}_{N-1}^{**}\}$, where $\mathbf{y}_{N-1}^* \neq \mathbf{y}_{N-1}^{**}$. Due to f_N it also follows that $y_N^* \neq y_N^{**}$. However, due to f_{N+1} one obtains only a unique x_N^* . Therefore, we can find for the corresponding $\mathbf{x}_N^* \in \mathcal{X}_N$ at least two possible elements in \mathcal{Y}_N , namely \mathbf{y}_N^* and \mathbf{y}_N^{**} . This is clearly a contradiction to the existence of a function $\mathbf{y}_N(\mathbf{x}_N)$.

Uniqueness can be derived also directly from Eq. (I.8). Since Eq. (I.8) admits for any given \mathbf{x}_{N-1} unique solutions to x_N , \mathbf{y}_{N-1} , and y_N , the variables \mathbf{x}_N and \mathbf{y}_N are also unique. The uniqueness can be obviously further deduced for \mathbf{c} with $c_i = x_i \frac{c_{\text{tot}}}{\xi_i}$ and for \mathbf{q} with $q_i = y_i \frac{q_{\text{tot}}}{\xi_i}$ for all $i = 1, \dots, N$. Since $\Omega(\mathbf{x}_{N-1}, \mathbf{y}_{N-1})$ is equivalent to $\Omega(\mathbf{x}_N, \mathbf{y}_N)$, which is in addition equivalent to $\Omega_{\mathcal{CH}}(\mathbf{c}, \mathbf{q})$, $\Omega(\mathbf{x}_{N-1}, \mathbf{y}_{N-1})$ is also equivalent to $\Omega_{\mathcal{CH}}(\mathbf{c}, \mathbf{q})$. Consequently also $\Omega_{\mathcal{CH}}(\mathbf{c}, \mathbf{q})$ implies the existence of $\mathbf{y}_{N-1}(\mathbf{x}_{N-1})$ as well as $\mathbf{y}_N(\mathbf{x}_N)$ and clearly also of a corresponding function without normalization $\mathbf{q}(\mathbf{c})$ since it is possible to

find for every $\mathbf{c} \in \mathcal{CH}$ a unique $\mathbf{q} \in \mathcal{QH}$, thus defining the function

$$\begin{aligned} \mathbf{q}(\mathbf{c}) : \mathcal{CH} &\rightarrow \mathcal{QH}, \\ \mathcal{CH} \subset \mathbb{R}^N, \mathcal{QH} &\subset \mathbb{R}^N. \end{aligned} \quad (\text{I.10})$$

In other words, the existence of $\mathbf{y}_{N-1}(\mathbf{x}_{N-1})$ for $\Omega(\mathbf{x}_{N-1}, \mathbf{y}_{N-1})$ implies $\mathbf{q}(\mathbf{c})$ for $\Omega_{\mathcal{CH}}(\mathbf{c}, \mathbf{q})$, the original equilibrium relations (5.2) complemented by a constant solution normality c_{tot} (5.3), thus restricting the domain in the space of fluid phase concentrations to a corresponding hyperplane \mathcal{CH} .

In a very similar way, one can show the existence of a function $\mathbf{c}(\mathbf{q})$ related to a function $\mathbf{x}_{N-1}(\mathbf{y}_{N-1})$. Again, Eq. (I.1) is partially rewritten similar to Eq. (I.2). In this case however, the x_i variables are considered to be the dependent ones resulting in

$$x_i = y_i \tilde{K}_{iN}^{-\frac{1}{\nu_i}} \left(\frac{x_N}{y_N} \right)^{\frac{\nu_N}{\nu_i}}, \quad i = 1, \dots, N-1, \quad (\text{I.11a})$$

$$0 = \sum_{i=1}^N y_i \tilde{K}_{iN}^{-\frac{1}{\nu_i}} \left(\frac{x_N}{y_N} \right)^{\frac{\nu_N}{\nu_i}} - 1. \quad (\text{I.11b})$$

Similarly, we introduce a new variable $\tilde{x} = \tilde{y}^{-1}$, thus obtaining a function $\eta(\tilde{x})$

$$0 = \sum_{i=1}^N y_i \tilde{K}_{iN}^{-\frac{1}{\nu_i}} \left(\frac{x_N}{y_N} \right)^{\frac{\nu_N}{\nu_i}} - 1 = \sum_{i=1}^N \beta_i \tilde{x}^{\frac{\nu_N}{\nu_i}} - 1 = \eta(\tilde{x}) \quad (\text{I.12})$$

for arbitrary but fixed \mathbf{y}_N . Since at least one β_m with $m \in \{1, \dots, N\}$ is non-zero and all other variables being equal or greater than zero, it is obvious that $\eta(\tilde{x})$ has the same properties as $\eta(\tilde{y})$ in (I.4) and (I.5) but now related to \tilde{x} . Consequently, there is a unique positive solution for \tilde{x} . In this case, y_N is uniquely obtained from $y_N = 1 - \sum_{i=1}^{N-1} y_i$, while the remaining x_i are obtained uniquely from

$$\begin{aligned} x_i &= y_i \tilde{K}_{iN}^{-\frac{1}{\nu_i}} \tilde{x}^{\frac{\nu_N}{\nu_i}}, \quad i \in \{1, \dots, N-1\}, \\ x_N &= 1 - \sum_{i=1}^N x_i. \end{aligned} \quad (\text{I.13})$$

Therefore, we find for every $\mathbf{y}_N \in \mathcal{Y}_N$ a unique $\mathbf{x}_N \in \mathcal{X}_N$, and $\Omega(\mathbf{x}_N, \mathbf{y}_N)$ implies also the existence of a function

$$\mathbf{x}_N(\mathbf{y}_N) : \mathcal{Y}_N \rightarrow \mathcal{X}_N, \quad (\text{I.14a})$$

$$\mathcal{X}_N \subset \mathbb{R}^N, \mathcal{Y}_N \subset \mathbb{R}^N. \quad (\text{I.14b})$$

Since the deduction of $\mathbf{x}_N(\mathbf{y}_N)$ is based on the same system $\Omega(\mathbf{x}_N, \mathbf{y}_N)$ as the deduction of $\mathbf{y}_N(\mathbf{x}_N)$, the same equivalences hold. Consequently, $\Omega(\mathbf{x}_N, \mathbf{y}_N)$,

$\Omega(\mathbf{x}_{N-1}, \mathbf{y}_{N-1})$, and $\Omega_{\mathcal{CH}}(\mathbf{c}, \mathbf{q})$ as well as $\mathbf{x}_N(\mathbf{y}_N)$ imply the existence of

$$\begin{aligned} \mathbf{x}_{N-1}(\mathbf{y}_{N-1}) &: \mathcal{Y}_{N-1} \rightarrow \mathcal{X}_{N-1}, \\ \mathcal{X}_{N-1} &\subset \mathbb{R}^{N-1}, \quad \mathcal{Y}_{N-1} \subset \mathbb{R}^{N-1}, \end{aligned} \quad (\text{I.15a})$$

$$\begin{aligned} \mathbf{c}(\mathbf{q}) &: \mathcal{QH} \rightarrow \mathcal{CH}, \\ \mathcal{CH} &\subset \mathbb{R}^N, \quad \mathcal{QH} \subset \mathbb{R}^N. \end{aligned} \quad (\text{I.15b})$$

Note, any of the functions in (I.14) and (I.15) implies the other two due to the equivalence of (I.1), (I.8), and $\Omega_{\mathcal{CH}}(\mathbf{c}, \mathbf{q})$. In other words the existence of all three functions in their respective domains is also equivalent, which is consistent with the equivalences that were already deduced for (I.7), (I.9), and (I.10).

It remains to verify that $\mathbf{x}_N(\mathbf{y}_N)$ is the inverse of $\mathbf{y}_N(\mathbf{x}_N)$. Clearly, the existence of both functions guarantees the uniqueness of any pair $(\mathbf{x}_N^*, \mathbf{y}_N^*) \in \mathcal{X}_N \times \mathcal{Y}_N$ that satisfies $\Omega(\mathbf{x}_N^*, \mathbf{y}_N^*) = 0$. As a result $\mathbf{y}_N^* = \mathbf{y}_N(\mathbf{x}_N^*)$ and $\mathbf{x}_N^* = \mathbf{x}_N(\mathbf{y}_N^*)$ holds, and we can write

$$\begin{aligned} \Omega(\mathbf{x}_N^*, \mathbf{y}_N^*) &= \Omega(\mathbf{x}_N^*, \mathbf{y}_N(\mathbf{x}_N^*)) = \Omega(\mathbf{x}_N^*, \mathbf{y}_N(\mathbf{x}_N(\mathbf{y}_N^*))) = 0 \\ \mathbf{y}_N(\mathbf{x}_N(\mathbf{y}_N^*)) &= \mathbf{y}_N^*, \end{aligned} \quad (\text{I.16a})$$

$$\begin{aligned} \Omega(\mathbf{x}_N^*, \mathbf{y}_N^*) &= \Omega(\mathbf{x}_N(\mathbf{y}_N^*), \mathbf{y}_N^*) = \Omega(\mathbf{x}_N(\mathbf{y}_N(\mathbf{x}_N^*)), \mathbf{y}_N^*) = 0 \\ \mathbf{x}_N(\mathbf{y}_N(\mathbf{x}_N^*)) &= \mathbf{x}_N^* \end{aligned} \quad (\text{I.16b})$$

for every $(\mathbf{x}_N^*, \mathbf{y}_N^*) \in \mathcal{X}_N \times \mathcal{Y}_N$. Hence, the function $\mathbf{y}_N(\mathbf{x}_N)$ is the inverse of $\mathbf{x}_N(\mathbf{y}_N)$ and vice versa. Both functions exist globally with respect to their domain. Using the equivalence of the existence of functions (I.14) and (I.15) as well as (I.7), (I.9), and (I.10), we can further deduce that the global existence of a function and its inverse is equivalent for all three cases. In other words, $\mathbf{y}_{N-1}(\mathbf{x}_{N-1})$ has the inverse $\mathbf{x}_{N-1}(\mathbf{y}_{N-1})$, and $\mathbf{q}(\mathbf{c})$ has the inverse $\mathbf{c}(\mathbf{q})$. In both cases the functions exist globally in their respective domains.

As a remark, the sets \mathcal{X}_N and \mathcal{Y}_N as well as \mathcal{X}_{N-1} and \mathcal{Y}_{N-1} are identical due to identical structure of the two closing conditions in (I.1b,I.1c) and (I.8b), respectively. Consequently, the sets \mathcal{CH} and \mathcal{QH} differ only in their linear scaling of the coordinates with scalars $\nu_i c_{\text{tot}}$ and $\nu_i q_{\text{tot}}$, respectively for each coordinate c_i and q_i . In particular one can find for every $\mathbf{c}^* \in \mathcal{CH}$ a $\mathbf{q}^* \in \mathcal{QH}$ with $\frac{c_i^*}{c_{\text{tot}}} = \frac{q_i^*}{q_{\text{tot}}}$ for all $i = 1, \dots, N$.

Appendix I.2 Application of the Global Inverse Theorem

Focus in this section is on representation $\Omega_{N-1}(\mathbf{x}_{N-1}, \mathbf{y}_{N-1})$ defined by Eq. (I.8), which is no restriction due to the equivalences presented in the previous section. The global inverse theorem by Hadamard states the following [110]

"Let $f : M_1 \rightarrow M_2$ be a \mathcal{C}^1 map between two connected N -dimensional manifolds whose Jacobian never vanishes, and which is "proper" in the sense that $f^{-1}(K)$

is compact whenever K is a compact subset of M_2 . Suppose further that M_2 is simply-connected. Then f is a homeomorphism. "

In the present case, the function $\mathbf{y}_{N-1}(\mathbf{x}_{N-1})$ is considered, which maps from $\mathcal{X}_{N-1} \subset \mathbb{R}^{N-1}$ to $\mathcal{Y}_{N-1} \subset \mathbb{R}^{N-1}$. Its existence is shown in the previous section.

It remains to show that all conditions of Hadamard's global inverse theorem are satisfied. Since both sets are subsets of \mathbb{R}^{N-1} , which is a simply connected space itself, they are both not only connected but also simply connected [111]. Further, $\mathbf{y}_{N-1}(\mathbf{x}_{N-1}) \in \mathcal{C}^1$ means that the function is continuously differentiable. It is well known by the differentiability theorem for multi-variable functions that $\mathbf{y}_{N-1}(\mathbf{x}_{N-1}) \in \mathcal{C}^1$ is satisfied if and only if all entries of the Jacobian \mathbf{J}_{N-1} of $\mathbf{y}_{N-1}(\mathbf{x}_{N-1})$ exist and are continuous themselves. This will be shown in the remainder, but first the remaining conditions are considered. Since the function $\mathbf{y}_{N-1}(\mathbf{x}_{N-1})$ will turn out to be differentiable, it is also continuous. Further, since \mathcal{X}_{N-1} is a bounded by N linear equations of the form (including the closing condition f_{N+1})

$$\begin{aligned} \mathbf{E}\mathbf{x} &\leq \mathbf{1}, \\ \mathbf{E} &= \mathbf{1}_N - \mathbf{I}_N \end{aligned} \tag{I.17}$$

containing also the boundary due to the equality constrained included in Eq. (I.17), the set \mathcal{X}_{N-1} is compact. In addition, $\mathcal{Y}_{N-1} \subset \mathbb{R}^{N-1}$ "is Hausdorff", i.e. the Hausdorff-property is induced on \mathcal{Y}_{N-1} by \mathbb{R}^{N-1} , which is a Hausdorff-space [112]. As a result the function $\mathbf{y}_{N-1}(\mathbf{x}_{N-1})$ is proper [113].

Finally, it remains to show that the Jacobian $\mathbf{J}_{N-1} = \frac{\partial \mathbf{y}_{N-1}}{\partial \mathbf{x}_{N-1}}$ exists, is continuous, and does not vanish everywhere in \mathcal{X}_{N-1} . It is clear that if \mathbf{J}_{N-1} is non-existent or discontinuous for some $\mathbf{x}_{N-1} \in \mathcal{X}_{N-1}$, it is a necessity that the same holds for the eigenvalues $\lambda_k(\mathbf{x}_{N-1})$ for all $k = 1, \dots, N-1$ since the related characteristic equation is not continuous in this case. Thus, it suffices to consider these eigenvalue functions. A particular form of the characteristic equation defining the eigenvalues for $\mathbf{\Omega}(\mathbf{x}_{N-1}, \mathbf{y}_{N-1})$ was already derived in Sections 4.3 and 5.3, here shown in a slightly different but equivalent representation

$$0 = f(\mathbf{x}_{N-1}, \lambda_k) = \sum_{i=1}^N \frac{1}{\nu_i} y_i \prod_{j \neq i} \left(\frac{y_j}{x_j} - \lambda_k \right), \quad k = 1, \dots, N-1. \tag{I.18}$$

From Eq. (I.18) it is clear that on the boundary, where at least one component l vanishes, i.e. $x_l = 0$ and therefore $y_l = 0$ (see equations f_i in (I.1)), exists an eigenvalue $\lambda_k = \frac{y_l}{x_l}$. The ratio $\frac{y_l}{x_l}$ exists since for $x_N \neq 0$

$$\frac{y_l}{x_l} = \tilde{K}_{iN}^{\frac{1}{\nu_i}} \left(\frac{y_N}{x_N} \right)^{\frac{\nu_N}{\nu_i}}, \quad l \neq N \tag{I.19}$$

is satisfied. If however $x_N = 0$, then we require that at least one other component m is non-zero for non-zero c_{tot} with

$$\frac{y_N}{x_N} = \tilde{K}_{mN}^{\frac{1}{\nu_m}} \left(\frac{y_m}{x_m} \right)^{\frac{\nu_m}{\nu_N}}, \quad m \neq N. \quad (\text{I.20})$$

The existence of $\frac{y_N}{x_N}$ together with f_i and $i \neq \{m, N\}$ guarantees the existence of all remaining ratios independently of the fact that component i has vanished or not. The only singularity occurs when $c_{\text{tot}} = 0$. This case, however, is of little interest since \mathcal{CH} reduces to a single point; the origin. In this case, obviously, normalized coordinates do not exist in the first place, and it is reasonable that only cases with $c_{\text{tot}} > 0$ are considered. Division of Eq. (I.18) by $\prod_{j=1}^N \left(\frac{y_j}{x_j} - \lambda_k \right)$ results in

$$0 = \sum_{i=1}^N \frac{\frac{1}{\nu_i} y_i}{\frac{y_i}{x_i} - \lambda_k}, \quad k = 1, \dots, N-1 \quad (\text{I.21})$$

similar to Eq. (4.15) and also Eq. (5.11) excluding $\lambda_N = 0$. The previous operation is valid only if $\lambda_k \neq \frac{y_l}{x_l}$ for every component l and every k , i.e. there exists no component l with $x_l = 0$, thus excluding the boundary $\partial\mathcal{X}_{N-1}$ and reversals. Based on the structure in Eq. (I.21) of the characteristic polynomial, the genuine non-linearity was shown in Appendix C, specifically in the interior of the positive orthant including the interior $\mathring{\mathcal{CH}}$ for $\mathbf{\Omega}_{\mathring{\mathcal{CH}}}(\mathbf{c}, \mathbf{q})$ and therefore also for the reduced system $\mathbf{\Omega}(\mathbf{x}_{N-1}, \mathbf{y}_{N-1})$ in $\mathring{\mathcal{X}}_{N-1}$, i.e.

$$\nabla \lambda_k \mathbf{r}_k \leq 0, \quad (\text{I.22})$$

where $\mathbf{r}_k \in \mathbb{R}^{N-1}$ are the eigenvectors of the reduced system as defined in Eq. (4.19). As a consequence, the gradient of every λ_k is known to exist in the interior $\mathring{\mathcal{X}}_{N-1}$ of \mathcal{X}_{N-1} including also reversals. This existence implies the continuity and existence of every λ_k itself, which in turn guarantees the existence and continuity of \mathbf{J}_{N-1} in $\mathring{\mathcal{X}}_{N-1}$. Based on Eq. (I.21), hyperbolicity can be easily concluded from the locations of the poles $\frac{y_i}{x_i}$ for all $i = 1, \dots, N$ that create $N-1$ intervals. Each interval contains a solution λ_k . Since the smallest value $\frac{y_N}{x_N} > 0$, the $N-1$ unique solutions λ_k are all positive, which is also satisfied for reversals (Sections 4.3 and 5.3). Hence, the Jacobian \mathbf{J}_{N-1} is non-vanishing everywhere in $\mathring{\mathcal{X}}_{N-1}$. Note, the result is valid independently of the existence of reversals in $\mathring{\mathcal{X}}_{N-1}$.

It remains to analyze the behavior of the eigenvalues on the boundary $\partial\mathcal{X}_{N-1}$. If N_L components vanish, i.e. $x_l = 0$ for all $l \in \mathcal{L}$, where \mathcal{L} with $\dim(\mathcal{L}) = N_L$ has a maximum number of $N-1$ elements, the division of Eq. (I.18) by $\prod_{j \notin \mathcal{L}} \left(\frac{y_j}{x_j} - \lambda_k \right)$ is valid, and the following equivalent formulation of the characteristic equation is obtained

$$0 = \prod_{l \in \mathcal{L}} \left(\frac{y_l}{x_l} - \lambda_k \right) \sum_{i \notin \mathcal{L}} \frac{\frac{1}{\nu_i} y_i}{\frac{y_i}{x_i} - \lambda_k}, \quad k = 1, \dots, N-1. \quad (\text{I.23})$$

It is evident that for all $l \in \mathcal{L}$ with $x_l = 0$ the eigenvalues $\lambda_k = \frac{y_l}{x_l}$ are solutions, while all other eigenvalues have to satisfy

$$0 = \sum_{i \notin \mathcal{L}} \frac{\frac{1}{\nu_i} y_i}{\frac{y_i}{x_i} - \lambda_k}. \quad (\text{I.24})$$

From Eq. (I.24) we can deduce that again an order is induced through $N - N_L$ poles defining $N - N_L - 1$ intervals containing the eigenvalues $\lambda_k \neq \frac{y_l}{x_l}$ for all $l \in \mathcal{L}$. The order of affinities as in Eq. (4.16) requires for $\lambda_k = \frac{y_l}{x_l}$ either $k = l$ or $k = l - 1$. Further there exists for every $l \in \mathcal{L}$ a corresponding eigenvalue $\lambda_m \neq \frac{y_l}{x_l}$ with $\frac{y_{l+1}}{x_{l+1}} > \lambda_m > \frac{y_{l-1}}{x_{l-1}}$ and $m + 1 \in \mathcal{L}$ or $m \in \mathcal{L}$. Hence, it is possible that two eigenvalues λ_k and λ_m with $k \in \{l - 1, l\}$ as well as $m \in \mathcal{L} \setminus \{k\}$ or $m + 1 \in \mathcal{L} \setminus \{k\}$ coincide on the boundary $\partial \mathcal{X}_{N-1}$. The maximal number of possibly coinciding pairs is N_L . The eigenvalue functions $\lambda_k \neq \frac{y_l}{x_l}$ defined by Eq. (I.24) do not depend on the x_l anymore, which is also an obvious consequence of $x_l = 0$ for all $l \in \mathcal{L}$. Therefore, $\frac{\partial \lambda_k}{\partial x_l} = 0$ holds for every $\lambda_k \neq \frac{y_l}{x_l}$. The remaining $N - N_L - 1$ entries of $\nabla \lambda_k$ also exist due to Eq. (I.24). This equation has the same structure as Eq. (I.21). Hence, it will imply the same properties only for a $N - N_L - 1$ -dimensional system with components $l \in \mathcal{L}$ being absent. In particular, all partial derivatives $\frac{\partial \lambda_k}{\partial x_i}$ for $\lambda_k \neq \frac{y_l}{x_l}$ and $i \in \{1, \dots, N\} \setminus \mathcal{L}$ exist, therefore $\nabla \lambda_k$ with $\lambda_k \neq \frac{y_l}{x_l}$ exists on $\partial \mathcal{X}_{N-1}$. It remains to show that for any $l \in \mathcal{L}$ and $\lambda_k = \frac{y_l}{x_l}$ the gradient $\nabla \lambda_k$ exists on $\partial \mathcal{X}_{N-1}$. On the boundary we have at least one non-vanishing component. In other words, there always exists an component $n \notin \mathcal{L}$ with $x_n \neq 0$. This component is used as reference component and we can write

$$y_j = x_j \tilde{K}_{jn}^{\frac{1}{\nu_j}} \left(\frac{y_n}{x_n} \right)^{\frac{\nu_n}{\nu_j}}, \quad j \neq n, \quad (\text{I.25a})$$

$$y_n = 1 - \sum_{j \notin \mathcal{L}} y_j, \quad j \neq n, \quad (\text{I.25b})$$

$$x_n = 1 - \sum_{j \notin \mathcal{L}} x_j, \quad j \neq n. \quad (\text{I.25c})$$

Additionally, for any eigenvalue $\lambda_k = \frac{y_l}{x_l}$ holds

$$\frac{\partial \lambda_k}{\partial x_j} = \frac{\partial \left(\frac{y_l}{x_l} \right)}{\partial x_j}, \quad j \neq n, \quad (\text{I.26a})$$

$$\frac{y_l}{x_l} = \tilde{K}_{ln}^{\frac{1}{\nu_l}} \left(\frac{y_n}{x_n} \right)^{\frac{\nu_n}{\nu_l}} = f(x_n, y_n). \quad (\text{I.26b})$$

Eqs. (I.25) and (I.26) define eigenvalues that do not depend on any $l \in \mathcal{L}$, hence

$$\frac{\partial \lambda_k}{\partial x_l} = 0 \quad (\text{I.27})$$

holds. These entries are trivial and do exist obviously. All remaining entries $i \notin \mathcal{L}$, $i \neq n$ follow from Eq. (I.26)

$$\frac{\partial \lambda_k}{\partial x_i} = \frac{\partial \left(\frac{y_l}{x_l} \right)}{\partial x_i} = \left(\frac{\partial f}{\partial x_n} \right)_{y_n} \frac{\partial x_n}{\partial x_i} + \left(\frac{\partial f}{\partial y_n} \right) \frac{\partial y_n}{\partial x_i}. \quad (\text{I.28})$$

Using Eqs. (I.25) and (I.26) one obtains

$$\frac{\partial \lambda_k}{\partial x_i} = \frac{\partial \left(\frac{y_l}{x_l} \right)}{\partial x_i} = \frac{y_l}{x_l} \frac{1}{y_n} \frac{\nu_n}{\nu_l} \left(\frac{y_n}{x_n} + \frac{\partial y_n}{\partial x_i} \right). \quad (\text{I.29})$$

The term $\frac{\partial y_n}{\partial x_i}$ can be obtained from implicit differentiation of combination of (I.25a) and (I.25b)

$$0 = g(\mathbf{x}_{N-N_L-1}, x_n, y_n) = 1 - \sum_{j \notin \mathcal{L}} x_j \tilde{K}_{jN}^{\frac{1}{\nu_j}} \left(\frac{y_n}{x_n} \right)^{\frac{\nu_n}{\nu_j}}, \quad (\text{I.30a})$$

$$\begin{aligned} \frac{\partial y_n}{\partial x_i} = - \left(\frac{\partial g}{\partial y_n} \right)_{\mathbf{x}_{N-N_L-1}, x_n}^{-1} & \left(\left(\frac{\partial g}{\partial x_i} \right)_{\mathbf{x}_{N-N_L-1} \setminus \{x_i\}, x_n, y_n} \right. \\ & \left. + \left(\frac{\partial g}{\partial x_n} \right)_{\mathbf{x}_{N-N_L-1}, y_n} \frac{x_n}{x_i} \right). \end{aligned} \quad (\text{I.30b})$$

Note, the vector $\mathbf{x}_{N-N_L-1} \in \mathbb{R}^{N-N_L-1}$ contains all components that have not vanished excluding the n th component. Finally, we obtain for the remaining entries of the gradient

$$\frac{\partial \lambda_k}{\partial x_i} = \frac{\partial \left(\frac{y_l}{x_l} \right)}{\partial x_i} = \frac{y_l}{x_l} \frac{1}{\nu_l} \left(\sum_{j \notin \mathcal{L}} \frac{y_j}{\nu_j} \right)^{-1} \left(\frac{y_n}{x_n} - \frac{y_i}{x_i} \right). \quad (\text{I.31})$$

Clearly, all terms in Eq. (I.31) are defined. Hence, gradient $\nabla \lambda_k$ exists for all $\lambda_k = \frac{y_l}{x_l}$ on $\partial \mathcal{X}_{N-1}$. Consequently, all gradients of any eigenvalue $\nabla \lambda_k$ exist on $\partial \mathcal{X}_{N-1}$. As for the interior $\overset{\circ}{\mathcal{X}}_{N-1}$, it follows that all eigenvalues are existent and continuous, which again leads to the conclusion of an existing and continuous Jacobian \mathbf{J}_{N-1} on $\partial \mathcal{X}_{N-1}$. All eigenvalues have $\frac{y_N}{x_N} > 0$ as lower bound, which makes the Jacobian \mathbf{J}_{N-1} non-vanishing everywhere on $\partial \mathcal{X}_{N-1}$.

It remains to show the continuity of $f(\mathbf{x}_{N-1}, \lambda_k)$ with respect to \mathbf{x}_{N-1} when approaching the boundary from the interior, thus showing the continuity of λ_k for every $k = 1, \dots, N-1$. Again, we have some arbitrary non-vanishing reference component n everywhere on the boundary, which is also present for every possible path that can approach the boundary from the interior. This is a consequence from the fact that at most $N-1$ components can vanish when transitioning from $\overset{\circ}{\mathcal{X}}_{N-1}$ to $\partial \mathcal{X}_{N-1}$. Using Eq. (I.30b), the y_n is differentiable with respect to all

x_i with $i \notin \mathcal{L}$ and trivially also with respect to all x_l with $l \in \mathcal{L}$. Clearly y_n is continuous. Using in addition Eq. (I.25a), all remaining y_j with $j \neq n$ are differentiable due to the differentiability of y_n , which can be readily derived from

$$\begin{aligned} \frac{\partial y_j}{\partial x_i} &= \left(\frac{\partial y_j}{\partial x_i} \right)_{x_n, y_n} + \left(\frac{\partial y_j}{\partial x_n} \right)_{x_i, y_n} \frac{\partial x_n}{\partial x_i} + \left(\frac{\partial y_j}{\partial y_n} \right)_{x_i, x_n} \frac{\partial y_n}{\partial x_i} \\ &= \delta_{ij} \frac{y_j}{x_j} + \frac{y_j}{\nu_j} \frac{\nu_n}{y_n} \left(\frac{y_n}{x_n} + \frac{\partial y_n}{\partial x_i} \right). \end{aligned} \quad (\text{I.32})$$

The differentiability of every y_i with $i = 1, \dots, N$ for any path from the interior $\mathbf{x}_{N-1} \in \mathcal{X}_{N-1}$ to the boundary $\mathbf{x}_{N-1}^* \in \partial \mathcal{X}_{N-1}$ implies their continuity

$$\lim_{\mathbf{x}_{N-1} \rightarrow \mathbf{x}_{N-1}^*} y_i(\mathbf{x}_{N-1}) = y_i(\mathbf{x}_{N-1}^*). \quad (\text{I.33})$$

Considering the corresponding limit behavior of $f(\mathbf{x}_{N-1}, \lambda_k)$ and using standard limit operator properties, we get

$$\begin{aligned} \lim_{\mathbf{x}_{N-1} \rightarrow \mathbf{x}_{N-1}^*} f(\mathbf{x}_{N-1}, \lambda_k) &= \lim_{\mathbf{x}_{N-1} \rightarrow \mathbf{x}_{N-1}^*} \left(\sum_{i=1}^N \frac{1}{\nu_i} y_i \prod_{j \neq i} \left(\frac{y_j}{x_j} - \lambda_k \right) \right) \\ &= \sum_{i=1}^N \frac{1}{\nu_i} \lim_{\mathbf{x}_{N-1} \rightarrow \mathbf{x}_{N-1}^*} y_i \prod_{j \neq i} \left(\frac{\lim_{\mathbf{x}_{N-1} \rightarrow \mathbf{x}_{N-1}^*} y_j}{\lim_{\mathbf{x}_{N-1} \rightarrow \mathbf{x}_{N-1}^*} x_j} - \lambda_k \right) \\ &= \sum_{i=1}^N \frac{1}{\nu_i} y_i(\mathbf{x}_{N-1}^*) \prod_{j \neq i} \left(\frac{y_j(\mathbf{x}_{N-1}^*)}{x_j^*} - \lambda_k \right) = f(\mathbf{x}_{N-1}^*, \lambda_k). \end{aligned} \quad (\text{I.34})$$

The resulting continuity of Eq. (I.18) in \mathcal{X}_{N-1} implies the continuity of all eigenvalue functions in $\mathcal{X}_{N-1} = \mathring{\mathcal{X}}_{N-1} \cup \partial \mathcal{X}_{N-1}$ also when approaching the boundary from the interior. Hence, the Jacobian exists everywhere in \mathcal{X}_{N-1} , and it is also continuous everywhere as well as non-vanishing. The last property follows readily from the preceding analysis of the eigenvalues in the interior and on the boundary using $\lambda_k > \frac{y_N}{x_N} > 0$. Ultimately, we can conclude from Hadamard's global inverse theorem that $\mathbf{y}_N(\mathbf{x}_N)$ is a homeomorphism. In other words the function $\mathbf{y}_{N-1}(\mathbf{x}_{N-1})$ is a continuous bijection for which a continuous inverse function $\mathbf{x}_{N-1}(\mathbf{y}_{N-1})$ exists globally in \mathcal{X}_{N-1} . The equivalence arguments of the previous section lead to the conclusion that in turn a continuous function $\mathbf{q}(\mathbf{c})$ is a bijection with a continuous inverse $\mathbf{c}(\mathbf{q})$ everywhere on \mathcal{CH} .

Appendix I.3 Remarks

First, the equation describing the watershed region is an $N - N_L - 2$ dimensional set. Assuming, as deduced in the previous section, that some non-trivial λ_k coincides with $\lambda_l = \frac{y_l}{x_l}$ (i.e. $x_l = 0$) on the part of boundary where $x_n \neq 0$ and using

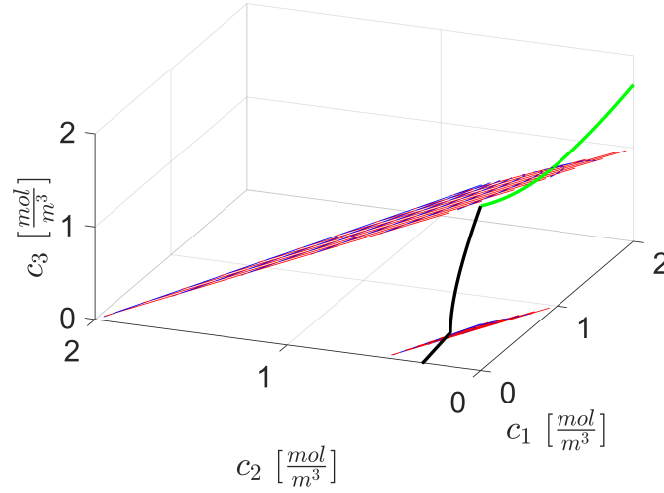


Figure Appendix I.1: The two existing watershed curves are shown for the example presented in Subsection 5.5.1. The green line is the watershed curve in the (c_1, c_3) plane, whereas the black line is the watershed curve in the (c_2, c_3) plane.

Eq. (I.24), this set is represented by

$$\begin{aligned}
 0 &= \sum_{i \notin \mathcal{L}} \frac{\frac{1}{\nu_i} x_i}{1 - \lambda_k \frac{x_i}{y_i}} = \sum_{i \notin \mathcal{L}} \frac{\frac{1}{\nu_i} x_i}{1 - \frac{y_l}{x_i} \frac{x_i}{y_i}} \\
 &= \sum_{i \notin \mathcal{L}} \frac{\frac{1}{\nu_i} x_i}{1 - \left(\tilde{K}_{li} \tilde{K}_{in}^{\frac{\nu_i - \nu_l}{\nu_i}} \right)^{\frac{1}{\nu_l}} \left(\frac{y_n}{x_n} \right)^{\nu_n \frac{\nu_i - \nu_l}{\nu_i \nu_l}}} = f(\mathbf{x}_{N-N_L-1})
 \end{aligned} \tag{I.35}$$

since also

$$x_n = 1 - \sum_{j \notin \mathcal{L}, j \neq n} x_j, \tag{I.36a}$$

$$y_j = y_j(\mathbf{x}_{N-N_L-1}), \quad j \notin \mathcal{L}, \quad j \neq n \tag{I.36b}$$

$$y_n = 1 - \sum_{j \notin \mathcal{L}, j \neq n} y_j = y_n(\mathbf{x}_{N-N_L-1}) \tag{I.36c}$$

holds. For illustration purposes, the watershed curves of the example from Section 5.5.1 (Tabs. 5.1, 5.2) are shown in Fig. Appendix I.1. Eq. (I.35) is used for their calculation in standard concentration variables. Since the solution normality is not fixed, the closing condition (I.36a) does not apply. Consequently, the watershed curve is of dimension $N - N_L - 1$, in particular the dimension is $3 - 1 - 1 = 1$. In this case, two watershed curves exist; one in the (c_1, c_3) plane, the other one in the (c_2, c_3) plane.

Second, the genuine non-linearity in Appendix C seems to be presented only for the interior of the concentration phase space. However, in this appendix, we have shown the existence of all entries in $\nabla\lambda_k$ for all possible k in \mathcal{X} , which is equivalent to their existence on \mathcal{CH} after simple scalar coordinate transformation. In addition, it is easy to show that only the entries of non-vanishing components are relevant. This can be easily deduced by rewriting Eq. (5.15)

$$\mathbf{r}_k = \left[\frac{\frac{q_1}{\nu_1}}{\frac{q_1}{c_1} - \lambda_k}, \dots, \frac{\frac{q_N}{\nu_N}}{\frac{q_N}{c_N} - \lambda_k} \right]^T. \quad (\text{I.37})$$

From Eq. (I.37) it is evident, that for all $\lambda_k \neq \frac{q_l}{c_l}$ and vanishing components $l \in \mathcal{L}$, the corresponding entry $r_{k,l}$ is zero and the proof in Appendix C reduces for these eigenvalues simply to all non-vanishing components $i \notin \mathcal{L}$ that satisfy Eq. (I.24), which admits the identical structure as Eq. (5.11). Together with Eq. (I.37), Eq. (I.24) admits the same proof as Eqs. (5.11) and (5.15) in Appendix C for genuine non-linearity. If $\lambda_k = \frac{q_l}{c_l}$, the trivial solution $\mathbf{r}_k = \mathbf{0}$ is available (see Eq. (5.14)) on the intersection of the corresponding integral curves with the boundary $\partial\mathcal{CH}$, which is a single (end)point where $\nabla\lambda_k\mathbf{r}_k|_{c_l=0} = 0$ would hold. Hence each of those points is a singular point on the corresponding integral curve of family k . However, this discontinuity can be avoided by a continuation of the non-trivial solution in Eq. (I.37). This continuation is justified due to the continuity of λ_l everywhere and the fact that we require only a one-sided continuous limit at the boundary. There is only a single critical entry in \mathbf{r}_l considering Eq. (I.37)

$$\frac{\frac{q_l}{\nu_l}}{\frac{q_l}{c_l} - \lambda_l}, \quad (\text{I.38})$$

all other entries in Eq. (I.37) are readily defined also on the boundary. A continuation can be found by using

$$0 = \sum_{i=1}^N \xi_i \frac{\frac{q_i}{\nu_i}}{\frac{q_i}{c_i} - \lambda_l}, \quad (\text{I.39a})$$

$$\xi_l \frac{\frac{q_l}{\nu_l}}{\frac{q_l}{c_l} - \lambda_l} = - \sum_{i \notin \mathcal{L}} \xi_i \frac{\frac{q_i}{\nu_i}}{\frac{q_i}{c_i} - \frac{q_l}{c_l}} \quad (\text{I.39b})$$

Eq. (I.39b) provides clearly a finite value that is the one-sided limit of Eq. (I.38) due to $\lambda_l \rightarrow \left(\frac{q_l}{c_l}\right)^-$ (or $\lambda_{l-1} \rightarrow \left(\frac{q_l}{c_l}\right)^+$ instead). Hence, the continuation of Eq. (I.38) on the boundary can be added

$$\frac{\frac{q_l}{\nu_l}}{\frac{q_l}{c_l} - \lambda_l} = \begin{cases} \frac{\frac{q_l}{\nu_l}}{\frac{q_l}{c_l} - \lambda_l}, & \mathbf{c} \in \mathring{\mathcal{CH}} \\ -\frac{1}{\xi_l} \sum_{i \notin \mathcal{L}} \xi_i \frac{\frac{q_i}{\nu_i}}{\frac{q_i}{c_i} - \frac{q_l}{c_l}}, & \mathbf{c} \in \partial\mathcal{CH}, c_l = 0 \end{cases} \quad (\text{I.40})$$

Consequently, the results in Appendix C readily include the eigenvalues with $\lambda_k = \frac{q_l}{c_l}$ on the boundary as well since identically structured equations (I.24) and (I.37) can be applied resulting in $\nabla \lambda_k \mathbf{r}_k|_{c_l=0} < 0$ for the non-trivial eigenvector solution (I.37) with (I.40).

Third, hyperbolicity prevails not only everywhere in \mathcal{CH} (see Eq. (5.12)) but also almost everywhere on the boundary of $\partial\mathcal{CH}$. Due to the results of the previous section, we know that the eigenvalue eigenvalues either satisfy $\lambda_k = \frac{q_l}{c_l}$ for any $l \in \mathcal{L}$ or else satisfy Eq. (I.24). Without loss of generality, we assume $\lambda_l = \frac{q_l}{c_l}$. Hence, the following holds

$$\frac{q_1}{c_1} > \lambda_1 > \frac{q_2}{c_2} > \dots > \frac{q_{l-1}}{c_{l-1}} > \lambda_{l-1} > \frac{q_{l+1}}{c_{l+1}} > \dots > \frac{q_N}{c_N} > \lambda_N = 0, \quad (\text{I.41a})$$

$$\frac{q_{l-1}}{c_{l-1}} > \frac{q_l}{c_l} = \lambda_l > \frac{q_{l+1}}{c_{l+1}}. \quad (\text{I.41b})$$

From Eq. (I.41) it is clear that the two eigenvalues λ_{l-1} and λ_l can assume identical values. However, this is possible only in water sheds, which are $N - N_L - 1$ dimensional subsets in boundary of dimension $N - 1$ if the solution normality is not fixed. Hence, strict hyperbolicity is admitted almost everywhere on the boundary $\partial\mathcal{CH}$ and therefore almost everywhere in \mathcal{CH} .

This page intentionally left blank.

Bibliography

- [1] H. Schmidt-Traub, M. Schulte, A. Seidel-Morgenstern, *Preparative Chromatography*, Wiley-VCH, Weinheim, 2012.
- [2] A. Rodrigues, *Simulated Moving Bed Technology: Principles, Design and Process Applications*, Butterworth-Heinemann, Waltham, 2015.
- [3] D. R. Stoll, P. W. Carr, Two-dimensional liquid chromatography: A state of the art tutorial, *Anal. Chem.* 89(1) (2017) 519–531.
- [4] C. Horváth, S. R. Lipsky, Column design in high pressure liquid chromatography, *J. Chromatogr. Sci.* 7(2) (1969) 109–116.
- [5] G. Carta, A. Jungbauer, *Protein Chromatography*, Vol. 1, WILEY-VCH Verlag GmbH & Co. KGaA, Weinheim, 2010.
- [6] S. Gallant, A. Kundu, S. Cramer, Modeling non-linear elution of proteins in ion-exchange chromatography, *Journal of Chromatography A* 702 (1995) 125–142.
- [7] D. Antos, A. Seidel-Morgenstern, Application of gradients in the simulated moving bed process, *Chem. Eng. Sci.* 56(23) (2001) 6667–6682.
- [8] A. Rajendran, G. Paredes, M. Mazzotti, Simulated moving bed chromatography for the separation of enantiomers, *J. Chrom. A* 1216 (2009) 709–738.
- [9] M. Mazzotti, G. Storti, M. Morbidelli, Optimal operation of simulated moving bed units for nonlinear chromatographic separations, *J. Chrom. A* 769 (1997) 3–24. doi:10.1016/S0021-9673(97)00048-4.
- [10] M. Mazzotti, A. Rajendran, Equilibrium theory-based analysis of nonlinear waves in separation processes, *Annual Review of Chemical and Biomolecular Engineering* 4 (2013) 119–141.
- [11] G. Guiochon, B. Lin, *Modeling for preparative chromatography*, Academic Press, Boston, 1994.
- [12] K.-U. Klatt, F. Hanisch, G. Dünnebier, S. Engell, Model-based optimization and control of chromatographic processes, *Comput. Chem. Eng.* 24 (2000) 1119–1126.

- [13] G. Guiochon, S. Golshan-Shirazi, A. Katti, *Fundamentals of Preparative and Nonlinear Chromatography*, Academic Press, Boston, 1994.
- [14] H.-K. Rhee, R. Aris, N. R. Amundson, *First-Order Partial Differential Equations: Volume I – Theory and Application of Single Equations*, Prentice Hall, New Jersey, 1986.
- [15] H.-K. Rhee, R. Aris, N. R. Amundson, *First-Order Partial Differential Equations: Volume II – Theory and Application of Hyperbolic Systems of Quasi-linear Equations*, Prentice Hall, New Jersey, 1989.
- [16] R. J. LeVeque, *Numerical Methods for Conservation Laws*, Birkhäuser Verlag, Basel, 1992.
- [17] A. Myers, J. Prausnitz, Thermodynamics of mixed-gas adsorption, *AIChE J.* 11 (1965) 121–127. doi:10.1002/aic.690110125.
- [18] A. B. Koudriavtsev, R. F. Jameson, W. Linert, *The law of Mass Action*, Vol. 1, Springer, New York, 2001.
- [19] I. Langmuir, The adsorption of gases on plane surfaces of glass, mica and platinum, *JACS* 40(9) (1918) 1361–1403.
- [20] D. M. Ruthven, *Principles of Adsorption and Adsorption Processes*, John Wiley & Sons, Hoboken, 1984.
- [21] G. Gamba, R. Rota, G. Storti, S. Carrà, M. Morbidelli, Adsorbed solution theory models for multicomponent adsorption equilibria, *AIChE J.* 35(6) (1989) 959–966.
- [22] G. Gamba, R. Rota, G. Storti, S. Carrà, M. Morbidelli, Vacancy solution theory of adsorption from gas mixtures, *AIChE J.* 26(1) (1980) 76–83.
- [23] A. Seidel-Morgenstern, Experimental determination of single solute and competitive adsorption isotherms, *J. Chrom. A* 1037 (2004) 225–272.
- [24] E. N. Rudisill, M. D. LeVan, Standard states for the adsorbed-solution theory, *Chem. Eng. Sci.* 47(5) (1992) 1239–1245.
- [25] C. J. Radke, J. M. Prausnitz, Thermodynamics of multi-solute adsorption from dilute liquid solutions, *AIChE J.* 18(4) (1972) 761–768. doi:10.1002/aic.690180417.
- [26] D. D. Do, *Adsorption Analysis: Equilibria and Kinetics*, Vol. 2 Series on Chemical Engineering, Imperial College Press, London, 1998.
- [27] D. Tondeur, *Theorie des colonnes d’change d’ions*, ph.D. Thesis, Universite de Nancy (1969).

- [28] F. G. Helfferich, G. Klein, *Multicomponent Chromatography. Theory of Interference*, M. Dekker, New York, 1970.
- [29] C. Brooks, S. Cramer, Steric mass-action ion exchange: Displacement profiles and induced salt gradients, *AIChE Journal* 38(12) (1992) 1969–1978.
- [30] S. Gallant, S. Vunnum, S. Cramer, Optimization of preparative ion-exchange chromatography of proteins: linear gradient separations, *Journal of Chromatography A* 725 (1996) 295–314.
- [31] S. Gallant, S. Vunnum, S. Cramer, Modeling gradient elution of proteins in ion-exchange chromatography, *AIChE Journal* 42(9) (1996) 2511–2520.
- [32] H. Karkov, L. Sejergaard, S. Cramer, Methods development in multimodal chromatography with mobilephase modifiers using the steric mass action model, *Journal of Chromatography A* 1318 (2013) 149–155.
- [33] J. Diedrich, W. Heymann, S. Leweke, S. Hunt, R. Todd, C. Kunert, W. Johnson, E. von Lieres, Multi-state steric mass action model and case study on complex high loading behavior of mab on ion exchange tentacle resin, *J. Chromatogr. A* 1525 (2017) 60–70. doi:10.1016/j.chroma.2017.09.039.
- [34] D. Nagrath, A. Messac, B. W. B. and S. M. Cramer, A hybrid model framework for the optimization of preparative chromatographic processes, *Biotechnol. Progr.* 20(1) (2004) 162–178.
- [35] A. Osberghaus, S. Hepbildikler, S. Nath, M. Haindl, E. von Lieres, J. Hubbuch, Optimizing a chromatographic three component separation: A comparison of mechanistic and empiric modeling approaches, *J. Chrom. A* 1237 (2012) 86–95.
- [36] W. E. Schiesser, *The Numerical Method of Lines Integration of Partial Differential Equations*, Academic Press, San Diego, 1991.
- [37] R. Köhler, K. D. Mohl, H. Schramm, M. Zeitz, A. Kienle, M. Mangold, E. Stein, E. D. Gilles, Methods of lines within the simulation environment DIVA for chemical processes, in: A. VandeWouwer, P. Saucez, W. Schiesser (Eds.), *Adaptive method of lines*, CRC Press, 2001, pp. 371–406.
- [38] V. Natarajan, S. Cramer, Comparison of linear gradient and displacement separations in ion-exchange systems, *Biotechnology and Bioengineering* 78(4) (2002) 365–375.
- [39] S. Leweke, E. von Lieres, *Chromatography analysis and design toolkit (cadet)*, *Comput. Chem. Eng.* 113 (2018) 274–294.

- [40] D. Kahaner, C. Moler, S. Nash, *Numerical Methods and Software*, Vol. 1, Prentice Hall, Inc., New Jersey, 1989.
- [41] H. O. R. Landa, D. Flockerzi, A. Seidel-Morgenstern, A method for efficiently solving the IAST equations with aqn application to adsorber dynamics, *AIChE Journal* 59 (2013) 1263–1277.
- [42] J. O'Brien, A. Myers, A comprehensive technique for equilibrium calculations in adsorbed mixtures: The generalized fastias method, *Ind. Eng. Chem. Res.* 27 (1988) 2085–2092. doi:10.1021/ie00083a021.
- [43] A. Myers, D. Valenzuela, Computer algorithm and graphical method for calculating adsorption equilibria of gas mixtures, *J. Chem. Eng. Jpn.* 19(5) (1986) 392–396. doi:10.1252/jcej.19.392.
- [44] J. O'Brien, A. Myers, Rapid calculations of multicomponent adsorption equilibria from pure isotherm data, *Ind. Eng. Chem. Process Des. Dev.* 24 (1985) 1188–1191. doi:10.1021/i200031a049.
- [45] M. Ilic, D. Flockerzi, A. Seidel-Morgenstern, A thermodynamically consistent explicit competitive adsorption isotherm model based on second order single component behavior, *Journal of Chromatography A* 1217 (2010) 2132–2137.
- [46] A. Tarafder, M. Mazzotti, A method for deriving explicit binary isotherms obeying the ideal adsorbed solution theory, *Chemical Engineering Technology* 35 (2012) 102–108.
- [47] D. Flockerzi, M. Kaspereit, A. Kienle, Spectral properties of Bi-Langmuir isotherms, *Chemical Engineering Science* 104 (2013) 957–959.
- [48] F. Ortner, S. Jermann, L. Joss, M. Mazzotti, Equilibrium theory analysis of a binary system subject to a mixed generalized Bi-Langmuir isotherm, *Industrial & Engineering Chemistry Research* 54 (2015) 11420–11437.
- [49] M. Mazzotti, Local equilibrium theory for the binary chromatography of species subject to a generalized Langmuir isotherm, *Industrial & Engineering Chemistry Research* 45 (2006) 5332–5350.
- [50] D. Tondeur, Theory of ion-exchange columns, *Chemical Engineering Journal* 1 (1970) 337–346.
- [51] F. G. Helfferich, Multiple steady states in multicomponent countercurrent mass-transfer processes, *Chemical Engineering Science* 48 (1993) 681–686.
- [52] A. Velayudhan, C. Horváth, Preparative chromatography of proteins analysis of the multivalent ion-exchange formalism, *J. Chrom.* 443 (1988) 13–29.

- [53] D. Frey, Local-equilibrium behavior of retained pH and ionic strength gradients in preparative chromatography, *Biotechnol. Prog.* 12 (1996) 65–72.
- [54] J. Pérez, D. Frey, Behavior of the inadvertent pH transient formed by a salt gradient in the ion-exchange chromatography of proteins, *Biotechnol. Prog.* 21 (2005) 902–910.
- [55] T. Pabst, G. Carta, pH transitions in cation exchange chromatographic columns containing weak acid groups, *J. Chrom. A* 1142 (2007) 19–31.
- [56] T. Pabst, G. Carta, Separation of protein charge variants with induced pH gradients using anion exchange chromatographic columns, *Biotechnol. Prog.* 24 (2008) 1096–1106.
- [57] M. Mazzotti, Giuseppe, M. Morbidelli, Shock layer analysis in multicomponent chromatography and countercurrent adsorption, *Chemical Engineering Science* 49 (1994) 1337–1355.
- [58] C. Migliorini, M. Mazzotti, M. Morbidelli, Robust design of countercurrent adsorption separation processes: 5. nonconstant selectivity, *AIChE J.* 46(7) (2000) 1384–1399.
- [59] J. M. Smith, H. C. V. Ness, M. M. Abbott, *Introduction to Chemical Engineering Thermodynamics*, McGraw-Hill, New York, 2005.
- [60] J. Janson, *Protein Purification*, Vol. 1, JOHN WILEY & SONS. INC., New Jersey, 2011.
- [61] R. R. Drager, F. E. Regnier, Application of the stoichiometric displacement model of retention to anion-exchange chromatography of nucleic acids, *J. Chrom.* 359 (1986) 147–155.
- [62] J. Smoller, *Shock Waves and Reaction–Diffusion Equations*, 2nd Edition, Springer, New York, 1994.
- [63] C. M. Dafermos, *Hyperbolic Conservation Laws in Continuum Physics*, Vol. 4, Springer, Berlin, 2016.
- [64] P. Lax, *Hyperbolic Systems of Conservation Laws and the Mathematical Theory of Shock Waves*, Vol. 1, CBMS-NSF Regional Conference Series in Applied Mathematics, 1973.
- [65] P. Saucez, W. E. Schiesser, A. V. Wouwer, Upwinding in the method of lines, *Math. Comput. Simul.* 56(2) (2001) 171–185.
- [66] K. Kaczmarski, D. Antos, Calculation of chromatographic band profiles with an implicit isotherm, *J. Chromatogr. A* 862(1) (1999) 1–16. doi:10.1016/S0021-9673(99)00901-2.

- [67] L. C. Young, Orthogonal collocation revisited, *Comput. Method. Appl. M.* 345 (2019) 1033–1076. doi:10.1016/j.cma.2018.10.019.
- [68] P. Rouchon, M. Schonauer, P. Valentin, G. Guiochon, Numerical simulation of band propagation in nonlinear chromatography, *Sep. Sci. Technol.* 22(8-10) (1987) 1793–1833. doi:10.1080/01496398708057614.
- [69] MATLAB, version 8.4.0 (R2014b), The MathWorks Inc., Natick, Massachusetts, 2014.
- [70] K. E. Brenan, S. L. Campbell, L. R. Petzold, *Numerical Solution of Initial Value Problems in Differential-Algebraic Equations*, North Holland & Elsevier Science Publishing Company, 1989.
- [71] P. Deuffhard, E. Hairer, J. Zugck, One-step and extrapolation methods for differential-algebraic systems, *Numerische Mathematik* 51 (1987) 501–516.
- [72] A. Hindmarsh, P. Brown, K. Grant, S. Lee, R. Serban, D. Shumaker, C. Woodward, SUNDIALS: Suite of nonlinear and differential/algebraic equation solvers, *ACM Transactions on Mathematical Software (TOMS)* 31 (3) (2005) 363–396.
- [73] J. Unger, A. Kröner, W. Marquardt, Structural analysis of differential-algebraic equation systems: Theory and applications, *Computers & Chemical Engineering* 19 (1995) 867–882.
- [74] M. Czok, G. Guiochon, The physical sense of simulation models of liquid chromatography: Propagation through a grid or solution of the mass balance equation, *Anal. Chem.* 62(2) (1990) 189–200. doi:10.1021/ac00201a020.
- [75] P. Kunkel, V. Mehrmann, *Differential-algebraic Equations: Analysis and Numerical Solution*, European Mathematical Society, Switzerland, Zürich, 2006.
- [76] E. Kvaalen, L. Neel, D. Tondeur, Directions of quasi-static mass and energy transfer between phases in multicomponent open systems, *Chemical Engineering Science* 40 (1985) 1191–1204.
- [77] R. Seydel, *Practical Bifurcation and Stability Analysis*, Springer-Verlag, New York, 1994.
- [78] P. Knabner, L. Angermann, *Numerical Methods for Elliptic and Parabolic Partial Differential Equations*, Springer-Verlag, New York, 2003.
- [79] A. Butté, G. Storti, M. Mazzotti, Shock formation in binary systems with nonlinear characteristic curves, *Chemical Engineering Science* 63 (2008) 4159–4170.

- [80] S. Grüner, A. Kienle, Equilibrium theory and nonlinear waves for reactive distillation columns and chromatographic reactors, *Chemical Engineering Science* 59 (2004) 901–918.
- [81] T. D. Vu, A. Seidel-Morgenstern, S. Grüner, A. Kienle, Analysis of ester hydrolysis reactions in a chromatographic reactor using equilibrium theory and a rate model, *Industrial & Engineering Chemistry Research* 44 (2005) 9565–9574.
- [82] S. Grüner, M. Mangold, A. Kienle, Dynamics of reaction separation processes in the limit of chemical equilibrium, *AIChE Journal* 52 (2006) 1010–1026.
- [83] G. Klein, D. Tondeur, T. Vermeulen, Multicomponent ion exchange in fixed beds, *Industrial & Engineering Chemistry Fundamentals* 6 (1967) 339–351.
- [84] H. P. Urbach, On the conservation laws of nonlinear chromatography for heterovalent ions, *Proceedings of the Royal Society A* 440 (1993) 303–322.
- [85] A. Kienle, W. Marquardt, Bifurcation analysis and steady-state multiplicity of multicomponent, non-equilibrium distillation processes, *Chemical Engineering Science* 46 (1991) 1757–1769.
- [86] H. Nagai, G. Carta, Lysine adsorption on cation exchange resin. i. ion exchange equilibrium and kinetics, *Sep. Sci. Technol.* 39(16) (2004) 3691–3710.
- [87] H. Nagai, G. Carta, Lysine adsorption on cation exchange resin. ii. column adsorption/desorption behavior and modeling, *Sep. Sci. Technol.* 39(16) (2004) 3711–3738.
- [88] G. Storti, M. Mazzotti, M. Morbidelli, Robust design of binary countercurrent adsorption separation processes, *AIChE J.* 39(3) (1993) 471–492.
- [89] C. Migliorini, M. Mazzotti, M. Morbidelli, Continuous chromatographic separation through simulated moving beds under linear and nonlinear conditions, *J. Chrom. A* 827(2) (1998) 161–173.
- [90] M. Mazzotti, R. Baciocchi, G. Storti, M. Morbidelli, Vapor-phase simulated moving bed adsorptive separation of linear/nonlinear paraffins, *Ind. Eng. Chem. Res.* 35(7) (1996) 2313–2321.
- [91] P. Li, G. Xiu, A. E. Rodrigues, Proteins separation and purification by salt gradient ion-exchange smb, *AIChE J.* 53(9) (2007) 2419–2431.
- [92] P. Li, J. Yu, G. Xiu, A. E. Rodrigues, Separation region and strategies for proteins separation by salt gradient ion-exchange smb, *Sep. Sci. Technol.* 43(1) (2008) 11–28.

- [93] T. Yang, M. C. Sundling, A. S. Freed, C. M. Breneman, S. M. Cramer, Prediction of pH-dependent chromatographic behavior in ion-exchange systems, *Anal. Chem.* 79(23) (2007) 8927–8939.
- [94] Q. Shi, Y. Zhou, Y. Sun, Influence of pH and ionic strength on the steric mass-action model parameters around the isoelectric point of protein, *Biotechnol. Progr.* 21(2) (2005) 516–523.
- [95] T. M. Pabst, D. Antos, G. Carta, N. Ramasubramanyan, A. K. Hunter, Protein separations with induced pH gradients using cation-exchange chromatographic columns containing weak acid groups, *J. Chrom. A* 1181(1-2) (2008) 83–94.
- [96] L. I. Tsonev, A. G. Hirsh, Theory and applications of a novel ion exchange chromatographic technology using controlled pH gradients for separating proteins on anionic and cationic stationary phases, *J. Chrom. A* 1200(2) (2008) 166–182.
- [97] M. A. Holstein, A. A. M. Nikfetrat, M. Gage, A. G. Hirsh, S. M. Cramer, Improving selectivity in multimodal chromatography using controlled pH gradient elution, *J. Chrom. A* 1233 (2012) 152–155.
- [98] J. A. Gerstner, J. A. Bell, S. M. Cramer, Gibbs free energy of adsorption for biomolecules in ion-exchange systems, *Biophys. Chem.* 52(2) (1994) 97–106.
- [99] J. C. Bosma, J. A. Wesselingh, pH dependence of ion-exchange equilibrium of proteins, *AIChE J.* 44(11) (1998) 2399–2409.
- [100] S. Kluters, F. Wittkopp, M. Jöhnck, C. Frech, Application of linear pH gradients for the modeling of ion exchange chromatography: Separation of monoclonal antibody monomer from aggregates, *J. Sep. Sci.* 39(4) (2015) 663–675.
- [101] F. Steinebach, M. Krättli, G. Storti, M. Morbidelli, Equilibrium theory based design space for the multicolumn countercurrent solvent gradient purification process, *Ind. Eng. Chem. Res.* 56(45) (2017) 13482–13489.
- [102] B. Guélat, G. Ströhlein, M. Lattuada, L. Delegrange, P. Valax, M. Morbidelli, Simulation model for overloaded monoclonal antibody variants separations in ion-exchange chromatography, *J. Chrom. A* 1253 (2012) 32–43.
- [103] H. Shen, D. D. Frey, Effect of charge regulation on steric mass-action equilibrium for the ion-exchange adsorption of proteins, *J. Chrom. A* 1079 (2005) 92–104.
- [104] E. Hackermann, H. Hasse, Influence of mixed electrolytes and pH on adsorption of bovine serum albumin in hydrophobic interaction chromatography, *J. Chrom. A* 1521 (2017) 73–79.

- [105] E. J. Klein, S. L. Rivera, Optimization of ion-exchange protein separations using a vector quantizing neural network, *Biotechnol. Progr.* 16(3) (2000) 506–512.
- [106] A. Susanto, K. Treier, E. Knieps-Grünhagen, E. von Lieres, J. Hubbuch, High throughput screening for the design and optimization of chromatographic processes: Automated optimization of chromatographic phase systems, *Chem. Eng. Technol.* 32(1) (2009) 140–154.
- [107] A. Creasy, G. Barker, Y. Yao, G. Carta, Systematic interpolation method predicts protein chromatographic elution from batch isotherm data without a detailed mechanistic isotherm model, *Biotechnol. J.* 10(9) (2015) 1400–1411.
- [108] K. McBride, K. Sundmacher, Overview of surrogate modeling in chemical process engineering, *Chem. Ing. Tech.* 91(3) (2019) 228–239.
- [109] K. V. Kumar, M. M. de Castro, M. Martinez-Escandell, M. Molina-Sabio, F. Rodriguez-Reinoso, A site energy distribution function from toth isotherm for adsorption of gases on heterogeneous surfaces, *Phys. Chem. Chem. Phys.* 13 (2011) 5753–5759. doi:10.1039/C0CP00902D.
- [110] W. B. Gordon, An application of hadamard’s inverse function theorem to algebra, *Am. Math. Mon.* 84(1) (1977) 28–29.
- [111] J. R. Munkres, *Topology*, Pearson, London, 1999.
- [112] F. Hausdorff, *Set Theory*, American Mathematical Soc., Providence (RI), 2005.
- [113] R. Brown, *Topology and Groupoids*, Deganwy, 2006.
URL www.groupoids.or.uk

Ehrenerklärung

Ich versichere hiermit, dass ich die vorliegende Arbeit ohne unzulässige Hilfe Dritter und ohne Benutzung anderer als der angegebenen Hilfsmittel angefertigt habe. Die Hilfe eines kommerziellen Promotionsberaters habe ich nicht in Anspruch genommen. Dritte haben von mir weder unmittelbar noch mittelbar geldwerte Leistungen für Arbeiten erhalten, die im Zusammenhang mit dem Inhalt der vorgelegten Dissertation stehen. Verwendete fremde und eigene Quellen sind als solche kenntlich gemacht.

Ich habe insbesondere nicht wissentlich:

- Ergebnisse erfunden oder widersprüchliche Ergebnisse verschwiegen,
- statistische Verfahren absichtlich missbraucht, um Daten in ungerechtfertigter Weise zu interpretieren,
- fremde Ergebnisse oder Veröffentlichungen plagiiert,
- fremde Forschungsergebnisse verzerrt wiedergegeben

Mir ist bekannt, dass Verstöße gegen das Urheberrecht Unterlassungs- und Schadensersatzansprüche des Urhebers sowie eine strafrechtliche Ahndung durch die Strafverfolgungsbehörden begründen kann.

Ich erkläre mich damit einverstanden, dass die Dissertation ggf. mit Mitteln der elektronischen Datenverarbeitung auf Plagiate überprüft werden kann.

Die Arbeit wurde bisher weder im Inland noch im Ausland in gleicher oder ähnlicher Form als Dissertation eingereicht und ist als Ganzes auch noch nicht veröffentlicht.

Magdeburg, 23.06.2020